JOURNAL OF RESEARCH

OF THE U.S. GEOLOGICAL SURVEY

JULY–AUGUST 1975
VOLUME 3, NUMBER 4

Scientific notes and summaries of investigations in geology, hydrology, and related fields

U.S. DEPARTMENT OF THE INTERIOR

UNITED STATES DEPARTMENT OF THE INTERIOR

GEOLOGICAL SURVEY

V. E. McKelvey, Director

For sale by the Superintendent of Documents, U.S. Government Printing Office, Washington, DC 20402. Order by SD Catalog No. JRGS. Annual subscription rate $18.90 (plus $4.75 for foreign mailing). Single copy $3.15. Make checks or money orders payable to the Superintendent of Documents.

Send all subscription inquiries and address changes to the Superintendent of Documents at the above address.

Purchase orders should not be sent to the U.S. Geological Survey library.

Library of Congress Catalog-card No. 72-600241.

The Journal of Research is published every 2 months by the U.S. Geological Survey. It contains papers by members of the Geological Survey and their professional colleagues on geologic, hydrologic, topographic, and other scientific and technical subjects.

Correspondence and inquiries concerning the Journal (other than subscription inquiries and address changes) should be directed to the Journal of Research, Publications Division, U.S. Geological Survey, National Center 321, Reston, VA 22092.

Papers for the Journal should be submitted through regular Division publication channels.

The Secretary of the Interior has determined that the publication of this periodical is necessary in the transaction of the public business required by law of this Department. Use of funds for printing this periodical has been approved by the Director of the Office of Management and Budget through June 30, 1980.

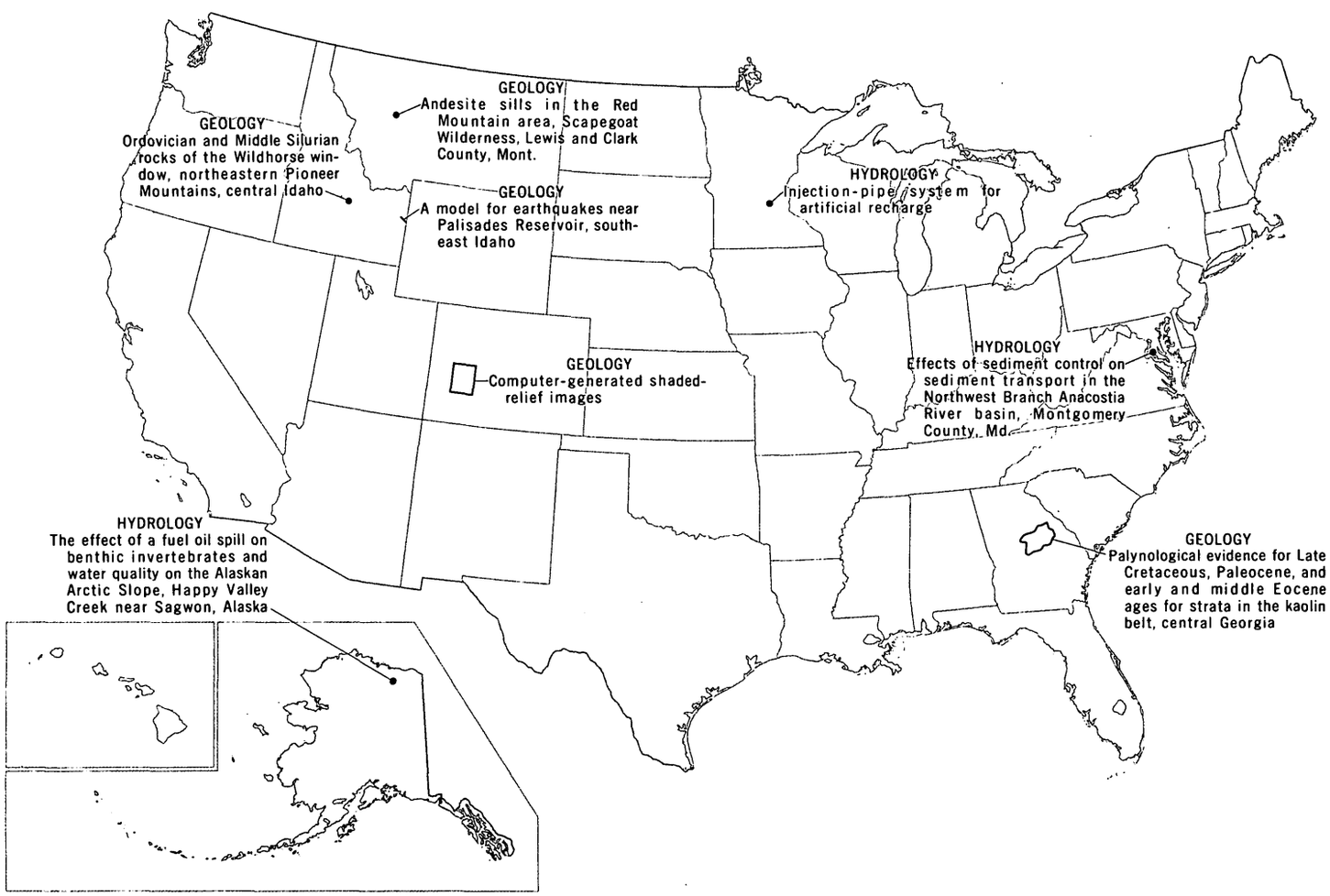

GEOGRAPHIC INDEX TO ARTICLES

See "Contents" for articles concerning areas outside the United States and articles without geographic orientation.

JOURNAL OF RESEARCH

of the

U.S. Geological Survey

Vol. 3 No. 4 July–Aug. 1975

CONTENTS

ABBREVIATIONS

A ---------angstrom
a_0 --------unit cell
acre-ft ----acre-foot
alt -------altitude
atm ------atmosphere
avg ------average
bbl -------barrel
B.P. ------before present
b.y. -------billion years
°C --------degree Celsius
cal -------calorie
calc ------calculated
cm -------centimetre
cm^2 -------square centimetre
COD ------chemical oxygen demand
colln. -----collection
concd -----concentrated
concn -----concentration
cP --------centipoise
c/s -------counts per second; cycles per second
D ---------debye unit
d ---------day
dB -------decibel
d.f. -------degree of freedom
diam ------diameter
DO -------dissolved oxygen
Eh --------oxidation-reduction potential
eq --------equation
EROS ----Earth Resources Observation System
ERTS ----Earth Resources Technology Satellite (now Landsat)
eU -------equivalent uranium
°F --------degree Fahrenheit
ft --------foot
ft^2 --------square foot
ft-c -------foot-candle
g ---------gram
gal -------gallon
h ---------hour
ha --------hectare
hm -------hectometre
in. -------inch
J ---------joule
K ---------kelvin
keV ------kiloelectronvolt
kg --------kilogram
km -------kilometre
km^2 -------square kilometre
kV -------kilovolt
kWh ------kilowatt-hour
l ---------litre
lat -------latitude
lb --------pound
LDMW ---locally derived meteoric water
lm --------lumen
log -------logarithm (common)
long ------longitude
M --------molarity, molar (concentration)
m --------molality, molal (concentration)
m ---------metre
m^2 --------square metre
mA -------milliampere
MBAS ----methylene blue active substance
MeV ------megaelectron volt
mg -------milligram
Mgal -----million gallons
mGal -----milligal
mi -------mile
mi^2 -------square mile
MIBK ----methyl isobutyl ketone
min ------minute
Ml -------million litres
ml -------millilitre
mm -------millimetre
mo -------month
mol ------mole
mV ------millivolt
m.y. ------million years
μcal ------microcalorie
μg --------microgram
μm -------micrometre
μmho -----micromho
N --------normality
n ---------neutron
NASA ----National Aeronautics and Space Administration
NOAA ----National Oceanic and Atmospheric Administration
nm -------nanometre
oz --------ounce
p ---------proton
P.d.t. -----Pacific daylight time
pH -------measure of hydrogen ion activity
ppb ------part per billion
ppm ------part per million
r/min ----revolutions per minute
s ---------second
(s) -------solid
SI --------Systeme International (International System)
SMOW ----standard mean ocean water
std -------standard
σ ---------population standard deviation
t ---------tonne
U.S.P. ----United States Pharmacopeia
UTM -----Universal Transverse Mercator
W --------watt
w/v ------weight per volume
yd -------yard
yr --------year

Jour. Research U.S. Geol. Survey
Vol. 3, No. 4, July–Aug. 1975, p. 379–392

ORIGIN OF LUNAR LIGHT PLAINS

By E. C. T. CHAO; CARROLL ANN HODGES; J. M. BOYCE, and L. A. SODERBLOM;
Reston, Va.; Menlo Park, Calif.; Flagstaff, Ariz.

Abstract.—Most Cayley-type Imbrian-age plains deposits and adjacent mantled slopes, including those at the Apollo 16 site, may be composed—at least near the surface—of ejecta from the Orientale basin, the youngest multiringed impact basin on the Moon. The distribution and apparent age of the plains deposits and preliminary data on the highly feldspathic breccias collected by the Apollo 16 crew indicate that these surficial materials are neither locally derived nor part of the Imbrium ejecta. Stratigraphic relations, crater size-frequency distributions, and dating by erosional morphology of superposed craters have established Cayley light-plains deposits as younger than the Imbrium basin and older than mare material. All such crater-dated Cayley-type plains on both the near and far sides of the Moon are contemporaneous within the limits of the technique. Furthermore, comparisons of the crater size-frequency distributions of the Hevelius Formation (Orientale ejecta) and the plains show that the Cayley and Hevelius Formations are indistinguishable in age. The surface and near-surface materials of the Apollo 16 plains, therefore, are contemporaneous with Orientale basin ejecta—not with Imbrium ejecta, in which both crater densities and crater degradation are greater than in the light plains. Imbrium ejecta may, however, be present on the surface at the Apollo 16 site where excavated by craters from depth. Limited age data now available on the Apollo 16 samples are consistent with this interpretation. We conclude that rocks of Orientale provenance may be predominant on and near the surface at the Apollo 16 site. This hypothesis implies that the catastrophic Orientale impact struck a highland area underlain by highly feldspathic material and spread it over much of the Moon. Thus, much of the lunar highlands crust need not consist of anorthositic materials to any significant depth. These conclusions apply to the plains at the Apollo 16 site and most of the other Cayley-type plains, but we do not exclude the possibility that, moonwide, the plains may be polygenetic.

Before the Apollo 16 mission, the light-plains deposits at the Descartes site were interpreted on the basis of photogeologic criteria as most likely volcanic, possibly old mare-type basalt or more silicic lavas and (or) pyroclastic materials (Milton, 1968; Wilhelms and McCauley, 1971; Milton and Hodges, 1972; Trask and McCauley, 1972; Head and Goetz, 1972; Elston and others, 1972). Free-fall or ash-flow tuff was suggested to explain the apparent differential compaction observed in other areas where plains and adjacent mantle of the terra seemed to be composed of the same material (Howard and Masursky, 1968; Cummings, 1972). Because impact breccias predominate in the returned Apollo 16 samples (Lunar Sample Preliminary Examination Team (LSPET), 1973; Wilshire and others, 1973; Chao, 1973b), the origin of these plains deposits must be reexamined.

Widespread distribution of ejecta from lunar basins was recognized by Gilbert (1893), and Cayley-type plains were interpreted as Imbrium ejecta by R. E. Eggleton and C. H. Marshall (unpub. data, 1962). After the Apollo 16 mission, this hypothesis was resurrected (Eggleton and Schaber, 1972). The similarity of the plains to patches of ejecta around very small craters was noted by Head (1972), and widespread plains were described as part of the continuous ejecta from Orientale (Eggleton and Schaber, 1972; Hodges and others, 1973).

In order to determine the origin of the Cayley-type light plains, we reexamined their physical properties, distribution, and relative ages on Apollo orbital and Lunar Orbiter photographs. All plains similar to those at the Apollo 16 site were remapped on both near and far sides between 45° N. and 45° S. (fig. 1; D. E. Wilhelms, written commun., 1973). Soderblom and Boyce (1972) studied crater frequency distributions and relative ages of these light plains. Hodges (Hodges and others, 1972, 1973) examined the photogeologic data and field relationships at and near the Apollo 16 site and around Orientale. Chao (1973a, b) considered the lithology, petrography, chemistry, and radiometric ages of the Apollo 16 samples and compared these with data from the Imbrium basin ejecta obtained on the Apollo 14 mission. We have also considered the modes of transportation and deposition of ejecta required to account for the origin and distribution of light plains. Continuous hummocky ejecta blankets are readily attributed to their source basins, but ejecta beyond these continuous deposits have not been sufficiently examined heretofore. In any large lunar cratering event, there must be a range of ejection velocities between that of the continuous ejecta and that of particles that escape the Moon. If ejection angles are small and

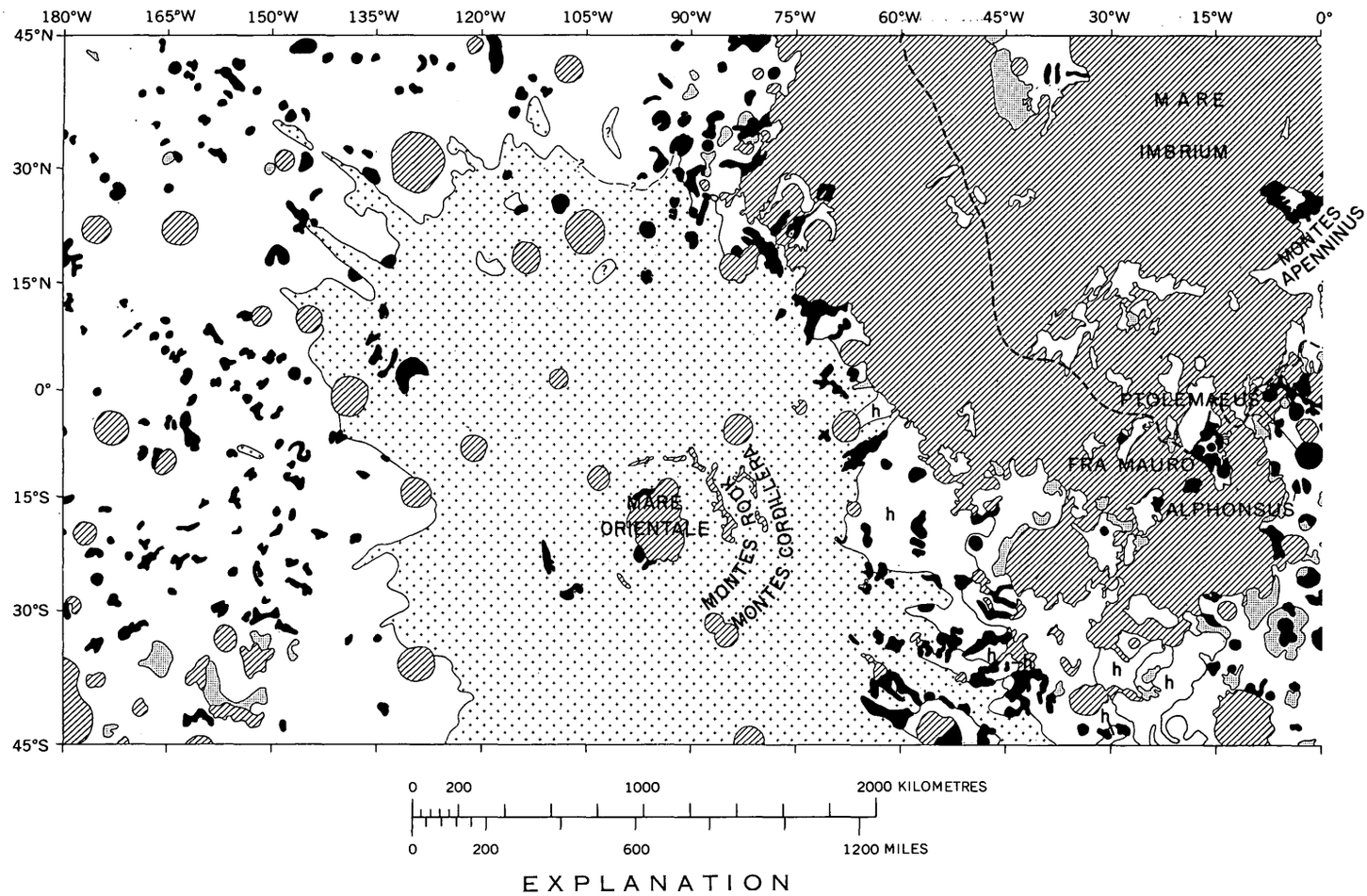

EXPLANATION

Light-colored plains deposits of Imbrian age (Cayley-type plains and other units). Near-planar deposits with lobate contacts and flow textures obviously part of Orientale basin ejecta are not included, nor are certain far-side deposits identified as old mare materials by presence of mare ridges.

Terra-mantling materials. Because of divergent conventions on source maps and uneven photographic coverage, this unit is mapped in more detail between 70° W. and 140° E. than elsewhere. Additional extensive deposits occur peripheral to Orientale deposits. In other areas, mantling materials are approximately proportional in abundance to Cayley-type plains deposits

Orientale deposits, including rugged rings of uplifted pre-basin rock, Hevelius Formation, plains and mantling materials obviously gradational with Hevelius Formation, and secondary impact craters

All materials (mostly mare and crater materials) younger than the Orientale and Cayley-type plains deposits. Craters Petavius and Humboldt may be older

All materials older than the Orientale and light-plains deposits. Certain enigmatic units near Orientale which are hilly and furrowed and hilly and pitted (h) are included but age relative to Orientale is uncertain

Approximate limit of Fra Mauro Formation

FIGURE 1.—Distribution of Cayley-type light-colored terra plains material, terra-mantling material, and previously mapped Orientale ejecta between 45° N. and 45° S. All convincingly identifiable patches of Cayley-type plains larger than 25 km are shown, as are mantle patches between 70° W. and 140° E. (see below). Patches of other units larger than 50 km are shown. Unmapped plains and mantle patches smaller than 25 km seem approximately proportional in number to mapped patches in any given area. Compiled by D. E. Wilhelms from the following sources: 70° W. to 70° E., Wilhelms and McCauley (1971); 70° E. to 140° E., Wilhelms and F. El-Baz (unpub. data, 1973); 140° E. to 140° W., D. E. Stuart-Alexander (unpub. data, 1973); 140° W. to 70° W., D. H. Scott, M. N. West, and J. F. McCauley (unpub. data, 1973). All areas previously mapped as plains were rechecked.

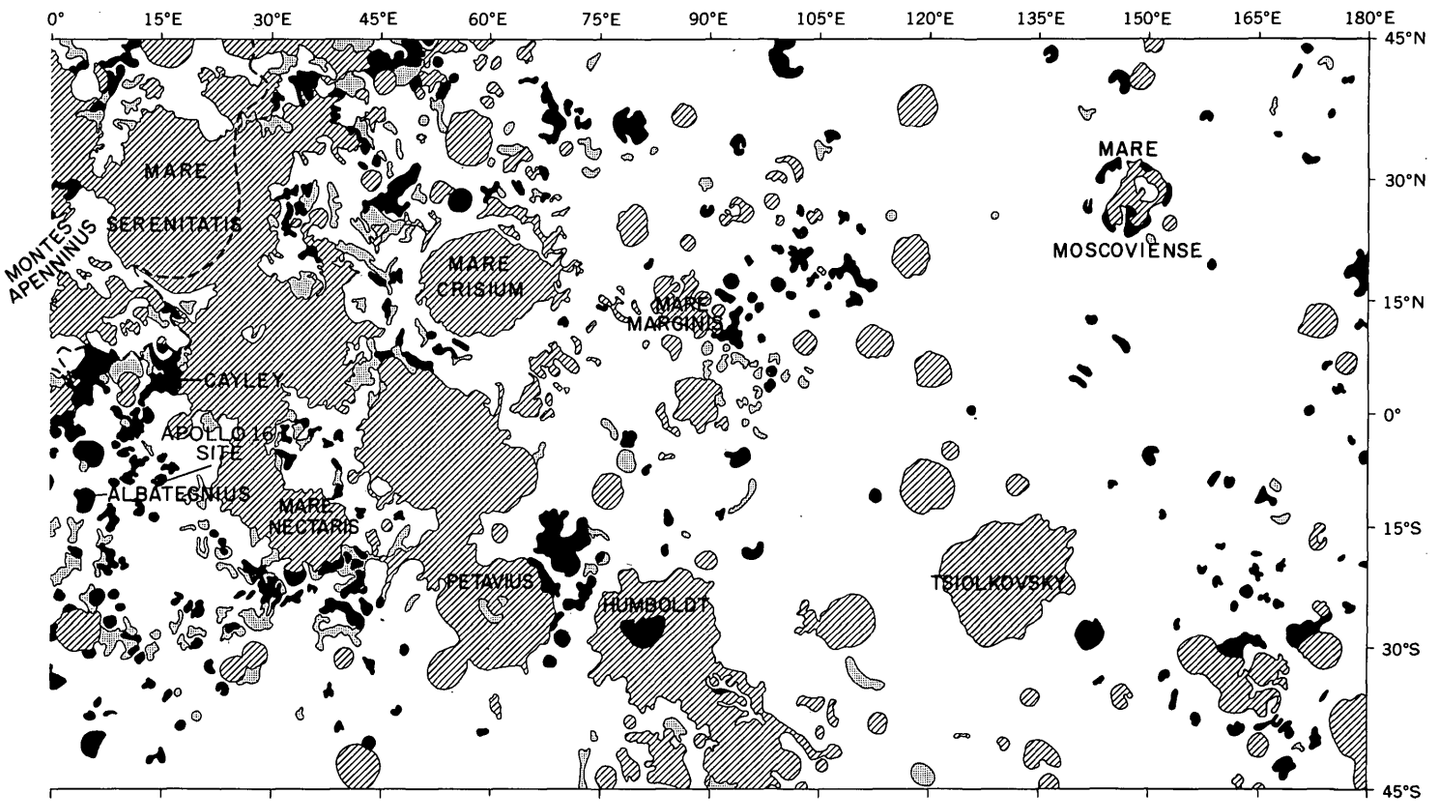

volume great, ejecta deposited at these velocities may be widespread enough to account for the light plains.

Our data and interpretations support the hypothesis that the surface and near-surface materials of some light plains, including those at the Apollo 16 site, are at least partly composed of ejecta from the Orientale basin and that the materials of many rugged areas, such as the Descartes highlands, are overlain by similar material.

Acknowledgments.—We are indebted to D. E. Wilhelms, who reexamined, rechecked, and remapped the lunar light-plains deposits of various areas, and to H. J. Moore and D. E. Wilhelms for their critical and constructive reviews of this manuscript. This study was conducted on behalf of the National Aeronautics and Space Administration under contract Nos. T-1167B (experiment S-222) and T-2357A.

RELATIVE AGE AND DISTRIBUTION OF CAYLEY-TYPE PLAINS

The Cayley Formation was defined as light-colored (intermediate albedo) terra plains deposits of Imbrian age in the central near side of the Moon (D. E. Wilhelms, unpub. data, 1965; Morris and Wilhelms, 1967; Wilhelms, 1970, p. F27–F28). The name was adopted for the plains at the Apollo 16 site (Milton, 1968; Milton and Hodges, 1972) because of similarity with plains at the type locality near the crater Cayley. In this paper, the term "Cayley-type" plains will be used in place of the formal Cayley Formation for units with the following characteristics: (1) Generally flat and smooth surfaces, as seen at telescopic resolution, (2) intermediate albedo between that of mare and that of very rugged uplands, (3) higher crater frequencies than those on mare material and less than those on the Fra Mauro Formation, (4) apparent lack of mare-type ridges, and (5) in some places, a population of large subdued craters that appears mantled. Light plains of other ages also occur but will not be considered further (Wilhelms and McCauley, 1971; Boyce and others, 1974).

Most Cayley-type plains occur in topographic lows, including circular craters and troughs concentric with multiringed basins. The deposits appear to transect structures and textures of the Fra Mauro Formation and Imbrium sculpture, as in the crater Ptolemaeus (fig. 2) and at the type area near the crater Cayley.

On telescopic and Lunar Orbiter photographs, many Cayley-type plains are similar in texture and albedo to adjacent terra. Some of these terra units have been mapped as thick mantling members of the Cayley Formation or as terra material of Imbrian age (1:1,000,000-scale maps of the U.S. Geological Survey's Geologic Atlas of the Moon; Wilhelms, 1970, p. F28). These units have about the same areal distribution as Cayley-type plains (fig. 1) and are especially abundant

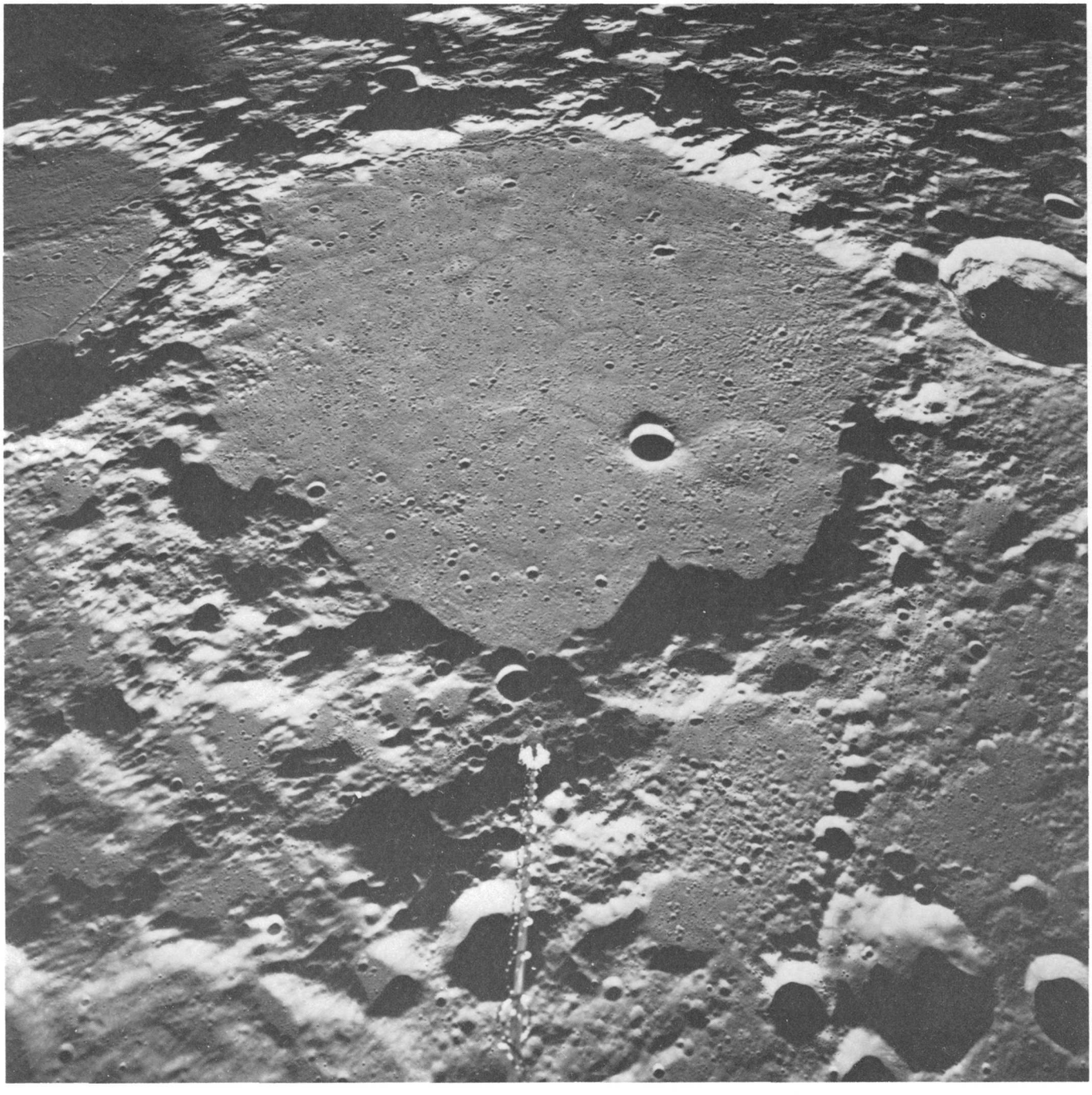

FIGURE 2.—Crater Ptolemaeus, 150 km in diameter (Apollo 16 orbital oblique photograph, A16–05781). Mare Imbrium is to the north on the right. Cayley-type plains deposits occupy crater floor. In this low-sun photography, topography mantled by the Cayley is clearly evident; continuations of lineaments on the unburied adjacent highlands are visible. These lineaments are part of the Imbrium basin radial system (Imbrium sculpture) and presumably formed when the basin formed. Cayley-type material probably also mantles the more rugged looking rim of Ptolemaeus as well as small crater depressions within the rim (lower left and lower central part of the rim area).

near Orientale (though not distinguished there in fig. 1). The terra units have been interpreted as contemporaneous with or somewhat older than the Cayley-type plains; that is, the "pools" of plains may represent either concentrations of a single widespread deposit or unrelated material that filled preexisting depressions. On the best Lunar Orbiter and Apollo high-resolution photographs, contacts between these

terra and plains units appear gradational, supporting the first interpretation. Most Cayley-type surfaces appear rolling and undulating (Wilhelms, 1972). The surficial materials of Cayley-type plains and adjacent terra may have a common origin as parts of a widespread blanketing material. Because the "blanket" is relatively thin, the underlying topography related to preexisting units and events can still be detected.

By means of a technique of crater morphology analysis, relative ages of light-plains deposits in many areas (including Ptolemaeus, fig. 2) on both near and far sides were obtained (Soderblom and Boyce, 1972; Boyce and others, 1974). The results are presented in terms of D_L, defined as the diameter of a crater which would be eroded to an arbitrary small slope (1°) under the impact flux that has accumulated on the surface in question (Soderblom and Lebofsky, 1972). The areas of Cayley-type deposits measured show a strikingly narrow range of ages (D_L, 500–600 m), indistinguishable within the limitations of the method. Measurements of D_L for the Fra Mauro Formation are greater than about 1,000 m. More recent work by Boyce, Dial, and Soderblom (1974) confirmed previous results showing that, in all localities measured, a distinct and consistent gap exists between D_L values for the Cayley-type plains and D_L for the Fra Mauro Formation and older plains contemporaneous with it (fig. 3).

The frequency distribution of craters per unit area also shows that Cayley-type plains are contemporaneous with one another and with the Hevelius Formation (McCauley, 1967) which comprises the continuous ejecta from the Orientale basin. Soderblom and Boyce (1972) and Boyce, Dial, and Soderblom (1974) measured the frequency distribution of craters larger than 500 m in diameter in Cayley-type plains. (Craters of this size were used because smaller craters might have reached a steady-state distribution.) A comparison of the crater-frequency distribution on the Hevelius Formation with that on the Cayley-type plains at different sites is shown in figure 4; frequency distributions of fresh craters larger than 500 m in diameter are indistinguishable between the Hevelius Formation and Cayley-type plains, within the error of measurement, indicating approximate contemporaneity of the two units. The distributions are also

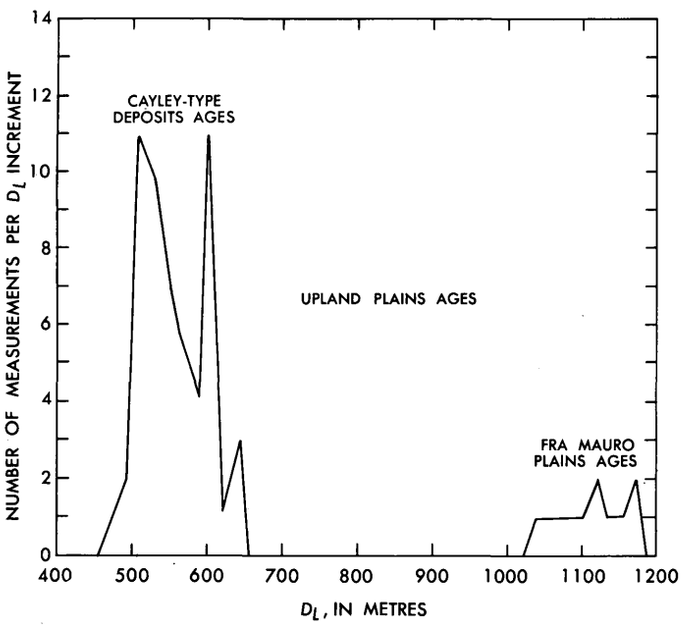

FIGURE 3.—Histogram of 90 relative ages (D_L, diameter of a crater eroded to 1°) determined for upland light-plains units moonwide. Note that there are two distinct age groups.

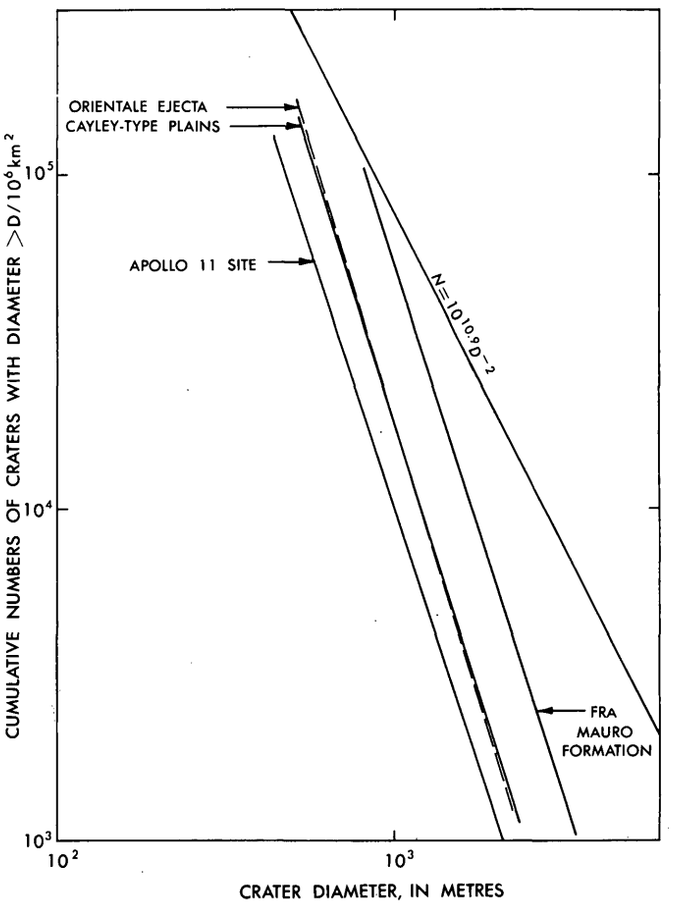

FIGURE 4.—Cumulative diameter frequency of craters on the Fra Mauro Formation (Swann and others, 1971; Soderblom and Boyce, 1972), Orientale ejecta (Ulrich, 1968; Boyce and others, 1974). Cayley-type plain (Soderblom and Boyce, 1972; Boyce and others, 1974; Grudewicz, 1974) and the Apollo 11 site (Morris and Shoemaker, 1968). The Apollo 11 curve and the steady-state curve of Trask (1966) are included for comparison. Note that the crater densities of the Cayley-type plains and the Orientale ejecta are similar and that they are both very different from the crater densities of the Fra Mauro Formation and of the mare at the Apollo 11 site.

equivalent to those older than mare basin materials within the Orientale basin (Ulrich, 1968).

Furthermore, craters larger than 8 km in diameter are less degraded and therefore younger on Cayley-type plains than on the Fra Mauro Formation but are identical morphologically with those on the Hevelius Formation, thus substantiating the correlative ages of the plains and Orientale (T. W. Offield, written commun., 1973) by yet a third method (Pohn and Offield, 1970; Offield and Pohn, 1970).

Cayley-type plains and terra that appear mantled are widespread over the entire lunar surface (fig. 1), but they are particularly abundant in belts peripheral to both the Imbrium and Orientale basins. Plains are concentrated adjacent to the Fra Mauro Formation (fig. 5) in the central near side (Eggleton and Schaber, 1972) and also occur in large patches north of the Imbrium basin (B. K. Lucchitta, unpub. data, 1974). The ages of all the latter northern plains have not been determined because of inadequate photographic coverage, but two localities have a relative age equivalent to that of the Fra Mauro Formation, older than Cayley-type plains (Boyce and others, 1974). Plains peripheral to the Hevelius Formation are abundant and are clearly identified as deposits of ejecta from the Orientale basin (Eggleton and Schaber, 1972, figs. 29-9–29-10; Moore and others, 1974). Cayley-type plains and the gradational terra unit are also concentrated inside and just outside the main ring of the Nectaris basin (including the occurrence at the Apollo 16 site).

The distribution pattern is incomplete because it is disrupted by younger mare basalts and crater ejecta, but it suggests that plains and mantled terra units are related genetically to multiringed basins (Eggleton and Schaber, 1972). Those Cayley-type plains peripheral to the Hevelius Formation include channels and lobes radial to Orientale, indicating that plains are formed by materials that are related and associated with the lineated Orientale ejecta (Eggleton and Schaber, 1972, fig. 29-10). Cayley-type plains peripheral to Imbrium are probably formed in part by similar ejecta from Imbrium that accumulated in the circum-Imbrium depressions and smoothed out irregularities. However, because the surface of these plains in the central near side is younger than the Fra Mauro Formation (Soderblom and Boyce, 1972), a post-Imbrium source or event is required to account for that surface.

THICKNESS OF PLAINS DEPOSITS

Cayley-type plains commonly overlie older but recognizable cratered surfaces, suggesting that a particular part of the plains may have had a complex history. Where plains deposits occupy the floor of an impact crater, estimates of thickness may be made by using the crater depth-diameter equations of Pike (1968, 1972). In Ptolemaeus, the apparent thickness of postcrater fill is 2 to 3 km; the central peak, if present, is entirely buried. Evidence suggests that this accumulation is composed of ejecta from at least three source craters or basins: Orientale, Imbrium, and Alphonsus. The pre-Imbrium crater Alphonsus overlaps Ptolemaeus; thus, its ejecta must be part of the earliest filling material. A population of large craters that appear mantled is visible in Ptolemaeus; the largest of these are probably secondary craters from Imbrium. A linear trough parallel to Imbrium sculpture is also discernible at low sun angle (fig. 2). Part of the filling deposit, therefore, is probably ejecta from the Imbrium basin. The range of ejecta from Imbrium is equivalent to that from Orientale in which a planar facies of ejecta occurs, intermingled with secondary craters (Moore and others, 1974); an analogous facies of planar ejecta from Imbrium is therefore postulated in this central highlands area peripheral to Fra Mauro Formation. The subdued large craters and sculpture suggest that a mantle of still younger material was emplaced.

In Albategnius, an adjacent large crater also containing Cayley-type plains, some mantled craters are subdued and rimless but well defined, permitting an estimate of thickness of overlying material. On the basis of an original rim height of a buried crater 4.5 km in diameter (Pike, 1972), this thickness is approximately 200 m. Mantled topography is also present, though not as conspicuous, in the vicinity of the Apollo 16 site (Eggleton and Schaber, 1972). Additionally, evidence of stratigraphic layering in Apollo 16 orbital and ground-based photographs of North Ray and South Ray craters (Ulrich, 1973; Apollo Field Geology Investigation Team (AFGIT), 1973), further supports the postulate of sequential deposits.

As shown by the crater-erosion model and the crater-frequency distributions in Ptolemaeus and Albategnius (fig. 4), the so-called crater-age clock of the surface has been reset. This modification can occur as a result of deposition, erosion, or both. An influx of material (such as crater ejecta) may be deposited on the surface, gradually building up a discrete layer, or material may impact the surface in amounts sufficient to erode—and thus subdue—the preexisting topography (Boyce and others, 1974). Where the influx of material occurs, the maximum size of craters obliterated is dependent mainly on the thickness of the subsequent deposit. Where material impacts the surface, a surficial deposit forms which progressively fills in craters and subdues

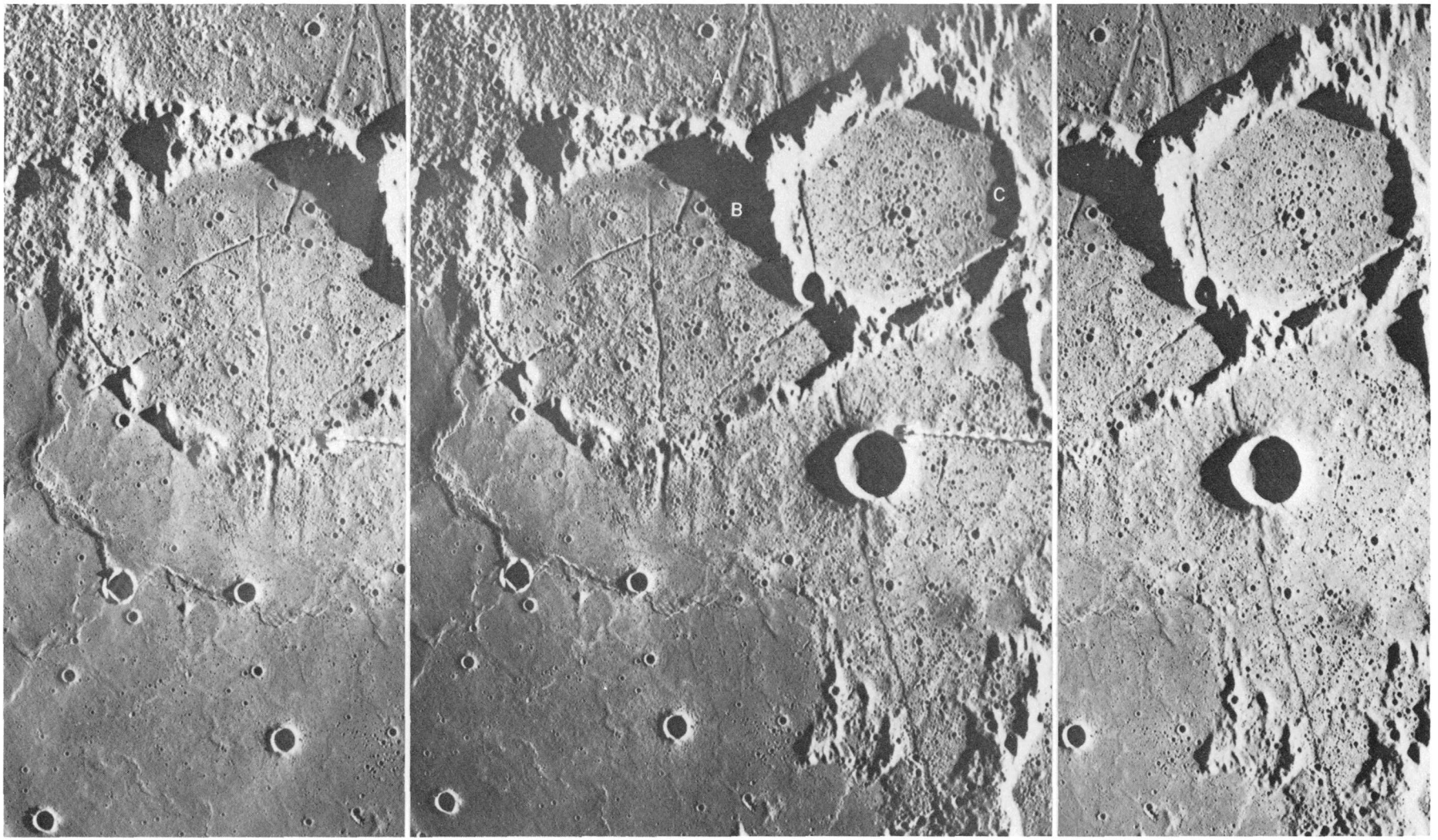

FIGURE 5.—Cayley-type plains south of the Apollo 14 Fra Mauro landing site. Large craters are Fra Mauro (A), Bonpland (B), and Parry (C). Rough terrain at upper left is distal part of Fra Mauro Formation. Elsewhere, the Cayley-type plains deposits partly bury the Fra Mauro, thinly in Bonpland, more thickly in Parry where little Imbrium radial structure is evident. Mantled lobate Fra Mauro materials, however, occur just south of the rim of Bonpland. Mantled ejecta in Bonpland is thicker and is filled by the material of the mantle to higher altitudes in the southern part than in the northern part. The Cayley is in turn buried by mare material. Note that the topographic features seen through the mantling materials are related to Imbrium but the crater density is Cayley. Stereophotograph from Apollo 16 metric photographs 1980, 1981, and 1982.

their rims, so that, depending on the flux distribution of material, craters smaller than a given size range are obliterated and those larger are subdued. In either circumstance, a substantial influx of debris is required, and the apparent contemporaneity of Cayley-type plains implies a common source and (or) process of deposition. The additional evidence of synchroneity with Orientale compels investigation of that basin as a potential source of surficial plains materials. We consider that the Cayley-type plains formed mainly as a depositional unit which effectively reset the preexisting crater-age clock.

DATA FROM RETURNED SAMPLES

Large impact basins probably have distributed a wide range of rock types as ejecta over much of the Moon because of the great vertical and lateral extent of the rocks excavated. The same process also appears to be the only one that can distribute a blanket of ejecta of relatively homogeneous composition widely over the lunar surface. The distinct highly feldspathic composition of the Apollo 16 returned samples and their radiometric ages suggest derivation of these rocks from such a source basin. The highly feldspathic rock suite probably contributes to and accounts for the albedo that is characteristic of the light plains. The sample data are discussed below in support of the hypothesis that a significant amount of ejecta from Orientale reached the Apollo 16 site and may be present to some extent at the Apollo 14 site as well.

Apollo 16 samples

The Apollo 16 samples are distinctly more feldspathic than those from other highlands sites. Breccias, hornfels, and crystalline rocks are all unusually high in alumina. Studies of coarse fines from 12 samples (Chao and J. A. Minkin, unpub. data, 1973) show that in addition to the white anorthositic rocks, among the light-gray to black lithic types, three types predominate: (1) Dark-gray to black olivine-plagioclase xenocryst-laden crystalline rock, (2) feldspathic micronoritic hornfels, and (3) plagioclase-dominant xenocryst-laden partly devitrified glass. Compared with coarse fines of the Apollo 14 Fra Mauro site, the Descartes samples are distinctly richer in CaO and Al_2O_3, MgO being dominant over FeO if the total mafic oxides are more than 10 weight percent. They are lower in FeO, TiO_2, K_2O, and P_2O_5. Although low-Al_2O_3 and high-K_2O breccias such as 60315 and 62235 are included in hand specimens from Apollo 16, they are rare among the coarse fines we have studied. The porous feldspathic breccias of Apollo 14, as represented by 14063, contain light-gray micronorite hornfels fragments (Chao and others, 1972) which are characterized by K-rich mesostasis, whereas fragments with K-rich mesostasis are exceedingly rare in Apollo 16 feldspathic breccias. Hence, both light-gray and dark lithic fragments which characterize the Apollo 16 breccias are different from those of the Apollo 14 Fra Mauro materials.

Because regolith is derived from underlying materials, its bulk chemical composition should essentially reflect that of the underlying deposit. Table 1 shows representative chemical analyses of regolith compositions at Apollo 14, 15, and 16 sites. The Apollo 14 Fra Mauro and the Apollo 15 Apennine Front materials are similarly low in Al_2O_3 (16–18 weight percent) and CaO (10–12 wt percent), whereas the Apollo 16 regolith is very high in Al_2O_3 (about 28 wt percent) and CaO (about 16 wt percent) and lower in FeO, MgO, K_2O, P_2O_5, and TiO_2 than the Apollo 14 and 15 ma-

TABLE 1.—*Chemical composition, in weight percent, of selected Apollo 14, 15, and 16 materials*
[N.d., not determined]

	Apollo 14			Apollo 15		Apollo 16	
	Fra Mauro material[1]						
	Annealed breccia 14303,34	Regolith microbreccia 14047,27	Fines[1] 14259,12	Regolith microbreccia[2] 15265	Fines[3] 15091,38	Regolith microbreccia[4] 61295,5	Fines[4] 61220,2
SiO_2	47.49	47.45	48.16	46.94	46.47	45.19	45.35
TiO_2	1.98	1.48	1.73	1.40	1.31	0.56	0.49
Al_2O_3	16.05	17.75	17.60	16.71	17.47	28.29	28.25
FeO	10.96	10.36	10.41	11.18	11.57	4.52	4.55
MgO	10.99	9.35	9.26	9.95	10.50	4.72	5.02
CaO	10.03	11.19	11.25	11.19	11.77	16.16	16.21
Na_2O	.87	.75	.61	.51	.41	.45	.42
K_2O	.46	.49	.51	.25	.18	.09	.09
P_2O_5	.56	.39	.53	.25	.16	.10	.10
MnO	.15	.13	.14	.15	.17	.06	.06
Cr_2O_3	.21	.22	.26	.33	.24	N.d.	N.d.
S	N.d.	N.d.	N.d.	.08	N.d.	.06	.06
Total	99.75	99.56	100.46	98.94	100.25	100.20	100.60

[1] Chao, Minkin, and Best (1972). [2] LSPET (1972). [3] Carron, Annell, Christian, Cuttitta, Dwornik, Ligon, and Rose (1972). [4] LSPET (1973).

terials. This distinction is pronounced and suggests that the highly feldspathic Apollo 16 materials did not come from the same local geochemical regime as the Fra Mauro or Apennine Front samples.

Unfortunately, a comparison of the distributions of the Cayley-type materials with the distribution of high-Al_2O_3 materials recorded by remote X-ray fluorescence measurements is impossible because of the large area of the cells sampled by the X-ray mapping (Adler and others, 1972a,b).

Contamination of Apollo 14 site by highly feldspathic material

If Orientale ejecta is as widespread as suggested here, some fraction of it certainly would be expected to occur at the Apollo 14 site, overlying the Fra Mauro breccias. To determine the possible influx of Cayley-type material at the Apollo 14 site, we compared the bulk composition of the fines and regolith breccias with that of the Fra Mauro breccias as classified by Chao (1973b). The typical Fra Mauro breccias are characterized by a high KREEP (potassium, rare-earth elements, phosphorus) component (Rose and others, 1972; Willis and others, 1972; Scoon, 1972; Taylor and others, 1972; Philpotts and others, 1972; and Strasheim and others, 1972). Inasmuch as the Apollo 16 Cayley-type materials are highly feldspathic and poor in KREEP, their contamination of the Apollo 14 regolith materials should cause an increase in Al_2O_3 and CaO and a decrease in K_2O or P_2O_5 as compared with the Fra Mauro materials. Table 2 lists the calculated amounts of the Apollo 16 type of fines which would be required to raise the Al_2O_3 content of 14303 to that of the Apollo 14 regolith. An estimated 14 to 17 weight percent of material similar in composition to Apollo 16 fines 61220 or 66081, respectively, is required. Feldspathic breccias such as 14063 also are present in the Fra Mauro Formation. To account for the higher Al_2O_3 content in the regolith, 27 percent of 14063 would be required (table 2). This amount appears to be much too high, judging from its scarcity in the boulders near Cone crater. Minor-element data are inadequate to make a meaningful comparison between the Apollo 14 regolith and the Fra Mauro breccias with respect to influx of the Cayley-type material.

The above data suggest contamination by a thin but chemically distinct deposit of Cayley-type materials at the Apollo 14 site; these materials may have been derived from Orientale. Such identification of a source basin according to chemical data is subject to uncertainty because the target material and the ejecta of even a single basin may be vertically and laterally variable. Nevertheless, the distinctions cited are suggestive of unrelated source areas.

Radiometric ages

The youngest possible age of a large impact event may be preserved in shocked ejecta samples, but at the Apollo 16 site the breccias have highly complex histories. In order to interpret the radiometric age of a rock it is essential to know (1) the ultimate source of the rock, (2) effects of subsequent thermal or shock metamorphism, and (3) degree of annealing, if any.

Dates from Apollo 14 Fra Mauro materials interpreted as Imbrium ejecta indicate the age of the Imbrium event to be about 3.9 b.y. (Chao, 1973a). The maximum age of Cayley-type material must be the youngest crystallization or metamorphic age of fragments in Apollo 16 breccias, provided that they have not been reset by post-Cayley craters. The minimum age must be that of the oldest known mare basalt; on the basis of the crater-erosion model (Soderblom and Lebofsky, 1972), relative ages of maria are everywhere younger than Cayley-type plains and Orientale ejecta.

TABLE 2.—*Chemical composition, in weight percent, of Apollo 14 Fra Mauro material, Apollo 14 and 16 fines, and mixtures of Apollo 14 Fra Mauro material and Apollo 16 fines*

[N.a., not available]

	Apollo 14 Fra Mauro material[1]			Apollo 14 fines[1]	Apollo 16 fines[2]		Mixtures (percentages given in parentheses)		
	Annealed breccia 14303,34	Feldspathic breccia 14063,46	Regolith microbreccia 14047,27	14259,12	66081,2	61220,2	14303,34(73) 14063,46(27)	14303,34(83) 66081,2(17)	14303,34(86) 661220,2(14)
SiO_2	47.49	44.69	47.45	48.16	45.38	45.35	46.73	47.13	47.19
TiO_2	1.98	1.48	1.48	1.73	.67	.49	1.84	1.76	1.77
Al_2O_3	16,05	22.31	17.75	17.60	26.22	28.25	17.75	17.75	17.75
FeO	10.96	6.71	10.36	10.41	5.85	4.55	9.80	10.11	10.06
MgO	10.99	10.80	9.35	9.26	6.39	5.02	10.93	10.22	10.15
CaO	10.03	12.70	11.19	11.25	15.28	16.21	10.75	10.90	10.90
Na_2O	.87	.76	.75	.61	.39	.42	.84	.78	.81
K_2O	.46	.15	.49	.51	.13	.09	.38	.40	.41
P_2O_5	.56	.22	.39	.53	.13	.10	.46	.49	.49
MnO	.15	.08	.13	.14	.08	.06	.13	.13	.14
Cr_2O_3	.21	.21	.22	.26	N.a.	N.a.	N.a.	N.a.	N.a.
Total	99.75	100.11	99.56	100.46	100.52	100.54	99.61	99.67	99.67

[1] Analysts: H. J. Rose and others, U.S. Geological Survey (Chao and others, 1972). [2] LSPET (1973).

Several Apollo 16 samples have been dated by either argon-40–argon-39 or rubidium-strontium methods; the youngest of these is 68415, a feldspathic basalt. The rubidium-strontium crystallization age of this rock is 3.84±0.01 b.y. (Papanastassiou and Wasserburg, 1972a). Ages of other samples range from 3.90 to 4.24 b.y. (Papanastassiou and Wasserburg, 1972b; Tera and others, 1973; Albee and others, 1973; Husain and Schaeffer, 1973). Sample 68415 was collected at station 8 from a mappable ray of South Ray crater, about 5.5 crater diameters away. At this distance, 68415 probably was derived from relatively shallow depth within the crater (Chao, 1973b). Its bulk composition (LSPET, 1973) is nearly identical with the representative Apollo 16 fines. Hence, 68415 is likely from the Cayley-type materials, and 3.84 b.y. may approximate the maximum age of the uppermost plains unit.

The oldest mare basalt ages so far determined are those of some Apollo 17 basalts from Taurus-Littrow. Rubidium-strontium ages reported for basalt 77035 are 3.83±0.1 b.y. (B. W. Chappell and others, oral commun., 4th Lunar Sci. Conf., Houston, Tex., 1973) and 3.82±0.06 b.y. (Evensen and others, 1973). The rubidium-strontium age of basalt 75055 is 3.83±0.12 b.y. (M. Tatsumoto and others, oral commun., 4th Lunar Sci. Conf., Houston, Tex., 1973), and the argon-40–argon-39 age of 75055 is 3.78±0.04 b.y. (Huneke and others, 1973).

Because the Cayley-type plains are contemporaneous with the Orientale basin, the age data indicate that the Orientale basin probably formed between 3.84 and 3.83 b.y. The means of deriving the plains materials from the Orientale basin is discussed below.

TRANSPORTATION, DEPOSITION, AND VOLUME OF ORIENTALE EJECTA

We have cited evidence indicating that the uppermost materials of Cayley-type plains and mantle deposits shown in figure 1 may be composed chiefly of Orientale ejecta. The topographic expression and distribution of these units can be accounted for by appropriate transport and deposition mechanisms. Figure 6 shows ranges of transport of ballistic ejecta, expressed in terms of the subtended angle on the lunar sphere (θ) plotted as a function of ejection angle γ_i and velocity (V_i). The Apollo 16 Descartes site is approximately 99° (3,000 km) from the Cordilleran rim of Orientale and 114° (3,450 km) from the basin center. Ejecta from Orientale can reach the Apollo 16 site and beyond at velocities of 1.6 to 2.3 km/s when ejection angles are 60° and less. Ejecta from lunar craters clearly have been deposited at distances greater than 3,000 km, as illustrated by the crater Tycho whose rays extend

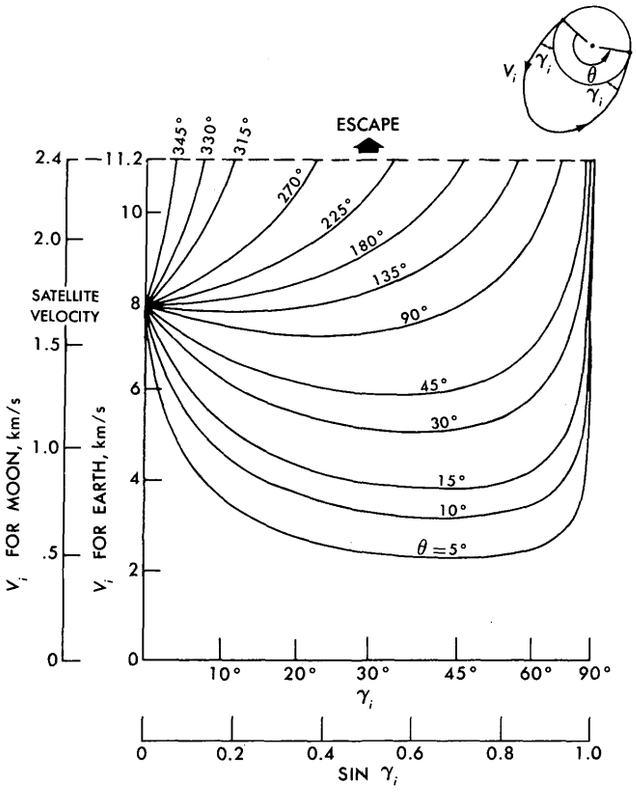

FIGURE 6.—Diagram showing the launch range in terms of the subtended angle θ (upper right corner) as related to launch velocity V_i and to the launch angle γ_i (D. R. Chapman, written commun., 1973).

more than 3,000 km (Baldwin, 1963). The ejecta ballistics model of Shoemaker (1962) would disperse ejecta from Copernicus some 5,500 km, or half the circumference of the Moon.

The plausibility of this hypothesis depends on widespread distribution of substantial quantities of Orientale ejecta. Estimates of the amount of ejecta from Orientale depend on a number of assumptions. Volumes of approximately 0.26 to 0.91 million cubic kilometres have been calculated using an empirical relationship between crater-radius and ejecta-thickness distribution in which basin radii of 195 and 310 km were assumed for Orientale (McGetchin and others, 1973). A geometric model of a basin using a spherical segment 390 km across and a depth-diameter ratio of 0.05 yields volumes of 0.61 to 1.82 million cubic kilometres depending on assumed slump conditions (Short and Forman, 1972). Much larger estimates of ejecta volumes from lunar basins also have been made. Dimensions cited by Dence, Grieve, and Plant (1974) for Imbrium, based on models for terrestrial impact craters, yield a volume of about 50 million cubic kilometres. This volume scaled down to Orientale, two-

thirds as large as Imbrium in diameter, is about 15 million cubic kilometres. Kaula and others (1974) obtained a difference in crustal thickness of 43 km between terra and mare near Serenitatis and Smythii and estimated the volume of a 300-km radius basin to be about 12 million cubic kilometres.

We estimate the volume of ejecta of Orientale to be about 8 million cubic kilometres. This estimate, probably as reasonable as any, assumes the basin to be a spherical segment (Short and Forman, 1972) 750 km across and 37.5 km deep (a depth-diameter ratio of 0.05). The depth of the present basin is about 6 to 8 km, but bulking of the brecciated floor materials, major isostatic adjustment, and subsequent flooding by mare materials have reduced the original depth. Selection of a diameter of 750 km is based on the following considerations. The innermost 400-km diameter ring of Orientale closely resembles the inner ring of the small double-ring basin Schrödinger (300-km outer-ring diameter) which appears to be intermediate between large craters with incipient rings of central peak blocks (for example, Humboldt) and the multiringed basins. This hummocky "peak ring" (Hartmann and Wood, 1971)—much lower topographically than the prominent outer rim—probably represents a transition from central peak to uplifted ring. Unlike the Cordilleran ring, the inner ring at Orientale shows no indication of superposed ejecta. The inner ring, therefore, probably formed in much the same manner as a central peak, uplifted from below (as implied by Baldwin, 1969, 1972). The continuity of the intermediate Rook ring, its circularity, and the regularity of its spacing from the Cordilleran scarp suggest that it too may have formed as a peak ring inside the transient cavity. The Cordillera of Orientale is equivalent to the third and most prominent ring of the Imbrium basin; these outermost rings are demonstrably equivalent to the rims of smaller craters (Moore and others, 1974). Some slumping from the Cordilleran scarp has undoubtedly occurred, just as smaller craters enlarge by formation of wall terraces. The transient basin cavity probably had a diameter somewhere between the Rook and Cordilleran rings; for convenience, we have used the approximate intermediate diameter of 750 km in our calculations.

Quantitative distributions of ejecta from lunar craters as a function of distance from the crater are poorly understood, and many models are possible (McGetchin and others, 1973). In lieu of a demonstrably valid model, about 10 to 20 percent of the total volume of Orientale ejecta is considered a reasonably conservative estimate of that fraction distributed beyond the continuous ejecta blanket (David Roddy, oral commun., 1973). Assuming that this fraction is dispersed evenly over the lunar surface (38 million square kilometres), a deposit 20 to 40 m thick would be produced. In reality, ejecta are concentrated along rays and lobes, so that actual thicknesses might range from zero to considerably greater than 20 to 40 m. Accordingly, thick deposits of Orientale ejecta are possible in Cayley-type plains and terra mantle units; 200 m or so of fill within Ptolemaeus and Albategnius is possible, and a significant deposit of Orientale ejecta can occur at Apollo 16. Locally, amounts may be very small, as at the Apollo 14 site.

The proposal that lunar light plains result solely from secondary impact debris (Oberbeck and others, 1974) is unlikely for the following reasons: (1) Young craters such as Theophilus and King (Howard, 1972) have smooth plains as ejecta facies, (2) Cayley-type plains near Orientale basin are clearly a facies of Orientale ejecta (Moore and others, 1974), (3) the relative ages of all terra light plains investigated fall into two distinct categories, corresponding to the Orientale and Imbrium events, and (4) ages of Apollo 16 samples are post-Imbrium, not pre-Imbrium like those of the surrounding terrain. Furthermore, moon-wide dispersal of ejecta from multiringed basins is theoretically probable. The impact of secondary projectiles undoubtedly caused some mixing of preexisting materials with the Cayley-type plains deposits, but the extent of mixing by metre-sized secondary ejecta fragments and by a blanket of ejecta are not likely to be significant (Chao, 1974).

GEOLOGIC IMPLICATIONS

The recognition of widespread ejecta from the youngest basin has important geologic implications: (1) It explains the origin and distribution of the Cayley-type plains deposits, (2) it accounts for the gradational relation between lunar light plains and mantle deposits, (3) it imposes geologic constraints on interpretations of orbital remote-sensing data, and (4) it constrains interpretations of the major highlands stratigraphic units.

If the Cayley-type plains and the closely associated mantle deposits (fig. 1) are Orientale ejecta, and if the Descartes highlands are older than the surficial plains deposits, then the Descartes materials at the Apollo 16 site must also be mantled by Cayley-type materials; the similarities among the returned samples (H. G. Wilshire, written commun., 1974) suggest this relation. Such a mantle probably prevented sampling of bedrock at Stone Mountain, so that Descartes rocks may have been returned only if North Ray crater penetrated them (Hodges and others, 1973).

We do not extrapolate our interpretation to all lunar light plains. Some of the patches east of Mare Marginis and Smythii have ridges that could be of the mare type; therefore, these may be old basalts. Other light plains, too small to map in figure 1, are locally derived impact ejecta from craters and basins, and larger patches may be also. For example, the plains and mantles in the floors of the craters Petavius and Humboldt cannot be ejecta from Orientale or any other basin if these craters are indeed younger than Orientale.

Proof of this hypothesis for the origin of the lunar light plains deposits is not conclusive, but it does account for much observational data. Chemical characteristics alone do not negate the possible Imbrium origin of some samples. The effect of secondary cratering at the Apollo 16 site, although present, does not preclude deposition of significant amounts of primary ejecta from both Imbrium and Orientale to form discrete deposits. The radiometric age data are consistent with the photogeologic evidence that the Cayley materials are younger than the Imbrium materials. However, ejecta from the Imbrium basin may be at the surface at the Apollo 16 site in ejecta of post-Cayley craters. Proximity to the Nectaris basin suggests that Nectaris ejecta is also present at depth (Hodges and others, 1972) and therefore could have been sampled, for example, by the North Ray Crater. Hence, the much younger North Ray Crater ejecta that overlie typical Cayley-type materials may contain "local" materials such as the older Imbrium or Nectaris ejecta.

SUMMARY

Evidence for a depositional, basin-related origin of the Cayley-type plains is as follows: (1) Localization and concentration peripheral to the lineated and hummocky ejecta of the large multiringed basins and (2) existence of a planar facies of continuous ejecta at Orientale and in the ejecta blankets of small craters. A direct relation of Cayley-type plains to Orientale is demonstrated by the equivalent crater-frequency and crater-erosion model ages. These plains are distinctly younger than the Fra Mauro Formation and remnant plains of Imbrium age. Therefore, although Cayley-type plains are common peripheral to the Fra Mauro Formation, the age of the surfaces requires deposition of younger material on probably planar ejecta from Imbrium. Furthermore, the Apollo 16 samples are distinctly different from those of Apollo 14.

According to this hypothesis, basin-forming impacts, exemplified by Orientale, produced ejecta which were distributed irregularly over the surface of the Moon, forming discontinuous deposits from zero to several tens of metres thick. Some contamination of plains deposits by preexisting local material probably occurred, but primary ejecta are dominant. Preexisting topography is observable in many places, and most Cayley-type plains are probably underlain by a planar facies of Imbrium ejecta, which—at least at the Apollo 16 site—overlies Nectaris ejecta. Cayley-type plains deposits include Orientale ejecta sufficiently thick to reset the crater-age clock. The composition of the plains samples implies that Orientale was formed in a highly feldspathic terrane, resulting in a widespread blanket of feldspathic breccias over much of the Moon. The lunar highland crust, therefore, may not be underlain by a continuous layer of anorthosite cumulate to any significant depth. The Orientale event probably occurred some time between 3.84 and 3.83 b.y.

We do not exclude the possibility that some Cayley-type plains may have a different origin.

REFERENCES CITED

Adler, Isidore, Trombka, J., Gerard, J., Lowman, P., Schmadebeck, R., Blodget, H., Eller, E., Yin, L., Lamothe, R., Gorenstein, P., and Bjorkholm, P., 1972a, Apollo 15 geochemical X-ray fluorescence experiment—Preliminary report: Science, v. 175, no. 4020, p. 436–440.

Adler, Isidore, Trombka, J., Gerard, J., Lowman, P., Schmadebeck, R., Blodget, H., Eller, E., Yin, L., Lamothe, R., Osswald, G., Gorenstein, P., Bjorkholm, P., Gursky, H., and Harris, B., 1972b, Apollo 16 geochemical X-ray fluorescence experiment—Preliminary report: Science, v. 177, no. 4045, p. 256–259.

Albee, A. L., Gancarz, A. J., and Chodos, A. A., 1973, Sanidinite facies metamorphism of Apollo 16 sample 65015 [abs.], *in* Lunar Science IV, Abstracts: Houston, Tex., Lunar Sci. Inst., p. 24–26.

Apollo Field Geology Investigation Team (AFGIT), 1973, Apollo 16 exploration of Descartes—A geologic summary: Science, v. 179, p. 62–69.

Baldwin, R. B., 1963, The measure of the moon: Chicago, Univ. Chicago Press, 488 p.

——— 1969, Ancient giant craters and the age of the lunar surface: Astron. Jour., v. 74, 570–571.

——— 1972, The tsunami model of the origin of ring structures concentric with large lunar craters: Physics Earth and Planetary Interiors, v. 6, p. 237–339.

Boyce, J. M., Dial, A. L., and Soderblom, L. A., 1974, Ages of the lunar near side light plains and maria, *in* Lunar Sci. Conf., 5th, Proc.: Geochim. Cosmochim. Acta, Supp. 5, v. 1, p. 11–23.

Carron, M. K., Annell, C. S., Christian, R. P., Cuttitta, Frank, Dwornik, E. J., Ligon, D. T., Jr., and Rose, H. J., Jr., 1972, Elemental analyses of lunar soil samples from Apollo 15 mission, *in* The Apollo 15 lunar samples: Houston, Tex., Lunar Sci. Inst., p. 198–199.

Chao, E. C. T., 1973a, Geologic implications of the Apollo 14 Fra Mauro breccias and comparison with ejecta from the Ries crater, Germany: U.S. Geol. Survey Jour. Research, v. 1, no. 1, p. 1–18.

——— 1973b, Preliminary genetic classification of Apollo 16 breccias [abs.], *in* Lunar Science IV, Abstracts: Houston, Tex., Lunar Sci. Inst., p. 129.

——— 1974, Impact cratering models and their application to lunar studies—A geologist's view, *in* Lunar Sci. Conf., 5th, Proc.: Geochim, Cosmochim. Acta, Supp. 5, v. 1, p. 35–52.

Chao, E. C. T., Minkin, J. A., and Best, J. B., 1972, Apollo 14 breccias: General characteristics and classification, *in* Lunar Sci. Conf., 3d, Proc.: Geochim. Cosmochim. Acta, Supp. 3, v. 1, p. 645–659.

Cummings, David, 1972, Geologic map of the Clavius quadrangle of the Moon: U.S. Geol. Survey Misc. Geol. Inv. Map I–706 (LAC–126).

Dence, M. R., Grieve, R. A. F., and Plant, A. G., 1974, The Imbrium basin and its ejecta [abs.], *in* Lunar Science V, Abstracts: Houston, Tex., Lunar Sci. Inst., p. 165–167.

Eggleton, R. E., and Schaber, G. G., 1972, Cayley Formation interpreted as basin ejecta, *in* Apollo 16 preliminary science report: U.S. Natl. Aeronautics and Space Admin. SP–315, p. 29-7 to 29-16.

Elston, D. P., Boudette, E. L., Schafer, J. P., Muehlberger, W. R., and Sevier, J. R., 1972, Apollo 16 field trips: Geotimes, v. 17, no. 3, p. 27–30.

Evensen, N. M., Murthy, V. R., and Coscio, M. R., Jr., 1973, Rb-Sr ages of some mare basalts and the isotopic and trace element systematics in lunar fines, *in* Lunar Sci. Conf., 4th, Proc.: Geochim. Cosmochim. Acta, Supp. 4, v. 2, p. 1707–1724.

Gilbert, G. K., 1893, The Moon's face, a study of the origin of its features: Philos. Soc. Washington Bull., v. 12, p. 241–292.

Grudewicz, E. B., 1974, Lunar upland plains relative age determinations and their bearing on the provenance of the Cayley Formation [abs.], *in* Lunar Science V, Abstracts: Houston, Tex., Lunar Sci. Inst., p. 301–303.

Hartmann, W. K., and Wood, C. A., 1971, Moon; origin and evolution of multiring basins: Moon, v. 3, no. 1, p. 3–78.

Head, J. W., III, 1972, Small-scale analogs of the Cayley Formation and Descartes mountains in impact-associated deposits, *in* Apollo 16 preliminary science report: U.S. Natl. Aeronautics and Space Admin. SP–315, p. 29-16 to 29-20.

Head, J. W., III, and Goetz, A. F. H., 1972, Descartes region—Evidence for Copernican-age volcanism: Jour. Geophys. Research, v. 77, no. 8, p. 1368–1374.

Hodges, C. A., Eggleton, R. E., Schaber, G. G., and Muehlberger, W. R., 1972, Some geologic implications of the Apollo 16 mission: Geol. Soc. America, Abs. with Programs, v. 4, no. 7, p. 540.

Hodges, C. A., Muehlberger, W. R., and Ulrich, G. E., 1973, Geologic setting of Apollo 16, *in* Lunar Sci. Conf., 4th, Proc.: Geochim. Cosmochim. Acta, Supp. 4, p. 1–25.

Howard, K. A., 1972, Ejecta blankets of large craters exemplified by King Crater, *in* Apollo 16 preliminary science report: U.S. Natl. Aeronautics and Space Admin. SP–315, p. 29-70 to 29-77.

Howard, K. A. and Masursky, Harold, 1968, Geologic map of the Ptolemaeus quadrangle of the Moon: U.S. Geol. Survey Misc. Geol. Inv. Map I–566 (LAC–77; RLC–13).

Huneke, J. C., Jessberger, E. K., Podosek, F. A., and Wasserburg, G. J., 1973, $^{40}Ar/^{39}Ar$ measurements in Apollo 16 and 17 samples and the chronology of metamorphic and volcanic activity in the Taurus-Littrow region, *in* Lunar Sci. Conf., 4th, Proc.: Geochim. Cosmochim. Acta, Supp. 4, v. 2, p. 1725–1756.

Husain, Liaquet, and Schaeffer, O. A., 1973, $^{40}Ar/^{39}Ar$ crystallization ages and $^{38}Ar/^{37}Ar$ cosmic ray exposure ages of samples from the vicinity of the Apollo 16 landing site [abs.], *in* Lunar Science IV, Abstracts: Houston, Tex., Lunar Sci. Inst., p. 406–407.

Kaula, W. H., Schubert, G., Lingenfelter, R. E., Sjogren, W. L., and Wollenhaupt, W. R., 1974, Apollo laser altimetry and inferences as to lunar structure, *in* Lunar Sci. Conf., 5th, Proc.: Geochim. Cosmochim. Acta, Supp. 5, v. 3, p. 3049–3058.

Lunar Sample Preliminary Examination Team (LSPET), 1972, The Apollo 15 lunar samples—A preliminary description: Science, v. 175, p. 363–375.

——— 1973, The Apollo 16 lunar samples—Petrographic and chemical description: Science, v. 179, p. 23–34.

McCauley, J. F., 1967, Geologic map of the Hevelius region of the moon: U. S. Geol. Survey Misc. Geol. Inv. Map I–491 (LAC–56).

McGetchin, T. R., Settle, M., and Head, J. W., 1973, Radial thickness variation in impact crater ejecta; implications for lunar basin deposits: Earth and Planetary Sci. Letters, v. 20, no. 2, p. 226–236.

Milton, D. J., 1968, Geologic map of the Theophilus quadrangle of the moon: U.S. Geol. Survey Misc. Geol. Inv. Map I–546 (LAC–78).

Milton, D. J., and Hodges, C. A., 1972, Geologic maps of the Descartes region of the moon, Apollo 16 pre-mission maps: U.S. Geol. Survey Misc. Geol. Inv. Map I–748, 2 sheets.

Moore, H. J., Hodges, C. A., and Scott, D. H., 1974, Multi-ringed basins—illustrated by Orientale and associated features, *in* Lunar Sci. Conf., 5th, Proc.: Geochim. Cosmochim. Acta, Supp. 5, v. 1, p. 71–100.

Morris, E. C., and Shoemaker, E. M., 1968, Television observations from Surveyor, *in* Surveyor project final report, Part 2, Science results: California Inst. Technology, Jet Propulsion Lab. Tech. Rept. 32–1265, p. 65–69.

Morris, E. C., and Wilhelms, D. E., 1967, Geologic map of the Julius Caesar quadrangle of the moon: U.S. Geol. Survey Misc. Geol. Inv. Map I–510 (LAC–60).

Oberbeck, V. R., Hörz, F., Morrison, R. H., Quaide, W. L., and Gault, D. E., 1974, Effects of formation of large craters and basins on emplacement of smooth plains material [abs.], *in* Lunar Science V, Abstracts: Houston, Tex., Lunar Sci. Inst., p. 568–570.

Offield, T. W., and Pohn, H. A., 1970, Lunar crater morphology and relative-age determination of lunar geologic units—Part 2, Applications: U.S. Geol. Survey Prof. Paper 700–C, p. C163–C169.

Papanastassiou, D. A., and Wasserburg, G. J., 1972a, The Rb-Sr age of a crystalline rock from Apollo 16: Earth and Planetary Sci. Letters, v. 16, no. 2, p. 289–298.

——— 1972b, Rb-Sr systematics of Luna 20 and Apollo 16 samples: Earth and Planetary Sci. Letters, v. 17, no. 1, p. 52–63.

Philpotts, J. A., Schnetzler, C. C., Nava, D. F., Bottino, M. L., Fullagar, P. D., Thomas, H. H., Schuhmann, S., and Kouns, C. W., 1972, Apollo 14–Some geochemical aspects, *in* Lunar Sci. Conf., 3d, Proc.: Geochim. Cosmochim. Acta. Supp. 3, v. 2, p. 1293–1305.

Pike, R. J., 1968, Meteoritic origin and consequent endogenic modification of large lunar craters: Ann Arbor, Univ. Michigan, Unpub. Ph. D. dissert., 404 p.

——— 1972, Geometric similitude of lunar and terrestrial craters: Internat. Geol. Cong., 24th, Montreal, Proc., Sec. 15, Programme no. 24, p. 41–47.

Pohn, H. A., and Offield, T. W., 1970, Lunar crater morphology and relative-age determination of lunar geologic units—Part 1, Classification: U.S. Geol. Survey Prof. Paper 700–C, p. C153–C162.

Rose, H. J., Jr., Cuttitta, Frank, Annell, C. S., Carron, M. K., Christian, R. P., Dwornik, E. J., Greenland, L. P., and Ligon, D. T., Jr., 1972, Compositional data for twenty-one Fra Mauro lunar materials, *in* Lunar Sci. Conf., 3d, Proc.: Geochim. Cosmochim. Acta, Supp. 3, v. 2, p. 1215–1229.

Scoon, J. H., 1972, Chemical analyses of lunar samples 14003, 14311, and 14321, *in* Lunar Sci. Conf., 3d, Proc.: Geochim. Cosmochim. Acta, Supp. 3, v. 2, p. 1335–1336.

Shoemaker, E. M., 1962, Interpretation of lunar craters, Chap. 8 *of* Zdenek, Kopal, ed., Physics and astronomy of the moon: New York, Academic Press, p. 283–359.

Short, N. M., and Forman, M. L., 1972, Thickness of impact crater ejecta on the lunar surface: Modern Geology, v. 3, no. 2, p. 69–91.

Soderblom, L. A., and Boyce, J. M., 1972, Ages of nearside and farside terra plains based on Apollo 16 metric photographs, *in* Apollo 16 preliminary science report: U.S. Natl. Aeronautics and Space Admin. SP–315, p. 29-3 to 29-6.

Soderblom, L. A., and Lebofsky, L. A., 1972, Technique for rapid determination of relative ages of lunar areas from orbital photography: Jour. Geophys. Research, v. 77, no. 2, p. 279–296.

Strasheim, A., Jackson, P. F. S., Coetzee, J. H. J., Strelow, F. W. E., Wybenga, F. T., Gricius, A. J., Kokot, M. L., and Scott, R. H., 1972, Analysis of lunar samples 14163, 14259, and 14321 with isotopic data for $^{7}Li/^{6}Li$, *in* Lunar Sci. Conf., 3d, Proc.: Geochim. Cosmochim. Acta, Supp. 3, v. 2, p. 1337–1342.

Swann, G. A., Bailey, N. G., Batson, R. M., Eggleton, R. E., Hait, M. H., Holt, H. E., Larson, K. B., McEwen, M. C., Michell, E. D., Schaber, G. G., Schafer, J. P., Shepard, A. B., Sutton, R. L., Trask, N. J., Ulrich, G. E., Wilshire, H. G,. and Wolfe, E. W., 1971, Preliminary geologic investigations of the Apollo 14 landing site, *in* Apollo 14 preliminary science report: U.S. Natl. Aeronautics and Space Admin. SP–272, p. 39–85.

Taylor, S. R., Kaye, Maureen, Muir, Patricia, Nance, W., Rudowski, R., and Ware, N. 1972, Composition of the lunar uplands—Chemistry of Apollo 14 samples from Fra Mauro, *in* Lunar Sci. Conf., 3d, Proc.: Geochim. Cosmochim. Acta, Supp. 3, v. 2, p. 1231–1249.

Tera, Fouad, Papanastassiou, D. A., and Wasserburg, G. J., 1973, A lunar cataclysm at ≈3.95 AE and the structure of the lunar crust [abs.], *in* Lunar Science IV, Abstracts: Houston, Tex., Lunar Sci. Inst. p. 723–725.

Trask, N. J., 1966, Size and spatial distribution of craters estimated from the Ranger photographs, *in* Ranger VIII and IX. Part 2, Experimenters' analyses and interpretations: California Inst. Technology, Jet Propulsion Lab. Tech. Rept. 32–800, p. 252–263.

Trask, N. J., and McCauley, J. F., 1972, Differentiation and volcanism in the lunar highlands; photogeologic evidence and Apollo 16 implications: Earth and Planetary Sci. Letters, v. 14, no. 2, p. 201–206.

Ulrich, G. E., 1968, Advanced systems traverse research project report: U.S. Geol. Survey open-file rept., 59 p.

——— 1973, A geologic model for North Ray crater and stratigraphic implications for the Descartes region; *in* Lunar Sci. Conf., 4th, Proc.: Geochim. Cosmochim. Acta, Supp. 4, p. 27–39.

Wilhelms, D. E., 1970, Summary of Lunar stratigraphy—Telescopic observations: U.S. Geol. Survey Prof. Paper 599–F, 47 p.

——— 1972, Preliminary geologic map of the region around the candidate Proclus Apollo landing site, *in* Apollo 15 preliminary science report: U.S. Natl. Aeronautics and Space Admin. SP–289, p. 25-72 to 25-75.

Wilhelms, D. E., and McCauley, J. F., 1971, Geologic map of the near side of the Moon: U.S. Geol. Survey Misc. Geol. Inv. Map I–703.

Willis, J. P., Erlank, A. J., Gurney, J. J., Theil, R. H., and Ahrens, L. H., 1972, Major, minor, and trace element data for some Apollo 11, 12, 14, and 15 samples, *in* Lunar Sci. Conf., 3d, Proc.: Geochim. Cosmochim. Acta, Supp. 3, v. 2, p. 1269–1273.

Wilshire, H. G., Stuart-Alexander, D. E., and Jackson, E. D., 1973, Petrology and classification of the Apollo 16 samples [abs.], *in* Lunar Science IV, Abstracts: Houston, Tex., Lunar Sci. Inst., p. 784–786.

Jour. Research U.S. Geol. Survey
Vol. 3, No. 4, July–Aug. 1975, p. 393–400

A MODEL FOR EARTHQUAKES NEAR PALISADES RESERVOIR, SOUTHEAST IDAHO

By DAVID SCHLEICHER, Denver, Colo.

Abstract.—The Palisades Reservoir seems to be triggering earthquakes: epicenters are concentrated near the reservoir, and quakes are concentrated in spring, when the reservoir level is highest or is rising most rapidly, and in fall, when the level is lowest. Both spring and fall quakes appear to be triggered by minor local stresses superposed on regional tectonic stresses; faulting is postulated to occur when the effective normal stress across a fault is decreased by a local increase in pore-fluid pressure. The spring quakes tend to occur when the reservoir level suddenly rises: increased pore pressure pushes apart the walls of the graben flooded by the reservoir, thus decreasing the effective normal stress across faults in the graben. The fall quakes tend to occur when the reservoir level is lowest: water that gradually infiltrated poorly permeable (fault-gouge?) zones during high reservoir stands is then under anomalously high pressure, which decreases the effective normal stress across faults in the poorly permeable zones.

This paper considers a seemingly anomalous concentration of epicenters in southeast Idaho, just west of the Palisades Reservoir (fig. 1). The reservoir is about 4 by 27 km (2.5 by 17 mi) and as much as 67 m (200 ft) deep at highest water level. It impounds the Snake River in Swan Valley, a northwest-trending graben between the Snake River Range on the northeast and the Caribou Range on the southwest. The bounding faults are the Grand Valley fault (northeast) and a series of parallel faults including the Swan Valley fault (southwest). The ranges comprise upper Paleozoic and Cretaceous sedimentary rocks.

The region including the Palisades Reservoir lies in the Rocky Mountain seismic belt (Ryall and others, 1966), which extends from northwest Arizona northward through central Utah, along the Idaho-Wyoming border, and through western Montana. The Palisades area has probably been seismically active through at least Quaternary time. Preliminary gravity data, for example, suggest a few kilometres of fill in the Swan Valley graben, (D. R. Mabey, oral commun., 1972), suggesting in turn that the faults bounding the graben are large structures, and thus that they have been active for a long time.

The Palisades Reservoir was filled in the fall of 1956. Before 1959 so few earthquakes were reported in the surrounding region that there is no direct evidence whether filling the reservoir has affected their frequency or magnitude. But indirect evidence—namely, the spatial and temporal distributions of the earthquakes—suggests that the reservoir has affected the local seismic pattern from 1960 to 1969, a period selected because seismic data are fairly complete.

SEISMIC PATTERN

The epicenters in the Caribou Range cluster were located by the Worldwide Seismograph Network of the NEIS (National Earthquake Information Service, formerly the U.S. Coast and Geodetic Survey), and plotted locations may differ from true locations by 10–40 km. Most of these epicenters are plotted at the intersections of 0.1° meridians and parallels.

Spatially, the epicenters form a distinct cluster centered about 20 km west of the Palisades Reservoir. It is plausible to assume that the precision of locating epicenters is better than the accuracy—in other words, that the techniques for location are good, but that the knowledge of local seismic-wave velocities is less good (L. C. Pakiser, oral commun., 1973). Thus it is reasonable to assume that the observed clustering is real, albeit possibly mislocated.

The number of epicenters in the cluster is consistently and atypically high: five epicenters are reported at one 0.1° grid intersection, four at or near three intersections, three at or near three intersections, and two at nine intersections. Contouring these numbers produces a reasonable contour pattern (fig. 2). The two-epicenter contour is about 50 km across. The four-epicenter contour defines an elongate high, plausibly nested within the overall anomaly. The high is most pronounced and most sharply defined at the north end of the concentration, where the four-epicenter "level" is about 5 km wide; its crestline extends about S. 45° E. —roughly parallel to the graben—for about 15–20 km before becoming less well defined.

The anomaly can be seen in regional perspective by examining the concentration of epicenters throughout a representative surrounding part of the Rocky Moun-

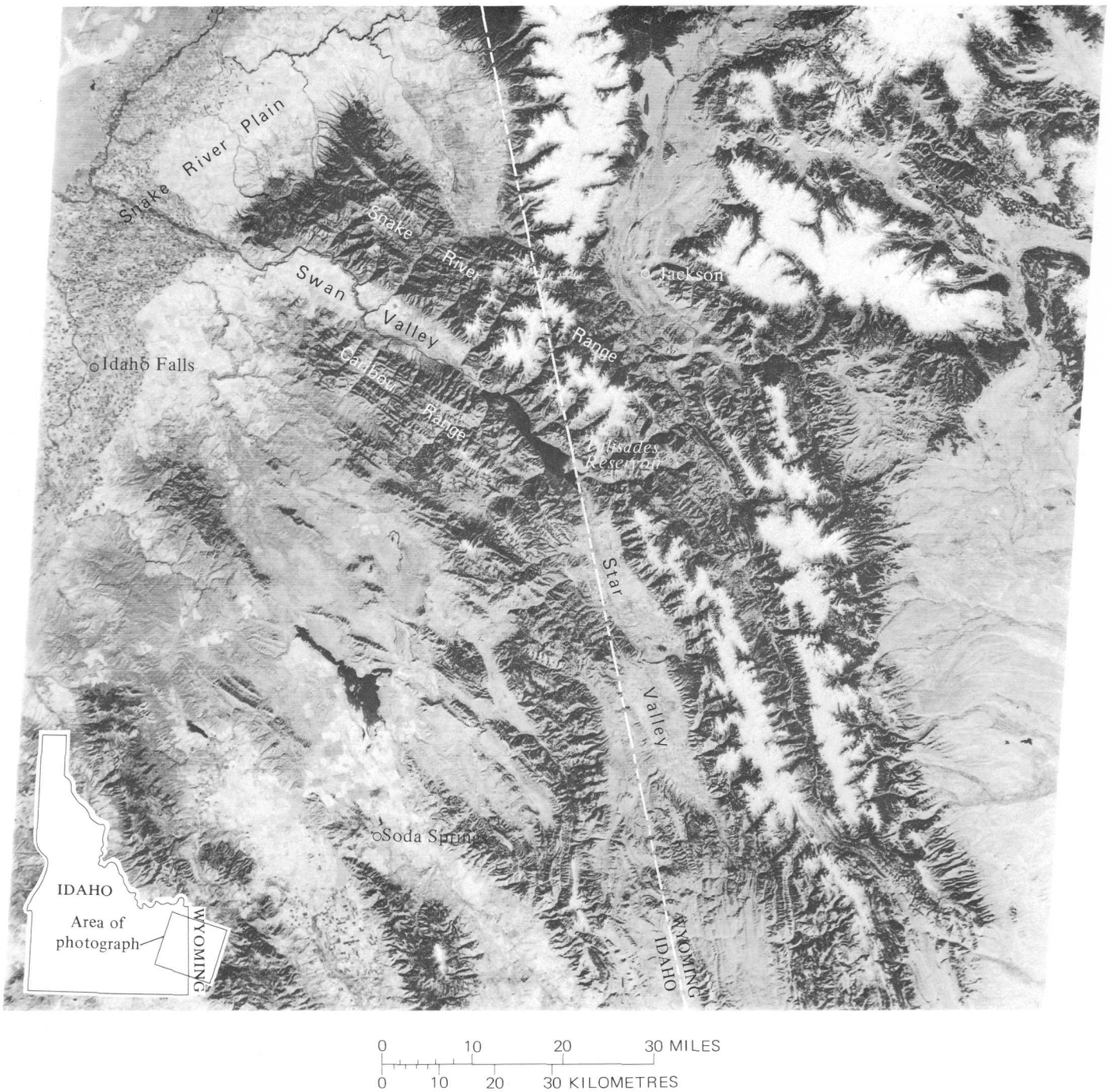

FIGURE 1.—Index and location map for Palisades Reservoir and surrounding area (ERTS photograph 1069–17411, Sept. 30, 1972).

tain seismic belt. The NEIS map of epicenters (U.S. Coast and Geodetic Survey, 1970) suggests that the coordinates 42°–44° N. and 110°–112° W., within which the reservoir is centered, generally circumscribe one cluster of epicenters. Concentrations of epicenters within this cluster were determined by counting the numbers of epicenters reported for 1960–69 in a 1,000-km² circle, using the technique employed for petrofabrics or structural geology, or recently for determining housing density from a topographic map (Bryant and Reed, 1972). The results (fig. 3) document a concentration of epicenters in the Caribou Range west of the reservoir, as well as a slightly smaller and less intense concentration southeast of Soda Springs. The results can be compared directly with Smith's (1972) observations of earthquake re-

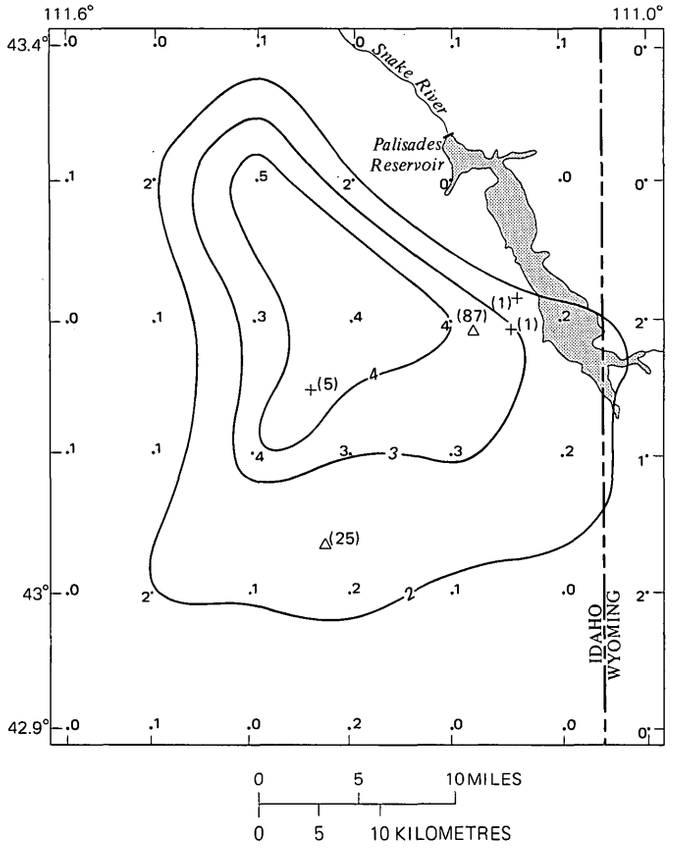

FIGURE 2.—Generalized contours showing concentration of epicenters, as plotted on a 0.1° meridian-parallel grid, 1960–69. Cross, epicenter located by Sbar and others (1972); open triangle, station at which Sbar and others (1972) detected other shocks; numbers in parentheses show number of shocks.

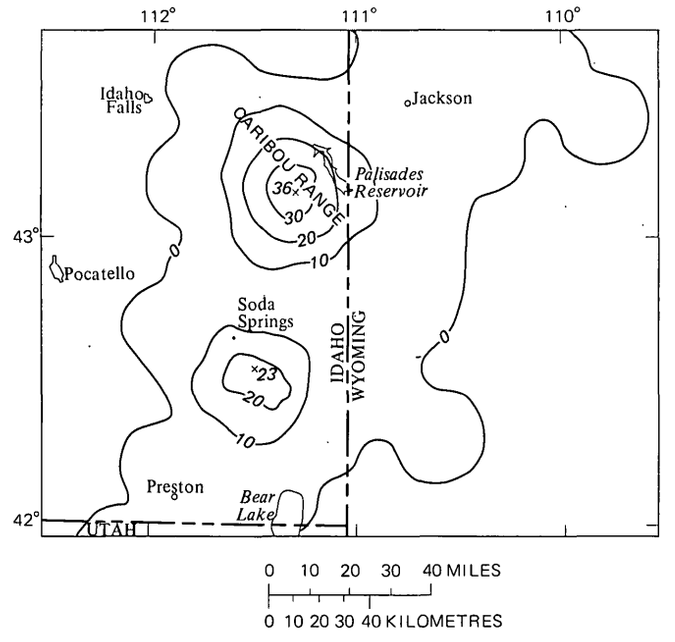

FIGURE 3.—Number of epicenters per 1,000 km², 1960–69. Total number of epicenters ≈120.

currence rates in the Rocky Mountain seismic belt. For an area of 1,000 km², he observes about one quake of Richter magnitude 3 or more per 2 yr. The Caribou Range cluster shows up to 36 quakes per 1,000 km² during the 10 yr considered here, the Soda Springs cluster up to 23. All the NEIS epicenters have magnitudes greater than 3, so both clusters represent anomalous numbers of quakes.

More accurate epicenter locations are available for the period 31 October to 27 November 1964, when Westphal and Lange (1966) monitored a local seismic net in the Caribou Range. They detected 264 microshocks scattered through the range. The largest cluster of epicenters lay about 10 km (6 mi) west of the reservoir. Sbar and others (1972) monitored a local net in the Caribou Range from 19 to 22 August 1969. They located seven epicenters in the range—five of them very near the center of the NEIS cluster, and two just west of the Palisades Reservoir (fig. 2). An additional 112 shocks were detected but not actually located. Of these, 87 shocks were detected by a station about 5 km (3 mi) west of the reservoir; 46 of these shocks were within 7 km (4 mi) of that station and less than 7 km deep. August and November typically have few quakes of magnitude 3 or more (compare next paragraph). Still, many of these August microshocks occurred so close to the reservoir that they may well have been triggered by it. Whether the more scattered November microshocks also were triggered by the reservoir remains equivocal.

The temporal distribution of the Caribou Range earthquakes (fig. 4*A*) independently suggests that some or all of them are triggered by the Palisades Reservoir. The quakes tend to cluster in spring (February, April, and June) and, very strongly, in fall (September and October). For points with two or more reported epicenters, the general pattern of clustering is much the same for swarms of quakes that occur no more than a few days apart as it is for all quakes. June has the highest average reservoir level for 1960–69, and September has the lowest. The suggestion is that both high and low reservoir levels can trigger quakes (fig. 4*B*). The spring quakes tend to occur when the reservoir level rises sharply (fig. 4*C*). By contrast, the fall quakes tend to occur when reservoir levels are lowest; this relation is clear if these low levels are rotated above the abscissa (fig. 4*B*).

Hagiwara and Ohtake (1972, p. 250–251) report that nearly 60 percent of the quakes near the Kurobe Dam in Japan occur between 1500 and 0300 hours. For the Palisades area, although the fall quakes are erratically distributed through the day, the spring quakes tend to occur around noon or midnight.

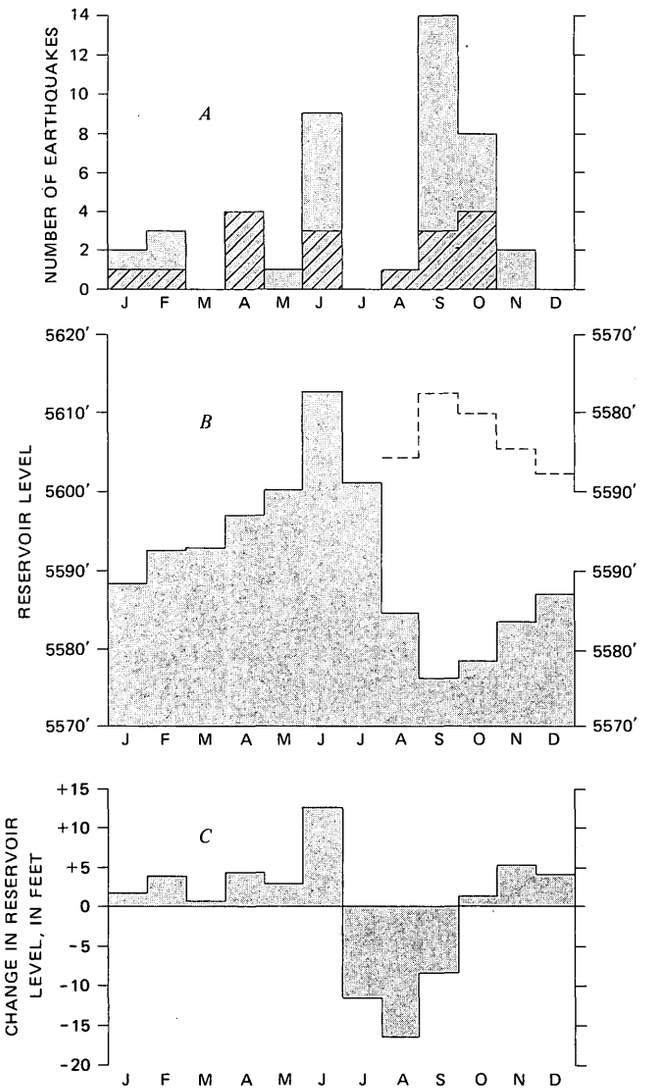

FIGURE 4.—Monthly distribution of earthquakes and data on reservoir level, 1960–69. *A*, Number of earthquakes by month in which they occurred; ruled bars represent only single earthquakes and the first earthquake of swarm. *B*, Average monthly reservoir levels, with August-December levels (dashed line) also plotted on inverted coordinates. *C*, Average monthly change in reservoir levels.

RELATED STUDIES

Lake Mead is perhaps the most studied example of a reservoir that seems to have triggered earthquakes (Carder, 1970). No quakes were reported in the sparsely inhabited area before the dam was built. The first was reported in September 1936, as the reservoir was being filled. Some thousands of quakes have been monitored since 1937, when seismographs were first set up. All but a few percent have occurred within about 80 km of the dam, and their average depth is probably less than 6 km (Carder, 1970, p. 52). All Richter magnitudes have been less than 5. As with the Palisades Reservoir, quakes tend to occur when the water level is highest or lowest.

Rothé (1969) has reported other reservoirs that seem to have triggered earthquakes. Typically, few or no quakes are noted before reservoir filling; after filling, the number increases and commonly shows some correlation with water level. Hypocenters are very close to the reservoir, and some, at least, are practically at the surface. Most of the quakes are small, but Richter magnitudes of 6 or more are reported for Grandval Dam (France), Kremasta Dam (Greece), Koyna Dam (India), and Lake Kariba (Rhodesia, Zambia). Earthquakes have also been attributed to reservoir filling in Japan (Hagiwara and Ohtake, 1972).

Similarly, earthquakes have apparently been triggered by injection of liquid wastes into a deep disposal well at the Rocky Mountain Arsenal near Denver, Colo. (Healy and others, 1968), and by injection of water for petroleum secondary-recovery operations near Rangely, Colo. (Raleigh, 1972).

TRIGGERING MECHANISMS

The means by which reservoirs may trigger earthquakes is poorly understood. The quakes are variously associated with high water levels (Carder, 1970; Rothé, 1970), with low levels (Carder, 1970), and with rapid changes in level (Rothé, 1969). The onset of faulting has been attributed to changes in pore-fluid pressure (Lane, 1971; Raleigh, 1972), to the load imposed by the water (Carder, 1970; Gough and Gough, 1970b), and to weakening of the rocks by water saturation (Hagiwara and Ohtake, 1972). Generally prompt seismic response suggests that quick-acting changes are responsible; changes in stress thus seem more likely than changes in mechanical properties. The geologic setting of the reservoirs is varied, and the exact mechanism of faulting is almost certainly dictated by the geologic units, by the prevailing stress field, and by the orientation and sense of displacement of the fault or faults affected by the reservoir.

In general, faulting is caused by changing stresses. The change ultimately leads to a stress difference so great that faulting occurs, again reducing the stress difference. In large part, the change of stress that causes faulting near some reservoirs is almost certainly tectonic. In unknown part, the change is probably due to modification of stresses at the depth of faulting by changes in load or pore pressure induced by changes in reservoir level. Apparently, this modification of stress—probably by much less than 1 percent—is great enough to trigger faulting.

Of the stresses causing normal faulting, as near the Palisades Reservoir, the vertical stress is the most com-

pressive principal stress (Hubbert and Willis, 1957, p. 157). It is thus tempting to think of the reservoir as simply an additional "load" that directly triggers faulting. But faulting is caused by critical differences in **effective stresses**—total stress minus pore-fluid pressure (Hubbert and Rubey, 1959, p. 134). It is thus likely that the weight of added water in the reservoir directly triggers faulting only if the reservoir water is perched, not merely the topmost part of a continuous ground-water column. The early quakes associated with observed settling around Lake Mead may fall into this category. Carder (1945, p. 191) suggests that at least some of them were due to reactivation of normal faults between granite and basin-fill sediments, and level surveys showed that the sediments had settled about 10 cm. Settling, however, appeared to have ceased by the time of a second level survey in 1941, and Carder (1970, p. 51) suggests that subsequent quakes have been triggered by seasonal load fluctuations. Gough and Gough (1970a) cite a very similar settling (as much as 23.5 cm) around Lake Kariba.

If, on the other hand, the reservoir water is merely the top of a continuous water column, the weight of the reservoir water cannot add directly to the effective vertical stress. Loading may trigger normal faulting for a short period (a few years?) after reservoir filling. Indeed, Gough and Gough (1970b) noted a marked decrease in seismicity after Lake Kariba had been filled. If earthquakes continue, however, the suggestion is that stresses are being modified by changes in pore-water pressure. Stresses may also be modified by the viscous effects of seasonal changes in ground-water flow through the porous materials beneath the reservoir.

PROPOSED MECHANISM FOR THE CARIBOU RANGE QUAKES

The exact means by which a reservoir may trigger earthquakes clearly depends on the geologic setting of the reservoir. If the Palisades Reservoir is triggering some or all of the Caribou Range quakes, the mechanism that follows may explain how. Even if the reservoir is not triggering these quakes, the proposed mechanism may apply to other reservoirs that fit the model described below.

The Palisades Reservoir occupies a graben. Southeast Idaho in general may be considered a region of tectonic relaxation (compare Hubbert and Willis, 1957, p. 158); that is, the region is currently being extended along normal faults. The most compressive principal stress (σ_3) is thus vertical; the least compressive principal stress (σ_1) is horizontal and perpendicular to the strike of the faults (fig. 5). Recurrence of faulting

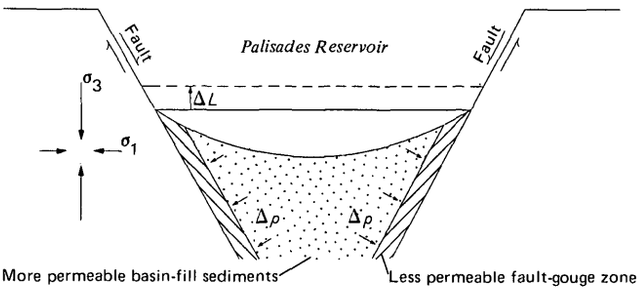

FIGURE 5.—Schematic section across graben. σ_1 and σ_3, tectonic stresses; ΔL, rise in reservoir level; Δp, rise in pore pressure.

suggests that σ_1 is continually decreasing. Hubbert and Willis (1957, p. 157) postulate that normal faulting occurs when σ_1 falls to about one-half to one-third of σ_3. The faulting increases σ_1, which then gradually decreases until it is again small enough to cause faulting. Except for the effects of erosion on the upthrown block and deposition on the downthrown block of a normal fault, σ_3 remains nearly constant and equal to the stress imposed by the weight of the overburden.

The area around the Palisades Reservoir would almost certainly be subject to earthquakes even if the reservoir were not there. Ryall, Slemmons, and Gedney (1966) show high seismic flux for the area before 1932, 24 years before the reservoir was filled. The effect of the reservoir must thus be merely to trigger faulting—that is, to modify its timing, intensity, or location—when tectonic stresses are on the verge of causing it anyway.

One explanation of how the Palisades Reservoir might trigger faulting depends on the following assumptions:

1. The geologic structure can be modeled as a trapezoidal prism of basin-fill sediments between the normal faults that bound the graben (fig. 5). Movement takes place on these faults or on normal faults in the graben (not shown in fig. 5).
2. The sediments in the graben are relatively permeable; near the reservoir, the water table in the sediments changes by about the same amount as the reservoir level.
3. At least parts of the fault zones bounding the graben are far less permeable than the sediments in the graben. The poor permeability of the fault zones means that water tables on opposite sides of each zone are practically independent. It is plausible to think of the poorly permeable zones as clayey fault gouge. (The model will also work if the fault zones are much more permeable than the basin-fill sediments.)
4. The water in the reservoir is not perched, but rather is part of a continuous ground-water column.

5. The effects of ground-water movement along the graben can be neglected. This presupposes that for intervals of a month or so, the water table in the graben is controlled predominantly by changes in reservoir level rather than by ground-water flow along the graben. A recharge dome a few times the length of the reservoir is likely.

A rise in reservoir level and the associated local rise in water table increase the pore-water pressure in the sediments filling the graben. Because the fault zones are relatively impermeable, the increased pore pressure pushes outward on both fault zones, slightly compressing the rocks outside the graben. But in the graben, σ_1 is decreased, and the likelihood of faulting is accordingly increased between the impermeable gouge zones. Note that the total range of variation in pore pressure throughout the entire year is about 1 bar, corresponding to about 10 m (30 ft) of change in reservoir level.

These spring quakes need not presuppose impermeable fault zones; they would follow from virtually the same mechanism if the bedrock walls of the graben are less permeable than the sediments of the graben.

Hubbert's famous sandbox (1951, fig. 1) suggests a mechanical analog. The sandbox is a rectangular box, open at the top, partly filled with sand. A partition in the box fits and moves like a piston in a cylinder. Imagine that the sandbox is modified by adding "ground water," saturating the sand to about equal levels on opposite sides of the movable partition, which is impermeable and leaks negligibly around the edges (fig. 6). If the partition is moved far enough to the right, normal faults will form in the left part of the box. If the movement of the partition could be stopped just before the onset of normal faulting, raising the water level in the left part of the box would nudge the partition just far enough to trigger the incipient faulting.

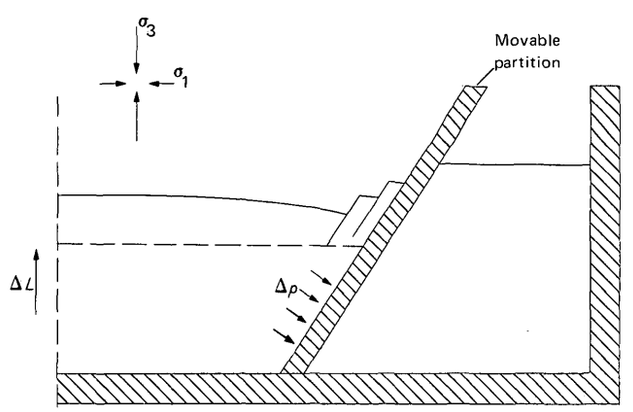

FIGURE 6.—Model sandbox, showing how normal faulting is triggered by increase in pore pressure (Δp) caused by rise in reservoir level (ΔL) when horizontal tectonic stress (σ_1) has been reduced almost to the point of faulting by moving partition to the right.

To make the sandbox further approach the model for the Palisades area, the partition should dip to the left about 60°, representing a poorly permeable normal-fault zone. The dimensions of the box parallel to the strike of the fault zone should be greatly increased. A mirror-image partition on the left would complete the "graben," and a dam would impound a reservoir on the sloping floor of the graben. The partitions would be moved very slowly to decrease σ_1. Each "spring," water would be added to the reservoir fast enough to maintain a ground-water recharge dome around the reservoir. Whenever the sand was on the verge of faulting, a sudden rise in reservoir level would impart a sudden nudge to both partitions, and that nudge would tend to trigger faulting in the graben. In the real graben, movement will probably occur on faults on the inner side of one or both fault zones (on the grabenward side of the least permeable part of the zone) or on faults in the graben neglected in this simplified model.

The fall quakes probably follow from a slightly different mechanism. It is likely that the zones of fault gouge are gradually permeated during spring, when the reservoir level is high (fig. 7). When the level again falls, pore water is trapped in the gouge zones, and its pressure is greater than that of the pore water in the more permeable sediments of the graben. The normal stress across shear surfaces in the fault zones is thus reduced (compare Hubbert and Rubey, 1959, p. 142), and normal faulting again becomes likely, despite the increase in σ_1 in the graben itself. In contrast to the spring faulting, this faulting is probably concentrated in the least permeable parts of the fault zones.

This mechanism can be modeled with three books and a plastic bag. Two of the books are stacked with the bag between them, and one end of the stacked books is rested on the third book. The slope of the stacked books should be such that the top book will almost slide off the stack. When the plastic bag is blown up, increasing the "pore-fluid" pressure above ambient (atmospheric) pressure, the top book immediately begins to slide.

RAMIFICATIONS

Strong earthquakes, regardless of their origin, are cause for concern. Rothé (1969, p. 29, 38) reports seven quakes of Richter magnitude 6 or more at four reservoirs; two of the areas were allegedly aseismic before the reservoirs were filled. It cannot, of course, be unequivocally demonstrated that filling the reservoirs "caused" the earthquakes, or that the quakes were more

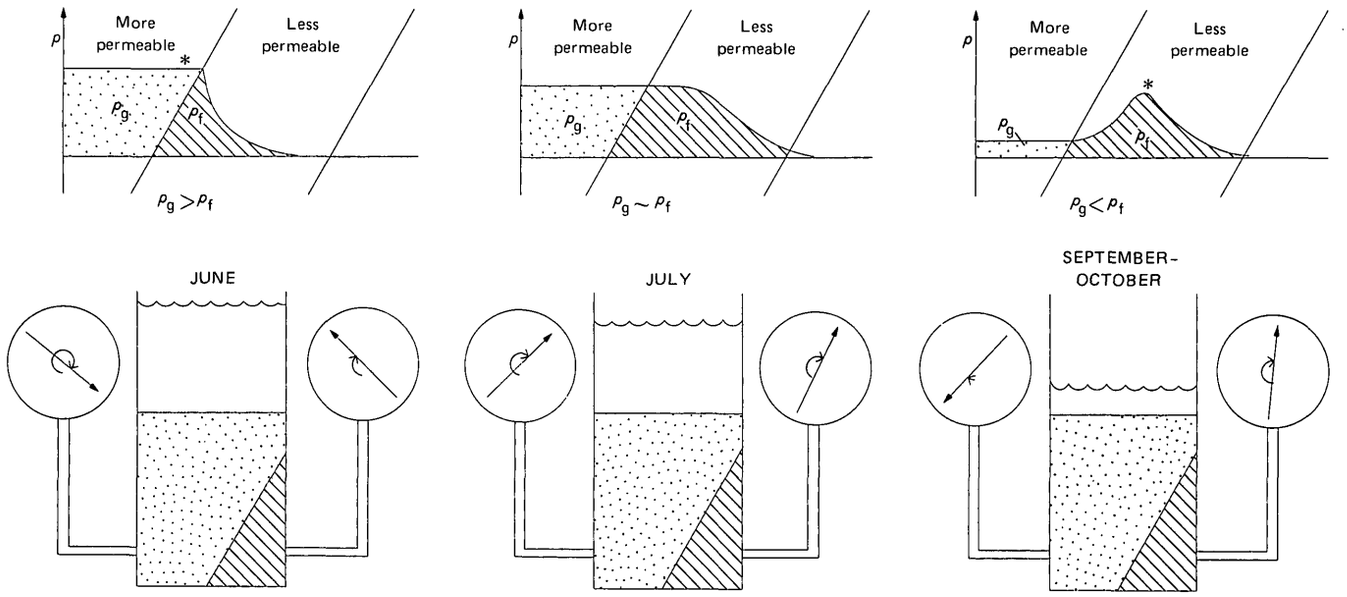

FIGURE 7.—Postulated distribution of pore-fluid pressure (p), showing how it varies with reservoir level; p_g, pressure in permeable sediments of graben) stipple pattern); p_f, pressure in less permeable fault-gouge zones (line pattern); *, locus of probable fault movement.

than a temporary response to filling. But the onset of seismicity in a previously aseismic area, or even an increase of seismicity in a known seismic area, can be unsettling. The 1967 Koyna, India, earthquake of Richter magnitude 6.4 killed 177, injured 2,300, and fractured the dam (Rothé, 1970, p. 232); repairs cost more than £1.5 million (Lancaster-Jones, 1972, p. 778). Clearly, a better understanding of mechanism is needed.

Fluctuating reservoirs, under the right circumstances, may provide a convenient way to trigger small quakes, thereby preventing tectonic stress differences from increasing to dangerous levels. If the dam is engineered to withstand the shocks, and if secondary complications such as landsliding do not occur, an increased frequency of small quakes associated with the reservoir may prove beneficial. But conversely, repeated triggering of movement along one part of a fault might increase the seismic danger elsewhere along the fault.

FURTHER STUDY

The Palisades Reservoir offers an unusual opportunity to study the effects of pore-fluid pressure on seismicity. The structural geometry of the graben is simple enough that it would be fairly easy to model. Seismic data for the area are becoming more abundant and accurate. Further study presupposes installation of a local seismic net to monitor quakes of intensity smaller than those detected by the current regional net, so as to locate hypocenters more accurately, to determine first motions, and to further study the peculiarly nonuniform distribution of quakes during the year. More accurate delineation of hypocenters may make it possible to detect seasonal variations in their position and to map out the geometry of one or more active faults at depth. The model proposed here implies dilatancy of the graben sediments before spring faulting; measurement of strain and seismic velocity will directly confirm or negate that hypothesis, and bear on dilatancy as a general premonitory effect (compare Scholz and others, 1973). Only rarely can the earth scientist conduct an experiment at this scale.

REFERENCES CITED

Bryant, Bruce, and Reed, J. C., Jr., 1972, Map showing approximate density of houses in the Evergreen quadrangle, Jefferson County, Colorado: U.S. Geol. Survey Misc. Inv. Map I–786–D.

Carder, D. S., 1945. Seismic investigations in the Boulder Dam area, 1940–1944, and the influence of reservoir loading on local earthquake activity: Seismol. Soc. America Bull., v. 35, no. 4, p. 175–192.

———1970, Reservoir loading and local earthquakes, *in* Adams, W. M., ed., Engineering seismology—the works of man: Geol. Soc. America Eng. Geology Case Histories, no. 8, p. 51–61.

Gough, D. I., and Gough, W. I., 1970a, Stress and deflection in the lithosphere near Lake Kariba—I: Royal Astron. Soc. Geophys. Jour., v. 21, no. 1, p. 65–78.

———1970b, Load-induced earthquakes at Lake Kariba—II: Royal Astron. Soc. Geophys. Jour., v. 21, no. 1, p. 79–101.

Hagiwara, T. and Ohtake, M., 1972, Seismic activity associated with the filling of the reservoir behind Kurobe Dam, Japan, 1963–1970: Tectonophysics, v. 15, no. 3, p. 241–254.

Healy, J. H., Rubey, W. W., Griggs, D. T., and Raleigh, C. B., 1968, The Denver earthquakes: Science, v. 161, no. 3848, p. 1301–1310.

Hubbert, M. K., 1951, Mechanical basis for certain familiar geologic structures: Geol. Soc. America Bull., v. 62, no. 4, p. 355–372.

Hubbert, M. K., and Rubey, W. W., 1959, Mechanics of fluid-filled porous solids and its application to overthrust faulting, [Pt.] 1 *of* Role of fluid pressure in mechanics of overthrust faulting: Geol. Soc. America Bull., v. 70, no. 2, p. 115–166.

Hubbert, M. K., and Willis, D. G., 1957, Mechanics of hydraulic fracturing: Am. Inst. Mining, Metall., and Petroleum Engineers Trans., v. 210, p. 153–166.

Lancaster-Jones, P., 1972, *in* Seismic activity at man-made reservoirs—discussion (of R. G. T. Lane): Inst. Civil Engineers Proc., v. 51, p. 777–778.

Lane, R. G. T., 1971, Seismic activity at man-made reservoirs: Inst. Civil Engineers Proc., v. 50, p. 15–24.

Raleigh, C. B., 1972, Investigation of seismic activity related to reservoirs, *in* Symposium on instrumentation—practical applications and results: Assoc. Eng. Geologists Bull., v. 9, no. 3, p. 177–183.

Rothé, J. P., 1969, Earthquakes and reservoir loadings: World Conf. Earthquake Eng., 4th, Santiago-de-Chile, Preprints A–1, p. 28–38 and addendum.

———1970, Seismes artificiels [in French with English summ.]: Tectonophysics, v. 9, p. 215–238.

Ryall, Alan, Slemmons, D. B., and Gedney, L. D., 1966, Seismicity, tectonism, and surface faulting in the western United States during historic time: Seismol. Soc. America Bull., v. 56, no. 5, p. 1105–1135.

Sbar, M. L., Barazangi, Muawia, Dorman, James, Scholtz, C. H., and Smith, R. B., 1972, Tectonics of the Intermountain Seismic Belt, western United States—microearthquake seismicity and composite fault plane solutions: Geol. Soc. America Bull., v. 83, no. 1, p. 13–28.

Scholz, C. H., Sykes, L. R., and Aggarwal, Y. P., 1973, Earthquake prediction—a physical basis: Science, v. 181, no. 4102, p. 803–810.

Smith, R. E. [R. B.], 1972, Contemporary seismicity, seismic gaps, and earthquake recurrences of the Wasatch Front, *in* Environmental geology of the Wasatch Front 1971: Utah Geol. Assoc. Pub. 1, p. I1–I9.

U.S. Coast and Geodetic Survey (Natl. Earthquake Inf. Center), 1970, Map NEIC–3012, *from* Seismicity of the United States: Washington, D.C., U.S. Dept. Commerce, Environmental Sci. Services Adm., 1 sheet.

Westphal, W. H., and Lange, A. L., 1966, Local seismic monitoring; final technical report: Stanford Research Inst. Rept., 242 p.

Jour. Research U.S. Geol. Survey
Vol. 3, No. 4, July–Aug. 1975, p. 401–408

COMPUTER-GENERATED SHADED-RELIEF IMAGES

By R. M. BATSON, KATHLEEN EDWARDS; and E. M. ELIASON,
Flagstaff, Ariz.; Menlo Park, Calif.

Abstract.—Digital image-processing techniques have been developed to make shaded-relief images from digitized topographic data. The resulting images have at least two advantages over aerial photographs: (1) The images are true map projections containing no relief-induced distortion, and (2) tonal variation is unambiguously identified with relief, rather than with snow, vegetation, or other albedo variations. Parallax can be introduced into these images in the computer, and stereoscopic pairs can thus be created.

The techniques of "hill-shading" or "shaded relief" have been used in cartography for many years to produce the illusion of a three-dimensional relief map.

Shaded-relief maps are useful because they convey an instant impression of the shape of the land if they are skillfully done. In this sense, they are better than photographs, which contain such a variety of image densities not related to relief that landforms are obscured or obliterated (fig. 1). Orthophotomaps with contour lines contain a wealth of information but still lack the impact of a good relief map from which information has been selectively deleted for clarity. Base maps upon which geologic maps or other colored overlays are placed must be carefully designed lest base tones distort the color and hence the interpretation of the final map. A high-contrast base consisting solely of lines is one answer to this dilemma, but a low-contrast shaded-relief base, in which tone variation is unambiguously identified with relief and no other surface characteristic, makes a dramatic improvement in the interpretability of a map.

Two methods are currently in use to produce shaded-relief maps. One method was developed by P. M. Bridges and J. L. Inge at the U.S. Air Force Aeronautical Chart and Information Center and Lowell Observatory in Flagstaff, Ariz., during the lunar mapping program in the 1960's. This method is based on interpretation of photographs and visual observation of the surface to be mapped (Inge, 1972). The method requires skill and training in photointerpretation and a well-developed ability to visualize and portray landforms accurately, regardless of their illumination and color on photographs. In a second, more traditional method, an illustrator utilizes topographic contour lines to determine the degree of shading required. This paper describes a technique in which a computer is used to produce shaded-relief maps by the second method.

Computerized production of shaded-relief maps utilizes techniques and concepts developed for planetary mapping from spacecraft television pictures (Levinthal and others, 1973). Relief is identifiable on photographs because natural surfaces reflect varying amounts of light as a function of the slope of the surface, the texture of the surface, the angle from which it is illuminated, and the location of the viewer (fig. 2). This phenomenon has been used in photometric studies of the lunar surface with telescopes, and complex laws have been proposed to define the luminance of the Moon with respect to the above geometric parameters (Minnaert, 1961; Hapke, 1963). No such complex functions, however, are necessary for simple portrayal of shaded relief. A relatively simple function such as the Lommel-Seeliger law is perfectly adequate. This law states that

$$I = \frac{1}{1 + \frac{\cos \epsilon}{\cos i}}, \qquad (1)$$

where I = the intensity of the reflectance,
ϵ = the angle between the observer and the slope normal, and
i = the angle between the sun and the slope normal.

This equation was used to produce the shaded-relief image in figure 3.

The data for this image were compiled by DMA (Defense Mapping Agency) from the Montrose 1:250,000 quadrangle (fig. 4). Personnel from this organization have measured altitudes by interpolation from contour lines at 100-m intervals. The values have been recorded on magnetic tape for each 1:250,000 quadrangle in the United States.

The computer program for shaded relief converted each pair of altitude values along each east-west line to a slope whose value was used in equation 1 to compute a brightness level for the interval between the pair of

FIGURE 1.—Part of ERTS image 1407–17190 of the area of the west half of the Montrose quadrangle, Colorado (1:250,000-scale topographic series). North is at top; east-west distance at center of photograph is about 55 mi (88 km).

altitudes. This set of values was then recorded on magnetic tape for input to an Optronics Corp. Photowrite device that produces film output from digital image playback.

The interpolation method used by DMA resulted in peculiar artifacts in parts of the image. These artifacts are clearly related, in form and location, to the contour lines from which the relief data were derived.

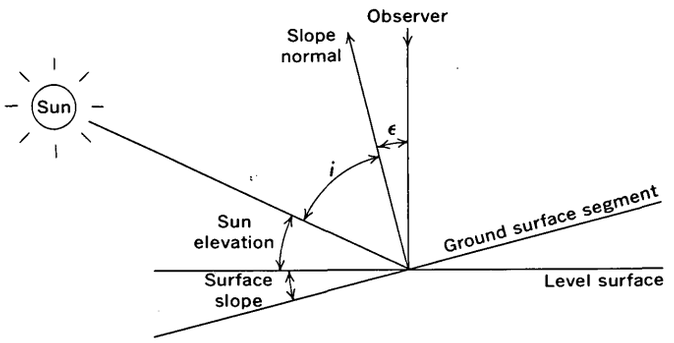

FIGURE 2.—Factors that affect the intensity of reflectance from the ground surface. The two factors most critical to determination of reflectance according to the Lommel-Seeliger law are angles i and ε. See text for discussion.

The artifacts can be prevented by higher order interpolation techniques.

The contrast of the image may be modified in the computer by redefining the brightness change for each slope increment, or by computing the brightness values with a lower or higher Sun. The illumination used to produce figure 3 was 30° above the western horizon. That for figure 5 was 5° above the western horizon, and that for figure 6 is 60° above the western horizon.

Simple manipulation of the digitized altitude data makes it possible to form stereoscopic shaded-relief images for additional clarification of surface structures. A detailed discussion of stereoscopic parallax is contained in Tewinkel, Schmid, Hallert, and Rosenfield (1966, p. 22–25). Introduction of stereoscopic parallax into a shaded-relief image requires only the very simple equation

$$\Delta p = \Delta h(K), \qquad (2)$$

where Δp is the displacement due to height, on the image plane, of an object whose height is Δh. K is a constant selected arbitrarily that will determine the strength of the stereoscopic illusion. Large values of K will result in exaggerated stereoscopic perception of relief, whereas small ones will produce a weak perception. A value of K was selected for figure 7 such that no value of Δp was greater than 2 mm.

An acceptable stereoscopic pair can be made by using the original, undistorted image and a second image into which parallax has been introduced. It is therefore possible to make a single, orthographic image of a large area and to make images with introduced parallax in selected parts of the area. Figure 7 is a stereogram in which parallax has been introduced into the left-hand member only.

The utility of shaded-relief drawings is not necessarily confined to the portrayal of topographic surfaces. Any data that can be contoured can be portrayed in this way.

The cost of making shaded-relief images by the method described in this paper depends largely on the cost of gathering topographic data for processing. Computer costs are small compared to the costs of encoding data. Generation of the image of figure 3 required about 30 min on a Digital Equipment Corp. PDP 11/45 computer. Generating the film image by the Optronics output device required less than 10 min.

An accurate, detailed, and efficient way to collect input data for the shaded-relief program would be to utilize stereoscopic plotting instruments with digital output capability. In particular, data might be gathered during orthophotomap compilation.

Many data of the kind required for this program have already been collected for other purposes. They reside in data banks throughout the country. If these data could be obtained and put into an acceptable format, large numbers of shaded-relief images could be compiled at relatively low cost.

Figures 3 through 7 follow "References Cited."

REFERENCES CITED

Hapke, B. W., 1963, A theoretical photometric function for the lunar surface: Jour. Geophys. Research, v. 68, p. 4571–4586.

Inge, J. L., 1972, Principles of lunar illustration: U.S. Air Force Aeronautical Chart and Inf. Center, ACIC Reference Pub., RP–72–1, 60 p.

Minnaert, M., 1961, Photometry of the moon, *in* Kuiper, G. P., and Middlehurst, B. M., eds., Planets and satellites, the solar system: Univ. Chicago Press, v. 3, p. 213–245.

Levinthal, E. C., Green, W. B., Cutts, J. A., Jahelka, E. D., Johansen, R. A., Sander, M. J., Seidman, J. B., Young, A. T., and Soderblom, L. A., 1973, Mariner 9—Image processing and products: Icarus, v. 18, p. 75–101.

Tewinkel, G. C., Schmid, H. H., Hallert, Bertil, and Rosenfield, G. H., 1966, Basic mathematics of photogrammetry, *in* Manual of photogrammetry: Am. Soc. Photogrammetry, v. 1, p. 17–65.

FIGURE 3.—Computer-generated shaded-relief image, west half of the Montrose quadrangle. Data from Montrose 1:250,000 quadrangle. The sun is assumed to be 30° above the western horizon. Scale 1:500,000 (1 in ≈ 8 mi; 1 cm = 5,000 m). North is at top.

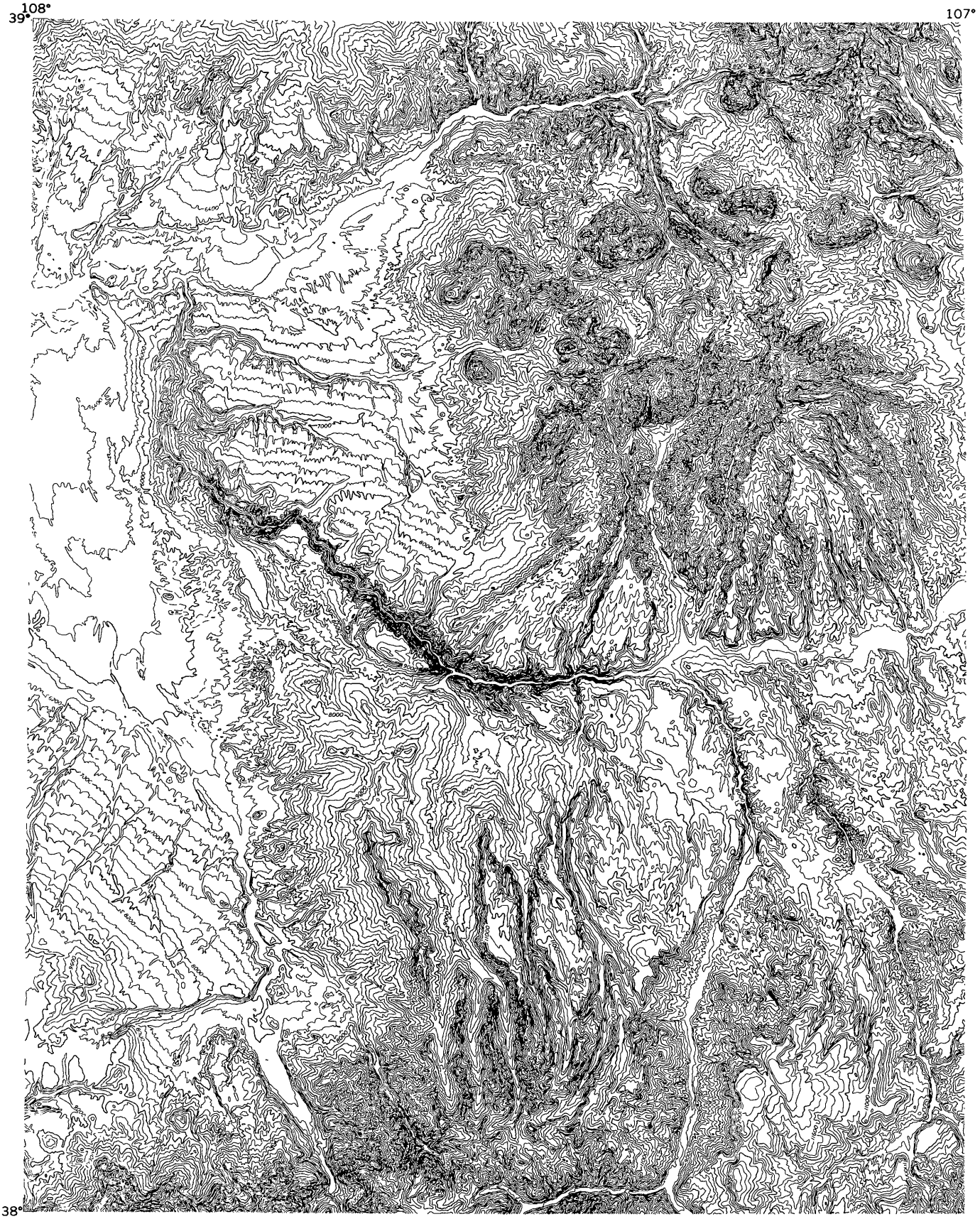

FIGURE 4.—Topographic contours, west half of the Montrose quadrangle. Contour interval, 200 ft; supplementary contours (dashed) at 100-ft interval in areas of low relief; scale 1:500,000. North is at top.

FIGURE 5.—Computer-generated shaded-relief image, west half of the Montrose quadrangle. Data from Montrose 1:250,000 quadrangle. The Sun is assumed to be 5° above the western horizon. Scale 1:500,000. North is at top.

FIGURE 6.—Computer-generated shaded-relief image, west half of the Montrose quadrangle. Data from Montrose 1:250,000 quadrangle. The Sun is assumed to be 60° above the western horizon. Scale 1:500,000. North is at top.

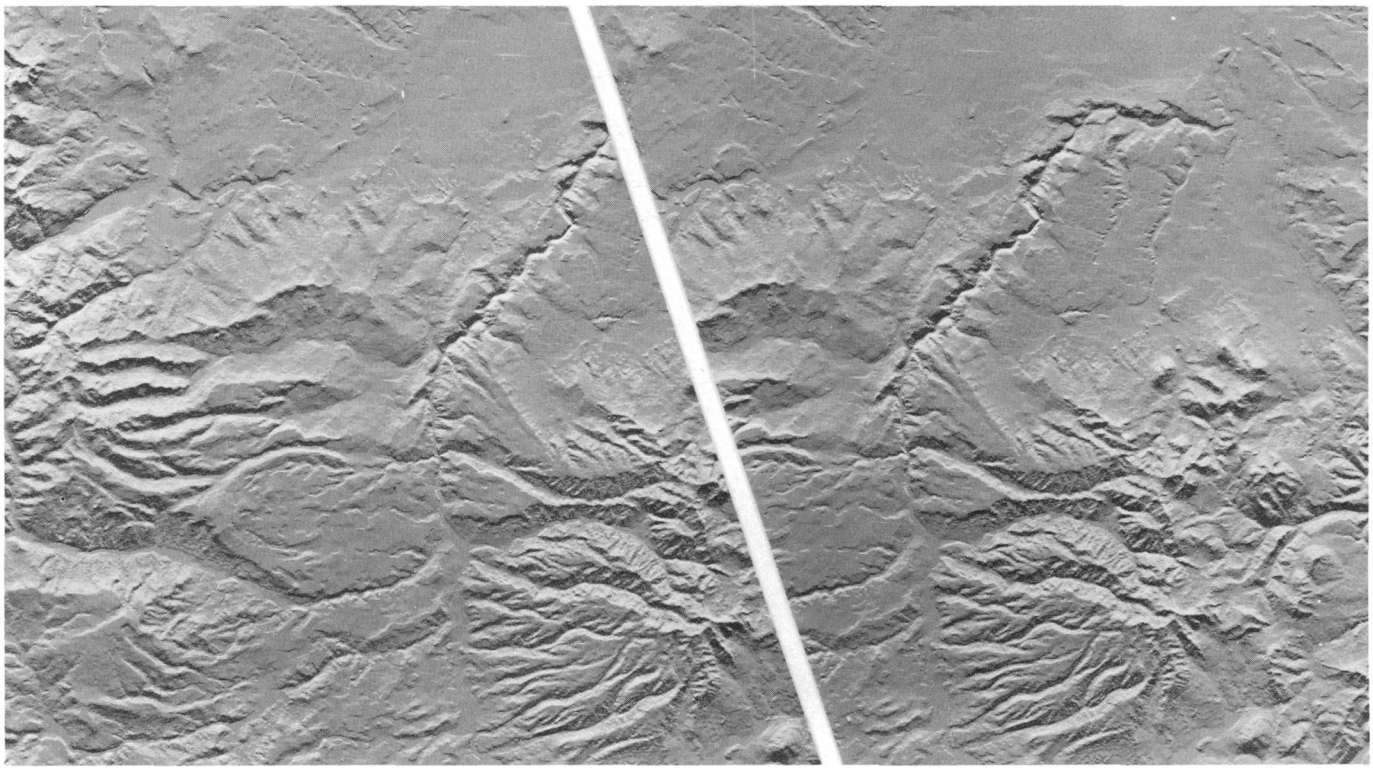

FIGURE 7.—Stereogram of computer-generated shaded-relief images of an area in the western part of the Montrose quadrangle. Data from Montrose 1:250,000 quadrangle. Scale approximately 1:833,333. North is to right.

Jour. Research U.S. Geol. Survey
Vol. 3, No. 4, July–Aug. 1975, p. 409–414

WHITLOCKITE AND APATITE OF SURFICIAL PHOSPHATE OCCURRENCES ON ENDERBURY ISLAND, PHOENIX ISLANDS, PACIFIC OCEAN

By R. A. GULBRANDSEN, Menlo, Park, Calif.

Abstract.—Whitlockite and apatite are the principal phosphate minerals in the surficial deposits of Enderbury Island; monetite and brushite are present in small amounts. All are derived from the guano of sea birds. The abundance of whitlockite discovered on Enderbury, and reported in samples from Remire Island in the Indian Ocean, indicates that the mineral is probably of common occurrence in young insular phosphate deposits. The composition of whitlockite from Enderbury Island is roughly $(Ca, Mg, Sr, Na)_3 (PO_4, CO_3)_2$, similar to the composition indicated for other insular occurrences by the sparse data available. The variety of apatite found on the island is carbonate fluor-hydroxylapatite, low in fluorine content. Whitlockite appears to have formed directly from guano components in surficial aqueous solutions, possibly accompanied by apatite. but changes with time to apatite.

Data on the nature and occurrence of insular whitlockite, a predominantly calcium orthophosphate somewhat similar to apatite in composition, are rare; Frondel's study (1943) of specimens from islands in the Caribbean Sea is still the main source of information. Braithwaite (1968) identified whitlockite in one specimen of phosphatic material on Remire Island in the Indian Ocean, and Trueman (1971) subsequently found that whitlockite was present in a number of Braithwaite's samples and is probably a common phosphate mineral on Remire Island. In this study of a small group of samples collected in the course of a reconnaissance of phosphate deposits on Enderbury Island, whitlockite was discovered to be at least as abundant in the samples of surficial deposits as apatite, the only other major phosphate mineral present. From these recent discoveries, it appears likely that whitlockite will be found to occur abundantly and widely on islands of similar type.

Insular apatite, carbonate hydroxyl-fluorapatite, is well known from the studies of Jacob, Hill, Marshall, and Reynolds (1933), McClellan and Lehr (1969), Trueman (1966), and Frondel (1943) and appears to be the principal phosphate mineral of insular deposits.

Mineralogical data on whitlockite and apatite, including chemical analyses and X-ray diffraction data, are presented here to provide more information about the phosphate minerals of insular deposits.

Enderbury Island, a small island about 5 km in length and a little less than 2 km in greatest breadth, is one of the atolls of the Phoenix Islands in the central equatorial Pacific Ocean (fig. 1). The highest point, the top of an old phosphate stockpile (fig. 1), is 10 m. The surface of the island forms a shallow depression with interior drainage. In the southern part of the island, a shallow saline lake occupies the site of a former lagoon that became filled with sediment; composition of lake water was reported by Brown and Gulbrandsen (1973). The climate is arid, having a mean annual rainfall of about 630 mm (Hutchinson, 1950, p. 166), and vegetation is sparse. Most of the island is coral, but shells of many kinds and other skeletal material are incorporated in the coral reefs and mixed with coral fragments in the sands of the beaches and of much of the interior of the island. The ridge rimming the island is made up of blocks of coral and beach rock. The coral is composed of aragonite; other skeletal materials are composed of aragonite or magnesium calcites.

Acknowledgments.—This study is an outgrowth of an investigation of the economic potential of phosphate deposits on Enderbury Island made for the protectorate nations (the United Kingdom and the United States) by Brian D. Hackman in behalf of the United Kingdom and by Joshua I. Tracey, Jr., and R. A. Gulbrandsen for the United States. The excellent organization, as well as support, of the project by John Holland and Maj. Forest Blair, both of the U.S. Air Force, is greatly appreciated. I especially thank the U.S. Air Force for the opportunity to make this study.

DISTRIBUTION AND OCCURRENCE OF PHOSPHATE

Phosphate, as guano and guano-derived phosphate rock and sediment, occurs widely on the island but is not now abundant. Hutchinson (1950, p. 180) estimated that about 100,000 tons of phosphate ore was

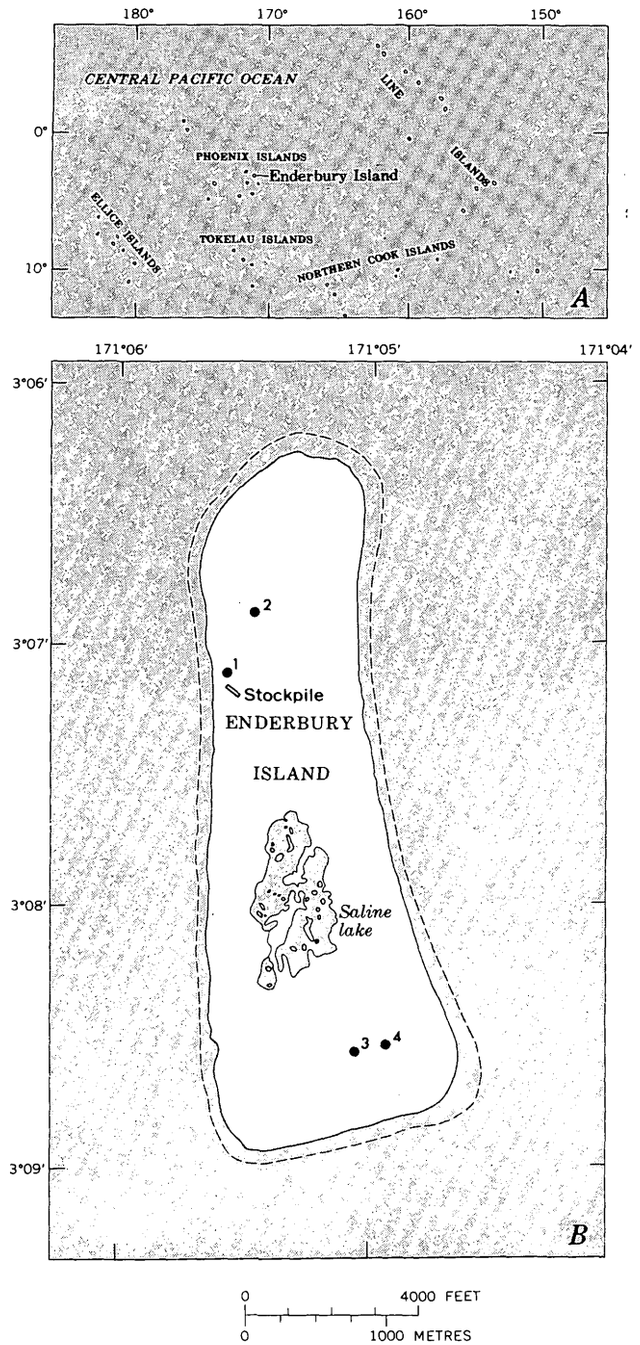

FIGURE 1.—Index map (*A*) showing location of Enderbury Island, and map of Enderbury Island (*B*) showing location of saline lake and sample localities 1, 2, 3, and 4. Dashed line around island marks the approximate position of low tide.

shipped from Enderbury in the latter half of the 19th century. A stockpile (see fig. 1) of a few thousand tons of material of very low grade, 5–10 percent P_2O_5, was left on the northwest side of the island. It is composed of medium-brown silt with numerous sand- and pebble-size fragments of carbonate rocks and is similar to much of the widespread unconsolidated sediment remaining on the island that is even lower in grade, generally 1–2 percent P_2O_5. Only two small patches of sediment were found to be moderately rich in phosphate, about 20 percent P_2O_5.

Guano accumulation since the period of mining is not large despite a huge population of sea birds—boobies, terns, frigate birds, and red-tailed tropic birds—that roost and nest on the island. Only in a few small groves, mostly of dead trees, where the birds roost, are guano piles conspicuous. Old diggings in both the north and south parts of the island expose phosphatic carbonate rock and phosphorite developed on the upper part of the ancient lagoonal reef platform. The phosphate has replaced carbonate and lined and filled cavities. One solid layer of phosphorite, about 3.5 cm thick and of local occurrence, shows ghost outlines of coral and represents both phosphate replacement and cavity-filling. Branched coral (finger-size) in an open framework of growth at one horizon has a thin veneer of medium-brown phosphate. In a small pit at the southern end of the island, coral fragments (thumb-size) have been almost entirely replaced by phosphate. In another occurrence of phosphate, unconsolidated sand-size grains make up a thin layer that may represent phosphate replacement of a carbonate lagoonal beach sand.

PHOSPHATE MINERALS

Phosphate minerals identified are whitlockite, apatite (carbonate fluor-hydroxylapatite), monetite, and brushite. Only whitlockite and apatite are widespread and abundant, probably about equally abundant overall, and neither is found entirely free of the other. Monetite and brushite are of local and separate occurrence; each is associated in occurrence with both whitlockite and apatite. Minerals of a sample of dry guano, a pile collected from a tree branch, have not been identified, but X-ray diffraction patterns show numerous peaks.

CHEMICAL ANALYSES

Chemical analyses of dry guano (loc. 1, fig. 1), a whitlockite-rich sample (loc. 2, fig. 1), and an apatite-rich sample (loc. 3, fig. 1) are presented in table 1.

The guano, because it was collected from the branch of a tree, represents material that has been leached of its more soluble components by rainwater but has not been modified in composition by contact with the calcium and magnesium carbonate minerals of the island. The relative proportions of the constituents in the guano, except for LOI (loss on ignition), H_2O—,

TABLE 1.—*Chemical analyses, in weight percent, of guano, whitlockite-rich sample, and apatite-rich sample from Enderbury Island*

[Lab No. M113330; analysts: S. T. Neil (SiO_2, MgO, CaO, H_2O-, P_2O_5, L.O.I.), L. B. Schlocker (Na_2O, K_2O), C. Huffman (F), B. P. Fabbi (SrO by X-ray spectrographic analysis); L.O.I. is loss on ignition, 105°–450°C, and represents largely organic matter. Lab No. M113328; analysts: S. T. Neil (MgO, CaO, H_2O-, P_2O_5, total C, CO_2), L. B. Schlocker (Na_2O, K_2O), M. Cremer (total H_2O), C. Huffman (F), N. H. Suhr (Al_2O_3, Fe_2O_3), B. P. Fabbi (SrO by X-ray spectrographic analysis), R. A. Gulbrandsen (L.O.I. 110°–1100°C); C (total) was determined gasometrically with the Leco carbon analyzer, CO_2 is carbonate carbon that was determined gravimetrically after liberation with H_3PO_4, and C(organic) is the difference between C(total) and carbonate carbon; Na_2O is the average of two determinations (1.33 and 1.39). Lab No. M113329; analysts: S. T. Neil (SiO_2, MgO, CaO, H_2O-, P_2O_5), M. Cremer (CO_2), L. B. Schlocker (Na_2O, K_2O), C. Huffman (F), H. N. Elsheimer (total H_2O), N. H. Suhr (Al_2O_3, Fe_2O_3), B. P. Fabbi (SrO by X-ray spectrographic analysis); CO_2 is carbonate carbon]

	Guano M113330	Whitlockite-rich sample M113328	Apatite-rich sample M113329
SiO_2	0.10	----	0.04
Al_2O_3	----	0.10	.07
Fe_2O_3 (total Fe)	----	.04	.02
MgO	.90	3.25	1.37
CaO	6.26	45.02	48.81
SrO	.03	.33	.37
Na_2O	.97	1.36	1.20
K_2O	2.55	.03	.04
P_2O_5	10.82	43.09	35.87
F	.06	.08	.72
CO_2	----	1.03	4.80
C(total)	----	.74	----
C(organic)	----	.46	----
H_2O+	----	2.61	4.42
H_2O-	4.34	.52	1.50
LOI	71.92	6.13	----
Subtotal	97.95	99.95	99.23
Less O (O=F)	.03	.03	.30
Total	97.92	[1] 99.92	98.93
Mn [2]	.0007	.0010	.0007
B [2]	<.0010	<.0010	.0020
Ba [2]	.0002	.0002	.0003
Cu [2]	.0020	.0007	.0010

[1] Sum excludes C(total), CO_2, C(organic), and H_2O+.
[2] Semiquantitative spectrographic analyses by R. E. Mays.

SrO, and SiO_2, are somewhat similar to proportions reported in fish, the food of the sea birds inhabiting the island. The amounts in fish (Bowen, 1966, p. 70), expressed here as weight percent, are 4.1 percent P_2O_5, 2.8 percent CaO, 1.4 percent K_2O, 1.1 percent Na_2O, 0.2 percent MgO, and 0.14 percent F.

The whitlockite sample contains a few percent of apatite as an impurity, enough to preclude making an accurate calculation of the cell contents of the mineral. The main components of the mineral, however, are clearly indicated by the analysis. In comparison with theoretical whitlockite (Frondel, 1941 and 1943), $Ca_3(PO_4)_2$, the general formula for whitlockite from Enderbury Island is $(Ca, Mg, Sr, Na)_3 (PO_4, CO_3)_2$. The C:P mole ratio for theoretical whitlockite is 1.5 as compared with the (Ca, Mg, Sr, Na): (P, C) mole ratio of 1.48 for the Enderbury whitlockite. Frondel (1943, p. 230) considered that the carbonate in his specimens of insular whitlockite occurred in a manner analogous to that of the carbonate apatites. The magnesium content reported here appears to be typical for whitlockite, and the small amount of strontium certainly accompanies calcium. Sodium has not been previously reported in whitlockite but cannot be otherwise accounted for in this occurrence; it serves here to approximately balance the charge loss due to the substitution of $(CO_3)^{-2}$ for $(PO_4)^{-3}$.

The significance of the 2.61 percent H_2O+ reported in the whitlockite analysis in table 1 is obscured by the presence in the sample of organic matter and apatite. Some hydrogen may be essential to the mineral, as proposed by Gopal and Calvo (1972) on the basis of a structural analysis of Palermo whitlockite (type whitlockite of Frondel, 1941), but direct confirmation is lacking.

Frondel (1943, p. 229) noted that carbonate whitlockites have distinctly lower indices of refraction than those without carbonate, a mean index of 1.600 to 1.6065 as compared with 1.625 to 1.6275. The mean index of microcrystalline aggregates of Enderbury whitlockite, about 1.600, is compatible with Frondel's observations.

The variety of apatite whose analysis is presented in table 1 is carbonate fluor-hydroxylapatite. The dominance of hydroxyl over fluorine in the mineral is indicated by the small amount of fluorine reported. The amount of carbonate in the apatite is obscured by the presence of some magnesium calcite and whitlockite impurities in the sample, but a calculation yields an amount of carbonate equivalent to 2.2 percent CO_2. This estimate utilizes formula 3 of McClellan and Lehr (1969, p. 1382), which relates the observed a cell dimension with the mineral contents of CO_3 and F. The equation was solved for CO_3, where the a dimension is 9.389 A and the F content is 0.8 percent, assuming about 10 percent impurities in the analyzed sample.

A large part of the magnesium reported in the analysis occurs in magnesium calcite and whitlockite, the chief impurities in the sample. The amount of sodium reported in table 1 is large in comparison with other insular apatite but similar to the values given for many marine apatites (Jacob and others, 1933, p. 23; McClellan and Lehr, 1969; and Trueman, 1966).

Probably the most notable compositional feature of insular apatites is the wide range of F contents that they exhibit, 0.38 to 3.42 percent F (Jacob and others, 1933, p. 39). Only the highest value, a sample from Makatea Island in the Pacific Ocean, appears to attain the amount required for end-member fluorapatite. Most insular apatite contains appreciably less F than does marine apatite, which is invariably

carbonate fluorapatite with a full compliment or an excess of F (Altschuler, 1973, p. 39). Altschuler (1973, p. 74) suggests that most of the F of insular apatite is acquired postdepositionally, replacing OH, from sea spray and sea wash. The amount of F taken up would then be related, at least partly, to the length of time the apatite was exposed to these conditions. The main deposits of such islands as Nauru, Ocean, and Christmas are older than the deposits on Enderbury and much higher in F content.

X-RAY DATA

X-ray diffraction data of whitlockite and carbonate fluor-hydroxylapatite from Enderbury are presented in table 2, and unit-cell parameters for whitlockite, in table 3. Whitlockite from the Palermo pegmatite in North Groton, N.H., is the type material described by Frondel (1941). The other samples, except for the one from Enderbury, are all of synthetic origin. The preparations of Ito (1968) show the contracting effect of the smaller Mg ion in replacement of Ca ion upon the a dimension, and the Enderbury and Palermo whitlockites both conform qualitatively in composition with this effect. The c dimension of Ito's products, however, is distinctly larger than that of the natural whitlockites. Of the whitlockites shown in the table, only the Enderbury is of low-temperature and guano-derived origin; better and more data are needed to relate the compositional components to the cell parameters.

TABLE 2.—*X-ray diffraction data of whitlockite and carbonate fluor-hydroxylapatite from Enderbury Island*

Calculated [1]		Observed		Calculated [1]		Observed	
hkl	*d*A	*d*A	*I*	*hkl*	*d*A	*d*A	*I*
Whitlockite [2]				**Whitlockite [2]—Continued**			
012	8.1	8.1	[3] 6	238	1.881	1.881	13
104	6.4	6.4	12	416	1.866	1.866	12
110	5.18	5.18	42	0.1.20	1.817	([4])	4
202	4.36	4.36	[3] 6	3.2.10	1.800	1.799	[3] 8
018	4.12	([4])	2	502	1.7859	([4])	5
024	4.04	4.04	16	054	1.7616	([4])	10
1.0.10	3.43	3.43	42	2.0.20	1.7147	1.7147	25
211	3.38	([4])	4	**Carbonate fluor-hydroxylapatite [5]**			
122	3.34	3.33	[3] 10				
208	3.22	([4])	6				
214	3.18	3.18	58				
300	2.99	2.99	14				
0.2.10	2.859	2.859	100	100	8.1	8.2	10
128	2.738	2.737	21	101	5.3	([4])	7
306	2.692	2.691	[3] 6	200	4.07	([4])	8
1.1.12	2.655	2.652	5	111	3.88	([4])	7
220	2.590	2.590	63	002	3.44	3.44	54
0.1.14	2.542	([4])	8	102	3.17	3.18	15
223	2.535			210	3.07	3.07	17
2.1.10	2.503	2.504	14	211	2.807	2.806	100
131	2.483	([4])	2	112	2.777	2.781	50
1.2.11	2.392	2.391	[3] 8	300	2.710	2.710	60
315	2.359	2.355	[3] 5	202	2.628	2.628	26
1.0.16	2.246	([4])	8	301	2.522	([4])	6
1.1.15	2.233	([4])	4	212	2.293	([4])	10
042	2.227	([4])	2	310	2.255	2.255	24
404	2.180	2.180	12	311	2.143	([4])	7
3.0.12	2.150	2.150	14	113	2.063	([4])	8
1.2.14	2.088	([4])	2	203	2.000	([4])	4
1.3.10	2.067	([4])	4	222	1.940	1.940	28
0.0.18	2.062			312	1.887	1.887	[3] 11
232	2.046	([4])	4	213	1.840	1.840	32
048	2.019	2.018	14	321	1.8006	([4])	11
3.1.11	2.002	([4])	5	410	1.7744	([4])	12
2.2.12	1.986	1.986	[3] 7	303	1.7522	([4])	11
4.0.10	1.920	1.919	23	402	1.7507		
327	1.919			004	1.7224	1.7215	19

[1] Indices and *d*-spacing refinement by computer program of Evans and others (1963) $\lambda = 1.54051$ A.

[2] For observed values, quartz internal standard, $(10\bar{1}0) = 4.255$ A. $(10\bar{1}1) = 3.343$ A, and $(11\bar{2}2) = 1.8178$ A. Diffractometer traverse rate = 0.5° 2θ/min. $\lambda = 1.54051$ A.

[3] Broad.

[4] Present but too poorly defined for accurate measurement.

[5] For observed values, quartz internal standard, $(10\bar{1}0) = 4.255$ A, $(10\bar{1}1) = 3.343$ A, $(11\bar{2}0) = 2.457$ A. $(10\bar{1}2) = 2.281$ A, $(20\bar{2}0) = 2.1275$ A, and $(11\bar{2}2) = 1.8178$ A. Diffractometer traverse rate = 0.5° 2θ/min. $\lambda = 1.54051$ A.

TABLE 3.—*Unit cell parameters (hexagonal) of whitlockite (space group R3C)*

Occurrence	a(A)	c(A)	V(A^3)	Reference
Enderbury Island: (Ca, Mg, Sr, Na)$_3$ (PO$_4$, CO$_3$)$_2$.	10.359	37.113	3449	This paper.
Palermo pegmatite, N.H.: $Ca_{54.7}$ $Mg_{4.1}$ $Fe^{+2}_{1.72}$ $Fe^{+3}_{1.38}$ $(PO_4)_{42}$ (21 formula units per hexagonal unit cell).	10.32	36.9	------	Frondel (1941, p. 152).
Palermo pegmatite, N.H.	10.32	37.0	------	Fisher (1960, p. 651).
Palermo pegmatite, N.H.: $Ca_{18.16}$ $Mg_{1.60}$ $Fe_{0.40}$ $(HPO_4)_{1.68}$ $(PO_4)_{12.32}$ (7 formula units per rhombohedral unit cell).	10.330	37.103	------	Gopal and Calvo (1972, p. 31).
Synthetic, 1120°C: Ca_7 Mg_2 $(PO_4)_6$.	10.31	37.25	------	Ito (1968, p. 355).
Synthetic, 1120°C: Ca_8 Mg $(PO_4)_6$.	10.36	37.24	------	Ito (1968, p. 355).
Synthetic, 1120°C: Ca_9 $(PO_4)_6$.	10.45	37.32	------	Ito (1968, p. 355).
Heated commercial sample: Ca_3 $(PO_4)_2$.	10.429	37.38	------	DeWolff (X-ray powder data file card 9–169).

Insular apatite is included in the broad study of natural apatites by McClellan and Lehr (1969), and it was their data relating the a cell dimension to the contents of carbonate and fluorine that was used to make an estimate, described above, of the carbonate content, as percent CO_2, in the Enderbury apatite sample. The unit-cell parameters of the Enderbury carbonate fluor-hydroxylapatite are:

$$a = 9.389 \pm 0.003 \text{ A},$$
$$c = 6.890 \pm 0.002 \text{ A},$$
and $$V = 526.0 \pm 0.3 \text{ A}^3.$$

WHITLOCKITE-APATITE RELATIONS

Hutchinson (1950, p. 482), in his monumental study of the biogeochemistry of vertebrate excretion, concluded, "All excretory products that accumulate as guano tend, as decomposition and leaching occur, to-

wards fluor-hydroxy/-carbonate-apatite * * *." Altschuler (1973, p. 74) suggests that there is a mineral evolution of the calcic phosphates from brushite-monetite to whitlockite to apatite that is accompanied by a parallel decline in organic, nitrogenous, and ammoniacal compounds.

The limited extent of sampling and of observations on Enderbury makes conclusions about the phosphate mineral relations on the island somewhat tentative, but the relations observed are in accord with those noted above. The few occurrences of brushite and monetite found do not reveal any definitive evidence about their relations with whitlockite and apatite. These minerals, together with whitlockite, do not appear to persist with time; only apatite has been identified in older phosphate deposits (not described in this report) that were encountered at depth in drill holes on the island.

Evidence for early formation of whitlockite from guano was found in a small pit (loc. 4, fig. 1) near the southern end of the island. A fine-grained brownish-black sediment, composed predominantly of whitlockite, covered part of the pit floor and surrounded a pile of guano. Only a small pond of water occupied the lowest part of the pit, but the distribution of sediment indicated that the water level had been higher at times and water had covered the entire pit floor. The sediment is rich in organic matter and contains, in addition to whitlockite, a few percent of apatite, a trace of brushite, and a significant amount of sodium chloride. Much of the apatite occurs as small bone fragments, probably fishbones not completely digested by the sea birds and passed along in the guano. The presence of sodium chloride signifies a contribution of seawater to the pond water, as sea spray or sea overwash, or by diffusion from underlying seawater that probably forms the ground water of the porous reef complex. The guano pile in the pit is situated directly below a tree branch that projects over the pit and served as roosting spot for the red-footed boobies that colonized the grove of trees along the edge of the pit. Other guano accumulations on the edge and side of the pit undoubtedly contributed material to the sediment in the pit.

Features of the whitlockite occurrence suggest a very close tie between whitlockite and guano and appear to demonstrate a present-day process in which whitlockite is formed from guano components in saline water. Brushite is possibly a short-lived preliminary product.

The experimental work of Rowles (1968) on the synthesis of whitlockite at low temperature provides some qualitative information about the whitlockite-apatite associations observed on the island. He found not only that the presence of magnesium in solution was necessary for the formation of whitlockite and that a significant amount of magnesium entered the structure of whitlockite but that nearly all of the whitlockite precipitates contained apatite. From solutions in which the ratio of Ca:Mg ranges from 5:1 to 20:1, he obtained precipitates whose proportion of whitlockite increased, at constant pH, with increasing Mg contents and decreased, at constant Ca:Mg, with increasing pH. These relations could account for the wide range of whitlockite-apatite proportions found in the samples from Enderbury, possibly signifying the occurrence of local variations in the chemical environment; yet an inexorable long-term change of whitlockite to apatite probably takes place in the overall surface environment and seemingly could produce the same effect.

REFERENCES CITED

Altschuler, Z. S., 1973, The weathering of phosphate deposits —geochemical and environmental aspects, *in* Griffith, E. J., Beeton, Alfred, Spencer, J. M., and Mitchell, D. T., eds., Environmental phosphorus handbook: New York, John Wiley and Sons, p. 33–96.

Bowen, H. J. M., 1966, Trace elements in biochemistry: New York, Academic Press, 241 p.

Braithwaite, C. J. R., 1968, Diagenesis of phosphatic carbonate rocks on Remire, Amirantes, Indian Ocean: Jour. Sed. Petrology, v. 38, p. 1194–1212.

Brown, D. W., and Gulbrandsen, R. A., 1973, Chemical composition of a saline lake on Enderbury Island, Phoenix Island group, Pacific Ocean: U.S. Geol. Survey Jour. Research, v. 1, no. 1, p. 105–111.

Evans, H. T., Jr., Appleman, D. E., and Handwerker, D. S., 1963, The least squares refinement of crystal unit cells with powder diffraction data by an automatic computer indexing method [abs.]: Am. Cryst. Assoc., Abs. of Ann. Mtg, Cambridge, Mass.

Fisher, D. J., 1960, Morinite-apatite-whitlockite: Am. Mineralogist, v. 45, nos. 5–6, p. 645–667.

Frondel, Clifford, 1941, Whitlockite—A new calcium phosphate, $Ca_3(PO_4)_2$: Am. Mineralogist, v. 26, p. 145–152.

——— 1943, Mineralogy of the calcium phosphates in insular phosphate rock: Am. Mineralogist, v. 28, p. 215–232.

Gopal, R., and Calvo, C., 1972, Structural relationship of whitlockite and β $Ca_3(PO_4)_2$: Nature (Phys. Sci), v. 237, no. 71, p. 30–32.

Hutchinson, G. E., 1950, The biogeochemistry of vertebrate excretion: Am. Mus. Nat. History Bull., v. 96, 594 p.

Ito, Jun, 1968, Synthesis of cerite: Natl. Bur. Standards Jour. Research, A. Phys. Chemistry, v. 72A, no. 4, p. 355–358.

Jacob, K. D., Hill, W. L., Marshall, H. L., and Reynolds, D. S., 1933, The composition and distribution of phosphate rock with special reference to the United States: U.S. Dept. Agriculture Bull. 364, p. 1–90.

McClellan, G. H., and Lehr, J. R., 1969. Crystal-chemical investigation of natural apatites: Am. Mineralogist, v. 54, nos. 9–10, p. 1374–1391.

Rowles, S. L., 1968, The precipitation of whitlockite from aqueous solutions, *in* Structure et propriétés des phosphates: Colloque Internat. Phosphates Minéraux Solides, Toulouse, Mai 16–20, 1967, v. 1, p. 151–155.

Trueman, N. A., 1966, Substitutions for phosphate ions in apatite: Nature, v. 210, no. 5039. p. 937–938.

——— 1971, A petrological study of some sedimentary phosphorite: Australian Minerals Devel. Lab. Bull., no. 11, p. 1–72.

Jour. Research U.S. Geol. Survey
Vol. 3, No. 4, July–Aug. 1975, p. 415–424

ANDESITE SILLS IN THE RED MOUNTAIN AREA, SCAPEGOAT WILDERNESS, LEWIS AND CLARK COUNTY, MONTANA

By ROBERT L. EARHART, Denver, Colo.

Abstract.—Sills 2–200 ft (0.6–60 m) thick in the Red Mountain area of the Scapegoat Wilderness in northwest Montana consist of altered andesite, basaltic andesite, and dacite and occur over a stratigraphic range of 8,000 ft (2,400 m) in the Helena and Snowslip Formations. The approximate compositional range of the sills is 50–80 percent plagioclase, 0–25 percent orthoclase, and 5–30 percent amphibole, pyroxene, and biotite; the uppermost sill contains about 15 percent quartz in the groundmass. Accessory minerals include quartz, magnetite, ilmenite, apatite, and pyrite. The petrology and alteration of the sills distinguish them from other sills in the region. Field observations and laboratory studies consisting of chemical, isotopic and X-ray analyses, and petrographic and mineralogic investigations suggest that the sills may have been emplaced in Precambrian Y time at about the same time as the extrusion of the Purcell Lava in the vicinity of Glacier National Park. Alternatively, the sills may represent a Precambrian igneous event not previously recognized in the Belt basin.

Sills ranging in composition from basaltic andesite to dacite were discovered during mapping of the Red Mountain area in the Scapegoat Wilderness, northwest Montana (fig. 1). The mapping, which was part of a program to evaluate the mineral resources of the wilderness, was done in the summer of 1970 by M. R. Mudge and R. L. Earhart. The sills are about 2–200 ft (0.6–60 m) thick and occur in Belt rocks over a stratigraphic range of approximately 8,000 ft (2,400 m). They are best exposed on the crest of a north- to northeast-trending ridge that includes Red Mountain (fig. 2). The sills are apparently unrelated to other igneous rocks known in the wilderness region; this observation prompted chemical, isotopic and X-ray analyses, and petrographic and mineralogic studies of the sills.

The Red Mountain area (fig. 2) covers about 18 mi² (47 km²) mostly in the southern part of the wilderness; a small part of the area lies outside the southern boundary. Red Mountain, which at an elevation of 9,411 ft (2,868 m) is the highest point in the wilderness, is named for its outcrops of red beds of the Snowslip Formation. Much of the area is above timberline and contains tarns, cirques, arêtes, and other features typical of alpine glaciation. The margins and bottoms of the valleys and cirques are covered with glacial till and colluvium. The area is accessible via a jeep trail that follows an old mine road along the west fork of Copper Creek. The jeep trail is a continuation of a good unpaved road that intersects State Highway 20 about 7 mi (11 km) east of Lincoln, Mont., and that goes along the main branch of Copper Creek.

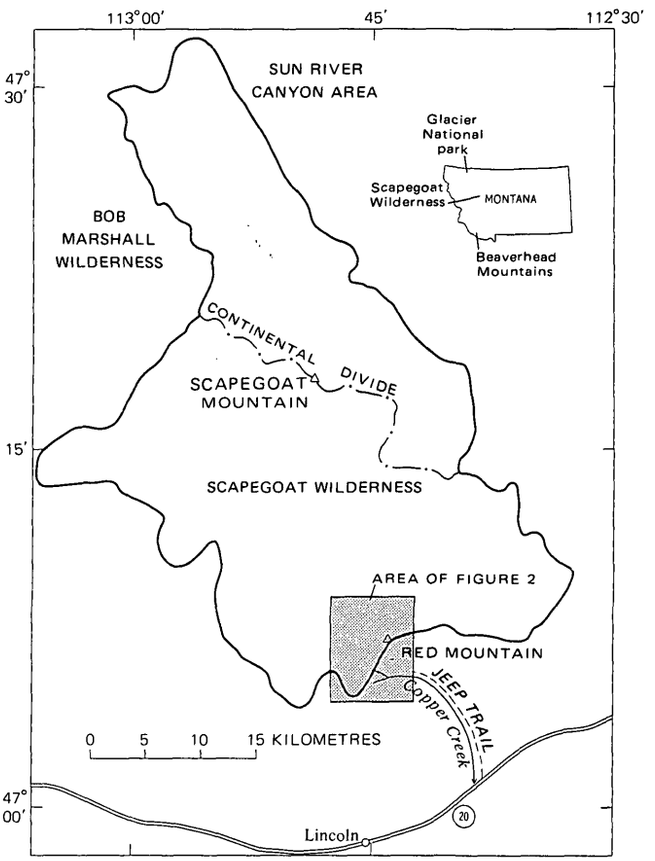

FIGURE 1.—Index map of the Red Mountain area.

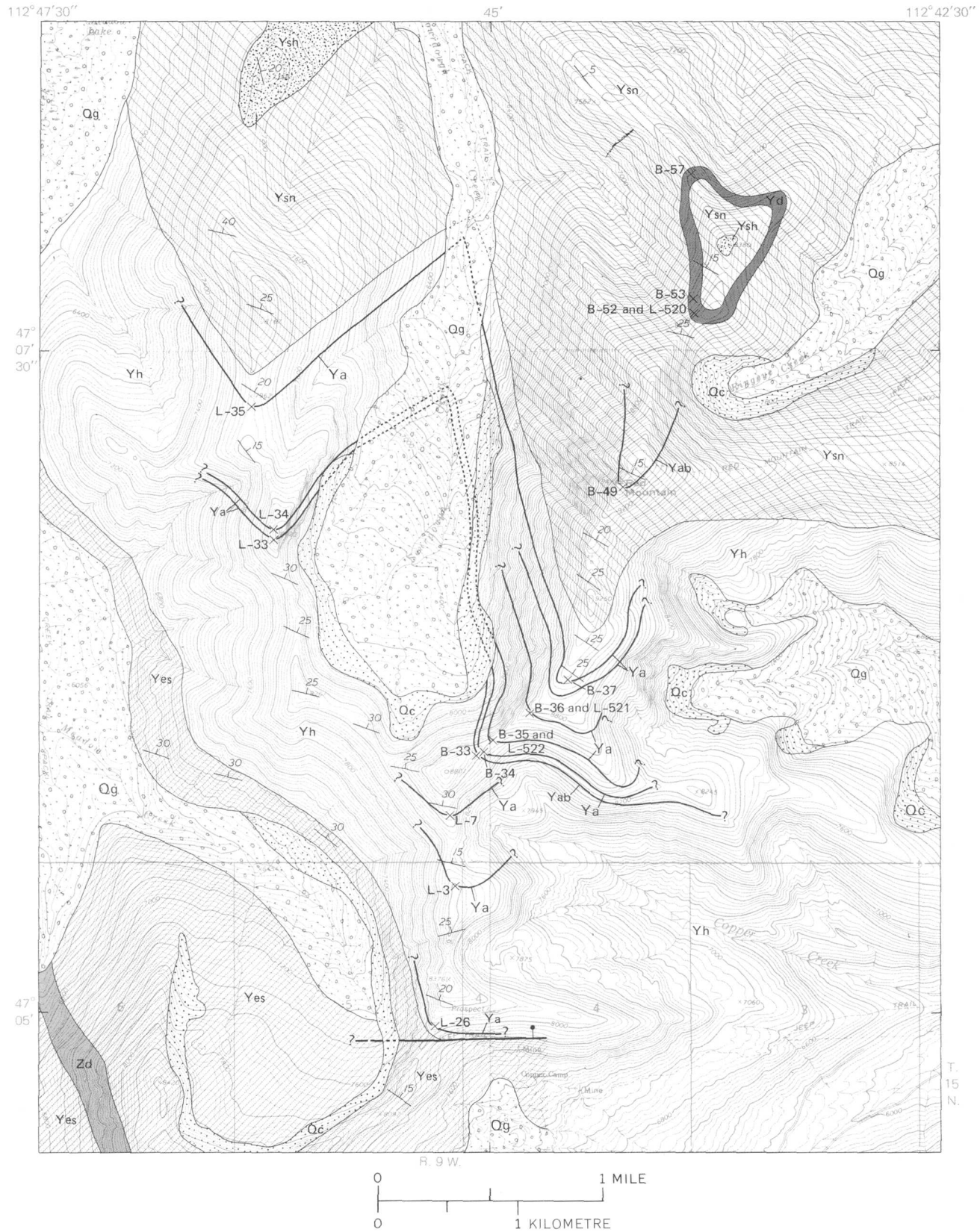

FIGURE 2.—Geologic map of the Red Mountain area, Scapegoat Wilderness. Geology mapped by M. R. Mudge and R. L. Earhart, 1970. Base from U.S. Geological Survey 1:24,000 topographic quadrangles: Olson Peak, Heart Lake, Arrastra Mountain, and Stonewall Mountain, 1968.

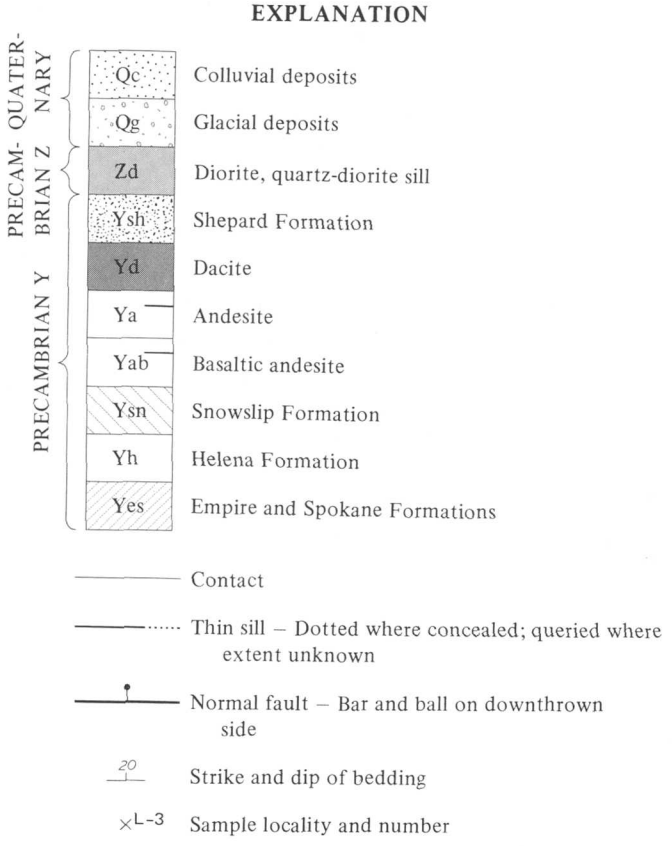

FIGURE 2.—Continued.

The geology of the Scapegoat Wilderness was mapped at a scale of 1:24,000 and compiled at a scale of 1:62,500 for inclusion in a mineral resources report (Mudge and others, 1974). The geologic map of the Red Mountain area (fig. 2) was compiled at the mapping scale and reduced for inclusion in this report. Eighteen samples were collected from 11 sills during mapping. All samples were analyzed for 30 elements by D. J. Grimes using a semiquantitative spectrographic method. Mineralogical data were obtained on 13 of the samples by X-ray diffraction methods and supplementary mineralogical information was obtained by thin-section study of some samples. The area was revisited during the summer of 1972 to collect four samples for K–Ar age determinations, including one sample from a diorite sill. These four samples were studied in thin-section; their major oxides were determined by P. L. D. Elmore using rapid-rock analytical techniques; and K–Ar age determinations were made on mineral concentrates by R. F. Marvin and H. H. Mehnert.

GEOLOGIC SETTING

The Red Mountain area is underlain by Precambrian metasedimentary rocks that form a northeastward-dipping homocline. These metasedimentary rocks are a part of the Belt Supergroup and have an accumulative thickness of approximately 16,000 ft (5,000 m). The only fault in the area is a high-angle normal fault with small displacement in the upper part of the Spokane and Empire Formations.

METASEDIMENTARY ROCKS

The metasedimentary rocks are divided into four conformable map units which from oldest to youngest are the Spokane and Empire undivided, Helena, Snowslip, and Shepard Formations, all of Precam-Y age.

The oldest rocks that are exposed in the area of figure 2 are in the Spokane Formation. They consist of reddish-brown and greenish-gray interbedded siltite and argillite with some very fine to medium-grained quartzite. The base of the unit is not exposed in the area. The Spokane is overlain by greenish-gray beds which are similar lithologically to the Spokane except that they contain increasing amounts of carbonate upward through the section. These beds are probably equivalent to the Empire Formation in the type locality at Marysville, Mont. (Knopf, 1963); however, in the Red Mountain area they contain numerous beds similar to the underlying Spokane, so the Spokane and Empire are undivided on the geologic map (fig. 2). Their total thickness is approximately 8,000 ft (2,400 m). The only fault that has a surface trace in the area occurs in the upper part of the Empire and Spokane Formations. It is a high-angle normal fault of small displacement.

The Helena Formation has a gradational contact with the underlying beds. The unit consists of thin to thick beds of impure gray dolomite and limestone with thin beds of calcareous siltite and quartzite. Stromatolites, oolites, flat-pebble conglomerates, and "molar tooth" structures are common features of the Helena. The thickness of the formation is about 5,500 ft (1,700 m).

The Snowslip Formation, which changes gradationally from the underlying Helena Formation, contains reddish-brown argillite, siltite, and fine- to medium-grained quartzite, with interlensing grayish-green beds of similar lithologies. Thin beds of limestone and limy clastic rocks are common, especially in the lower part of the formation. The unit is about 2,500 ft (760 m) thick.

Less than 100 ft (30 m) of the lower part of the Shepard Formation, a yellowish-gray silty dolomite, is exposed in the area.

The sedimentary rocks are regionally metamorphosed to the chlorite subfacies. Ferromagnesian min-

erals in the green and red beds are almost completely altered to chlorite. The color of the green beds is due to chlorite which locally comprises an estimated 5–10 percent of the rock.

SILL DESCRIPTIONS AND COMPOSITIONS

General features

Eleven sills, consisting of meta-andesite, metabasaltic andesite, and metadacite, in order of abundance, intrude the Helena and Snowslip Formations in the vicinity of Red Mountain. These sills are 2–200 ft (0.6–60 m) thick, have a maximum strike length of about 9,000 ft (2,750 m), and occur within a stratigraphic interval of about the same distance. All but the uppermost sill, which is light gray to pinkish gray, are medium to dark greenish gray. They are fine grained, porphyritic with randomly oriented minerals; the phenocrysts are about 1–6 mm long. The grain size of the metabasaltic andesite and meta-andesite sills tends to increase with sill thickness; however, the uppermost sill, which is the thickest in the sequence, has a fine-grained to subvitrophyric groundmass with phenocrysts that range in length from 3 to 10 mm.

The approximate compositional range of the sills throughout the system is 50–80 percent plagioclase, 0–25 percent orthoclase, and 5–30 percent altered amphibole, pyroxene, and biotite. In addition, the uppermost sill contains about 15 percent quartz in the groundmass. In most of this sill the predominant mafic mineral was hornblende, now mostly altered to chlorite. Two of the sills consist of metabasaltic andesite and contain 10–15 percent chloritized pyroxene and biotite. Accessory minerals in all sills include quartz, magnetite, ilmenite, apatite, and pyrite.

The thicker sills have very fine grained or aphanitic chilled zones extending 2–5 cm from the contacts. The thin sills, which are 2–5 ft (0.6–1.5 m) thick, are aphanitic throughout and chilled contacts are not megascopically detectable. One thick sill that intrudes argillaceous carbonate rocks in the Helena Formation has metamorphosed the wallrocks to calc-hornfels for a maximum of about 6 in (15 cm) above and 2 ft (60 cm) below the sill. Elsewhere contact metamorphism is either nonexistent or it is masked by the effects of regional metamorphism which has apparently altered the ferromagnesian minerals to chlorite both in the sills and in the metasedimentary rocks that enclose them.

Metabasaltic andesite

Two of the sills, represented by samples B–33 and B–49, are dark-greenish-gray metabasaltic andesite (fig. 3*B*). The groundmass is fine grained and equigranular and consists principally of randomly oriented, subhedral to euhedral crystals of plagioclase, augite, biotite, and hornblende. Moderate amounts of calcite are interstitial between the grains of the other minerals in the groundmass. The plagioclase ranges from anorthite to andesine; the average composition is An_{53} (andesine-labradorite). In places, the plagioclase is zoned from anorthite to andesine within individual crystals. The phenocrysts are predominantly biotite in grains as much as 1 mm wide and plagioclase in slender prisms as much as 2 mm long. The biotite phenocrysts are commonly highly pleochroic. The biotite, augite, and hornblende are in large part altered to chlorite. The chlorite mineral is believed to be chromiferous clinochlore, at least in part, which is reflected by the high chromium values in samples B–33 and B–49 (table 1). Accessory minerals include magnetite and ilmenite.

Meta-andesite

Eight of the sills are porphyritic meta-andesite. The groundmass contains about 60–75 percent plagioclase which ranges in composition from labradorite to oligoclase, although most of the feldspar is in the An_{35-45} range. In some sills the principal mafic mineral is biotite; in others it is hornblende. Augite was noted in sample L–522 (fig. 3*A*), and moderate amounts of calcite in sample L–521. The phenocrysts are plagioclase, biotite, and hornblende in crystals as much as 2 mm long. The ferromagnesian minerals are in large part altered to chlorite and in some sills (sample L–522) chlorite replacement is nearly complete. Locally, the plagioclase is partially altered to sericite. Accessory minerals are quartz and magnetite; a few of the sills contain trace amounts of pyrite, apatite, and ilmenite.

Metadacite

The uppermost and thickest sill is metadacite. The groundmass is extremely fine grained to subvitrophyric (fig. 3*C*) and is almost entirely feldspar (80 percent) and quartz (15 percent). The rock contains abundant phenocrysts of predominantly white to pink plagioclase and orthoclase up to 5 mm long. Mafic minerals constitute only about 5 percent of the rock and of these hornblende is the most abundant, followed by biotite.

DIORITE SILLS OF PRECAMBRIAN Z AGE

In addition to the meta-andesite and related sills, diorite sills crop out in this region. Notable occurrences have been mapped in the southern part of the

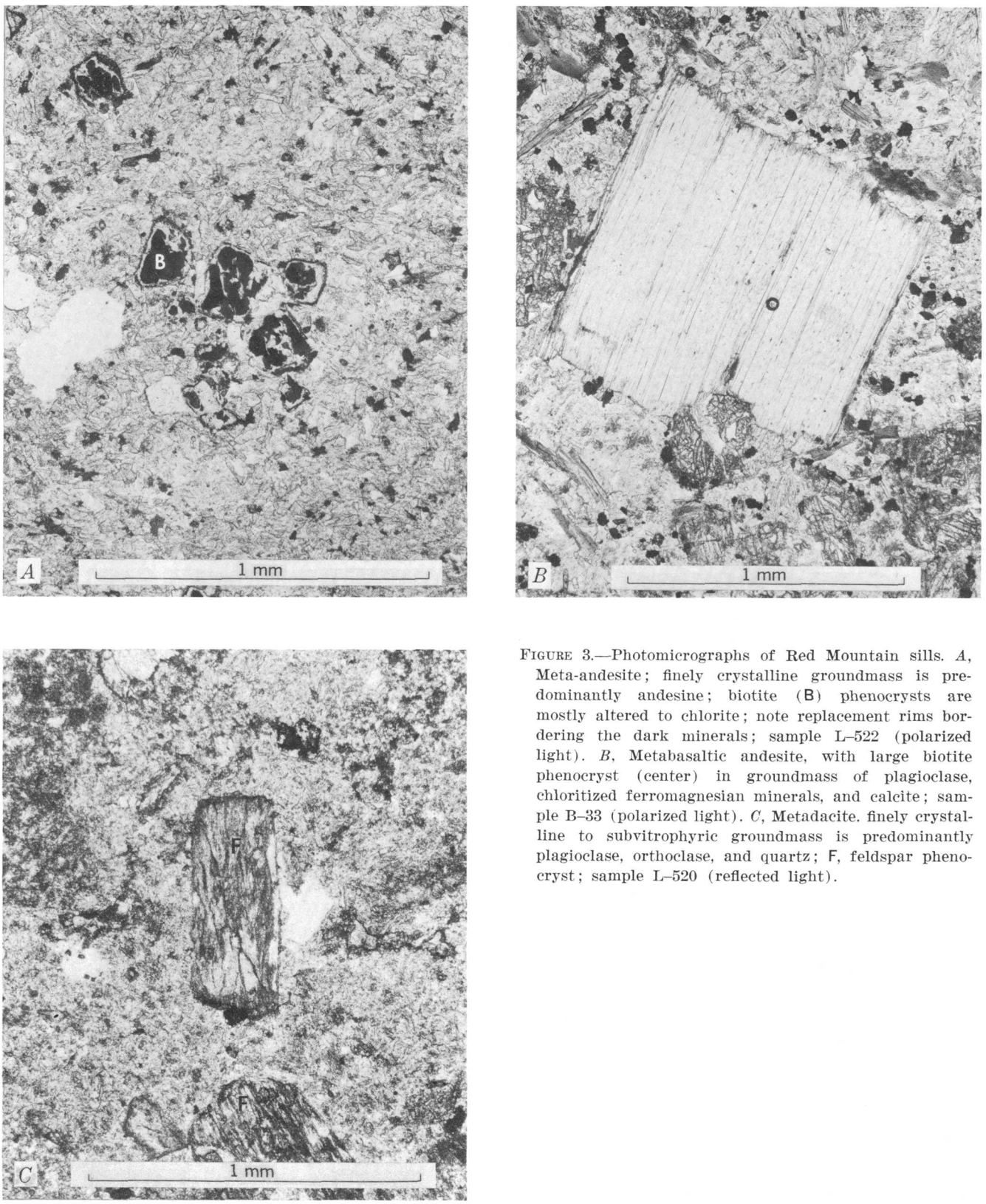

FIGURE 3.—Photomicrographs of Red Mountain sills. *A*, Meta-andesite; finely crystalline groundmass is predominantly andesine; biotite (B) phenocrysts are mostly altered to chlorite; note replacement rims bordering the dark minerals; sample L–522 (polarized light). *B*, Metabasaltic andesite, with large biotite phenocryst (center) in groundmass of plagioclase, chloritized ferromagnesian minerals, and calcite; sample B–33 (polarized light). *C*, Metadacite. finely crystalline to subvitrophyric groundmass is predominantly plagioclase, orthoclase, and quartz; F, feldspar phenocryst; sample L–520 (reflected light).

TABLE 1.—*Semiquantitative spectrographic analyses of sill and lava samples, Montana*

[All data are in parts per million except data for Fe. Mg, Ca, and Ti, which are in percent. Analysts D. J. Grimes and J. A. Domenico. ND, not detected; D, detected in amounts less than the lowest reporting step. Looked for but not found in detectable amounts: Ag, As, Au, Be, Bi, Cd, Mo, Nb, Sb, Sn, and W]

Sample No.	Fe	Mg	Ca	Ti	B	Ba	Co	Cr	Cu	La	Mn	Ni	Pb	Sc	Sr	V	Y	Zn	Zr
Sill samples from Red Mountain area																			
L–3	7	2	2	0.3	10	700	20	20	70	20	1,500	15	10	20	300	150	15	D	100
7	7	7	2	.3	ND	>5,000	30	30	30	50	1,000	20	10	20	300	150	20	D	150
26	3	1	2	.15	15	500	15	10	70	50	700	10	10	10	1,000	100	15	D	70
33	5	2	1.5	.3	D	1,500	30	15	70	ND	700	7	10	15	200	150	15	D	100
34	3	3	2	.2	D	1,000	20	70	50	20	500	15	D	15	300	100	15	D	100
35	3	1.5	2	.3	10	1,000	15	20	30	50	700	15	15	15	1,000	150	20	D	150
B–33	7	5	7	.3	ND	3,000	50	500	100	ND	1,000	70	D	30	700	150	10	D	30
34	7	3	5	.3	15	1,000	50	50	150	ND	1,000	20	D	30	200	150	15	D	50
35	7	3	5	.3	15	1,000	50	30	150	ND	700	20	15	30	300	100	15	D	50
36	5	3	3	.2	10	3,000	15	15	30	30	700	10	ND	15	300	100	10	D	70
37	7	3	2	.3	D	700	30	150	30	D	700	30	D	20	200	100	15	D	70
49	7	5	5	.3	20	700	50	500	70	20	1,000	50	D	30	1,500	150	15	D	70
52	3	1	1.5	.2	30	1,000	10	20	50	30	1,000	10	D	5	700	70	15	D	150
53	5	1	2	.2	15	1,000	10	30	50	50	1,000	10	10	7	1,500	70	15	D	150
57	5	1	1.5	.3	10	1,000	15	30	15	50	1,000	15	20	10	1,500	70	15	D	150
Sill samples from outside Red Mountain area																			
L–92	5	2	3	0.3	ND	1,000	15	30	50	30	1,500	15	20	10	1,500	100	20	D	150
397	5	1.5	2	.15	D	1,500	7	20	20	D	1,000	D	10	7	700	50	10	D	30
400	2	1	1.5	.15	D	1,000	7	10	10	20	700	5	10	5	1,000	30	10	D	70
Samples of Purcell Lava from Glacier National Park																			
PL–1	10	7	3	>1	D	1,500	50	70	700	20	700	30	50	30	D	150	70	ND	100
2	7	5	2	.2	30	300	20	50	20	20	1,500	30	15	10	ND	70	30	D	150
3	15	7	1.5	>1	D	700	50	30	30	ND	500	30	70	20	D	150	30	300	150
4	10	7	.7	>1	D	500	30	50	15	30	300	30	30	20	ND	150	30	300	150
5	15	7	.5	>1	D	3,000	30	30	15	30	300	30	ND	20	100	150	50	300	150
6	5	2	.07	.3	50	500	15	30	20	20	150	30	30	7	D	70	30	ND	150

Scapegoat Wilderness and in various parts of the Bob Marshall Wilderness to the north; similar sills are common elsewhere in northwest Montana. These sills range from a few feet to 600 ft (185 m) in thickness; some show minor quartz diorite, diorite-gabbro, gabbro, and monzonite facies (Mudge, 1972). One of these diorite sills, approximately 400 ft (123 m) thick, cuts the Spokane and Empire Formations undivided in the extreme southwest corner of the Red Mountain area (fig. 2). Commonly, these sills are medium grained and equigranular. Thin sills and chilled contacts of the thicker sills are finely crystalline, whereas centers of the thicker sills are coarsely crystalline. The diorite sills are easily distinguished from the meta-andesite sills on the basis of texture and mineralogy. Texture of the diorite is phaneritic and equigranular, whereas the texture of the meta-andesite–metadacite sills is commonly aphanitic and porphyritic. Diorite sills locally contain as much as 50 percent mafic minerals compared to 5–25 percent in the meta-andesite sills.

A K–Ar hornblende age of 750±25 m.y. was obtained for a diorite sill in the Sun River Canyon area (Mudge, 1972, p. A75). The diorite sill in the Red Mountain area gave a K–Ar hornblende age of 730±30 m.y. (table 3). These two ages suggest that the diorite sills in this region are probably all Precambrian Z in age.

CHEMICAL COMPOSITION OF THE SILLS

Eighteen samples from the sills were analyzed for 30 elements by a semiquantitative spectrographic method (table 1). The precision of this analytical method has been documented by Harrison and Grimes (1970) who concluded from replicate analyses that, except for strontium, the elements reported in table 1 have greater than 80 percent analytical precision within plus-or-minus-one reporting step. Values for strontium are probably less precise. Histograms (fig. 4) were constructed from the data shown in table 1 plus data for nine selected elements determined for diorite sills in the Scapegoat Wilderness (Mudge and others, 1974) and the Bob Marshall Wilderness (unpub. data, 1974). These histograms show the compositional differences between the meta-andesite and diorite sills for iron, titanium, and several minor elements.

The four samples collected for K–Ar age determinations were analyzed for major oxide chemistry by rapid-rock-analysis methods supplemented by atomic absorption (table 2). The feldspar norms of quartz diorite (sample L–519) reflect the difference in feld-

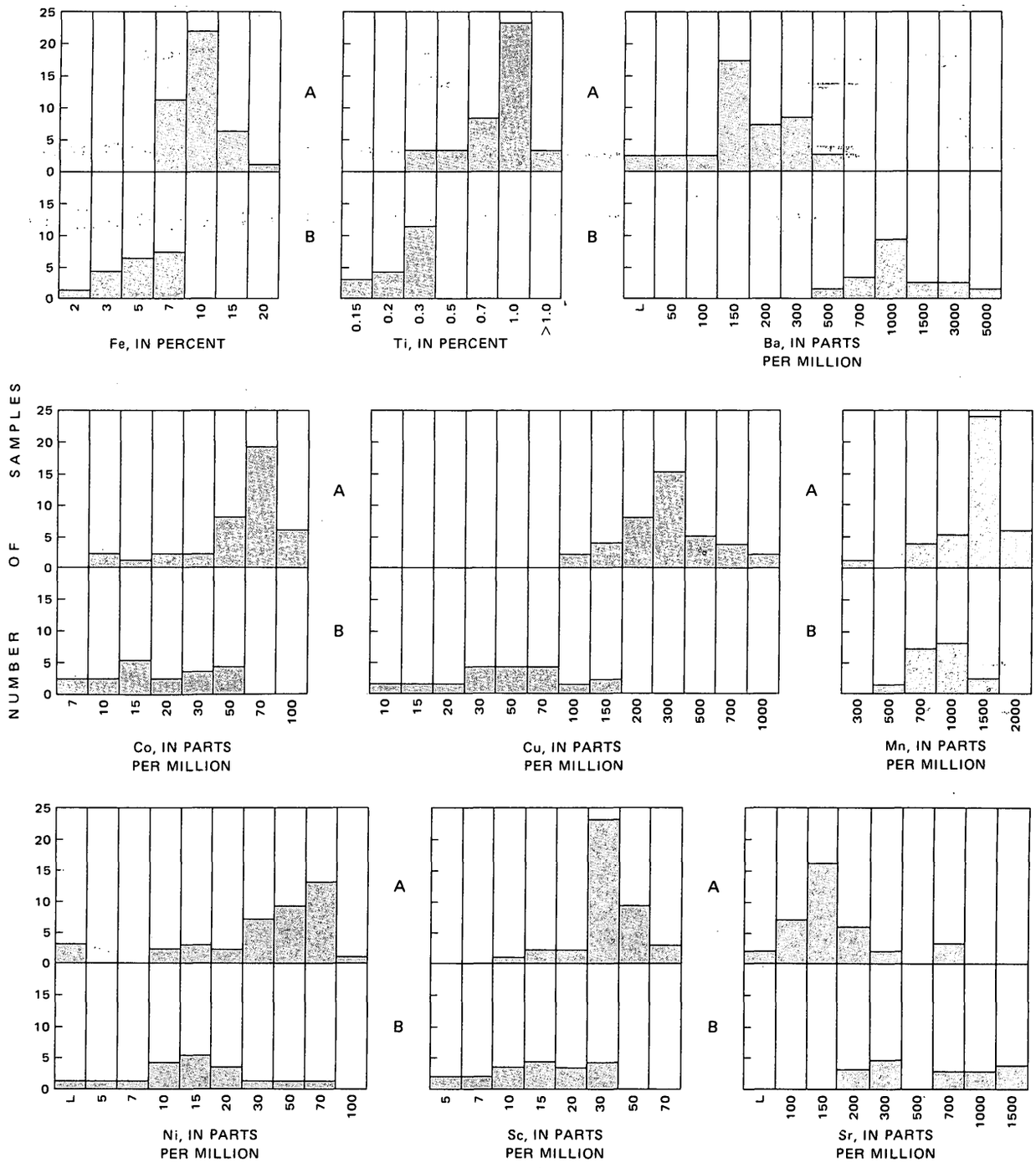

FIGURE 4.—Histograms of selected elements from diorite sills (A) and andesite sills (B). L, present but below limits of detection.

spar mineralogy between this rock type and the metaandesite and related sills. The norms of the metadacite sample (L–520) indicate the relatively high silica and low ferromagnesian content of the uppermost sill as compared to the underlying sills (samples L–521 and L–522), which are silica deficient and relatively ferromagnesian rich.

Because a possible temporal connection was suspected between the Red Mountain sills and the Purcell Lava, the latter was sampled at six localities along the Granite Chalet trail near the Continental Divide in Glacier National Park in order to compare the geochemical properties of the Purcell Lava with those of the Red Mountain sills. The semiquantitative spec-

TABLE 2.—*Analyses and norms of sills in the Red Mountain area*

[Rapid rock analysis by P. L. D. Elmore, U.S. Geological Survey. Methods used are those described by Shapiro and Brannock (1962) supplemented by atomic absorption (based on 500-mg samples). Sample numbers are given in parentheses. All data in percent]

	Quartz diorite (L–519)	Meta-dacite (L–520)	Meta-andesite (L–521)	Meta-andesite (L–522)
Chemical analyses				
SiO_2	60.0	62.9	53.0	51.8
Al_2O_3	13.6	17.4	16.7	15.6
Fe_2O_3	2.0	2.0	3.1	2.5
FeO	9.6	2.0	4.7	5.8
MgO	1.2	1.3	2.5	5.0
CaO	5.0	4.0	4.2	4.8
Na_2O	2.8	4.6	4.5	3.4
K_2O	2.2	3.0	3.8	3.0
H_2O+	1.6	1.7	2.5	3.5
H_2O-	.04	.18	.10	.23
TiO_2	1.2	.44	.92	1.0
P_2O_5	.53	.23	.64	.77
MnO	.19	.08	.11	.10
CO_2	<.05	.13	3.2	2.4
Total	100	100	100	100
CIPW norms				
Quartz	19.4	14.9	2.0	1.9
Orthoclase	12.8	17.8	22.2	17.8
Albite	23.6	38.8	38.3	28.8
Anorthite	28.1	16.7	14.2	18.3
Other	16.1	11.8	23.3	33.2
Total	100	100	100	100

trographic analyses (table 1) of these samples indicate that the lava contains more iron, magnesium and titanium but less calcium than the sills, a reflection of higher concentration of ferromagnesian minerals in the lava. There is a close geochemical correlation between the rocks of each area for the minor elements of barium, cobalt, chromium, copper, scandium, vanadium, and zirconium. Other minor elements show less correlation or none at all.

PETROGENESIS OF META-ANDESITE AND RELATED SILLS

If the sills in the Red Mountain area (except the diorite sill) are related to the same magmatic event, then the compositional variations represented by the metabasaltic-andesite, meta-andesite, and metadacite suggest that the sills differ in composition because of crystal fractionation of the parent magma, and further, that the sills were intruded in three phases. The first phase magma was iron, magnesium, calcium, and sodium rich. Calcic plagioclase and pyroxene were the first minerals to form followed by minor replacement of the pyroxene with amphibole and the formation of intermediate plagioclase. The second phase magma intruded stratigraphic horizons below, between, and above the first phase sills and contained increased amounts of sodium and potassium and lesser amounts of calcium. Early formed calcic plagioclase was replaced largely by intermediate plagioclase followed by the formation of hornblende, biotite, and potassium feldspar. The third phase magma intruded a stratigraphic horizon above the earlier sills and was deficient in iron and magnesium and contained increased amounts of potassium and silica resulting in the crystallization of soda plagioclase, minor hornblende, quartz, and potassium feldspar in proportions approximating the composition of dacite. The subvitrophyric texture of the third phase sill suggests a relatively shallow depth of intrusion.

Superposition of the sills, their short lateral continuity, and their subvolcanic character suggest that they originally occupied a position directly above the parent intrusive. However, the sills and their host rocks are part of an allochthon formed by thrust faulting that transposed basinward rocks eastward for many miles during Late Cretaceous and early Tertiary time (Mudge, 1970). As a result, the parent intrusive may be in the autochthon many miles to the west of the present position of the sills. Magnetic and gravity anomalies approximately 2 mi (3 km) southwest of the sills were discovered during the mineral investigations of the Scapegoat Wilderness, but these anomalies apparently reflect unrelated magnetite-bearing diorite sills (Mudge and others, 1974), rather than the source of the meta-andesite sills.

AGE OF THE SILLS

The results of field and mineralogical investigations suggest that the sills probably were intruded prior to regional metamorphism of the host rocks. Chloritization is a ubiquitous feature of the sills, and the degree of alteration is compatible with the chlorite subfacies metamorphic grade of the host rock. Only at one locality, where a sill is in contact with carbonate rock, was a weak development of calc-hornfels noted in the host rock. Contact metamorphism near the other sills, if it existed, has been masked by regional metamorphism.

If the Red Mountain sills predate regional metamorphism, as the degree of chloritization suggests, then they were intruded prior to the emplacement of the unmetamorphosed diorite sills, which are 730–750 m.y. old. The intrusive relationship of the Red Mountain sills indicates that they are younger than the upper part of the Snowslip Formation. The Snowslip is stratigraphically older than the McNamara Formation which has been dated at about 1,100 m.y. in the Sun River area by Obradovich and Peterman (1968). The age of the Snowslip is therefore inferred to be between 1,200 and 1,100 m.y.

As previously noted, the compositional variations of the sills suggest that they came from a common

magma source, with the compositional differences due to crystal fractionation in the magma chamber. Also, the subvitropheric texture of the metadacite suggests that intrusion occurred at a relatively shallow depth. If these assumptions are correct, then the sills were probably emplaced sometime between 1,200 and 1,100 m.y. ago.

The sills may be coeval with the Purcell Lava which is exposed in Glacier National Park, 110 mi (177 km) to the north. The Purcell Lava also occurs in the upper part of the Snowslip Formation and has been described by Daly (1912) as a chloritized andesite. It has been dated by Hunt (1962) as 1,075 m.y. old. This age is somewhat younger than that assumed for the Red Mountain sills. The difference may be due to two factors: (1) The apparent K–Ar biotite age of 1,075 m.y. may be slightly younger than the actual age of the Purcell Lava, and (2) deposition of Snowslip sediments could have continued for a longer time in the Glacier National Park area than in the Red Mountain area, thus creating a time-stratigraphic lag where intrusive and extrusive rocks of somewhat different ages occupy approximately the same stratigraphic position.

The preceding discussion of age is based mainly on the comparable degree of alteration of the host rock and the sills. It is possible that the alteration of the sills is deuteric and that the sills were intruded after regional metamorphism. To test this possibility, radiometric ages were determined by the K–Ar method for three of the sills. Owing to the altered condition of the sills, it was unlikely that the time of intrusion could be obtained. Because the biotite and other femics were extensively chloritized, sericitized feldspar concentrates were analyzed with the understanding that feldspars from intrusive sills or dikes often do not quantitatively retain radiogenic argon and thus the K–Ar age obtained would be a minimum age for the sill. The calculated K–Ar age for the metadacite sill indicates that it is at least as old as Late Triassic (202 m.y.), and the calculated K–Ar ages for two metaandesite sills indicate that they are as old as Late Pennsylvanian (283–293 m.y.) (table 3). The radiometric ages also indicate that the sills are not related to the Cretaceous igneous activity that resulted in the Elkhorn Mountains Volcanics, the Boulder batholith, and other nearby intrusives in southwestern Montana (Robinson and others, 1968; Tilling and others, 1968). Neither are they related to Cretaceous-Tertiary trachyandesite sills in the Sun River Canyon area (Mudge, 1972).

During the whole timespan of the Paleozoic and early Mesozoic, the sedimentary record indicates no igneous activity in Montana or surrounding regions (Kent, 1972) that would correlate with these apparent K–Ar ages. However, because some of the sedimentary record has been removed by erosion, evidence of a period of igneous activity may have been lost with the eroded sediments. Plutonic activity did occur about 440 m.y. ago (Scholten and Ramspott, 1968, p. 21) in the southern Beaverhead Mountains in the extreme southwestern corner of Montana. In the extreme northwestern corner of Montana, the Rainy Creek Complex of Boettcher (1967), an alkaline-ultramafic igneous complex intruded possibly as early as Permian (McDowell, 1971) or as late as Early Cretaceous (Boettcher, 1967). These areas are so far removed from the Red Mountain area that a connection with either area seems unlikely.

In summary, the combined metamorphic, radiometric, geologic, and petrologic evidence suggests that the age of the Red Mountain sills is Precambrian Y and that they may be related to the Purcell extrusive episode (Hunt, 1962). A less likely alternative is that the sills represent a Precambrian igneous event not previously recognized in the Belt basin.

TABLE 3.—*Analytical data for* K-Ar *age determinations on samples from Lewis and Clark County, Mont.*

[Constants: $K^{40}\lambda_e = 0.585\times10^{-10}yr^{-1}$; $\lambda_s = 4.72\times10^{-10}yr^{-1}$. Abundance: $K^{40} = 1.19\times10^{-4}$ atom percent. Potassium determinations made with an Instrumentation Laboratories flame photometer with a lithium internal standard. Analysts: R. F. Marvin, H. H. Mehnert, and Violet Merritt]

Sample No.	Analyzed mineral	K_2O (percent)	Radiogenic argon		Age (m.y. $\pm 2\sigma$)
			10^{-10} mol/g	Percent	
L–519--	Hornblende ---	1.26, 1.27	16.64	86	730±30
L–520--	Sericitized feldspar.	3.33, 3.30	10.46	94	202±7
L–521--	----do -------	4.25, 4.26	19.93	94	293±10
L–522--	----do -------	3.89, 3.92	17.58	95	283±10

NOTE.—Rock type and sample locality:
L–519: Quartz diorite, collected at lat 47°03′06″ N., long 112°45′58″ W., Arrastra Mountain quadrangle (outside of map area, fig. 2).
L–520: Metadacite, collected at lat 47°07′38″ N., long 112°43′50″ W., Stonewall Mountain quadrangle.
L–521: Meta-andesite, collected at lat 47°06′08″ N., long 112°44′46″ W., Stonewall Mountain quadrangle.
L–522: Meta-andesite, collected at lat 47°06′02″ N., long 112°44′58″ W., Arrastra Mountain quadrangle.

REFERENCES CITED

Boettcher, A. L., 1967, The Rainy Creek alkaline-ultramafic igneous complex near Libby, Montana—[Pt.] 1, Ultramafic rocks and fenite: Jour. Geology, v. 75, p. 526–553.

Daly, R. A., 1912, Geology of the North American cordillera at the forty-ninth parallel: Canada Geol. Survey Mem. 38, p. 207. [1915?]

Harrison, J. E., and Grimes, D. J., 1970, Mineralogy and geochemistry of some Belt rocks, Montana and Idaho: U.S. Geol. Survey Bull. 1312-O, 49 p.

Hunt, Graham, 1962, Time of Purcell eruption in southeastern British Columbia and southwestern Alberta: Alberta Soc. Petroleum Geologists Jour., v. 10, no. 7, p. 438–442.

Kent, H. C., 1972, Review of Phanerozoic history, *in* Mallory,

W. W., ed., Geologic atlas of the Rocky Mountain region: Denver, Rocky Mtn. Assoc. Geologists, p. 57–59.

Knopf, Adolph, 1963, Geology of the northern part of the Boulder bathylith and adjacent area, Montana: U.S. Geol. Survey Misc. Geol. Inv. Map I–381.

McDowell, F. W., 1971, K–Ar ages of igneous rocks from the western United States: Isochron/West, no. 2, p. 1–16.

Mudge, M. R., 1970, Origin of the disturbed belt in northwestern Montana: Geol. Soc. America Bull., v. 81, no. 2, p. 377–392.

——— 1972, Pre-Quaternary rocks in the Sun River Canyon area, northwest Montana: U.S. Geol. Survey Prof. Paper 663–A, 142 p.

Mudge, M. R., Earhart, R. L., Watts, K. C., Jr., Tuchek, E. T., and Rice, W. L., 1974, Mineral resources of the Scapegoat Wilderness, Powell and Lewis and Clark Counties, Montana, *with a section on* Geophysical surveys, by D. L. Peterson: U.S. Geol. Survey Bull. 1385–B, 82 p.

Obradovich, J. D., and Peterman, Z. E., 1968, Geochronology of the Belt Series, Montana, *in* Geochronology of Precambrian stratified rocks—Internat. Conf., Edmonton, Alberta, 1967, Papers: Canadian Jour. Earth Sci., v. 5, no. 3, pt. 2, p. 737–747.

Robinson, G. D., Klepper, M. R., and Obradovich, J. D., 1968, Overlapping plutonism, volcanism, and tectonism in the Boulder batholith region, western Montana, *in* Studies in volcanology—A memoir in honor of Howel Williams: Geol. Soc. America Mem. 116, p. 557–576.

Scholten, Robert, and Ramspott, L. D., 1968, Tectonic mechanisms indicated by structural framework of central Beaverhead Range, Idaho–Montana: Geol. Soc. America Spec. Paper 104, 71 p.

Shapiro, Leonard, and Brannock, W. W., 1962, Rapid analysis of silicate, carbonate, and phosphate rocks: U.S. Geol. Survey Bull. 1144–A, p. A1–A56.

Tilling, R. I., Klepper, M. R., and Obradovich, J. D., 1968, K–Ar ages and time span of emplacement of the Boulder batholith, Montana: Am. Jour. Sci., v. 266, no. 8, p. 671–689.

Jour. Research U.S. Geol. Survey
Vol. 3, No. 4, July–Aug. 1975, p. 425–429

AGE PROVINCES IN THE BASEMENT ROCKS OF LIBERIA

By CARL E. HEDGE, RICHARD F. MARVIN, and CHARLES W. NAESER,
Denver, Colo.

Abstract.—Fourteen new Rb-Sr ages and 17 new K-Ar ages, when combined with published ages, confirm the previous subdivision of the basement rocks of Liberia into 3 age provinces. The Liberian age province was metamorphosed and intruded 2,700 m.y. ago, but the data suggest that many of the rocks of this province are probably considerably older. The Eburnean age province was metamorphosed approximately 2,150 m.y. ago. Rocks of the Pan-African age province were originally part of the Liberian province, but underwent a relatively intense metamorphism 500 m.y. ago. The K-Ar age patterns suggest that the Pan-African province was uplifted relative to the Liberian province sometime after 500 m.y. ago, but fission-track ages of apatites indicate that any such relative vertical displacements must have occurred prior to 120 m.y. ago.

Hurley, Leo, White, and Fairbairn (1971) subdivided the basement rocks of Liberia into three age provinces. Most of the interior of Liberia, the interior of Sierra Leone, and some of the western part of Ivory Coast are underlain by basement rocks approximately 2,700 m.y. old (Liberian age province). In southeastern Liberia the basement rocks yield younger apparent ages of 1,900–2,300 m.y. (Eburnean age province). The boundary between these two age provinces has not been clearly recognized in the geological relationships. A. H. Chidester (written commun., 1974) considers the dominantly schistose terrane of southeastern Liberia to be younger than the dominantly gneissic Liberian age province; however, this geologically defined boundary does not correspond to the boundary defined by the radiometric ages (Hurley and others, 1971).

The third basement age province is in the narrow fault-bounded coastal block of west-central and northwest Liberia where radiometric ages are approximately 550 m.y.—typical of other Pan-African age belts. Both the character (C. H. Thorman, written commun., 1974) and the dating of the rocks suggest that the Pan-African province in Liberia represents a remetamorphism of the Liberian age province terrane.

This study was undertaken to provide a more detailed time framework for the evaluation of the basement rocks in Liberia. The work was done as part of a geologic exploration program undertaken cooperatively by the Liberian Geological Survey and the U.S. Geological Survey, and was sponsored by the Government of Liberia and the Agency for International Development, U.S. Department of State.

Acknowledgments.—Rock samples were provided by J. F. Seitz, C. H. Thorman, Sam Rosenblum, R. G. Tysdale, M. R. Brock, and A. H. Chidester, all of the USGS.

DATA AND DISCUSSION

Localities and descriptions of samples dated in this study, Rb-Sr data, and K-Ar data are given in tables 1, 2, and 3, respectively. Figure 1 shows the localities of and the ages obtained for samples used in this study and shows most of the ages reported by Hurley, Leo, White, and Fairbairn (1971; sample descriptions, localities, and analytical data given in Hurley and others, 1970). We have omitted a few of the published ages where the interpretations seemed ambiguous. For example, several of the samples whose analyses are given by Hurley, Leo, White, and Fairbairn (1970) are so poor in radiogenic Sr^{87} that their ages cannot truly be assigned independently.

The new ages from the Liberian age province support the conclusion of Hurley, Leo, White, and Fairbairn (1971) that this terrane went through a period of regional metamorphism and was locally intruded by granitic rocks about 2,700 m.y. ago. However, on several important aspects of the evolution of the Liberian province we disagree with Hurley, Leo, White, and Fairbairn. They interpreted the scatter of their whole-rock Rb-Sr ages in northwestern Liberia as being due to effects induced by the nearby Pan-African event approximately 550 m.y. ago. We conclude that much of the age scattering in the Liberian province results because many of the rocks are significantly older than 2,700 m.y.; the only post-2,700-m.y. effects we see in the

TABLE 1.—*Sample localities and descriptions*

[In the field numbers, letters identify the collectors, as follows: SZ, J. F. Seitz; RO, Sam Rosenblum; TN, C. H. Thorman; TY, R. G. Tysdale; and BC, M. R. Brock and A. H. Chidester]

Sample	Field No.	Locality		Rock type
		Lat N.	Long W.	
1	SZ–65B	8°20′	10°10′	Mafic dike.
2	SZ–67D	8°23′	9°48′	Basalt flow.
3	RO–231E	8°01′	9°36′	Granite.
4	RO–129D	7°06′	8°59′	Metanorite.
5	TN–101A	6°45′	11°20′	Norite.
6	TN–94A–1	6°54′	10°55′	Amphibolite.
7	TN–94A–2a	6°54′	10°55′	Granodioritic gneiss.
8	TN–94A–2b	6°54′	10°55′	Do.
9	TN–94A–3	6°54′	10°55′	Granitic gneiss.
10	TN–100A	6°49′	10°20′	Quartz-biotite schist.
11	TN–100B	6°49′	10°20′	Granitic gneiss.
12	TN–100C	6°49′	10°20′	Do.
13	RO–241B	6°23′	10°34′	Mafic granulite gneiss.
14	TN–86E–1	6°18′	10°21′	Amphibolite.
15	TN–86E–2a	6°18′	10°21′	Granitic gneiss.
16	TN–86E–2b	6°18′	10°21′	Do.
17	TY–107E	5°57′	9°58′	Amphibolite.
18	RO–230B	6°02′	9°52′	Charnockite.
19	TY–116A	5°25′	9°36′	Diorite dike.
20	TY–390A	5°21′	8°54′	Syenite stock.
21	BC–13C–1	4°22′	7°44′	Felsic gneiss.
22	BC–13C–2	4°22′	7°44′	Amphibolite.

TABLE 2.—*Rubidium-strontium analytical data*

[See table 1 for sample localities and descriptions. Age calculated assuming an initial Sr^{87}/Sr^{86} value of 0.703. Analysts: C. E. Hedge, R. A. Hildreth, and W. H. Henderson. Constants: Rb^{87} $\lambda_\beta = 1.39 \times 10^{-11}$/yr, $Rb^{87} = 0.283$ g/g Rb]

Sample	Material analyzed	Rb (ppm)	Sr (ppm)	Rb^{87}/Sr^{86}	Sr^{87}/Sr^{86}	Age (m.y.)
3	Granite	80.9	250.0	0.9400	0.7429	2,950
6	Amphibolite	49.3	257.0	.5563	.7145	1,470
7	Gneiss	144.0	232.0	1.811	.7842	3,160
8	do	87.0	302.0	.8367	.7422	3,290
9	do	116.0	181.0	1.879	.7825	2,980
10	Schist	203.0	9.6	84.51	3.995	2,750
11	Gneiss	90.5	186.0	1.420	.7702	2,750±50
11	Microcline	288.0	265.0	3.189	.8142	1,760±50
11	Plagioclase	83.0	257.0	.9389	.7589	1,760±50
12	Gneiss	98.8	16.5	18.60	1.4392	2,750±50
13	Granulite	1.9	448.0	.0125	.7052	Indeterminate
15	Gneiss	69.1	146.0	1.371	.7195	480±60
16	do	104.0	175.0	1.730	.7219	480±60
18	Charnockite	71.2	295.0	.6991	.7302	2,750

TABLE 3.—*Potassium-argon analytical data*

[See table 1 for sample localities and descriptions. K_2O values are the average of two or more determinations made with an Instrumentation Laboratories flame photometer with a lithium internal standard; analysts, L. B. Schlocker and Violet Merritt (samples 2 and 3). Radiogenic argon analyzed by R. F. Marvin and H. H. Mehnert. Constants: K^{40} $\lambda_\epsilon = 0.585 \times 10^{-10}$/yr, $\lambda_\beta = 4.72 \times 10^{-10}$/yr; atomic abundance, $K^{40} = 1.19 \times 10^{-4}$]

Sample	Material analyzed	K_2O (percent)	Radiogenic Ar^{40}		Age (m.y. $\pm 2\sigma$)
			10^{-10} mol/g	Percent	
1	Hornblende	1.123	110.1	100	2,850±60
2	Whole rock	.28	1.984	87	428±44
3	Biotite	8.56	437.6	99	1,960±70
4	Hornblende	.413	26.03	98	2,230±60
5	Plagioclase	.158	1.125	83	429±12
6	Hornblende	.780	37.66	99	1,900±50
10	Biotite	8.95	447.8	99	1,940±40
13	Hornblende	1.751	15.30	97	515±11
14	do	.824	7.520	92	535±15
15	Biotite	8.66	70.32	96	483±11
17	Hornblende	1.246	10.62	95	504±11
19	Biotite	9.24	73.05	96	472±10
19	Hornblende	1.393	10.88	98	467±10
20	Biotite	8.88	86.43	97	566±12
21	do	9.05	411.3	99	1,830±40
21	Hornblende	.956	49.16	99	1,970±60
22	do	.431	19.46	96	1,820±50

Liberian province are not Pan-African in age, but correspond to the Eburnean event.

Hurley, Leo, White, and Fairbairn (1971) published an isochron age of 2,650 m.y. for a group of granitic and gneissic rocks from northern Liberia. We obtained 2,750-m.y. ages from a schist (sample 10) and from two granitic gneisses (samples 11 and 12), all from the Bong Mine iron deposit. These results indicate that the iron-formation is at least 2,750 m.y. old. The charnockite sample (No. 18) also has a 2,750-m.y. age. Our other ages from the Liberian province are older, however. The metamorphosed mafic dike (sample 1) and granite sample (No. 3) yield ages of 2,850 and 2,950 m.y. respectively. Four samples from the Bomi Hills iron mine (Nos. 6, 7, 8, and 9) have discordant ages, but the granodiorite gneiss may be as old as 3,200 m.y. and the granitic gneiss, 3,000 m.y.

The possible antiquity of these gneisses is illustrated in figure 3. The Sr^{87}/Sr^{86} ratios have been extrapolated back in time, in proportion to their Rb^{87}/Sr^{86} ratios. At 2,750 m.y. many of the samples had Sr^{87}/Sr^{86} ratios considerably higher than the mantle value at that time, indicating a pre-2,750-m.y. crustal history. We suggest that a continental crust formed about 3,200 m.y. ago and that the iron-formation and associated metasedimentary and metavolcanic rocks were deposited sometime during the interval from 3,200 to 2,750 m.y. ago. The entire assemblage was then folded, metamorphosed, and intruded by granitic rocks 2,750 m.y. ago.

At this time, our knowledge is not sufficient to develop a meaningful interpretation of the extent and geologic history of the Eburnean age province. Besides the general lack of data bearing on the problem there is the paradox of the lithological-geophysical boundary not corresponding with the few age determinations. Hurley, Leo, White, and Fairbairn (1970) obtained whole-rock Rb-Sr ages of about 2,100 m.y. for four samples of granites and gneisses from a belt northwest of the lithological-geophysical boundary. We can see no reason to discount these four ages. We can only suggest that granites and granitic gneisses of 2,100-m.y. age are lithologically and geophysically too similar to 2,700-m.y.-age rocks to be distinguished by reconnaissance-type studies. The boundary between the Liberian and Eburnean age provinces may be approximately where Hurley, Leo, White, and Fairbairn (1971) suggested; but any detailed delineation of the boundary must consider the fact that the northwestern

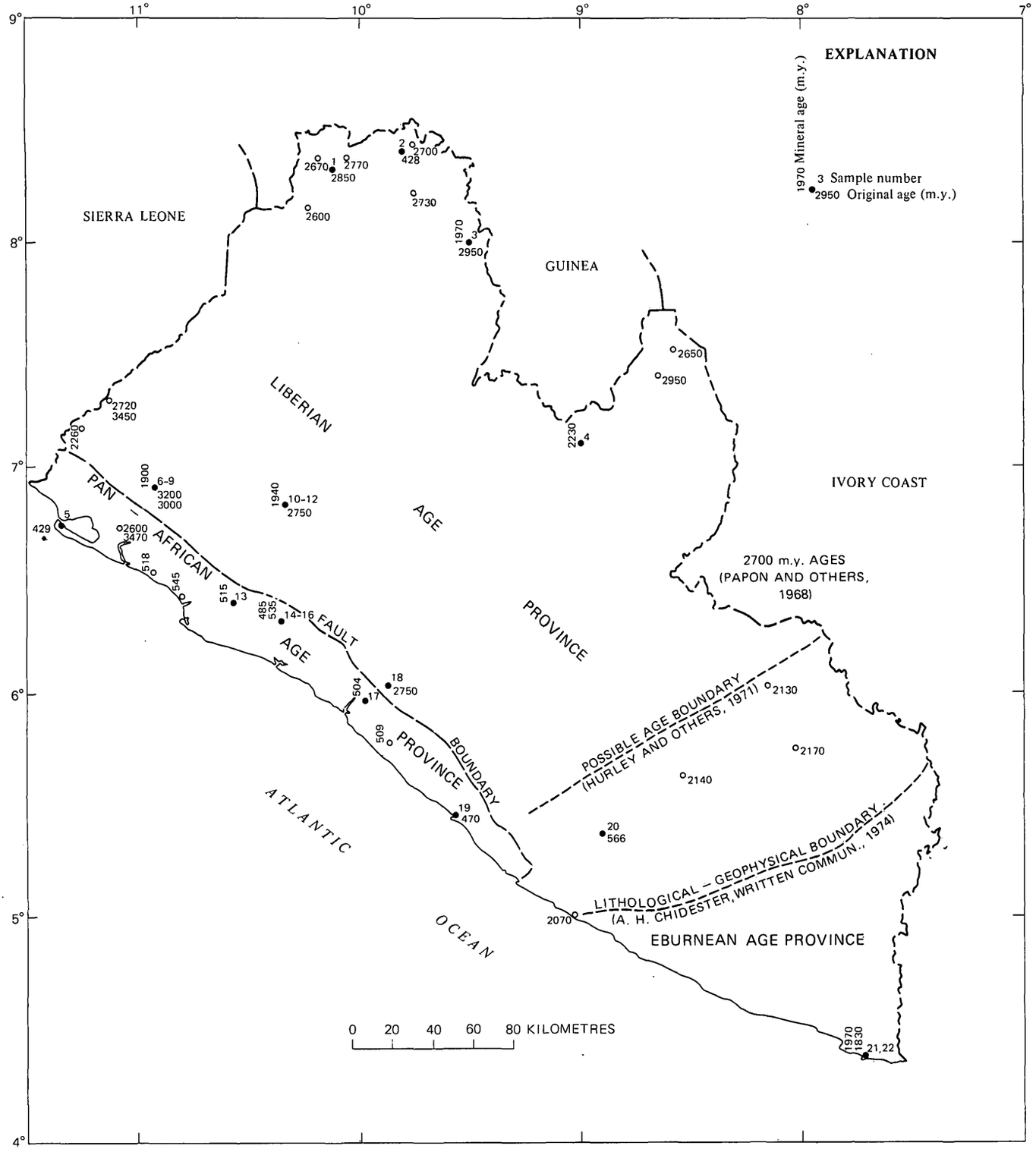

FIGURE 1.—Map of Liberia showing sample localities and ages. Solid circles indicate data from present study; open circles, data from Hurley, Leo, White, and Fairbairn (1970). Except for a few K-Ar mineral ages on essentially unmetamorphosed igneous rocks, horizontally written ages are whole-rock Rb-Sr ages and are believed to represent approximate age of the rock; vertically written ages are mineral ages believed to reflect later thermal effects.

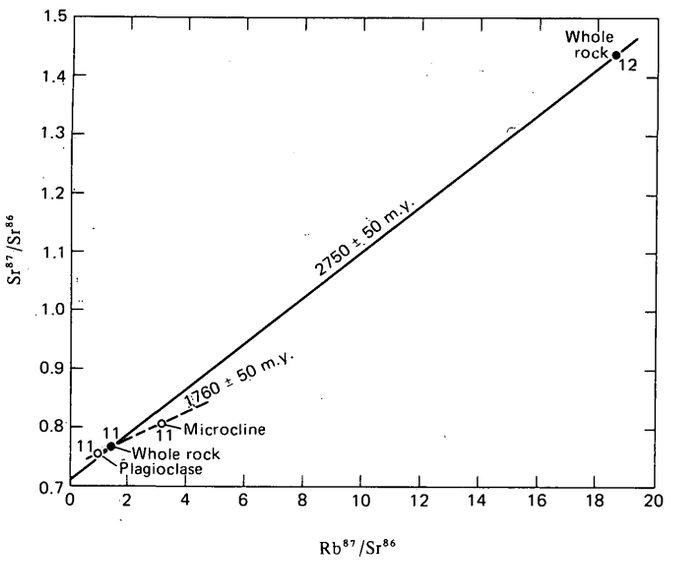

FIGURE 2.—Isochron plot of Rb-Sr data for samples 11 and 12 and feldspar separates from sample 11.

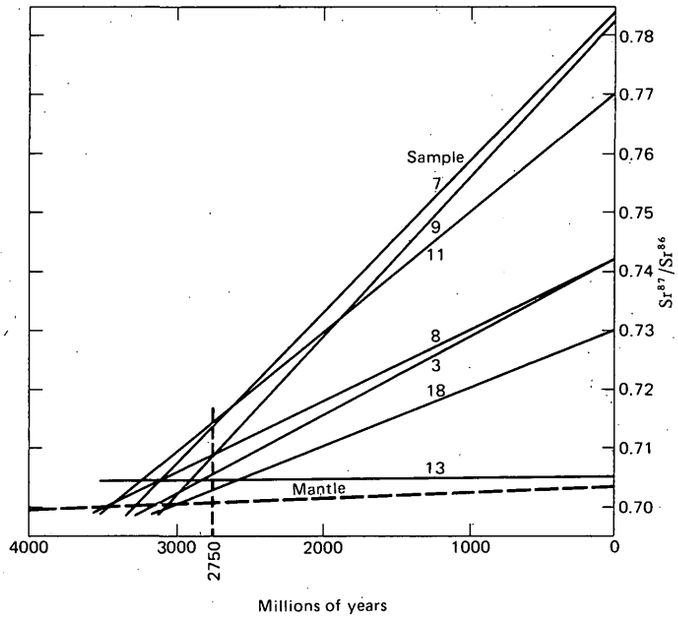

FIGURE 3.—Sr^{87}/Sr^{86} evolution diagrams.

part of the Eburnean age province in Liberia is lithologically similar to the Liberian age province (dominantly gneissic rocks), although the southeastern part of the Eburnean age province is dominantly schistose.

Whatever the nature or position of the Liberian-Eburnean boundary, the exact age of the Eburnean province rocks is still in question. Besides the ages by Hurley, Leo, White, and Fairbairn (1970), we have K-Ar mineral ages of 2,230–1,830 m.y. in both the Eburnean and Liberian provinces. Dating to the east of Liberia (Legrand, 1971; Grant, 1970; Brunnschweiler, 1974) indicates a fairly distinct period of igneous and metamorphic activity 2,100–2,200 m.y. ago. This time period corresponds to the whole-rock Rb-Sr ages measured by Hurley, Leo, White, and Fairbairn (1970) in Liberia. The time interval from 2,100 to 2,200 m.y., therefore, appears to represent the correct age assignment for Eburnean igneous and metamorphic activity. The wide range in K-Ar mineral ages (2,100–1,830 m.y.) is probably the result of uplift and cooling following the 2,100- to 2,200-m.y. event.

C. H. Thorman (written commun., 1974) considers the Pan-African province to be a remetamorphosed block of the Liberian province. This interpretation is supported by apparent whole-rock Rb-Sr ages of 2,600 and 3,470 m.y. determined by Hurley, Leo, White, and Fairbairn (1970) from within the Pan-African age province in western Liberia. We did Rb-Sr analyses of two adjacent gneiss samples (Nos. 15 and 16) that were interpreted as having been "sweated out" of a thick amphibolite sequence. The results indicate that the gneisses formed 480±60 m.y. ago from material of indeterminate, but significantly older, age.

Pan-African age igneous activity is indicated by a sample from a basalt flow (No. 2) in the northern part of the Liberian age province and by one from a syenite stock (No. 20) in the Eburnean age province. A norite body (sample 5) and a diorite dike (sample 19) indicate igneous as well as metamorphic activity within the Pan-African age province. The age of the norite could be determined only on plagioclase and hence may be somewhat low.

Surprisingly, other than the two igneous rocks just-mentioned, there appears to be no manifestation of this relatively profound geological event in the adjacent older provinces. For example, hornblende and biotite from sample localities 6 and 10 give K-Ar ages of 1,900 and 1,940 m.y.—similar to ages in the distant Eburnean province—and sample 6 is only 12 km from the Pan-African province boundary. This lack of evidence in rocks of the older terranes of effects caused by the Pan-African event suggests that there was probably very significant movement on the faults which bound the Pan-African province (Thorman, 1972). It is possible, for instance, that 500 m.y. ago the Pan-African province rock was deep (and hot) while the rocks of the adjacent provinces were nearer the surface. According to this hypothesis, subsequent uplift along the boundary faults would then have brought the respective blocks into their present juxtaposition.

In hopes of testing such a hypothesis, we determined fission-track ages on apatites from six samples—three from the Pan-African age province and three from the adjacent Liberian age province. Fission tracks in apa-

tites will be annealed at temperatures ranging from about 100° to 150°C (Naeser and Faul, 1969). Fission-track ages of apatite should therefore reflect the time at which a rock was uplifted to within about 3 km of the surface. The ages obtained for these six apatites are essentially the same—about 120 m.y. (table 4). That is, during Cretaceous time, the Pan-African and Liberian age provinces were in juxtaposition and together were uplifted to within 3 km of the surface.

TABLE 4.—*Fission-track data*

[ρs, fossil tracks/cm^2; ρi, induced tracks/cm^2; ϕ, neutrons/cm^2; T, years $\pm\sigma$; λ, 6.85×10^{-17}/yr. Numbers shown in parentheses represent total number of tracks counted. Analyst: C. W. Naeser]

Sample No.	$\rho s\times10^5$	$\rho i\times10^5$	$\phi\times10^{15}$	$T\times10^6$
6	9.34(772)	8.47(713)	1.67	112±11
10	8.33(902)	7.71(1,607)	1.69	111±11
13	1.94(404)	1.63(340)	1.70	123±12
14	1.85(385)	1.75(364)	1.66	107±11
17	1.69(352)	1.37(286)	1.72	128±13
18	2.58(538)	2.05(428)	1.71	131±13

REFERENCES CITED

Brunnschweiler, R. O., 1974, New K-Ar age determinations from the West African shield in the Niger Republic: Geology, v. 2, p. 17–20.

Grant, N. K., 1970, Geochronology of Precambrian rocks from Ibadan, southwestern Nigeria: Earth and Planetary Sci. Letters, v. 10, p. 29–38.

Hurley, P. M., Leo, G. W., White, R. W., and Fairnbairn, H. W., 1970, The Liberian age province (ca. 2700 m.y.) and adjacent provinces in Liberia and Sierra Leone, *in* Hurley, P. M., ed., Variations in isotopic abundances of strontium, calcium and argon and related topics: Massachusetts Inst. Technology 18th Ann. Prog. Rept. to U.S. Atomic Energy Comm., no. 1381–18, p. 17–37.

———1971, Liberian age province (about 2,700 m.y.) and adjacent provinces in Liberia and Sierra Leone: Geol. Soc. America Bull., v. 82, p. 3483–3490.

Legrand, J. M., 1971, Presidions sur l'evolution du cycle birrimian obtenue par de nouvelles mesures d'ages par la methode U/Pb sur des zircons de granites eburneens de Haute Volta [with English summ.]: Soc. Geol. Belgique Annales, v. 94, p. 237–248.

Naeser, C. W., and Faul, H., 1969, Fission track annealing in apatite and sphene: Jour. Geophys. Research, v. 74, p. 705–710.

Papon, Andre, Roques, Maurice, and Vachette, Michelle, 1968, Age de 2700 millions d'annees, determine par la methode au strontium, pour la serie charnockitique de Man, en Cote-d'Ivoire: Acad. Sci. Comptes Rendus, ser. D, v. 266, p. 2046–2048.

Thorman, C. H.. 1972. The boundary between the Pan-African and the Liberian age provinces, Liberia, West Africa: Geol. Soc. America Abs. with Programs, v. 4, no. 7, p. 690.

Jour. Research U.S. Geol. Survey
Vol. 3, No. 4, July–Aug. 1975, p. 431–436

ORDOVICIAN AND MIDDLE SILURIAN ROCKS OF THE WILDHORSE WINDOW, NORTHEASTERN PIONEER MOUNTAINS, CENTRAL IDAHO

By JAMES H. DOVER and REUBEN JAMES ROSS, Jr., Denver, Colo.

Abstract.—Along Wildhorse Creek in the northeastern Pioneer Mountains, autochthonous Ordovician and Silurian rocks of an eastern carbonate assemblage are exposed in a structural window through allochthonous flysch deposits of the Mississippian Copper Basin Group. Graptolite-bearing Middle and Upper Ordovician dolomite and cherty dolomite 210 ft (64 m) thick are lithologically and faunally similar to the Hanson Creek Formation of central Nevada and the Saturday Mountain Formation of central Idaho. *Monograptus*-bearing Middle Silurian platy limestone at least 130 ft (40 m) thick resembles the Roberts Mountains Formation of central Nevada and rocks improperly designated Trail Creek Formation in the Bayhorse region of central Idaho. Allochthonous age-equivalent units of a more western transitional assemblage (the type Phi Kappa and Trail Creek Formations) occur 5 mi (8 km) west of the Wildhorse window, along the crest of the Pioneer Mountains.

In the northeastern Pioneer Mountains of central Idaho, two small structural windows through the allochthonous upper Paleozoic Copper Basin Group of Paull and others (1972) are known informally as the Wildhorse and Dry Canyon windows (figs. 1, 2). This paper describes autochthonous Ordovician and Silurian rocks exposed in part of the Wildhorse window. The Ordovician strata are similar lithologically and faunally to the Hanson Creek Formation of the Monitor and Toquima Ranges of central Nevada and to the Saturday Mountain Formation as generally understood in central Idaho (C. P. Ross, 1937, 1947). The Silurian strata resemble the Roberts Mountains Formation of central Nevada and the so-called Trail Creek Formation at Malm Gulch, 32 mi (53 km) to the north, in the Bayhorse region of central Idaho (Ross, 1937).

W. B. N. Berry examined all graptolite collections to verify graptolite identifications made by R. J. Ross. Conodonts were prepared and examined by L. A. Wilson and J. W. Huddle.

PALEOZOIC SEQUENCES OF THE PIONEER MOUNTAINS REGION

In the Pioneer Mountains region, major thrusting of late Mesozoic age has modified Paleozoic depositional and orogenic patterns (Dover, 1969). Although general paleofacies distribution has been discussed or inferred by Scholten (1957), Thomasson (1959), Ross (1962), Churkin (1962), and King (1969), accurate reconstruction of Paleozoic facies patterns still is hindered in this region by the areal extent of allochthonous cover, by uncertainties as to the amount and time(s) of facies telescoping by thrusting, and by extensive intrusion and postthrusting volcanism. Even so, some authors, most notably Churkin (1962) and

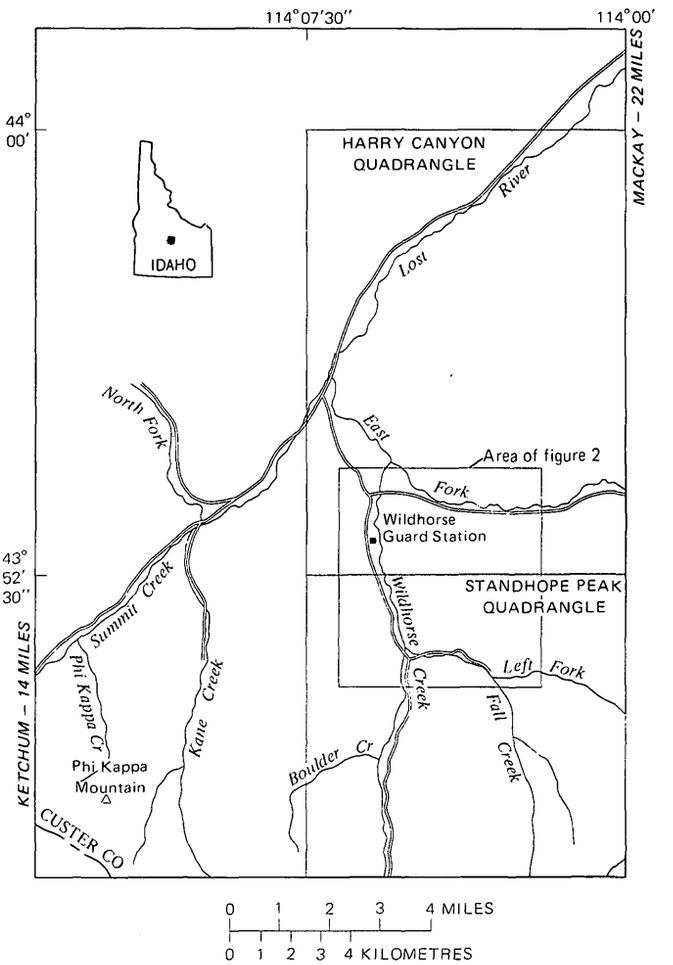

FIGURE 1.—Map of part of the Pioneer Mountains, central Idaho.

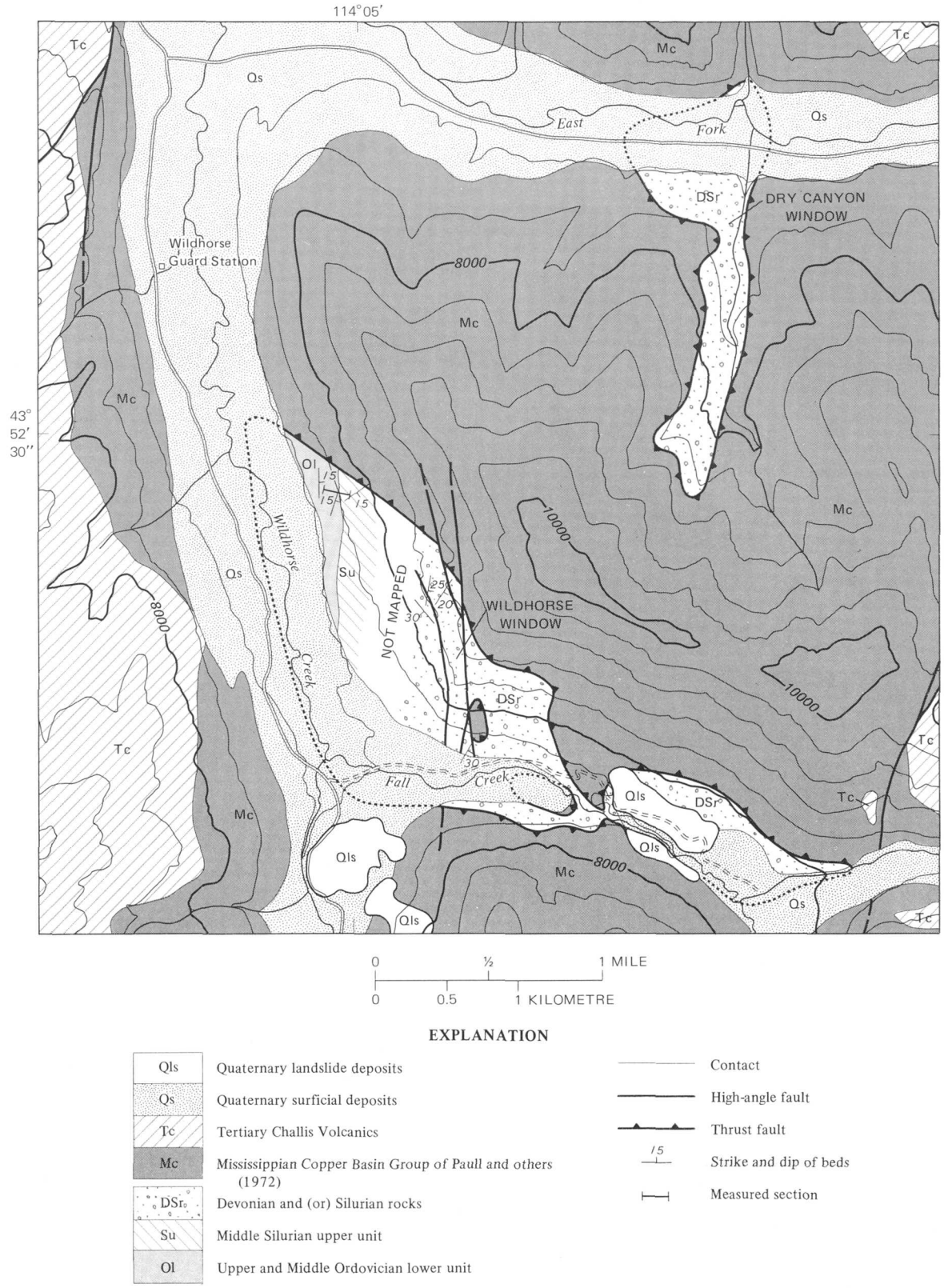

FIGURE 2.—*Geologic map of the Wildhorse and Dry Canyon windows. Geology mapped in 1973. Base from parts of the U.S. Geological Survey Harry Canyon and Standhope Peak 7½-minute topographic quadrangles, 1967.*

Roberts and Thomasson (1964), have been impressed by a remarkable similarity of the Paleozoic stratigraphic framework of central Idaho to that of the Antler belt in Nevada.

Autochthonous(?) lower and middle Paleozoic rocks of the Lost River Range, 20–30 mi (32–48 km) east of the Pioneers, include Ordovician Kinnikinic Quartzite and Saturday Mountain Formation, Silurian Laketown Dolomite, and Devonian Jefferson and Grand View Dolomites and Three Forks Limestone (Mapel and others, 1965). This assemblage of fairly clean carbonates and quartzites represents an eastern carbonate assemblage (according to the usage of Roberts, 1964) that probably was deposited nearer the craton than were similar rocks in central Nevada.

Lower and middle Paleozoic rocks of the Wood River region 15 mi (24 km) to the west and the western Pioneer Mountains all are allochthonous; these include quartzite and black graptolitic slate and shale of the Ordovician Phi Kappa and Silurian Trail Creek Formations, and dark phyllitic argillite and subordinate limestone of the Devonian Milligen Formation (Umpleby and others, 1930; Churkin, 1962, 1963; Dover, 1969; studies by C. A. Sandberg, W. E. Hall, and J. N. Batchelder, in U.S. Geological Survey, 1973, p. 167). These rocks generally are regarded as transitional between the eastern carbonate assemblage and a western siliceous and volcanic assemblage (Roberts, 1964) inferred to have been deposited in and (or) west of the area now occupied by the Idaho batholith.

In the eastern Pioneer Mountains the transitional assemblage and the eastern carbonate assemblage are separated by a thick thrust sheet of dominantly clastic Mississippian rocks correlative with the Copper Basin Group of Paull and others (1972). (New unpublished paleontological data suggests that the upper rocks of the Copper Basin Group questionably assigned a Pennsylvanian age by Paull and others (1972) are more likely Mississippian in age. Thus we regard the type Copper Basin Group as entirely Mississippian.) The amount of eastward transport of the Copper Basin Group allochthon is uncertain but may be considerable.

The Ordovician and Silurian strata described herein represent a part of the eastern carbonate assemblage that is exposed in a small window through the Copper Basin Group allochthon. In the absence of positive stratigraphic, petrologic, or local mapping evidence for major internal thrusting, the Wildhorse window sequence is considered to be essentially autochthonous or possibly parautochthonous. Minor shearing can be observed locally along at least one lithologic contact between units of widely contrasting competence in a structurally high part of the window, but that same contact generally is depositional and unsheared elsewhere along strike. Contrary to the report of Paull and Rothwell (1973), we find no place, within the window, where older stratigraphic units are thrust over younger. Moreover, minor high-angle faults and gentle warping as reflected by bedding attitudes within the window can be readily explained by drag related to the overriding Copper Basin Group allochthon and (or) postthrusting high-angle faults that cut the window.

WILDHORSE WINDOW ROCKS

Previous work

The rocks of the Wildhorse window were first assigned to the Permian and Pennsylvanian Wood River Formation by Umpleby, Westgate, and Ross (1930, pl. 1). Roberts and Thomasson (1964, fig. 122.3*B*) included the window rocks in undifferentiated Mississippian rocks. Dover (1969, p. 33) recognized (1) that the window rocks are tectonically overlain by dominantly clastic rocks now correlated with the Copper Basin Group, and (2) that the Wildhorse carbonate units are lithloogically distinct from other carbonate units of the central and western Pioneer Mountains, but he did not separately map the window carbonates and allochthonous Mississippian carbonates of the eastern Pioneers. B. G. Rothwell (Univ. Wisconsin, Milwaukee) has mapped in an area that includes the Wildhorse window. Preliminary thicknesses and age assignments of both the Wildhorse and Dry Canyon window rocks were reported by Paull and Rothwell (1973). Our subsequent work in the summer of 1973 shows their data to be incomplete and forms the basis of this report.

Measured section

A total of 340 ft (103.8 m) of section (fig. 3) was measured in gently southeastward dipping beds on the east side of Wildhorse Creek, 1.2 mi (2 km) north of the junction of Fall Creek (Idaho coordinates, central zone: E 477,500 ft, N 802,560 ft; UTM coordinates, zone 11: E734,180 m, N4,861,220 m). Exposures appear to be limited to the northwestern corner of the window (fig. 2). The section is incomplete, because the rocks above and below are covered. Two mappable units are present (fig. 3)—a lower unit of Middle to Upper Ordovician dolomite and cherty dolomite and an upper unit of Middle Silurian cherty dolomite and massive to platy limestone. Only these units, which represent the stratigraphically and structurally lowest part of the Wildhorse window section, were studied in detail. The lower unit resembles the Hanson Creek Formation (Nolan and others, 1956) and the Saturday Mountain

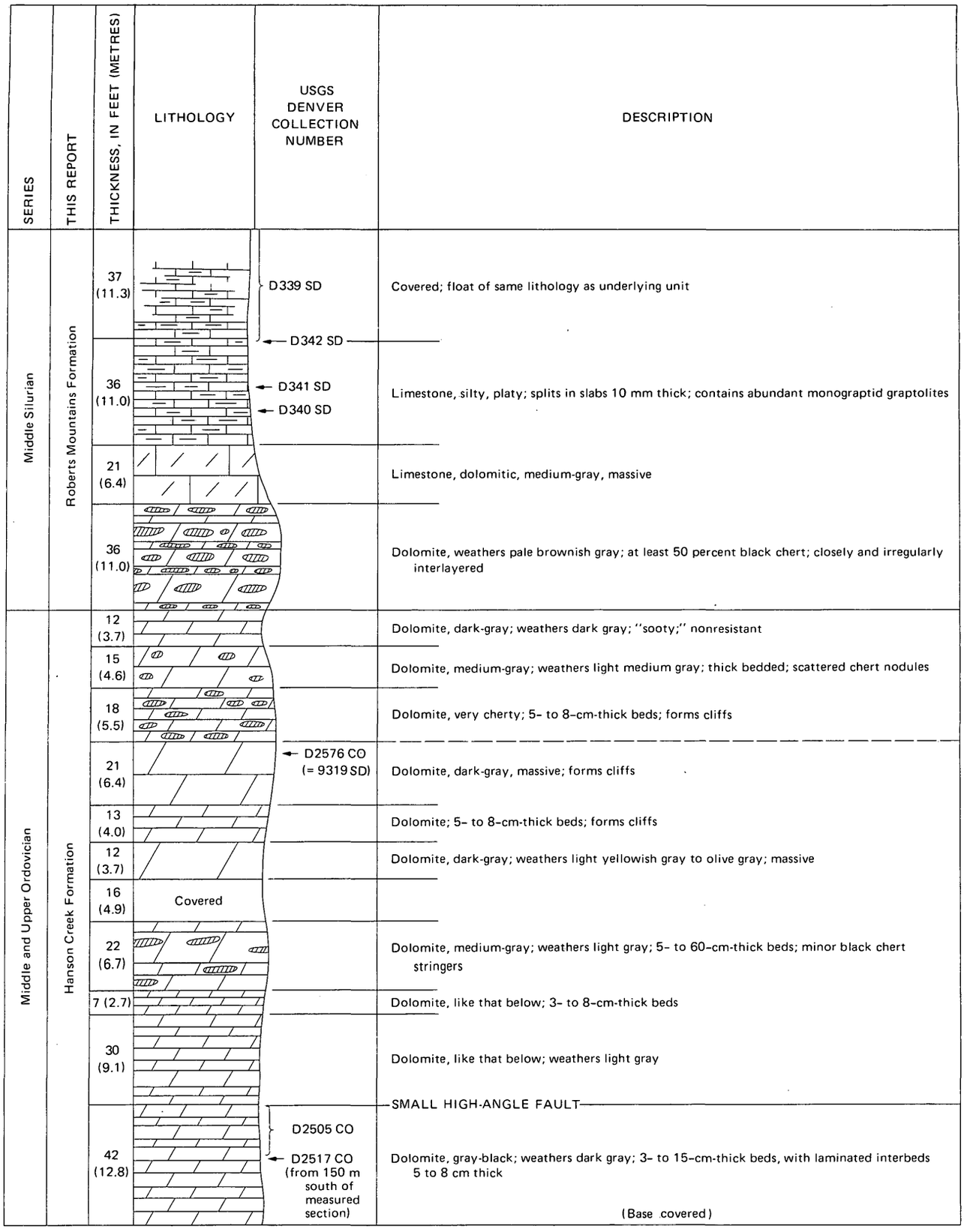

FIGURE 3.—Schematic section of Middle and Upper Ordovician and Middle Silurian rocks of the Wildhorse window. Location of measured section shown in figure 2.

Formation (Ross, 1937, 1947). The upper unit resembles the Roberts Mountains Formation (Nolan and others, 1956) and the Trail Creek Formation at Malm Gulch (Ross, 1937, pl. 1).

Paleontology

Fossils identified in seven collections, all from the Standhope Peak quadrangle, are listed below:

USGS colln. D339 SD. Roberts Mountains Formation; Idaho coordinates E 477,700, N 802,500.
Monograptus flemingii
a monoclimacid?
Age: Wenlock.

USGS colln. D340 SD. Roberts Mountains Formation, 12 ft (3.7 m) above base of platy limestone; Idaho coordinates E 477,500, N 802,560.
Cyrtograptus perneri?
Monograptus flemingii?
Age: Silurian—possibly about mid-Wenlock.

USGS colln. D341 SD. Roberts Mountains Formation, 18 ft (5.5 m) above base of platy limestone; Idaho coordinates E 477,500, N 802,560.
Cyrtograptus?
Monograptus sp. (of *M. priodon—M. flemingii* type)
pristiograptid?
Age: Silurian—possibly about mid-Wenlock.

USGS colln. D342 SD. Roberts Mountains Formation, 35 ft (10.7 m) above base of platy limestone; Idaho coordinates E 477,500, N 802,560.
Cyrtograptid fragment?
Monograptus sp.
Age: Silurian—possibly Wenlock.

USGS colln. D2576 CO (=USGS colln. 9319 SD). Hanson Creek Formation, 18 ft (5.5 m) above base of massive, cliff-forming dolomite; Idaho coordinates E 477,500, N 802,560. Conodonts (determined by J. W. Huddle).
Belodella sp.
Belodina compressa? (Branson and Mehl)
Belodina profunda? (Branson and Mehl)
Cordylodus sp.
Drepandodus suberectus (Branson and Mehl)
Ligonodina sp.
Lonchodina sp.
Panderodus sp.
P. sp.
Plectospathodus n. sp.
Age: probably Late Ordovician.

USGS colln. D2505 CO. Hanson Creek or Saturday Mountain Formation in top 20 ft (6.1 m) of gray-black dolomite; Idaho coordinates E 477,500, N 802,560.
Climacograptus sp.
Orthograptus sp. (robust form)
Age: Middle-Late Ordovician, probably in span of zones 12–14 (*Climacograptus bicornis–Orthograptus quadrimucronatus* zones) of Berry (1960) (=zones 10–13 of Elles and Wood, 1914).

USGS colln. D2517 CO. Hanson Creek Formation from 150 m south of colln. D2505 CO; Idaho coordinates E 477, 375, N 801,460.
Climacograptus hastatus martini
Orthograptus truncatus cf. var. *intermedius*
Orthograptus sp.
Age: Ordovician zone 13 (*Orthograptus truncatus intermedius* zone) most likely, although zone 14 (*O. quadrimucronatus* zone) cannot be fully ruled out.

Regional correlation

Lithologically and faunally these basal units of the Wildhorse window closely resemble the Ordovician Hanson Creek and Silurian Roberts Mountains Formations of the Antelope Valley sequence in central Nevada (Merriam, 1963). The Silurian part of the window section in particular closely resembles not only the Roberts Mountains Formation of the northern Monitor Range but also the upper cherty part of the Gatecliff Formation and the slabby, platy limestone of the Masket Shale, both formations of Kay and Crawford (1964) in the Toquima Range of Nevada. In Idaho, lithic and temporal equivalents are the Ordovician Saturday Mountain Formation and the Silurian Trail Creek Formation at the Malm Gulch locality in the Bayhorse area 30 mi to the north (Ross, 1937). Partly equivalent rocks are exposed in a similar structural window near Fish Creek Reservoir in the southern Pioneer Mountains 40 mi to the southeast (Skipp and Sandberg, 1972). Conceivably the name Saturday Mountain might be applied to the Ordovician part or lower unit of the Wildhorse window section, but the name Trail Creek for the Silurian part or upper unit should not be applied. The Trail Creek problem results from what may be an inappropriate extension of that name from the type locality along upper Trail Creek (Rock Roll Canyon quadrangle; 10 mi northwest of the Wildhorse window) in the north-central Pioneer Mountains (Umpleby and others, 1930) to Malm Gulch in the Bayhorse area (Ross, 1937). A reexamination in progress shows that the type Trail Creek consists of siliceous argillite and quartzite with thin shaly, graptolitic partings; it is lithologically distinct from, and probably represents a more westerly facies than, the limy Malm Gulch and Wildhorse window Silurian.

Regional implications

The Wildhorse window exposures indicate that (1) much if not all of the Copper Basin Group in the northeastern Pioneer Mountains is allochthonous and (2) Ordovician-Silurian strata similar to those in the Lost River Range to the east underlie the Copper Basin Group allochthon.

The window rocks show that an eastern carbonate assemblage extended at least as far west as the northeastern Pioneer Mountains in Ordovician-Silurian time. In addition, they represent the nearest approach (to within about 5 mi or 8 km) of the carbonate assemblage to allochthonous age-equivalent transitional

assemblage rocks (the type Phi Kappa and Trail Creek Formations) known in central Idaho. Nowhere are these two assemblages in direct tectonic contact.

Striking lithologic and faunal similarities of these window rocks with units from northern and central Nevada demonstrate the continuity of lower and middle Paleozoic facies through the Nevada and Idaho parts of the Cordilleran geosyncline.

REFERENCES CITED

Berry, W. B. N., 1960, Graptolite faunas of the Marathon region, west Texas: Texas Univ. Pub. 6005, 179 p.

Churkin, Michael, Jr., 1962, Facies across Paleozoic miogeosynclinal margin of central Idaho: Am. Assoc. Petroleum Geologists Bull., v. 46, no. 5, p. 569–591.

———1963, Graptolite beds in thrust plates in central Idaho and their correlation with sequences in Nevada: Am. Assoc. Petroleum Geologists Bull., v. 47, no. 8, p. 1611–1623.

Dover, J. H., 1969, Bedrock geology of the Pioneer Mountains, Blaine and Custer Counties, central Idaho: Idaho Bur. Mines and Geology Pamph. 142, 65 p.

Elles, G. L., and Wood, E. M. R., 1914, A monograph of British graptolites, Part 10: Palaeontographical Soc. [London], v. 67, p. 487–526.

Kay, Marshall, and Crawford, J. P., 1964, Paleozoic facies from the miogeosynclinal to the eugeosynclinal belt in thrust slices, central Nevada: Geol. Soc. America Bull., v. 75, no. 5, p. 425–454.

King, P. B., 1969, Tectonic map of North America: U.S. Geol. Survey, scale 1:5,000,000.

Mapel, W. J., Read, W. H., and Smith, R. K., 1965, Geologic map and sections of the Doublespring quadrangle, Custer and Lemhi Counties, Idaho: U.S. Geol. Survey Geol. Quad. Map GQ–464.

Merriam, C. W., 1963, Paleozoic rocks of Antelope Valley, Eureka and Nye Counties, Nevada: U.S. Geol. Survey Prof. Paper 423, 67 p.

Nolan, T. B., Merriam, C. W., and Williams, J. S., 1956, The stratigraphic section in the vicinity of Eureka, Nevada: U.S. Geol. Survey Prof. Paper 276, 77 p.

Paull, R. A., and Rothwell, B. G., 1973, Miogeosynclinal and transitional Silurian and Devonian rocks, central Pioneer Mountains, south-central Idaho: Geol. Soc. America Abs. with Programs, v. 5, no. 6, p. 500–501.

Paull, R. A., Wolbrink, M. A., Volkmann, R. G., and Grover, R. L., 1972, Stratigraphy of the Copper Basin Group, Pioneer Mountains, south-central Idaho: Am. Assoc. Petroleum Geologists Bull., v. 56, no. 8, p. 1370–1401.

Roberts, R. J., 1964, Stratigraphy and structure of the Antler Peak quadrangle, Humboldt and Lander Counties, Nevada: U.S. Geol. Survey Prof. Paper 459–A, 93 p.

Roberts, R. J., and Thomasson, M. R., 1964, Comparison of late Paleozoic depositional history of northern Nevada and central Idaho, *in* Short papers in geology and hydrology: U.S. Geol. Survey Prof. Paper 475–D, p. D1–D6.

Ross, C. P., 1937, Geology and ore deposits of the Bayhorse region, Custer County, Idaho: U.S. Geol. Survey Bull. 877, 161 p.

———1947, Geology of the Borah Peak quadrangle, Idaho: Geol. Soc. America Bull., v. 58, no. 12, p. 1085–1160.

———1962, Paleozoic seas of central Idaho: Geol. Soc. America Bull., v. 73, no. 6, p. 769–794.

Scholten, Robert, 1957, Paleozoic evolution of the geosynclinal margin north of the Snake River Plain, Idaho-Montana: Geol. Soc. America Bull., v. 68, no. 2, p. 151–170.

Skipp, Betty, and Sandberg, C. A., 1972, Window of Silurian and Devonian miogeosynclinal and transitional rocks, west of Craters of the Moon National Monument, central Idaho: Geol. Soc. America Abs. with Programs, v. 4, no. 6, p. 411.

Thomasson, M. R., 1959, Late Paleozoic stratigraphy and paleotectonics of central and eastern Idaho: Wisconsin Univ., Ph. D. dissert., 244 p.

Umpleby, J. B., Westgate, L. G., and Ross, C. P., 1930, Geology and ore deposits of the Wood River region, Idaho, with a description of the Minnie Moore and near-by mines, by D. F. Hewett: U.S. Geol. Survey Bull. 814, 250 p.

U.S. Geological Survey, 1973, Geological Survey research 1973: U.S. Geol. Survey Prof. Paper 850, 366 p. [1974].

Jour. Research U.S. Geol. Survey
Vol. 3, No. 4, July–Aug. 1975, p. 437–445

PALYNOLOGICAL EVIDENCE FOR LATE CRETACEOUS, PALEOCENE, AND EARLY AND MIDDLE EOCENE AGES FOR STRATA IN THE KAOLIN BELT, CENTRAL GEORGIA

By ROBERT H. TSCHUDY and SAM H. PATTERSON, Denver, Colo., Reston, Va.

Abstract.—Palynomorphs of Late Cretaceous (Maestrichtian), Paleocene, Paleocene or early Eocene (Wilcox), and middle Eocene (Claiborne) ages have been found in lignitic and carbonaceous clays and silts in the Tuscaloosa Formation, as used in central and east-central Georgia. The occurrence of palynomorphs of Maestrichtian (Navarro) age above thick kaolin deposits at one locality and a suite of Claiborne age fossils below a thick deposit at another locality establish that kaolins of both Late Cretaceous and middle Eocene or younger ages are present. However, the recognition of the Paleocene and middle Eocene beds in the Tuscaloosa Formation of several authors indicates that part of it is much younger than previously thought. The palynomorphs and other characteristics of the carbonaceous materials of Cretaceous and middle Eocene ages indicate freshwater accumulation. The beds of Paleocene age contain both terrestrial and marine forms indicating deposition in marine swamps or estuaries. These findings and the range in ages support the conclusion that the depositional history of the Late Cretaceous and early Tertiary formations in Georgia is complex.

This paper is concerned with the age and stratigraphic relations of sedimentary rocks assigned to the Tuscaloosa Formation of Cooke (1943) in the kaolin belt of central and east-central Georgia (fig. 1). Its purpose is to (1) record the presence of palynomorphs of Cretaceous, Paleocene, and middle Eocene ages in these beds; (2) present a comparison of these palynomorphs with previously described assemblages of known ages from other parts of the Gulf Coast and Mississippi embayment; (3) comment on the stratigraphic value of these age determinations; (4) verify the observations of other geologists (Buie and Fountain, 1968; Scrudato and Bond, 1972; Cousminer, 1973; Cousminer and Terris, 1973) that much of the kaolin mined in Georgia is of Tertiary age, rather than all of it being of Cretaceous age; and (5) suggest the nature of the environment under which the sediments yielding these fossils were deposited.

The palynological investigations were done by the senior author in laboratories of the U.S. Geological Survey, Denver, Colo. Samples reported on herein were selected from a larger group collected by the second author. Collecting localities and simplified regional geology are shown in figure 1, and localities are located by the Transverse Mercator 1,000-m grid in table 1. The samples were collected in strip mines and selected from company drill cores. The material selected for study consisted of dark-gray or black clay and carbonaceous and lignitic clay and silt, because such lithotypes are more likely than others to yield identifiable palynomorphs. The general lithological characteristics of beds associated with the material sampled and very tentative correlations resulting from these studies are shown in figure 2.

Acknowledgments.—Company geologists and management personnel aided by granting permission for sampling and investigations in kaolin strip mines and by supplying drill cores, locations and logs of drill holes, and other information. Among those to whom we wish to express thanks are L. K. Terris, J. M. Smith, and Doral Mills of Georgia Kaolin Co.; Jack Rogers and R. B. Hall of J. M. Huber, Inc.; and D. W. L. Spry, C. W. Gronow, and William Mallory of Anglo-American Clay Co. B. F. Buie of Florida State University and S. M. Herrick, formerly of the U.S. Geological Survey, read and commented on the manuscript and aided the second author in numerous ways during the field investigations and report preparation. S. M. Pickering, Jr., State geologist of Georgia, discussed problems concerning stratigraphy and ages of beds in the region with the second author on several occasions, and he also aided in collecting some of the pollen samples. L. P. Stafford and P. F. Huddlestun, of the Georgia Geological Survey, read the manuscript and made suggestions for improving it.

STRATIGRAPHY

The beds with which this report is concerned occur between the much older crystalline rocks on which they

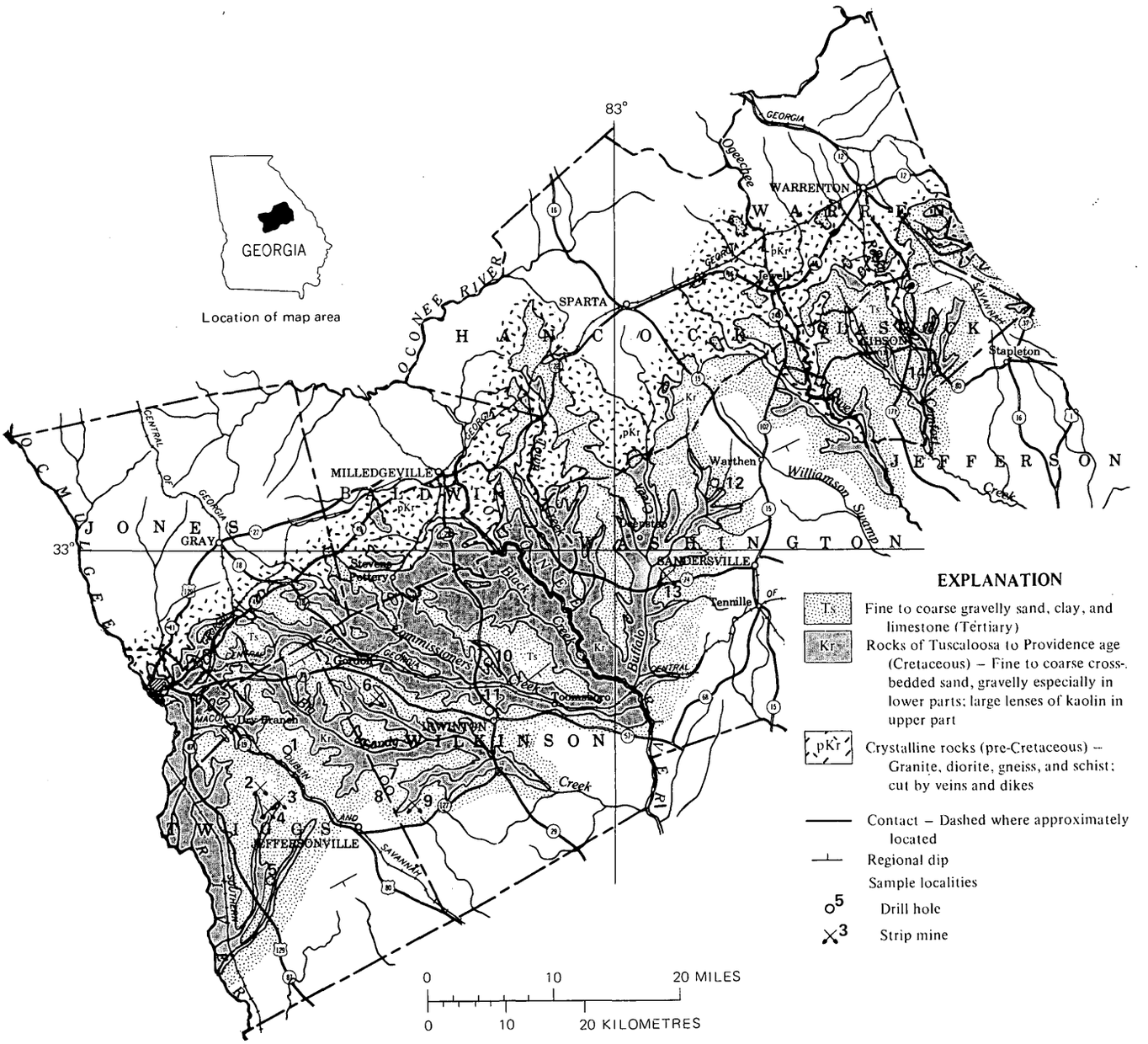

FIGURE 1.—Locations of strip mines and drill holes from which palynological samples were obtained. Geology modified from Eargle (1955, pl. 1).

rest unconformably and the overlying younger marine strata. They consist mainly of arkosic or clayey, poorly consolidated, crossbedded, channel fill, and lenticular sand and kaolin units. Most beds have typical nonmarine characteristics. In most places the overlying marine beds are of Jackson (late Eocene) age, but probable marine beds of Claiborne (middle Eocene) age were thought to be present at a few localities (Lang and others, 1965, p. 4, pl. 1). Most exposures of the beds with which this report is concerned are no more than a few tens of metres thick, but in the subsurface they may be as much as 200 m thick (Herrick, 1961).

The ages and correlations of the beds between the crystalline rocks and the marine formations have long been problematical. In the early part of this century they were variously correlated with the Tuscaloosa Formation of Alabama, the Potomac Group of the Middle Atlantic region, and the Middendorf and Black Creek Formations of South Carolina (Cooke, 1943, p. 8). Stephenson (1912), on the basis of identification of fossil plants by E. W. Berry, called these rocks in eastern Alabama and their equivalents in Georgia Lower Cretaceous. Later Berry (1923) reassigned the fossil plants to the Tuscaloosa of Late Cretaceous age.

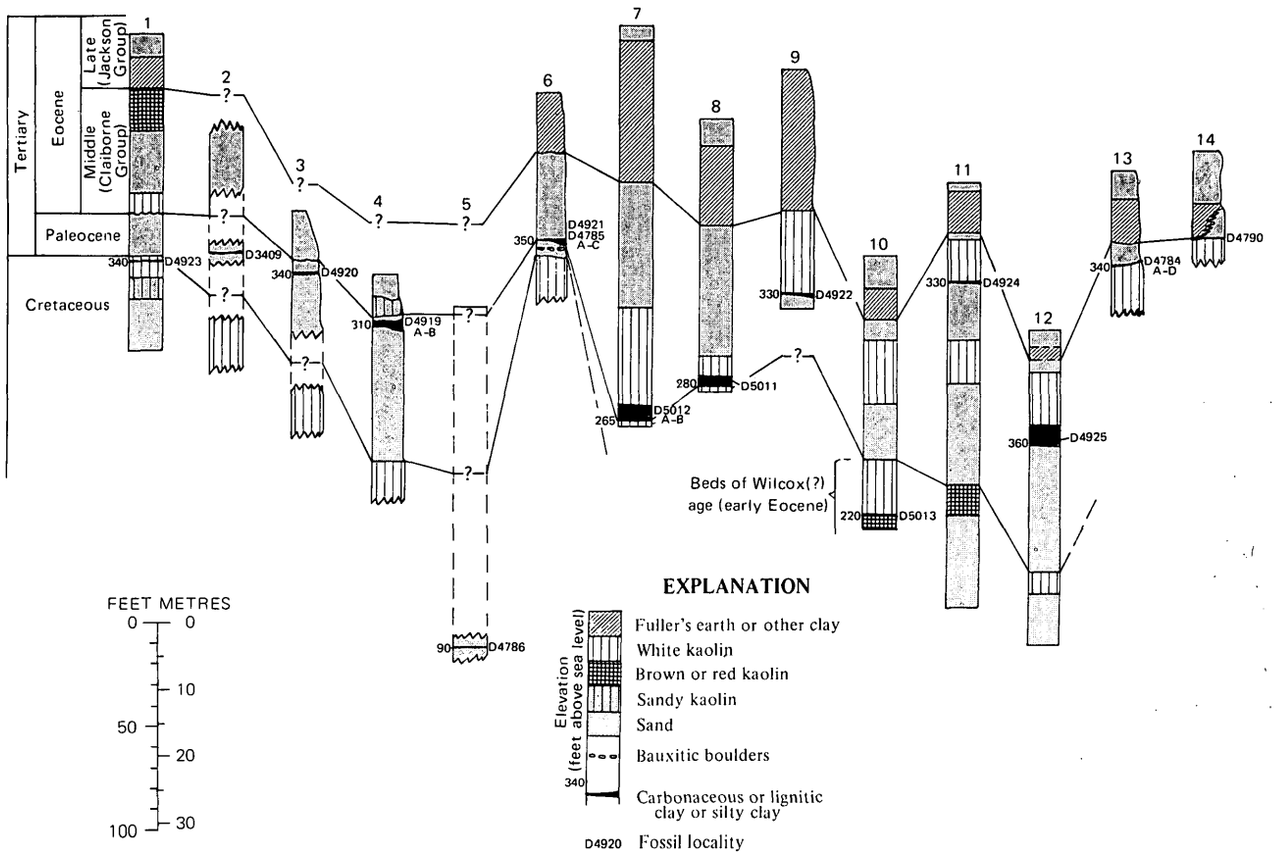

FIGURE 2.—Tentative correlations of beds containing palynological material exposed in strip mines and penetrated in drilling. Localities are shown in figure 1.

The Late Cretaceous plant *Phyllites asplenioides* was also identified by R. W. Brown in a sample of carbonaceous clay from the Martin kaolin mine (La Moreaux, 1946, p. 44), which is located about 2 mi (3 km) north of mine 6 (fig. 1). Paleobotany is emphasized in these correlations because only plant fossils had been found in these strata. Recently external molds of a sparse fauna of marine invertebrates have been found at a few localities (Buie and Fountain, 1968).

After a study of regional relationships, Cooke (1936, p. 17; 1943, p. 8–13) applied the name Tuscaloosa Formation to a group of Upper Cretaceous beds extending along the inner margin of the Coastal Plain from North Carolina, through Georgia, to Mississippi, and northward into Tennessee. The geologists who have in general followed Cooke's usage of this formational name include LaMoreaux (1946), LeGrand and Furcron (1956), LeGrand (1962), Kesler (1963), Herrick (1961), and Herrick and Vorhis (1963). However, some geologists (Scrudato and Bond, 1972) use the name Middendorf Formation for these beds in part of this region. The authors doubt that the beds referred to in this article can be precisely correlated with the Middendorf Formation in South Carolina.

Eargle (1955, p. 83–84, pl. 1) concluded that the true Tuscaloosa Formation of this area (fig. 1) apparently was restricted to the lowermost part of this formation as used by the authors noted in the foregoing paragraph and that strata correlating with Upper Cretaceous formations in west-central Georgia were present. He used the term "rocks of Tuscaloosa to Providence age, undifferentiated" on his geologic map. That the regional relationships of the Tuscaloosa Formation and associated beds is uncertain is also indicated by Lang, Warren, Thompson, and Overstreet (1965, p. 3), who described the correlation of the Tuscaloosa Formation as tentative and used the term "Cretaceous undifferentiated" on their geologic map.

The possibility that the beds, which several authors followed Cooke (1943) in calling the Tuscaloosa Formation, contained lower Tertiary strata was suspected by several geologists working in the World War II period and shortly thereafter, including Bridge (1950, p. 189), Eargle (1955, p. 86) and S. M. Herrick (written commun., 1974). However, none found convincing evidence to support this belief. The long delay in the recognition of the presence of younger beds is mainly

because of the following: (1) Lithologies characteristic of nonmarine deposits throughout these beds, (2) the presence of large economic kaolin deposits in both the older and younger parts, (3) the limited exposures in the region, and (4) the fact that the only fossils found until recently were plant remains. Furthermore, the paleobotany studies historically were on plant megafossils, and palynological studies were made only in recent years. Palynological data have provided information permitting refinements in age determinations not possible using plant megafossils.

About 10 years ago, company geologists began to suspect that much of the kaolin mined was of Tertiary age. The principal reasons for this supposition were differences in stratigraphic positions and lithologies of deposits. The lithologic differences included (1) much more abundant vermicular kaolin crystals in deposits of Cretaceous age, and (2) a very slight light-green tinge, abundant very fine grained heavy minerals, and common tubular bryozoalike structures in deposits thought to be of Tertiary age. Also, the so-called soft kaolins were thought to be older than the hard ones. Tschudy's unpublished palynological work (1964) on a carbonaceous clay sample from the J. M. Huber mine 14 (figs. 1 and 2, loc. 2) indicated that some of the Georgia kaolin was of Tertiary age. Buie and Fountain (1968) reported the presence of abundant, small, poorly preserved Tertiary mollusks from below mined kaolin and so concluded that Georgia kaolin deposits were of both Cretaceous and Tertiary age. These mollusk fossils were identified as equivalent in age to the Gosport Sand or the Moodys Branch Formation (B. F. Buie, oral commun., 1972). The first formation is in the Claiborne Group, and the second is in the Jackson Group. The palynological species in the carbonaceous clay from mine 14 were originally identified by Tschudy as being of late Paleocene or early Eocene age. A more recent evaluation indicated a definite Paleocene age for this sample. Other identifications of Eocene or Tertiary ages of pollen from carbonaceous material associated with kaolin were made by Scrudato (1969), Scrudato and Bond (1972), L. Terris (written commun., 1970), Cousminer (1973), and Cousminer and Terris (1973).

AGE IMPLICATIONS AND PROBABLE REGIONAL CORRELATIONS

The ages attributed to the samples included in this report are based upon published and unpublished records of palynomorphs from the Mississippi embayment region. One of the first pertinent reports is that of Elsik (1968); he described a pollen assemblage from the Paleocene Rockdale Lignite of Texas. Later, Fairchild and Elsik (1969) presented the stratigraphic distribution of some lower Tertiary palynomorphs from the Gulf Coast. Stratigraphic information relative to Mississippi embayment palynomorphs was supplemented by Tschudy (1970, 1973a, b). Tschudy (1973b) examined pollen assemblages from type and other well-documented localities of many of the Eocene formations of the Mississippi embayment region and included the stratigraphic distribution of the more significant taxa. Tschudy (1975) also presented the stratigraphic distribution of the Normapolles genera and species found in Upper Cretaceous and lower Tertiary rocks of the Mississippi embayment. On the basis of the above reports, supplemented by unpublished data from the Denver palynological laboratory of the U.S. Geological Survey, the taxa that serve to characterize several segments of the stratigraphic column were chosen for inclusion in figure 3.

The stratigraphic ranges of the fossil pollen mentioned in table 1 are all included in figure 3. The age determinations were based upon the entire assemblages present in the samples and not exclusively upon the taxa mentioned and included in figure 3.

Several palynomorphs in a drill-core sample from above a thick kaolin deposit (loc. 1, fig. 2 and table 1), particularly *Rugubivesiculites*, are clearly characteristic of Late Cretaceous (Maestrichtian) assemblages. This sample probably represents the equivalent of the McNairy Sand Member of the Ripley Formation in the Mississippi embayment. The drill core from considerable depth (table 1, loc. 5) also contains a limited suite of pollen that is definitely of Cretaceous age. Probably this flora is somewhat older than the material from location 1, and it may be equivalent in age to the Coffee or Cusseta Sand or the lowermost part of the Ripley Formation.

Samples from two nearby strip mines (locs. 3 and 4) yielded assemblages of definite Paleocene age. These assemblages are similar to those described from the Porters Creek Clay (Herrick and Tschudy, 1967) and the Clayton Formation. This Paleocene age determination marks the first recognition of beds of this age in the part of central Georgia east of the Ocmulgee River. The beds in which this Paleocene pollen occurs presumably are about the same age as sandy fossiliferous limestone and bedded brown clay in the Midway Group mapped in the region southwest of this area (LeGrand, 1962, p. 27, fig. 2) and in the Andersonville district, Georgia (Zapp, 1965, pl. 1). The following Foraminifera were identified by E. H. Rainwater (Southeastern Geological Society, 1944, p. 51) from clay in the Andersonville district: *Bolivina midwayensis* Cush-

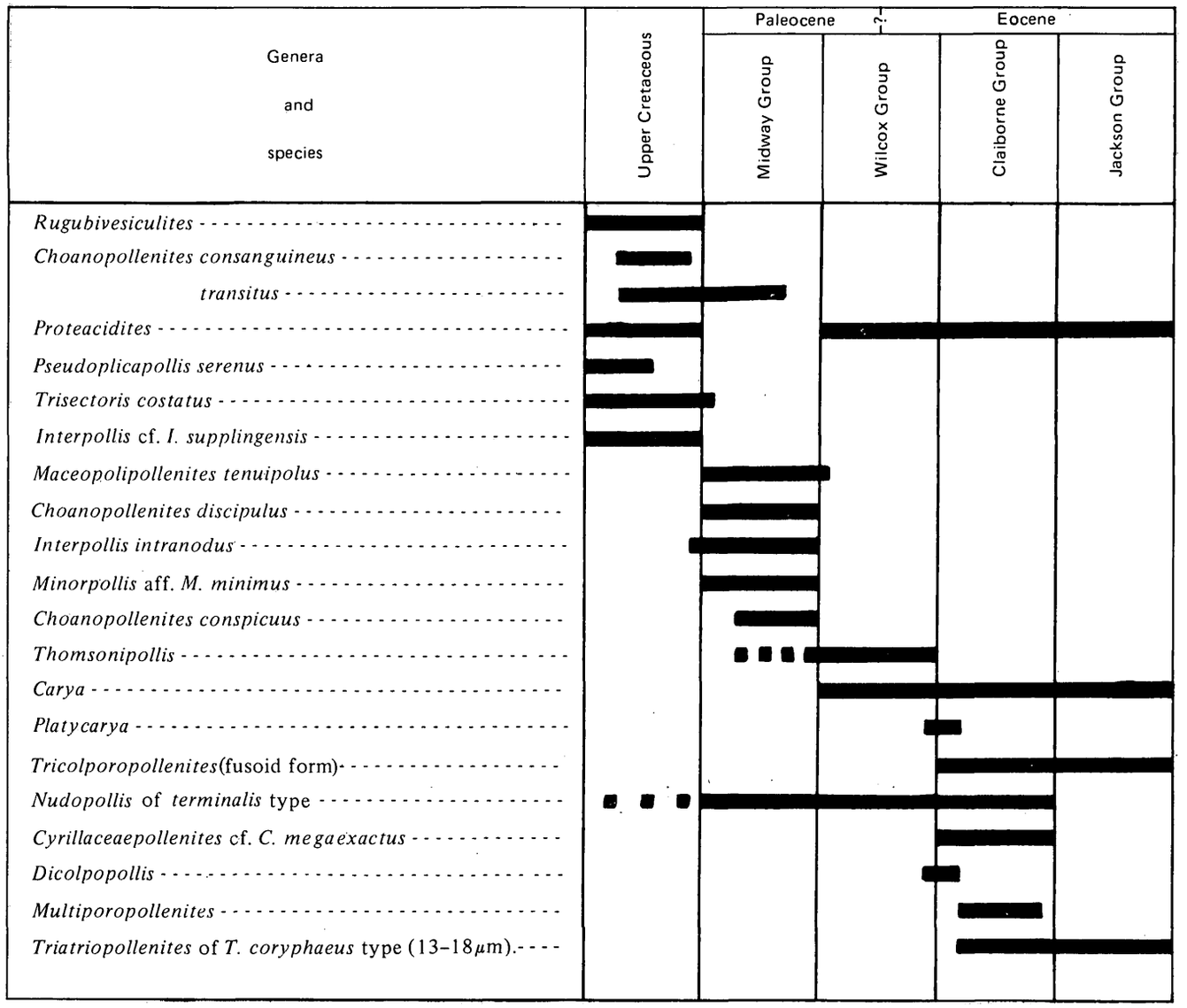

FIGURE 3.—Stratigraphic ranges of selected fossil pollen taxa.

man, *Cibicides* cf. *praecursorius* (Schwager), *Discorbis midwayensis* Cushman, *Globorotalia* sp., and *Gyroidina aequilateralis* (Plummer). Ostracodes of early Paleocene age also were found in material from beds of about this same stratigraphic position near Montezuma, Ga. (Ogren, 1970).

In addition to the foregoing paleontologic evidence for a post-Cretaceous age for some of the kaolin, Pickering (1971) found several "sediment balls" in kaolin clay which contained Tertiary Foraminifera. These "sediment balls" consisted chiefly of sand, and they occurred in an impure lenticular kaolin deposit that was stripped with the overburden in Georgia Kaolin Co. mine 59B (located near mine 6, fig. 1). The sandy "sediment balls" were of quite different lithology from the kaolin enclosing them, and their origin was not determined with certainty. Possible origins advanced by geologists who observed them include (1) water-transported masses from a preexisting sandy bed, and (2) sand fillings of the nesting cavities of burrowing animals such as *Callianassa*. Regardless of their origin these rounded sandy masses were found to contain Bryozoa and Foraminifera. The Foraminifera (tentatively) identified as *Textularia* sp., *Nonion inexcavatus*, *Eponides jacksonensis*, *Cibicides lobatulus*, *Cibicides americanus antiquus*, *Discorbis assulatus*, and *Valvulineria jacksonensis* are of Eocene age (Pickering, 1971).

Black clay from one drill core (loc. 10, fig. 2 and table 1) contains pollen of *Carya*, which has not been observed in material older than Nanafalia Formation samples, and *Thomsonipollis*, which is absent from all

TABLE 1.—*Locations and summary of age determinations and environmental implications of palynological samples*

Locality (figs. 1, 2)	Sample	Location, Transverse Mercator grid	Description of sample	Age and observations
1	D4923	3626600N, 274200E	Black clay from drill core at depth of 107–109 ft (32.6–32.9 m).	Late Cretaceous (Maestrichtian), yielded diagnostic palynomorphs including *Rugubivesiculites*, *Choanopollenites consanguineus*, *C. transitus*, and *Proteacidites*.
2	D3409	3622500N, 266400E	Black clay exposed in J. M. Huber mine 14.	Paleocene, yielded *Minorpollis* cf. *M. minimus*, *Maceopolipollenites tenuipolus*, *Choanopollenites transitus*, and *C. discipulus*. Marine acritarchs and dinoflagellates and the freshwater alga *Botryococcus* suggest near-shore marine deposition.
3	D4920	3620100N, 269200E	Black clay containing abundant plant remains exposed in strip mines.	Yielded a characteristic Paleocene assemblage including *Minorpollis* cf. *M. minimus*, *Maceopolipollenites tenuipolus*, *Choanopollenites discipulus*, and *Interpollis intranodus*, as well as the following marine fossils, dinoflagellates, *Micrhystridium* and *Pterospermopsis*.
4	D4919B	3619200N, 267900E	Upper 3 ft (1 m) of black clay exposed in strip mine.	Samples from this location yielded the same characteristic Paleocene taxa as did the sample from location 3. Fewer accessory taxa were noted from location 4.
	D4919A	3619200N, 267900E	Lower 3 ft (1 m) of same unit------	Do.
5	D4786	3610600N, 268300E	Black clay from depth 228.5–229 ft (69.7–69.9 m), drill hole Faulk No. 1.	Definite Cretaceous palynomorphs included the following: *Proteacidites*, *Rugubivesiculites*, *Interpollis* cf. *I. supplingensis*, *Pseudoplicapollis serenus*, and *Trisectoris costatus*. This sample is probably somewhat older than the sample from location 1.
6	D4921	3636400N, 282800E	Black carbonaceous clay, 1 ft (0.3 m) thick 15 ft (4.6 m) above kaolin, exposed in south wall of kaolin mine.	Definitely of middle Eocene age (probably early Claiborne); pollen identified include *Platycarya*, *Tricolporopollenites* (fusoid form), *Nudopollis* of the *terminalis* type, and *Cyrillaceaepollenites* cf. *C. megaexactus*.
	D4785C	3636400N, 282800E	Black carbonaceous clay 2.5–4 ft (0.7–1.3 m) above base; exposed in north wall of above mine.	Do.
	D4785B	3636400N, 282800E	Same as above, 1–2.5 ft (0.3–0.7 m) above base.	Do.
	D4785A	3636400N, 282800E	Same as above, 0–1 ft (0–0.3 m) above base; base 5 ft (1.7 m) above kaolin mined.	Do.
7	D5012B	3625750N, 283610E	Black clay from drill hole from depth 185–187 ft (56.4–57 m).	Definitely of middle Eocene age (probably early Claiborne). Fossils identified include *Platycarya*, *Tricolporopollenites* (fusoid form), *Nudopollis* of the *terminalis* type, *Cyrillaceaepollenites* cf. *C. megaexactus*, and *Dicolpopollis*.
	D5012A	3625750N, 283610E	Black clay from drill hole from depth 187–189 ft (57–57.6 m).	Do.
8	D5011	3625100N, 283950E	Black clay from drill hole, from depth 126–128 ft (38.4–39 m).	Middle Eocene (probably early Claiborne); yielded all the diagnostic taxa mentioned from locality 7 except *Dicolpopollis*.
9	D4922	3623950N, 288100E	Black lignitic clay, 1 ft (0.3 m) thick, contains carbonized logs and limbs; from below kaolin 40 ft (12.2 m) thick in strip-mine face.	Definitely middle Eocene (probably early Claiborne); all the diagnostic taxa found in locality 8 were also present in this sample.
10	D5013	3639700N, 297500E	Black clay from drill core at depth of 124 ft (37.8 m).	Paleocene–early Eocene (Wilcox) indicated by the presence of pollen of the two taxa *Carya* and *Thomsonipollis*.
11	D4924	3632700N, 296000E	Black clay from drill core at depth of 46–48 ft (14–14.6 m).	This sample was poor but yielded *Nudopollis* of the *terminalis* type and *Platycarya*, indicating a middle Eocene (probably early Claiborne) age. Abundant algal cysts and the alga *Tetraporina* were observed which suggest freshwater deposition.
12	D4925	3649700N, 319810E	Black clay from drill-hole core at depth of 50–52 ft (15.2–15.8 m).	This sample also was poor but yielded virtually the same assemblage as was found in locality 11.

TABLE 1.—*Locations and summary of age determinations and environmental implications of palynological samples*—Continued

Locality (figs. 1, 2)	Sample	Location Transverse Mercator grid	Description of sample	Age and observations
13	D4784D	3659700N, 325800E	Black carbonaceous clay containing plant remains 10–12 in (25–30 cm) above base of clay.	Middle Eocene, probable early Claiborne, age pollen including *Platycarya*, *Nudopollis* of the *terminalis* type, *Tricolporopollenites* (fusoid form), *Cyrillaceaepollenites* cf. *C. megaexactus*, and *Dicolpopollis*. Pollen is similar to that of the other three samples from locality 13.
	D4784C	3659700N, 325800E	Same as above, 8–10 in (20–25 cm) above base.	Do.
	D4784B	3659700N, 325800E	Same as above, 6–8 in (15–20 cm) above base.	Do.
	D4784A	3659700N, 325800E	Same as above, 0–6 in (0–15 cm) above base; base is in a channel depression in kaolin mined.	Do.
14	D4790	3675300N, 353500E	Silty clay containing abundant carbonaceous plant remains, about 1 ft (0.3 m) thick, above kaolin in strip mine, described by Sandy, Carver, and Crawford (1966).	Middle Eocene, probably of early or middle Claiborne age as indicated by the presence of the following taxa: *Multiporopollenites*, *Triatriopollenites* of the *T. coryphaeus* type (13–18 μm), *Nudopollis* of the *terminalis* type, *Cyrillaceaepollenites* cf. *C. megaexactus*, and *Platycarya*?.

post-Hatchetigbee assemblages. Therefore, this material is assigned a Paleocene–early Eocene (Wilcox) age. The sample from locality 2, a collection site now under water, is of Paleocene age.

Definite middle Eocene age determinations were made for the samples collected from localities 6, 7, and 9, and those from 8, 11, 12, 13, and 14 are most probably of the same age. Furthermore, sufficient diagnostic species were present in the first group to make it probable that these assemblages are not only middle Eocene but represent the equivalent of the lower part of the Claiborne. The definite middle Eocene age determinations are based primarily on the presence of *Platycarya*, *Nudopollis* of the *terminalis* type, *Tricolporopollenites* (fusoid forms), and *Cyrillaceaepollenites* cf. *C. megaexactus* (see fig. 3).

ENVIRONMENT OF DEPOSITION

The presence of carbonaceous and lignitic material of the type sampled is itself ordinarily considered to represent deposition in a swampy or marshy freshwater environment. This generality seems to be valid for the deposits represented by the two samples of Cretaceous age (locs. 1 and 5, table 1), which contain only terrestrial fossils. This conclusion is also in general agreement with (1) the plant fossils identified by Berry (1923) and by Brown (in LaMoreaux, 1946, p. 44) from the Tuscaloosa Formation in Georgia, and (2) the crossbedded and arkosic characteristics of the formation.

Freshwater deposition of the material from beds of middle Eocene (Claiborne) ages is strongly suggested by the presence of abundant freshwater algal cysts and *Tetraporina* in several samples, as well as by the finely divided nature of the organic matter. This evidence for freshwater deposition is from beds rather closely associated stratigraphically with sand in which B. F. Buie found marine fossils (Buie and Fountain, 1968). This freshwater-marine relationship seems to establish that at least one advance or retreat of the sea occurred in middle Eocene time. It also suggests that organic materials and clay were deposited in near-shore environments, perhaps similar to the one existing near the present coast of Georgia, which is characterized by winding swampy streams discharging into shallow marshy estuaries.

The groups of samples of Paleocene age (locs. 2, 3, and 4; table 1) contain both terrestrial and marine fossils. This establishes the presence of near-shore depositional conditions in at least part of Paleocene time. The environment of deposition could well have been similar to that outlined for the middle Eocene above, except that the samples studied represent material deposited in the seaward and dominantly marine parts of estuaries or in marine swamps near the coast.

CONCLUSIONS

The palynomorphs of Cretaceous (Maestrichtian) age above a thick kaolin deposit (loc. 1, fig. 2 and table 1) verify that the Cretaceous age assignment for the extensive kaolins, applied for many decades, is in part correct. However, the conclusions by authors cited in the introduction that many of the kaolin deposits are of Tertiary age is also supported by the middle Eocene pollen in the sample from below the thick kaolin mined at locality 9 (table 1, fig. 2) and by the

stratigraphic relations of other pollen-bearing material with mined deposits.

Results of these investigations, including recognition of beds of Maestrichtian, Paleocene, and possible early and definite middle Eocene ages, establish that the depositional history of the Coastal Plain formations in Georgia during Late Cretaceous and early Tertiary time was complex. As would be expected, these results provide further evidence of advancements and withdrawals of the sea. Such movements took place in Paleocene and middle Eocene times. It also seems more firmly established that much of the kaolin was deposited in a near-shore environment, which is in agreement with conclusions by Kesler (1963) and Scrudato (1973).

Beds assigned to the Tuscaloosa Formation are now known to be at least as old as Late Cretaceous and as young as middle Eocene (Claiborne). Whether or not rocks as old as Cenomanian, which have been identified by fossil palynomorph evidence in the Tuscaloosa Formation elsewhere in southern and southeastern United States (Phillips and Felix, 1971a, b; Tschudy, 1973a), are present in the area of this report (fig. 1) was not resolved by this investigation. However, it is clear that the Tuscaloosa Formation in central Georgia contains strata considerably younger than does the formation at the type locality. For this reason as well as the confusing history of the use of this term, the abandonment of the name Tuscaloosa in central Georgia is desirable. Sufficient basis for subdividing the Tuscaloosa Formation and the introduction of new formational terms is likely to be found in the results of additional field and laboratory investigations. The beds assigned to this formation in central Georgia contain considerable evidence for what could be called intraformational unconformities, such as channel-fill deposits, lenticular units, and irregular and undulating contacts between units of different lithologies. Some of these features may be found to represent stratigraphic breaks that can be recognized throughout the region. Therefore, on the basis of lithology it may be possible to separate the Cretaceous and Tertiary parts of the Tuscaloosa Formation in this region into two new formations.

REFERENCES CITED

Berry, E. W., 1923, The age of the supposed Lower Cretaceous of Alabama: Washington Acad. Sci. Jour., v. 13, no. 20, p. 433–435.

Bridge, Josiah, 1950, Bauxite deposits of the southeastern United States, *in* Snyder, F. G., ed., Symposium on mineral resources of the southeastern United States: Knoxville, Tennessee Univ. Press, p. 170–201.

Buie, B. F., and Fountain, R. C., 1968, Tertiary and Cretaceous age of kaolin deposits in Georgia and South Carolina [abs.]: Geol. Soc. America Spec. Paper 115, p. 465.

Cooke, C. W., 1936, Geology of the Coastal Plain of South Carolina: U.S. Geol. Survey Bull. 867, 196 p.

——— 1943, Geology of the Coastal Plain of Georgia: U.S. Geol. Survey Bull. 941, 121 p. [1944].

Cousminer, H. L., 1973, Paleogene palynology of basal Coastal Plain sediments, Irwinton district, Georgia: Geol. Soc. America Abs. with Programs, v. 5, no. 7, p. 584–585.

Cousminer, H. L., and Terris, L., 1973, Palynology of Paleocene clays from Georgia: Am. Assoc. Strat. Palynologists, 5th Ann. Mtg., Abs. of Papers, p. 72–73.

Eargle, D. H.. 1955, Stratigraphy of the outcropping Cretaceous rocks of Georgia: U.S. Geol. Survey Bull. 1014, 101 p.

Elsik, W. C., 1968, Palynology of a Paleocene Rockdale Lignite, Milam County, Texas, [pt.] 2, Morphology and Taxonomy (end): Pollen et Spores, v. 10, no. 3, p. 599–664.

Fairchild, W. W., and Elsik, W. C., 1969, Characteristic palynomorphs of the lower Tertiary in the Gulf Coast: Palaeontographica, sec. B, v. 128, nos. 3–6, p. 81–89.

Herrick, S. M., 1961, Well logs of the Coastal Plain of Georgia: Georgia Geol. Survey Bull. 70, 462 p.

Herrick, S. M., and Tschudy, R. H., 1967, Microfossil evidence for correlation of Paleocene strata in Ballard County, Kentucky, with the lower part of the Porters Creek Clay, *in* Geological Survey research 1967: U.S. Geol. Survey Prof. Paper 575–B, p. B40–B44.

Herrick, S. M., and Vorhis, R. C., 1963, Subsurface geology of the Georgia Coastal Plain: Georgia Geol. Survey Inf. Circ. 25, 79 p.

Kesler, T. L., 1963, Environment and origin of the Cretaceous kaolin deposits of Georgia and South Carolina: Georgia Mineral Newsletter, v. 16, nos. 1–2, p. 3–11.

LaMoreaux, P. E., 1946, Geology and ground-water resources of the coastal plain of east-central Georgia: Georgia Geol. Survey Bull. 52, 173 p.

Lang. W. B., Warren, W. C., Thompson, R. M., and Overstreet, E. F., 1965, Bauxite and kaolin deposits of the Irwinton district, Georgia: U.S. Geol. Survey Bull. 1199–J, 26 p.

LeGrand, H. E., 1962, Geology and ground-water resources of the Macon area, Georgia: Georgia Geol. Survey Bull. 72, 68 p.

LeGrand, H. E., and Furcron, A. S., 1956, Geology and groundwater resources of central-east Georgia: Georgia Geol. Survey Bull. 64, 113 p.

Ogren, D. E., 1970, Ostracoda from the Paleocene Clayton Formation in central Georgia: Georgia Acad. Sci. Bull., v. 28, no. 4, p. 149–152.

Phillips, P. P., and Felix, C. J., 1971a, A study of Lower and Middle Cretaceous spores and pollen from the southeastern United States—1, Spores: Pollen et Spores, v. 13, no. 2, p. 279–348.

——— 1971b, A Study of Lower and Middle Cretaceous spores and pollen from the southeastern United States—2, Pollen: Pollen et Spores, v. 13, no. 3, p. 447–473.

Pickering, S. M., Jr., 1971, Lithostratigraphy and biostratigraphy of the north-central Georgia Coastal Plain: Georgia Geol. Soc., 6th Ann. Field Trip, Oct. 8–9, 1971, 8 p.

Sandy, John, Carver, R. E., and Crawford, T. J., 1966. Stratigraphy and economic geology of the coastal plain of the central Savannah River area, Georgia: Geol. Soc. America, Southeastern Sec., Guidebook, Field Trip 3, 1966, 30 p.

Scrudato, R. J., 1969, Origin of east-central Georgia kaolin deposits: Geol. Soc. America Abs. with Programs, pt. 7, p. 203.

——— 1973, Coastal marsh-depositional environment for the Georgia and South Carolina kaolin deposits: Geol. Soc. America Abs. with Programs, v. 5, no. 5, p. 433–434.

Scrudato, R. J., and Bond, T. A., 1972, Cretaceous-Tertiary boundary of east-central Georgia and west-central South Carolina: Southeastern Geology, v. 14, no. 4, p. 233–239.

Southeastern Geological Society, 1944, Second field trip, southwestern Georgia, Nov. 15, 16, 1944:63 p.

Stephenson, L. W., 1912. Alabama, Georgia and South Carolina, sec. I 16–17, *in* Willis, Bailey, Index to the stratigraphy of North America: U.S. Geol. Survey Prof. Paper 71, p. 605–606.

Tschudy, R. H., 1970, Two new pollen genera (Late Cretaceous and Paleocene) with possible affinity to the Illiciaceae: U.S. Geol. Survey Prof. Paper 643–F, 13 p.

——— 1973a, *Complexiopollis* pollen lineage in Mississippi Embayment rocks: U.S. Geol. Survey Prof. Paper 743–C, 15 p.

——— 1973b, Stratigraphic distribution of significant Eocene palynomorphs of the Mississippi embayment: U.S. Geol. Survey Prof. Paper 743–B, 24 p.

——— 1975, Normapolles pollen from the Mississippi Embayment: U.S. Geol. Survey Prof. Paper 865. (In press.)

Zapp, A. D., 1965, Bauxite deposits of the Andersonville district, Georgia: U.S. Geol. Survey Bull. 1199–G, 37 p.

Jour. Research U.S. Geol. Survey
Vol. 3, No. 4, July–Aug. 1975, p. 447–450

EARLY ORDOVICIAN GASTROPOD OPERCULA AND EPICONTINENTAL SEAS

By ELLIS L. YOCHELSON, Washington, D.C.

Abstract.—Collections made for some years from Lower Ordovician rocks by many geologists have established that the heavy calcareous operculum of the gastropod *Ceratopea* is almost never found associated with a shell and that commonly this operculum is secondarily silicified. *Ceratopea* may have lived in a stressed habitat and may have been essentially the only shelled invertebrate present. Presumably these animals grazed on algal mats and mounds growing in areas of water slightly more saline than open marine water and were killed by an influx of hypersaline water. Subsequent decay of soft parts would permit the operculum to rot off and would also lighten the shell so that it could float away. Penecontemporaneous silicification of calcareous opercula on the Ordovician sea bottom is postulated.

Some Middle Ordovician opercula of the Middle to Late Ordovician genus *Maclurites* serve to test this speculation. These opercula also occur in geologic settings which may be interpreted in terms of kill of animal, wafting away of shell, and secondary silicification of operculum.

This note is based to a large extent on speculation over the occurrence of a curious fossil. Random observations have been made in different parts of North America for nearly two decades. The idea presented here can only be tested, if at all, by further field observations and geochemical investigations. It is given in the hope of explaining a fossil distribution which otherwise seems inexplicable.

THE GASTROPOD *CERATOPEA*

Ceratopea Ulrich ranges through the upper half of Lower Ordovician strata (Yochelson and Bridge, 1957). It has been reported from outcrops in New Mexico, western Texas, central Texas, Colorado, Oklahoma, Arkansas, Alabama, Georgia, Tennessee, Virginia, Maryland, Pennsylvania, New York, Newfoundland, Greenland, and Spitsbergen. Not all species occur in each area, but some easily recognizable species do have geographic ranges measured in hundreds of miles.

Much of the Lower Ordovician carbonate sequence is poorly fossiliferous, at least in terms of larger invertebrates. Because species of *Ceratopea* are widespread and undergo change, a sequence of stratigraphically useful forms has been established. Insofar as it can be tested by correlation based on other fossils in the same rock units, including brachiopods, cephalopods, and trilobites, the widespread distribution of *Ceratopea* species in a definite sequence has been established.

MODE OF OCCURRENCE AND PRESUMED LIFE HABIT OF *CERATOPEA*

Ceratopea is an atypical gastropod in that the operculum, a platelike structure that seals the aperture when the soft parts are withdrawn, is calcified. An operculum occurs on all modern benthic marine gastropods except broad, low, conical forms that cling to rocks, but in only a few living genera, such as *Turbo* or *Nerita*, is it calcified. Many modern opercula have either spiral growth or lateral increments added around the margins of a plate. The operculum of *Ceratopea* differs in that ever larger layers were sequentially added to the posterior of the juvenile operculum. The shell aperture and operculum conform in shape, and the enlargement of the operculum by incremental growth insured that they conformed in size. As a consequence of this mode of growth, the operculum is quite thick and is both massive and heavy. The original carbonate mineral composition is unknown; indirect evidence, based on appearance at the outcrop, suggests to me that it may have been wholly or in large part aragonite rather than calcite.

Ceratopean opercula are well-known fossils, and one of the species was described more than six decades ago. In striking contrast, little is known of the shell. The opercula are virtually never associated with any gastropod shells, and they are almost never associated with other kinds of benthic fossils. The scarcity of shells relative to opercula is not a happenstance of collecting but is a fact that can be confirmed at many outcrops.

The statement about the rarity of ceratopean gastropod shells and the general scarcity of other macroinvertebrates does require a bit of qualification. The younger beds in the zone of *Ceratopea* do contain a more diverse fauna than the older beds; this fauna is predominantly molluscan. One life association of shell

and operculum has been found (Yochelson and Wise, 1972), but even in the younger beds where Early Ordovician mollusks are abundant, shells of *Ceratopea* are exceptionally rare relative to opercula.

One reason that opercula of *Ceratopea* are so useful in stratigraphy is that many of them are silicified. This increases their resistance to weathering, and as a consequence they may be found in residual soils and in rubble from outcrop weathering, this also increases the likelihood of their being seen on outcrops. Classically, subdivisions of the Knox Group of Tennessee were established on the basis of specimens picked from the deep residuum. The validity of this general approach has been tested in the regolith from similar Lower Ordovician rocks in northeastern Arkansas. The sequence of occurrences of opercula obtained from carbonate bedrock in Oklahoma has been checked in outcrops in northwest Georgia. The novel approach of etching specimens free from the rocks as a field procedure for mapping (Charles Cressler, oral commun., 1970) was used in Georgia.

One might argue that differential weathering is the reason for the absence of shells associated with residuum specimens of opercula. This argument fails when bedrock exposures are examined. Shells simply are not present at most outcrops or are exceedingly rare when they are present. Although some of the opercula are silicified, calcified specimens do occur at most outcrops. The percentage of silicified specimens relative to calcified ones and the degree of silica replacement appear highly variable. It seems likely that opercula in residuum are secondarily hardened by silica, and their relative rarity compared with some bedrock occurrences may be a result of the vagaries of weathering.

Charles Cressler (oral commun., 1970) has noted that at some localities in Georgia, where rare specimens lie along a distinct bedding plane in limestone, the part of an operculum above a bedding plane may be silicified but the part below has not been replaced. This observation has not been checked in other areas since it was first called to my attention, but in retrospect the observation seems likely to be valid for other regions where *Ceratopea* occurs.

Recently attention has been directed to low algal mounds in the Lower Ordovician carbonate rocks of Oklahoma and western Texas (Toomey and Ham, 1967; Toomey, 1970; Riding and Toomey, 1972). Similar mounds occur in the Lower Ordovician of Arkansas and in the Knox Group of Tennessee. Where observations can be made of bedrock occurrences, at least some *Ceratopea* opercula occur near such mounds. Many of the *Ceratopea* opercula observed in bedrock do not occur in association with mounds. However, some do occur in laminated limestones suggestive of algal-mat deposition.

Most primitive marine gastropods are herbivores. It is a reasonable assumption that *Ceratopea* followed this mode of life and grazed on the algae that formed mats and mounds on the sea floor. Thus, the ceratopean opercula could be in more or less life association with algae in a shallow-water marine assemblage. Depths are uncertain, but a depth of less than 20 feet (6m) is certainly reasonable from what is known of present analogues of Paleozoic algae.

MODE OF DEATH OF *CERATOPEA*

Implausible though it may be, the most reasonable hypothesis to explain the separation of the operculum from the shell of *Ceratopea* is for the shell to have floated away posthumously (Yochelson and Copeland, 1974). Upon death of the animal, the operculum eventually would be separated from the foot by distintegration of the soft parts. Enough of the other soft parts could be left to putrefy within the shell so that the gas generated by their decay would lighten the shell. Even if it would not float, the shell then could be readily moved by relatively weak currents.

One obvious difficulty with this suggestion is that it implies that the soft parts remained undisturbed for the period of days to weeks required for them to rot away. In present marine habitats, scavengers make short work of soft parts; modern buoyant marine gastropod shells apparently have not been reported or observed. One method of circumventing this problem is to suggest a mechanism that would prevent scavengers from being in the area where *Ceratopea* lived; again this is difficult to envision.

I speculate that *Ceratopea* lived in an environment slightly more saline than that of the open ocean; the more restricted parts of the Red Sea provide a present analogue. Algae would fluorish, but few macroinvertebrates except *Ceratopea* could survive. In particular, the scavengers and carnivores would be excluded. Were the waters to become abruptly more saline, this would not interfere with algal growth. The gastropods, however, would retract into their shells and eventually die. In these more saline waters the dead animal could decay without being disturbed by predators. The operculum could then rot off and the shell be moved away by light currents. There may then have been some moderate wave action to concentrate opercula as a lag; in some rocks, as in part of the Kindblade Formation of Oklahoma, opercula occur in profusion.

Large silicified *Ceratopea* opercula are common, and small ones are quite rare. To a certain extent, this may

be a consequence of collecting free specimens exposed in weathered material and mixed with pebbles. At the few localities where specimens have been etched from limestones or at the outcrops where a more diverse fauna is present, small individuals do occur. Nothing resembling a possible life population is known, but the size distribution in these occurrences does point in that direction.

DIAGENESIS OF *CERATOPEA*

Like other former living organisms, *Ceratopea* specimens show individual variation. In some collections, this variation may be exceptionally great for a species, judging by other groups of gastropods. I have consistently suggested wear of the opercula as one source of individual variation, subjectively assuming that rather violent current and wave action was needed to destroy the gastropod shell. However, J. W. Pierce (oral commun., 1972) has suggested that some of the "wear" shown by opercula may actually be the result of solution. I know of no way to confirm this observation, but it appears quite reasonable.

Harris (1973) has proposed a model of the Early Ordovician epicontinental seas which implies a salinity gradient such that the water toward the midcontinent of North America was more saline than that near the periphery. The curious features of *Ceratopea* opercula occurrence and preservation seem to fit this model.

If *Ceratopea* was widely tolerant of saline waters, it might have lived in a broad zone of slightly greater salinity where algae could fluorish but where most other marine herbivores that could have grazed down the algal mats were excluded. Evaporation of the shallow sea to "landward" would increase salinity. An associated increase in alkalinity of that body of water is plausible. Certainly under conditions of evaporation, as suggested by Harris (1973), the waters would be unlike those in the present oceans.

A further consequence of evaporation would be heat imbalance. Eventually this imbalance should be enough to generate storm winds that would move these hypersaline waters outward, killing the gastropods. Subsequently, a stillstand of this water would allow time for decay of soft parts. A later modest amount of wind drift would move the buoyant shells away.

The alkalinity of this hypersaline water in the extremely shallow sea could corrode and modify the heavy calcareous opercula. If, as a consequence of its greater salinity and alkalinity, the water contained a relatively high amount of silica in solution, this would provide a first necssary step for replacement of the opercula. After some time of more or less stillstand, a further change in conditions could cause deposition of silica. Because of the wide occurrence of thin Lower Ordovician cherts, some of which can be traced for miles (Helmuth Wedow, Jr., oral commun., 1973), changes in water chemistry seem most likely. A triggering mechanism that would have abruptly released the silica is appealing. Perhaps a decrease of salinity may be postulated. A reversal of wind circulation so that waters blew inshore would dilute salinity abruptly and result in deposition of chert and in silicification.

Not all Lower Ordovician chert is a replacement of original algal deposits, but it is becoming increasingly apparent that many of the cherts in the southern Appalachian area are replacements of stromatolites and mats. The algal deposits and *Ceratopea* opercula have in common more original organic material and greater porosity than have fine carbonate muds. Perhaps one or both of these factors localized silica deposition. It is difficult to understand how extensive replacement could have taken place after burial in carbonate mud, though this possibility cannot be ruled out. In some Early Ordovician localities, silicified fossils commonly are well preserved on the part that is up relative to the bedding plane and less well preserved on the underside. Often the lower part of the specimen may be welded to a chert layer. How would fluids moving through sediment silicify materials in this manner? If silicification of shells lying free on the sea floor was from the top downward and if the propensity for deposition of silica increased when the silica-rich water came in contact with the substrate, the phenomenon is more understandable.

Many of the Lower Ordovician carbonate rocks are dolomites. Much argument revolves around the problem of primary, penecontemporaneous, and secondary dolomitization. The opercula shed some light on this question, for their silicification must have preceded dolomitization or they would not have been preserved.

A PARTIAL TEST OF THE MODEL

Ceratopea is not unique in its possession of a calcified operculum. The Middle to Late Ordovician genus *Maclurites* also had such a structure, and, because of superficial similarity, the two opercula have been confused; the mode of growth and overall morphology of the two opercula is different, however.

The shell of *Maclurites* is extremely common in some areas, though opercula are quite rare. Indeed, many localities, for example those near Plattsburg, N.Y., which have yielded a profusion of shells have produced remarkably few opercula. However, at a few Middle Ordovician localities in Tennessee, *Maclurites* opercula occur in greater number than the shells.

Where *Maclurites* opercula are present, there is commonly some evidence within the carbonate rocks of algal mats or stromatolitic buildup. The opercula may be silicified, and in such areas, chert blebs and thin stringers of chert, possibly replacing algal mats, are present.

I do not wish to indicate that Middle Ordovician *Maclurites* and Early Ordovician *Ceratopea* lived in exactly the same habitat or that all species of each genus had the same environmental requirements. Nevertheless, the similarity in biological and geological features is evident. It suggests to me the plausibility of similar occasional erratic changes in the water composition of the shallow Middle Ordovician seas, as outlined above for Early Ordovician occurrences.

REFERENCES CITED

Harris, L. D., 1973, Dolomitization model for Upper Cambrian and Lower Ordovician carbonate rocks in the eastern United States: U.S. Geological Survey Jour. Research, v. 1, no. 1, p. 63–78.

Riding, Robert, and Toomey, D. F., 1972, The sedimentological role of *Epiphyton* and *Renalcis* in Lower Ordovician mounds, southern Oklahoma: Jour. Paleontology, v. 46, no. 4, p. 509–519.

Toomey, D. F., 1970, An unhurried look at a Lower Ordovician mound horizon, southern Franklin Mountains, West Texas: Jour. Sed. Petrology, v. 40, no. 4, p. 1318–1334.

Toomey, D. F., and Ham, W. E., 1967, *Pulchrilamina*, a new mound-building organism from Lower Ordovician rocks of West Texas and southern Oklahoma: Jour. Paleontology, v. 41, no. 4, p. 981–987.

Yochelson, E. L., and Bridge, Josiah, 1957, The Lower Ordovician gastropod *Ceratopea*: U.S. Geol. Survey Prof. Paper 294–H, p. 281–304 [1958].

Yochelson, E. L., and Copeland, M. J., 1974, Taphonomy and taxonomy of the Early Ordovician gastropod *Ceratopea canadensis* (Billings) 1865: Canadian Jour. Earth Sci., v. 11, p. 189–207.

Yochelson, E. L., and Wise, O. A., Jr., 1972, A life association of shell and operculum in the Early Ordovician gastropod *Ceratopea unguis*: Jour. Paleontology, v. 46, no. 5, p. 681–685.

Jour. Research U.S. Geol. Survey
Vol. 3, No. 4, July–Aug. 1975, p. 451–465

MORPHOLOGY AND PHYLOGENY OF THE COCCOLITHOPHYCEAN FAMILY CERATOLITHACEAE

By STEFAN GARTNER [1] and DAVID BUKRY,
Miami, Fla., La Jolla, Calif.

Abstract.—The family Ceratolithaceae includes a group of horseshoe-shaped calcareous nannofossils and contains ten species which are assignable to two genera: *Amaurolithus* n. gen. and *Ceratolithus*. Species of *Amaurolithus* are characterized by showing faint or no birefringence in cross-polarized light when viewed in preferred orientation. Included in *Amaurolithus* are *A. amplificus* (Bukry and Percival), *A. bizzarus* (Bukry), *A. delicatus* n. sp., *A. primus* (Bukry and Percival), and *A. tricorniculatus* (Gartner). Species of *Ceratolithus* are characterized by their strong birefringence in cross-polarized light when viewed in preferred orientation. *Ceratolithus* includes *C. acutus* Gartner and Bukry, *C. armatus* Müller, *C. cristatus* Kamptner, *C. rugosus* Bukry and Bramlette, and *C. telesmus* Norris. The family first appears in the geologic record during the late Miocene, represented by the nonbirefringent-appearing species that constitute the genus *Amaurolithus*. A succession of these species persists into the early Pliocene. The distinctly birefringent forms assigned to the genus *Ceratolithus* first appear near the base of the Pliocene; the succession has persisted to modern time.

The family Ceratolithaceae includes a group of late Neogene calcareous nannofossils found in association with coccoliths and discoasters in marine sediment. Ceratoliths generally have the shape of an asymmetrical horseshoe, unique among nannofossils, and hence are readily distinguishable in nannofossil assemblages. This distinctive appearance coupled with the relatively short geologic ranges of several species contributes to the usefulness of the family for biostratigraphy of late Miocene to Holocene marine sediments.

Bukry and Bramlette (1968) summarized the data on the stratigraphic significance of three distinctive species represented by ceratoliths, as then known from the pioneer studies of Bramlette on the biostratigraphy of coccolithophyceans: The still living *Ceratolithus cristatus* Kamptner (1950), a newly named *C. rugosus* of the Pliocene, and *C. tricorniculatus* of Gartner. Gartner's species was found to belong in a distinctive group that Bramlette had differentiated primarily on a very characteristic difference in showing little or none of the strong birefringence of calcite in the normal flat orientation because the optic axis is vertical in that orientation, as with the discoasters. This marked difference from typical species of *Ceratolithus* is the basis for placing some species formerly assigned to *Ceratolithus* in a new genus—*Amaurolithus*.

Acknowledgment.—We are indebted to Dr. M. N. Bramlette, Scripps Institution of Oceanography, for many fruitful discussions on the nature of ceratoliths. We thank Dr. Bramlette and Dr. W. W. Hay, University of Miami, for reviewing the manuscript. Research was supported by National Science Foundation grant GA–35991.

THE LIVING ORGANISM

Although the common skeletal remains of ceratolith-secreting organisms have been known since 1950, Norris (1965) was the first to describe the living organisms from the Indian Ocean. The cells of these organisms, unlike other coccolithophyceans, do not have flagellae, but they bear two types of coccoliths. One type is the horseshoe-shaped ceratolith that occurs singly, surrounding the cell, and the other is a delicate circular to elliptical hoop of which numerous individual specimens are attached to the outer, spherical sheath. This second type is described in some detail by Norris (1971), although the tiny delicate coccoliths are not known to be preserved in sediments.

MORPHOLOGY AND ULTRASTRUCTURE OF CERATOLITHS

The unusual shape and ornamentation of ceratoliths makes it difficult to describe these forms accurately without a specialized terminology. The various terms applied to ceratolith morphology are shown in figure 1.

Ceratoliths were first named by Kamptner (1950), who later (1954) described the species *Ceratolithus cristatus* in detail from optical-microscope observations in ordinary transmitted light and in polarized light. *C. cristatus* has the shape of an asymmetrical horseshoe

[1] School of Marine and Atmospheric Sciences, University of Miami.

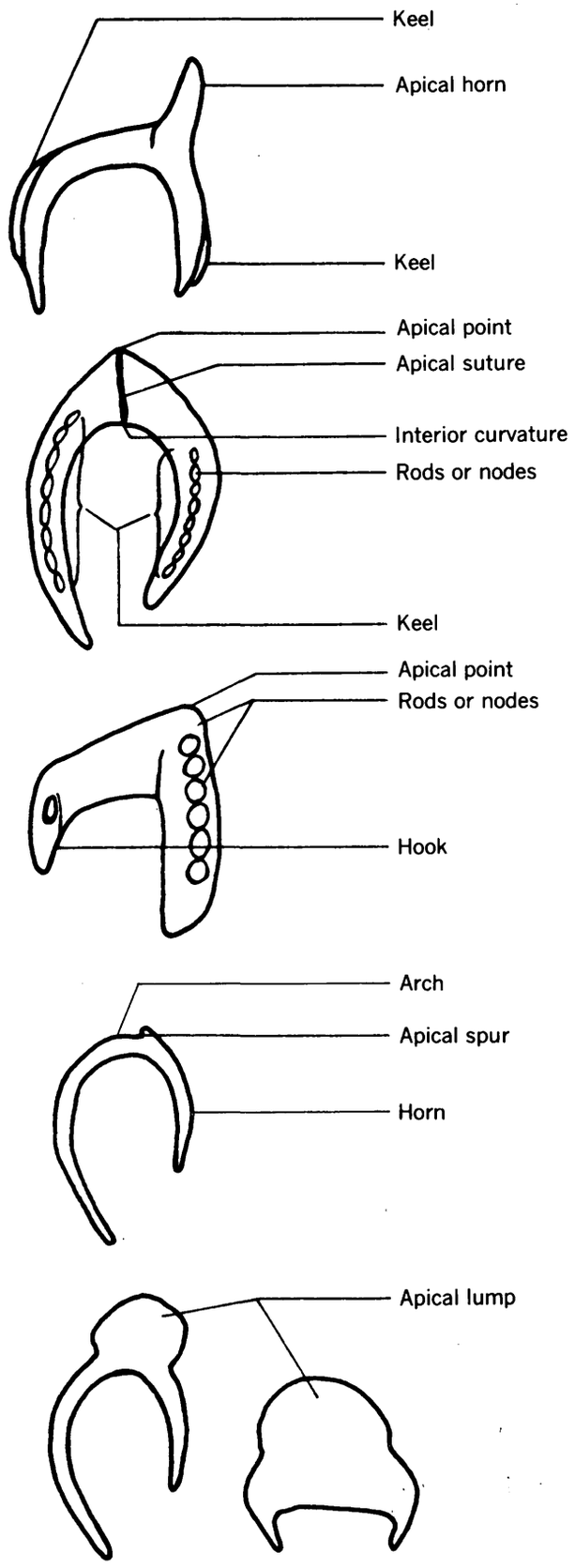

FIGURE 1.—Terms applied to ceratolith morphology.

because one side is shorter than the other (fig. 2). Kamptner describes the ultrastructure, here supplemented by some new observations using the electron microscope, as follows: With the ceratolith oriented so that the open end is upward and the shorter horn is to the left, a bladelike structure protrudes from either side perpendicular to the plane of the ceratolith horns. On the proximal surface (toward the viewer) this bladelike structure is composed of robust rods protruding along the median line of the ceratolith horns, each rod being joined to the adjacent rods along its edges. On the shorter horn the rods are perpendicular to the plane of the ceratolith, whereas on the longer horn the rods are inclined toward the point of the horn. The keel formed by these rods remains perpendicular to the plane of the ceratolith horns. Another keel protrudes in a similar fashion on the opposite side of the ceratolith (away from the viewer); this keel is featureless and very delicate. The inside of the horseshoe is smoothly but unevenly curved, the curvature being sharpest near the base of the shorter horn. The outside curvature is similar except for a blunt point that marks the near midpoint of the horseshoe. A thickening, commonly resembling a suture or ridge, extends from this blunt point to the inside of the horseshoe. The tips of the horns are regularly terminated, and the longer horn generally has a sharper point.

CRYSTALLOGRAPHY OF CERATOLITHS

Ceratoliths are constructed of calcite, and crystallographically every specimen behaves as a single calcite crystallite. But not all ceratoliths have the same crystallographic orientation relative to their general shape. On the basis of their appearance in cross-polarized light the various species can be divided into two groups, and this optical characteristic is used in this paper to assign ceratoliths to two genera. Species which

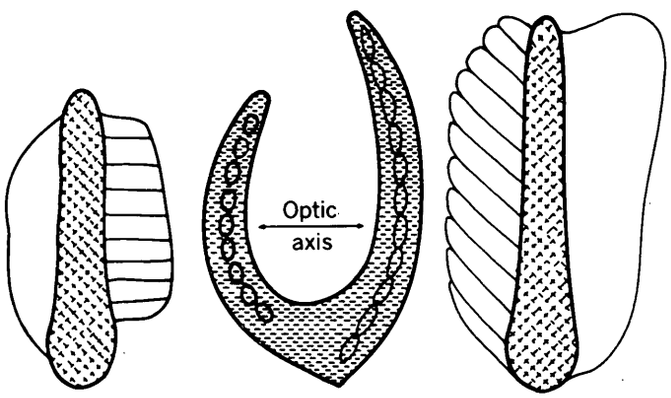

FIGURE 2.—Sketch of *Ceratolithus cristatus*, showing morphology and crystallography.

in preferred orientation show maximum birefringence are assigned to the genus *Ceratolithus* and are referred to as birefringent. Species which in preferred orientation show little or no birefringence are assigned to the genus *Amaurolithus* and for purposes of discussion are called nonbirefringent, although, strictly speaking, calcite is always birefringent, the apparent lack of birefringence being a result of orientation of the calcite optic axis.

The genus *Ceratolithus* includes *C. acutus*, *C. armatus*, *C. cristatus*, *C. rugosus*, and *C. telesmus*. The nonbirefringent species are *Amaurolithus amplificus*, *A. bizzarus*, *A. delicatus*, *A. tricorniculatus*, and *A. primus*. Of these, *A. amplificus* and *A. tricorniculatus* may appear weakly birefringent, but this seems to be due to tilting of the specimens which causes the plane of the ceratolith to be inclined to the direction of illumination.

Kamptner (1954) determined that the crystallographic *c* axis (the optic axis of calcite) for *C. cristatus* is in the plane of the ceratolith and approximately at right angles to the long axis of the ceratolith (see fig. 2). All species assigned to *Ceratolithus* share these crystallographic and optical properties. For the nonbirefrigent forms, the crystallographic optic axis is perpendicular to the plane of the ceratolith, as with most discoasters. When the specimens are viewed in preferred orientation, which is with the plane of the ceratolith perpendicular to the direction of illumination, they remain dark in polarized light. As most such specimens do not extinguish completely (become completely black) in cross-polarized light but rather remain a dark gray (except when tilted), one may infer that a slight amount of random variation occurs in the position of the optic axis. Some specimens have either two arms of different thickness or overgrowths of calcite that can tilt the plane of the optic axis slightly, causing the effect in cross-polarized light.

The species of *Amaurolithus* that commonly show weak birefringence, *A. amplificus* and *A. tricorniculatus*, have accessory structures that cause specimens to come to rest on a flat surface in such a way that the plane of the ceratolith is somewhat tilted with respect to the surface of the slide, and hence the crystallographic optic axis is inclined slightly to the direction of illumination. On *A. amplificus* the tilting caused by accessory structures, probably nodes or rods homologous with the keel-forming rods of *C. cristatus*, is commonly in the direction in which the horns point, or at right angles to this direction. As a consequence, weakly birefringent specimens of this species generally are brightest with the horns pointing about 45° toward the direction of polarization. Rarely, specimens are tilted at a random angle and in such orientations the position of brightest image is also random.

For the species *Amaurolithus tricorniculatus*, the tilt direction is generally determined by a spur below the base of the apical horn. Thus the crystallographic optic axis is usually inclined such that its projection in a surface perpendicular to the direction of illumination makes an angle about 45° with the direction in which the horns point. The brighter image for these specimens is therefore obtained when the horns are parallel to the direction of polarization.

Subtle differences in birefringence alone are not sufficient criteria for making species distinctions.

PHYLOGENY OF CERATOLITHACEAE

The earliest ceratolith-like nannofossils are of the rare species *Ceratolithina hamata* Martini (1967) from the Albian. This rather large species has a pronounced hook at the tip of one horn, is constructed of a single crystallographic unit, and shows birefringence in cross-polarized light. *Ceratolithoides kamptneri* Bramlette and Martini (1964) is a late Maestrichtian form on which the two horns are constructed of differently oriented calcite units. The late middle Eocene *Ceratolithina? vesca* Bukry and Percival (1971) also is constructed of a single crystallographic unit, but this species has relatively straight horns separated by about 75°. All three of the above species represent a discontinuous record of objects similar in shape but not lineally related to Neogene ceratoliths.

The origin of the family Ceratolithaceae remains unclear. The family first appears in the late Miocene, but among the diverse nannofossils of the middle and late Miocene there is no likely candidate for an ancestral ceratolith. Gartner (1967) suggested a possible relation between the genus *Ceratolithus* and *Triquetrorhabdulus rugosus* Bramlette and Wilcoxon (=*Ceratolithus farnsworthii* Gartner) but pointed out that the resemblance was closest to the Pleistocene and Holocene species *Ceratolithus cristatus* rather than the earlier representatives of the family, some of which coexisted with *T. rugosus*. Hence this relation must remain a remote possibility.

Norris (1965, 1971) has described delicate hoop-shaped coccoliths occurring on the surface of ceratolith-bearing cells, and this suggests another avenue by which ancestral ceratoliths may be sought. Unfortunately, these hoop-shaped coccoliths are so delicate that they are not likely to be preserved in the fossil record, and, indeed, none are known. Among the more robust types of coccoliths that might be considered in this context because of its hoop shape is the Oligocene to middle Miocene species *Coronocyclus nitescens;* there

is, however, no structural evidence of any relation between delicate and robust types.

A probable scheme of evolutionary succession of the various species of the family Ceratolithaceae is suggested in figure 3. *Amaurolithus primus* is the earliest ceratolith, but *A. delicatus* appears about the same time. Within the resolution limits of pelagic-ooze sediments, it is not possible to determine which is ancestral to the other. It may be important that the heavily calcified forms of *A. primus* are most abundant in samples from tropical latitudes, whereas *A. delicatus* seems to have a wider latitudinal distribution. This would suggest that some ecological preference existed among these two species and that some differentiation of the parent organism occurred prior to the appearance of these species in the fossil record. A close relation between *A. delicatus* and *A. primus* is suggested by their common optical properties. In preferred orientation, with the plane of the ceratolith at right angles to the direction of illumination, both species are nonbirefringent; that is, they do not become alternately bright and dark when rotated in cross-polarized light but rather remain gray. Horns of these early ceratoliths are either featureless or bear only weak keels, nodes, or other structures. The most obvious secondary structures, when present, are confined to the apical region, where they most commonly take the form of apical spurs or lumps.

The next ceratolith to appear is *Amaurolithus amplificus*. Morphologically this species differs from the two earlier species in these respects: Specimens are generally robust and relatively large with the horns diverging from the apical region at about 80°. One of the horns bears a hook, the other one a row of median nodes similar to but shorter and more robust than the rods which form the keel of *Ceratolithus cristatus*. Commonly, these nodes are secondarily calcified and very irregular in size. Optically, *A. amplificus* is similar to *A. delicatus* and *A. primus* in birefringence. However, specimens of this species are commonly tilted, probably because of the nodes developed on one side, and consequently they show slight birefringence.

Two more nonbirefringent species appear later in the record: *Amaurolithus bizzarus* and *A. tricorniculatus*. *A. bizzarus* is rare but seemingly restricted to the early Pliocene, whereas *A. tricorniculatus* may occur in late Miocene but primarily in early Pliocene sediments. Clearly these two species are closely related, but whether they evolve from *A. amplificus* or from *A. delicatus* and *A. primus* is not clear. The delicate construction and overall shape of the horseshoe probably point to *A. delicatus* as being the most likely ancestor, although the apical structure of *A. amplificus* is more similar to the apical structures found in *A. bizzarus* and *A. tricorniculatus*.

All the remaining species show strong birefringence in cross-polarized light, hence an evolutionary jump has to be made. The earliest species having this property is *Ceratolithus acutus*, a species that morphologically most closely resembles *Amaurolithus amplificus*. During the early Pliocene a change in crystallite orientation came about that remains unexplained. From this time on, the evolution of the genus seems much more straightforward in that some of the remaining species grade into one another almost imperceptibly. *C. rugosus* is readily distinguishable from *C. acutus* and *C. armatus* but not from *C. cristatus*. In most well-preserved sediment, the two could not be distinguished readily, although the propensity of *C. rugosus* to calcify and to be transformed into heavy, rugose specimens, within the organism or after being shed, makes the identification of most specimens relatively easy. *C. telesmus*, the most recently developed species in the lineage, is, in its extreme development, also readily distinguished. But specimens transitional between it and its probable ancestor, *C. cristatus*, are not uncommon.

The earliest species of Ceratolithaceae appear in the fossil record with no likely ancestral forms. Although this can be explained by assuming that the ancestral form developed in a noncalcifying state, it is nevertheless not unusual for a genus to appear abruptly without its having an obvious predecessor in the fossil record of calcareous nannoplankton.

SYSTEMATIC PALEONTOLOGY

Family CERATOLITHACEAE Norris, 1965
Genus *AMAUROLITHUS* n. gen.

Type species.—*Ceratolithus tricorniculatus* Gartner s. str.

Description.—The genus *Amaurolithus* consists of a group of horseshoe-shaped calcareous bodies, usually slightly asymmetrical and occasionally ornamented. Individual specimens behave as a single crystallographic unit, as with *Ceratolithus*, but the optic orientation is such that if specimens in preferred orientation are rotated in cross-polarized light they remain dark gray because the optic (*c*) axis is approximately perpendicular to the preferred orientation (with the plane of the ceratolith perpendicular to the direction of illumination).

***Amaurolithus amplificus* (Bukry and Percival) n. comb.**

Figure 6*g–l*

Ceratolithus tricorniculatus Gartner. Gartner, 1969 [in part], Gulf Coast Assoc. Geol. Socs. Trans., v. 19, p. 596, pl. 2, fig. 1.

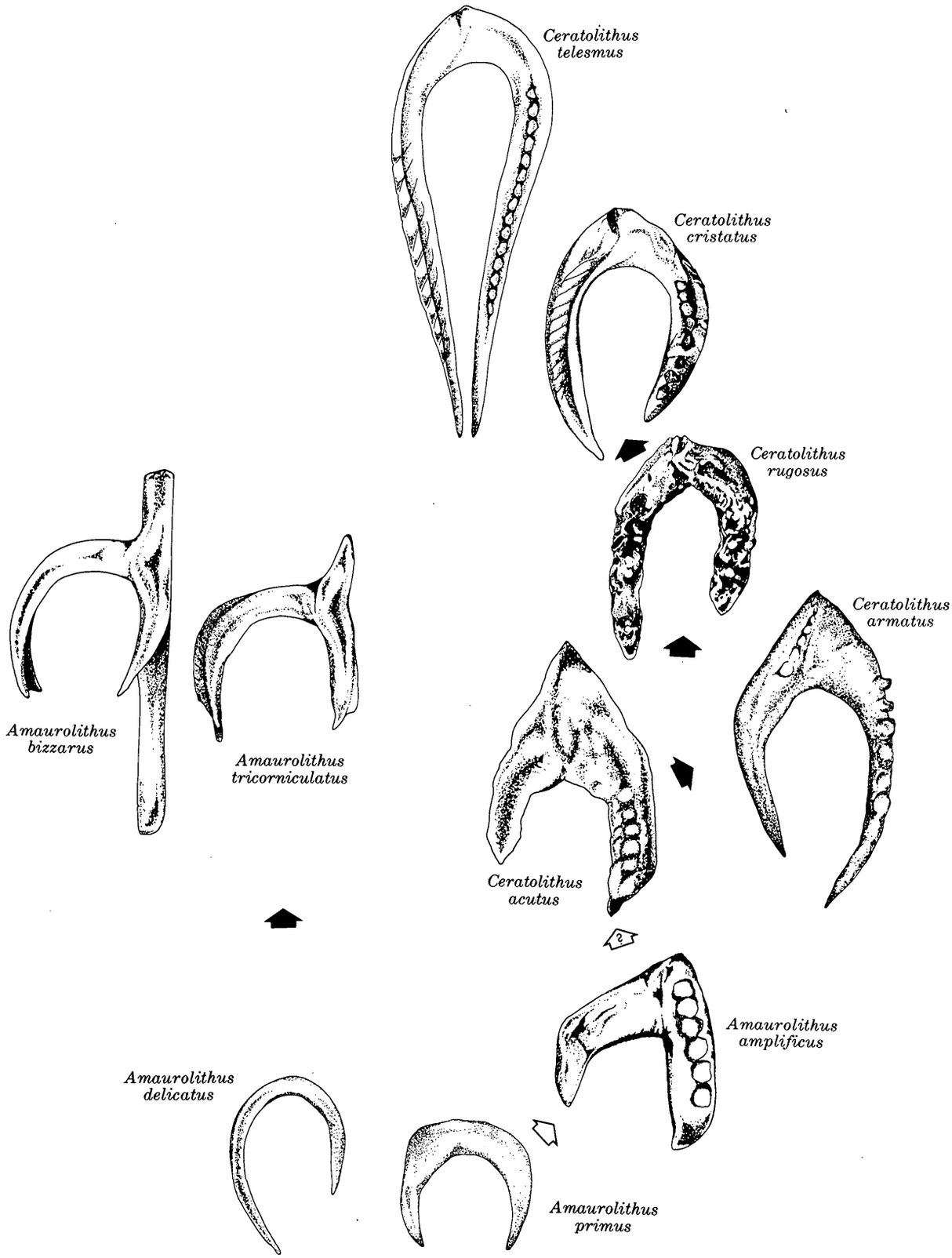

FIGURE 3.—Phylogenetic lineage of the family Ceratolithaceae. Only the end members, which constitute distinct species, are shown; for some branches, intermediate forms are recognizable. Solid arrows indicate a more direct relation between species than do open arrows.

Ceratolithus amplificus Bukry and Percival, 1971, Tulane Studies Geology and Paleontology, v. 8, p. 125, pl. 1, figs. 9–11.
Ceratolithus dentatus Bukry, 1973, Deep Sea Drilling Proj. Initial Repts., v. 16, p. 676, pl. 2, figs. 1–3.
Ceratolithus amplificus Bukry and Percival. Gartner and Bukry, 1974, Tulane Studies Geology and Paleontology, v, 11, p. 116, pl. 1, figs. 5–7.

Description.—Amaurolithus amplificus is a robust, strongly asymmetrical horseshoe-shaped species with a short but thick apical spine. The apical spine is located above the shorter of the two horns and is continuous with it and its row of nodes. The longer horn has a pronounced hook at its end. On well-preserved specimens, one surface of the most robust horn bears a line of nodes; on secondarily calcified specimens, these nodes are rough and commonly uneven. On many specimens, a keel may be visible in place of the nodes. In the preferred orientation, *A. amplificus* shows no birefringence. Tilted specimens show weak birefringence that varies with tilting of the specimen.

Remarks.—Amaurolithus amplificus is similar in form to *Ceratolithus acutus*, from which it differs by the more asymmetrical position of the apical spine and the lack of strong birefringence in cross-polarized light. *Amaurolithus tricorniculatus* is similar to *A. amplificus* but is much more delicate. Although both species may be weakly birefringent, *A. tricorniculatus* is most birefringent with the horns parallel to the direction of polarization. The pronounced curvature or hook at the tip of the longer horn of *A. amplificus* may give this species an angular appearance. The nodes on the surface of this species are no doubt predecessors of the rods that form the proximal keel in *Ceratolithus cristatus*. An intermediate development of this accessory structure can be seen well-preserved specimens of *C. acutus*, *C. armatus*, and *C. rugosus*.

Occurrence.—Amaurolithus amplificus occurs in late Miocene sediments in association with *A. primus* and *A. delicatus*. Its earliest occurrence is somewhat above the first occurrence of these two species, and it disappears from the record at about the level of the first occurrence of *Ceratolithus acutus*.

Amaurolithus bizzarus (Bukry) n. comb.

Figure 8*a*, *b*

Ceratolithus tricorniculatus Gartner. Bukry and Bramlette, 1968 [in part], Tulane Studies Geology, v. 6, p. 152, pl. 2, figs. 2, 4.
Ceratolithus bizzarus Bukry, 1973, Deep Sea Drilling Proj. Initial Repts., v. 16, p. 676, pl. 1, figs. 6–10.
Hekel, 1973, Deep Sea Drilling Proj. Initial Repts., v. 20, p. 236, pl. 1, figs. 17.

Description.—Amaurolithus bizzarus consists of an asymmetrical horseshoe-shaped body to which is attached a long straight rod along a line through the part of the shorter horn and the apical spine. The straight rod and the horseshoe of this ceratolith may not be in the same plane. The horseshoe may have keel-like accessory structures that protrude at the same angle to the plane of the ceratolith, as in *A. tricorniculatus*, so that the horseshoe appears double and shifts laterally when a specimen is focused at different levels. This species generally appears nonbirefringent, but may be weakly birefringent. Because of its unusual shape, specimens generally lie at some random angle relative to the direction of illumination. When weak birefringence is manifest in specimens nearly perpendicular to the direction of illumination, the specimen appears brightest with the horns subparallel to one direction of polarization.

Remarks.—Amaurolithus bizzarus appears to be a monstrosity but, as its geographic occurrence is sufficiently widespread, this form should not be dismissed as a local variant. Morphologically and optically it is most similar to *A. tricorniculatus*, with which it occurs commonly and to which it is closely related.

Occurrence.—Amaurolithus bizzarus is always rare and is commonly overlooked. It occurs consistently in early Pliocene pelagic sediments in which other ceratolith species are more common.

Amaurolithus delicatus n. sp.

Figure 7*a–f*

Ceratolithus tricorniculatus Gartner. Bukry and Bramlette, 1968 [in part], Tulane Studies Geology, v. 6, p. 152, pl. 2, fig. 1.
Gartner, 1969 [in part], Gulf Coast Assoc. Geol. Socs. Trans., v. 19, p. 596, pl. 2, fig. 2.
Stradner, 1973 [in part], Deep Sea Drilling Proj. Initial Repts., v. 13, p. 1197, pl. 36, figs. 4–6.
Müller, 1974 [in part], Deep Sea Drilling Proj. Initial Repts., v. 25, p. 591, pl. 11, figs. 7–9.
Ceratolithus primus Bukry and Percival. Bukry, 1973, Deep Sea Drilling Proj. Initial Repts., v. 16, p. 676, pl. 1, fig. 11.
Hekel, 1973, Deep Sea Drilling Proj. Initial Repts., v. 20, p. 236, figs. 15, 16.

Description.—Amaurolithus delicatus has a delicate, slightly asymmetrical horseshoe-shaped form. The two horns of the ceratolith are unequal to subequal in length and point together so as to indicate closure of the open end of the horseshoe. The horns are of about equal thickness and taper regularly to a point. The arch may be no thicker than the horns or it may be slightly thickened. The arch of the horseshoe generally is smoothly curved but occasionally it may bear a small asymmetrically placed spur or a large apical lump. *A. delicatus* is nonbirefringent and remains gray when rotated in cross-polarized light.

Remarks.—Amaurolithus delicatus is similar to *A. primus*, with which it occurs. They differ from one an-

other in that *A. delicatus* is distinctly longer than wide and has delicate, uniformly thick horns and arch. *A. delicatus* differs from *A. tricorniculatus* with which it occurs in the early Pliocene in that it lacks the third horn or apical spine and generally has longer horns. *A. delicatus* is no doubt closely related to *A. primus*, with which it may be associated throughout its range, although commonly in many samples only one of the two species is present, suggesting a possible ecologic relation. *A. delicatus* along with *A. primus* was formerly included in one broadly defined species under the name *Ceratolithus tricorniculatus* (=*Amaurolithus tricorniculatus*). Morphologic and stratigraphic differences, however, suggest that three distinct taxa may be differentiated.

Occurrence.—*Amaurolithus delicatus* occurs in late Miocene and early Pliocene sediments. Its earliest occurrence follows closely the earliest occurrence of *A. primus* and the latest occurrence of *Discoaster neohamatus*. Its last occurrence is less reliable in some areas, especially in deep-pelagic sediments. It may be recorded no higher than slightly above the earliest occurrence of *Ceratolithus acutus*. Elsewhere it may be found substantially higher, overlapping in part the range of *C. rugosus*. Its youngest well dated occurrence seems to be in the uppermost event of the Gilbert reversed polarity epoch, at about 3.6 m.y., B.P.

Holotype.—Figure 7*e*.

Type locality.—DSDP 22–214–9–3, 22–23 cm; Indian Ocean (lat 11°20′ S.; long 88°43′ E.).

***Amaurolithus primus* (Bukry and Percival) n. comb.**

Figure 7*g–l*

Ceratolithus primus Bukry and Percival, 1971, Tulane Studies Geology and Paleontology, v. 8, p. 126, pl. 1, figs. 12–14.

Ceratolithus tricorniculatus Gartner, Stradner, 1973 [in part] Deep Sea Drilling Proj. Initial Repts., v. 13, p. 1197, pl. 37, figs. 1, 2.

Ceratolithus primus Bukry and Percival. Müller, 1974, Deep Sea Drilling Proj. Initial Repts., v. 25, p. 591, pl. 11, fig. 3.

Ceratolithus sp. Müller, 1974, Deep Sea Drilling Proj. Initial Repts., v. 25, p. 616, pl. 11, fig. 2.

Description.—*Amaurolithus primus* is a usually asymmetrical crescentic form. The two horns are unequal or subequal and pointed: they may point inward as in an incomplete circle, or they may be nearly parallel and point forward. The apical region may be slightly or heavily thickened with heavy calcification along the inner curvature of the crescent. Along the outer curvature of the crescent, an asymmetrical apical lump or a small apical spur may be developed, or specimens may lack any apical structure. Optically *A. primus* is nonbirefringent in the preferred orientation and remains uniformly gray when rotated in cross-polarized light.

Remarks.—*Amaurolithus primus* is most similar to *A. delicatus*, with which it occurs. It differs from that species by being approximately equidimensional in length and width and by having more a robust arch and shorter horns. The two species are closely related and both were at one time included in one species with *A. tricorniculatus*. The three are sufficiently different, however, to be separated on the specific level.

Occurrence.—*Amaurolithus primus* occurs in late Miocene and early Pliocene sediments. It is first recorded, along with *A. delicatus*, from above the level of extinction of *Discoaster neohamatus*. Its last occurrence is slightly higher than the first occurrence of *Ceratolithus acutus* in the lower part of the Gilbert reversed polarity epoch, or about 4.8 m.y. B.P., in the upper part of the *A. tricorniculatus* Zone.

***Amaurolithus tricorniculatus* (Gartner) n. comb.**

Figure 8*c–h*

Ceratolithus tricorniculatus Gartner, 1967, Kansas Univ. Paleont. Contr., Paper 29, p. 5, pl. 10, figs. 4–6.

Bukry and Bramlette, 1968 [in part], Tulane Studies Geology, v. 6, p. 152, pl. 2, fig. 3.

Bukry and Bramlette. 1969, Deep Sea Drilling Proj. Initial Repts., v. 1, p. 378, pl. 7, fig. A.

Ellis, Lohman, and Wray, 1972, Colorado School Mines Quart., v. 67, p. 58, pl. 18, figs. 2, 3.

Stradner, 1973 [in part], Deep Sea Drilling Proj. Initial Repts., v. 13, p. 1197, pl. 36, figs. 6–8; pl. 37, figs. 3, 4, 5?, 6.

Ceratolithus amplificus Bukry and Percival. Hekel, 1973, Deep Sea Drilling Proj. Initial Repts., v. 20, p. 236, pl. 1, figs. 12, 13. [Birefringence caused by thick, irregular overgrowth].

Ceratolithus tricorniculatus Gartner, Müller, 1974 [in part]. Deep Sea Drilling Proj. Initial Repts., v. 25, p. 591, pl. 11, figs. 11, 12; pl. 19, fig. 1.

Description.—*Amaurolithus tricorniculatus* is a slightly asymmetrical horseshoe-shaped species on which a pronounced apical spine is present on one side of the arch and more or less in line with the shorter of the two horns. Both horns may bear a keel that protrudes at some irregular angle to the plane of the ceratolith. The apical spine may be straight or curved, and frequently is broken. Ceratoliths of this species commonly are delicate; a few robust specimens may be found. In cross-polarized light this species may show slight or no birefringence. When birefringence is slight, the specimen is brightest with the horns parallel to the direction of polarization and darkest with the horns about 45° to the direction of polarization.

Remarks.—*Amaurolithus tricorniculatus* is similar to *A. bizzarus* but differs from that form by lacking the long, straight bar. *A. delicatus* is similar but lacks the pronounced apical spine and has horns close together. Specimens of *A. tricorniculatus* that are weakly

birefringent may owe this feature to the presence of a spur on one horn, which causes these specimens to be tilted slightly on a flat surface. Hence the natural orientation of some specimens of *A. tricorniculatus* may not be with the plane of the ceratolith perpendicular to the direction of illumination.

Occurrence.—Amaurolithus tricorniculatus is a late Miocene and early Pliocene species but is most common in early Pliocene deposits.

Genus *CERATOLITHUS* Kamptner 1950

Type species.—Ceratolithus cristatus Kamptner, 1950.

Description.—The genus *Ceratolithus* is comprised of a group of minute calcareous bodies more or less in the shape of an asymmetrical horseshoe. Individual specimens behave as a single crystallographic unit; specimens in preferred orientation rotated in cross-polarized light are alternately bright and dark.

Ceratolithus acutus Gartner and Bukry

Figure 6*a–f*

Ceratolithus amplificus, in Bukry, 1971, San Diego Soc. Nat. History Trans., v. 16, p. 305, 306, tables 1, 2.

Ceratolithus sp., in Gartner, 1973, Geol. Soc. America Bull., v. 84, p. 2024, 2026, 2027, 2030, 2031, figs. 2, 3, 6.

Ceratolithus acutus Gartner and Bukry, 1974, Tulane Studies Geology and Paleontology, v. 11, p. 115, pl. 1, figs. 1–4.

Description.—Ceratolithus acutus is a robust species that has unequal horns and a broad but pronounced apical spine and apical suture. This apical structure can be slightly asymmetrical, but typically is a ridge symmetrically alined with the bisectrix line between the two horns. The ridge is not an extension of the horns or their nodes or keels. In the preferred orientation, with the plane of the ceratolith perpendicular to the direction of illumination, *C. acutus* is highly birefringent. Specimens are brightest when the horns are at about 45° to the polarizing directions of the crossed nicols and go to extinction when the horns are parallel to the direction of polarization.

Remarks.—Ceratolithus acutus is similar to the closely related species *C. rugosus* in its optical properties in cross-polarized light. It differs by having a pronounced apical spine. *Amaurolithus amplificus* is only weakly birefringent and has the apical spine more asymmetrically located. *C. armatus* is strongly birefringent and has a pointed arch but is distinguished by the distinctly asymmetric orientation of its apical ridge, which is only an extension of a line of nodes or a keel of one of the horns. *C. armatus* is a regional variant of the more widespread *C. acutus*. *C. acutus* was formerly included in *C. amplificus*, but the type level of *C. amplificus* is in the upper Miocene, below the extinction level of *Discoaster quinqueramus*. The highly birefringent ceratoliths, of which *C. acutus* is the oldest, did not appear until after the extinction of *D. quinqueramus*.

Occurrence.—Ceratolithus acutus is most common in lower Pliocene sediment. At the Capo Rossello in Sicily, this species occurs in the Trubi Formation from about 6 m to about 48 m above the base. In the equatorial Pacific, the species first appears near the middle of the lowermost event in the Gilbert reversed polarity epoch (core RC 12–66) and apparently ranges no higher than the Gilbert "b" event (core V24–59).

Ceratolithus armatus Müller

Figure 5*f–i*

Ceratolithus armatus Müller, 1974, Deep Sea Drilling Proj. Initial Repts., v. 25, p. 591, pl. 11, figs. 4–6; pl. 19, figs. 3, 4.

Description.—Ceratolithus armatus is a large species of ceratolith with curved, uneven horns, both of which taper uniformly to a sharp point. The apical region is deltoid and nearly symmetrical. The apical region on one surface is divided into two unequal parts by a ridge that extends from the apical point to the interior curvature. On the opposite surface, a row of pronounced nodes, present along the surface of the longer horn, extends along the edge on one side of the apical region; the keel from the shorter horn extends along the margin to the apex on the opposite side of the apical region. In cross-polarized light, this species shows strong birefringence.

Remarks.—Ceratolithus armatus is distinguished from the related species *C. rugosus* by its distinctly pointed arch. It is distinguished from the closely related *C. acutus* by the taper and curvature of the horns and by the asymmetry of the ridge in the deltoid apical region. For various specimens some differences are obscured, others accentuated, by different states of preservation.

Occurrence.—Ceratolithus armatus is presently known only from the Indian Ocean at DSDP 242 in the early Pliocene interval of core 4. It appears to be a locally successful derivation of the more widespread *C. acutus*. Stratigraphically, *C. armatus* appears to occur slightly higher than *C. acutus*.

Ceratolithus cristatus Kamptner

Figure 4*a–c*

Ceratolithus cristatus Kamptner, 1950, Österreichische Akad. Wiss., Math.-Naturw. Kl. Anz. 87, p. 154.

Kamptner, 1954, Archiv Protistenkunde, v. 100, p. 43, figs. 44, 45.

Bukry and Bramlette, 1968 [in part], Tulane Studies Geology, v. 6, p. 150, pl. 1, figs. 1–2, 4.

Ellis, Lohman, and Wray, 1972, Colorado School Mines Quart., v. 67, no. 3, p. 57, pl. 17, figs. 5, 6.

Müller, 1974, Deep Sea Drilling Proj. Initial Repts., v. 25, p. 591, pl. 11, fig. 10.

Description.—Ceratolithus cristatus is an asymetrical horseshoe-shaped species with unequal to subequal horns. On each side of the horseshoe, and centered along the median line of each horn, a keel is developed. Oriented with the open end of the horseshoe upward and the shorter horn to the left, the proximal keel is seen to be constructed of a row of rods. On the shorter horn, the rods are perpendicular to the plane of the horseshoe; on the longer horn, inclined forward, toward the point of the horn. The distal keel is delicate and is constructed of minute laths nearly perpendicular to the plane of the horseshoe. The two horns are joined along a thickened part that protrudes slightly to form a blunt apical angle along the outer curvature of the horseshoe. The inner curvature is smooth. Optically, *C. cristatus* is highly birefringent in the preferred orientation; it is brightest with the horns at about 45° to the direction of polarization and goes to extinction with the horns about parallel to the direction of polarization.

Remarks.—Ceratolithus cristatus is similar crystallographically to *C. acutus*, *C. rugosus*, and *C. telesmus*. Morphologically, *C. cristatus* is readily distinguished from *C. acutus* by the latter's pronounced triangular apical spine and generally featureless surface, and readily differentiated from *C. telesmus* by this species' long horns that nearly touch at their tip. *C. rugosus* commonly is much more robust than *C. cristatus* and has more parallel and closely appressed horns, but occasionally well preserved specimens of *C. rugosus* from sediments as old as middle Pliocene cannot be easily differentiated. Clearly *C. cristatus* has evolved rather directly from *C. rugosus* from which species it seems to differ chiefly by the curvature of its horns and by its lack of propensity to calcify heavily.

Occurrence.—Ceratolithus cristatus is a Pleistocene and Holocene species; its earliest occurrence is commonly noted at the base of the Pleistocene. But as it evolved rather directly from a Pliocene species, the precise level of speciation in continuous sections is a qualitative judgment. Many specimens are obviously transitional, especially near the Pliocene-Pleistocene boundary.

Ceratolithus rugosus Bukry and Bramlette

Figure 5*a–e*

Ceratolithus rugosus Bukry and Bramlette, 1968, Tulane Studies Geology v. 6, p. 152, pl. 1, figs. 5–9.

Ceratolithus rugosus Bramlette and Wilcoxon. Gartner, 1969, Gulf Coast Assoc. Geol. Socs. Trans., v. 19, p. 594, pl. 1, fig. 10.

Ceratolithus rugosus Bukry and Bramlette. Ellis, Lohman, and Wray, 1972, Colorado School Mines Quart., v. 67, no. 3, p. 58, pl. 18, fig. 1.

Colithus rugosus Bukry and Bramlette. Stradner, 1973, Deep Sea Drilling Proj. Initial Repts., v. 13, p. 1197, pl. 36, fig. 9.

Ceratolithus rugosus Bukry and Bramlette. Hekel, 1973, Deep Sea Drilling Proj. Initial Repts., v. 20, p. 236, pl. 1, figs. 18–21.

Müller, 1974, Deep Sea Drilling Proj. Initial Repts., v. 25, p. 591, pl. 11, fig. 1.

Description.—Ceratolithus rugosus is a roughly horseshoe-shaped body on which the relative size of horns may vary from nearly equal to very unequal. Specimens are generally robust and rough in appearance seen with a light microscope. The horns are relatively parallel. With the electron microscope a proximal keel can be recognized on both horns of well-preserved specimens. The keel is constructed of cylindrical rods, as in *C. cristatus*, although it is not clear whether the rods are perpendicular to the plane of the ceratolith on both horns or only on one. A distal keel has not been observed. The apical region is commonly thickened on one side, most commonly over the short horn; occasionally over the long horn, no apical spine or spur is present. In the preferred orientation, *C. rugosus* is highly birefringent in cross-polarized light. Specimens are brightest with the horns pointing about 45° to the direction of polarization and are extinct with the horns parallel to the direction of polarization.

Remarks.—Ceratolithus rugosus is most similar to *C. cristatus*, into which it evolves in the late Pliocene or early Pleistocene; at the transition level, it is difficult to separate them. The horns of *C. rugosus* have less curature and are more closely appressed than those of *C. cristatus*. *C. acutus* is very similar optically, but has pronounced pointed apical spine. The three species without doubt represent a direct evolutionary lineage from the earliest Pliocene to Pleistocene. *C. rugosus* commonly is heavily calcified, both horns as well as the apical region being subject to secondary overgrowth. The general lack of calcified specimens in marly and clayey sediments suggests that this overgrowth is at least in part postdepositional.

Occurrence.—Ceratolithus rugosus is restricted to Pliocene sediments. Its oldest occurrence is in the upper part of the Gilbert "c" magnetic event about 4.4 m.y. B.P. Its youngest occurrence is unclear because it evolves rather directly into *C. cristatus* at about the level of the Pliocene-Pleistocene boundary.

Ceratolithus telesmus Norris

Figure 4*d–h*

Ceratolithus telesmus Norris, 1965, Archiv Protistenkunde, v. 108, p. 21, pl. 11, figs. 5–7; pl. 13, figs. 1–3.

Ceratolithus cristatus Kamptner. Bukry and Bramlette, 1968 [in part], Tulane Studies Geology, v. 6, p. 150, pl. 1, fig. 3.

Description.—The ceratolith of *Ceratolithus telesmus* is slightly asymmetrical, horseshoe shaped, with subequal long horns. The horns are uniformly tapered, nearly straight, and sharply pointed, but may be inflected near the points. The length of the horns is about twice the width of the horseshoe. Both proximal and distal keels are present; the proximal keel is constructed of rods as in *C. cristatus*, the distal appears structureless in the light microscope. The apical region is the thickest part of the ceratolith and has an asymmetrically placed seam or suture. In the preferred orientation, *C. telesmus* is highly birefringent in cross-polarized light. It is brightest with the horns about 45° to the direction of polarization and is extinct with the horns about parallel to the direction of polarization.

Remarks.—*Ceratolithus telesmus* is most similar to *C. cristatus*, from which it differs chiefly by having longer and more delicate horns.

Occurrence.—Ceratoliths of *Ceratolithus telesmus* are found in late Pleistocene and Holocene calcareous pelagic sediments. The oldest occurrence of the species is difficult to determine because it evolved from *C. cristatus* with which it occurs and which it resembles closely when the tips of the long, delicate horns are broken off. Norris (1965) noted that the living cells of *C. telesmus* are found chiefly in the equatorial region of the Indian Ocean, whereas *C. cristatus* cells have a wider latitudinal distribution.

Figures 4 through 8 follow "References Cited."

REFERENCES CITED

Bramlette, M. N., and Martini, E., 1964, The great change in calcareous nannoplankton fossils between the Maestrichtian and Danian: Micropaleontology, v. 10, p. 291–322.

Bukry, David, 1971, Cenozoic calcareous nannofossils from the Pacific Ocean: San Diego Soc. Nat. History Trans., v. 16, p. 303–327.

——— 1973, Coccolith stratigraphy, eastern equatorial Pacific, Leg 16 Deep Sea Drilling Project: Deep Sea Drilling Proj. Initial Repts., v. 16, p. 653–711.

Bukry, David, and Bramlette, M. N., 1968, Stratigraphic significance of two genera of Tertiary calcareous nannofossils: Tulane Studies Geology, v. 6, p. 149–155.

——— 1969, Coccolith age determinations, Leg 1, Deep Sea Drilling Project: Deep Sea Drilling Proj. Initial Repts., v. 1, p. 369–387.

Bukry, David and Percival, S. F., Jr., 1971, New Tertiary calcareous nannofossils: Tulane Studies Geology and Paleontology, v. 8, p. 123–146.

Ellis, H. C., Lohman, W. H., and Wray, J. L., 1972, Upper Cenozoic calcareous nannofossils from the Gulf of Mexico (Deep Sea Drilling Project, Leg 1, Site 3): Colorado Mines Quart., v. 67, no. 3, 103 p.

Gartner, Stefan Jr., 1967, Calcareous nannofossils from Neogene of Trinidad, Jamaica, and Gulf of Mexico: Kansas Univ. Paleont. Contr., Paper 29, 7 p.

——— 1969, Correlation of Neogene planktonic foraminifer and calcareous nannofossil zones: Gulf Coast Assoc. Geol. Socs. Trans., v. 19, p. 585–599.

——— 1973, Absolute chronology of the late Neogene calcareous nannofossil succession in the equatorial Pacific: Geol. Soc. America Bull., v. 84, p. 2021–2034.

Gartner, Stefan, and Bukry, David, 1974, *Ceratolithus acutus* Gartner and Bukry n. sp. and *Ceratolithus amplificus* Bukry and Percival—nomenclatural clarification: Tulane Studies Geology and Paleontology, v. 11, p. 115–118.

Hekel, Heinz, 1973, Nannofossil biostratigraphy, Leg 20, Deep Sea Drilling Project: Deep Sea Drilling Proj. Initial Repts., v. 20, p. 221–247.

Kamptner, Erwin, 1950, Über den submikroskopischen Aufbau der Coccolithen: Österreichische Akad. Wiss., Math-Naturw. Kl., Anz., v. 87, p. 152–158.

——— 1954, Untersuchungen über den Feinbau der Coccolithen: Archiv Protistenkunde, v. 100, no. 1, 90 p.

Martini, E., 1967, *Ceratolithina hamata*, n.g., n. sp., aus dem Alb von N-Deutschland (Nannoplankton incertae sedis): Neues Jahrb. Geologie u. Paläontologie Abh., v. 128, p. 294–298.

Müller, Carla, 1974, Calcareous nannoplankton, Leg 25 (western Indian Ocean): Deep Sea Drilling Proj. Initial Repts., v. 25, p. 579–633.

Norris, R. E., 1965, Living cells of *Ceratolithus cristatus* (Coccolithophorineae): Archiv Protistenkunde, v. 108, p. 19–24.

——— 1971, Extant calcareous nannoplankton from the Indian Ocean: 2d Planktonic Conf., Roma 1971, Proc., p. 899–909.

Stradner, Herbert, 1973, Catalogue of calcareous nannoplankton from sediments of Neogene age in the eastern North Atlantic and the Mediterranean Sea: Deep Sea Drilling Proj. Initial Repts., v. 13, p. 1137–1199.

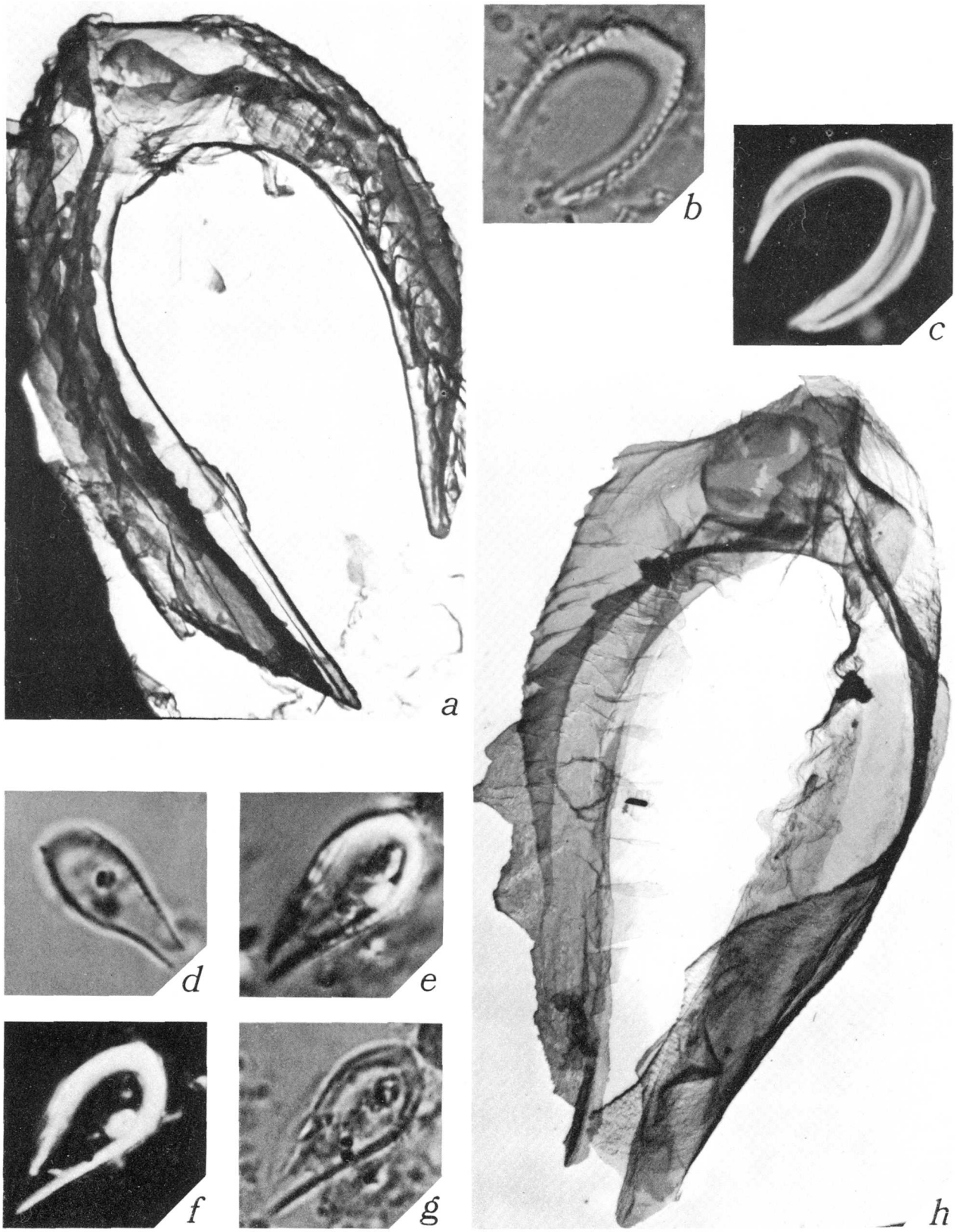

FIGURE 4.—*Ceratolithus.*

a–c. *Ceratolithus cristatus* Kamptner. Holocene, Caribbean. *a*, Transmission electron micrograph, × 9,400. *b,c*, Photomicrographs × 2,400. *b*, Transmitted light. *c*, Cross-polarized light.

d–h. *Ceratolithus telesmus* Norris.
d–g, Photomicrographs, × 2,400, Holocene, southeast Pacific. *d,g*, Transmitted light. *e*, Interference contrast. *f*. Cross-polarized light. *h*. Transmission electron micrograph, × 9,400, Holocene, Caribbean.

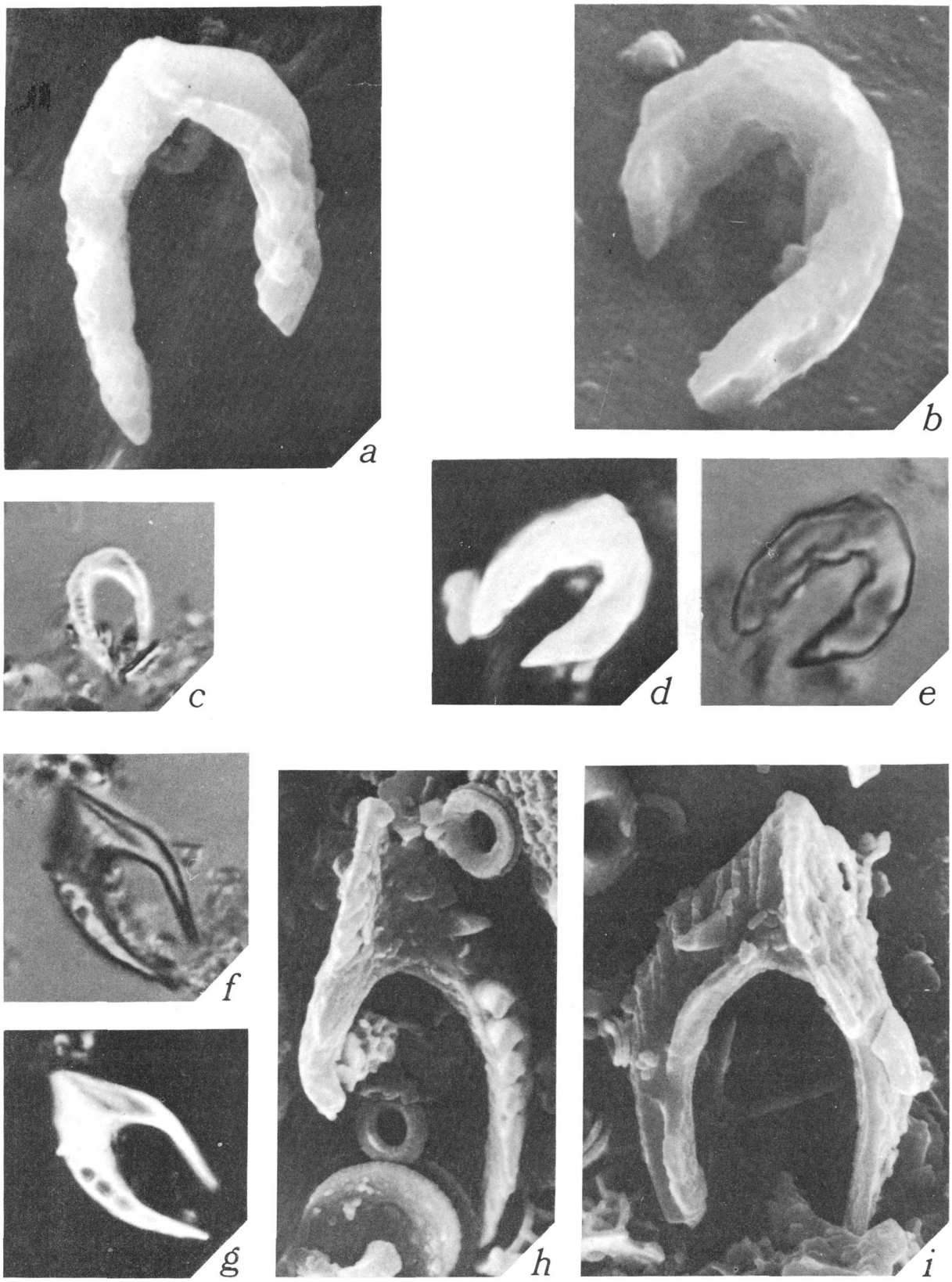

FIGURE 5.—*Ceratolithus.*

a–e. *Ceratolithus rugosus* Bukry and Bramlette.
a,b, Scanning electron micrographs, × 4,700, Pliocene. *a,* Northeast Atlantic. *b,* Equatorial Pacific. *c–e,* Photomicrographs, × 2,400, Pliocene, equatorial Pacific. *c,* Interference contrast. *d,* Cross-polarized light, long axis at about 45° to polarizing direction. *e,* Transmitted light.

f–i. *Ceratolithus armatus* Müller.
f,g, Photomicrographs, × 2,400, Pliocene, Indian Ocean. *f,* Transmitted light, *g,* Cross-polarized light, long axis at about 45° to polarizing direction. *h,i,* Scanning electron micrographs, Pliocene, Indian Ocean. *h,* × 5,600. *i,* × 6,600.

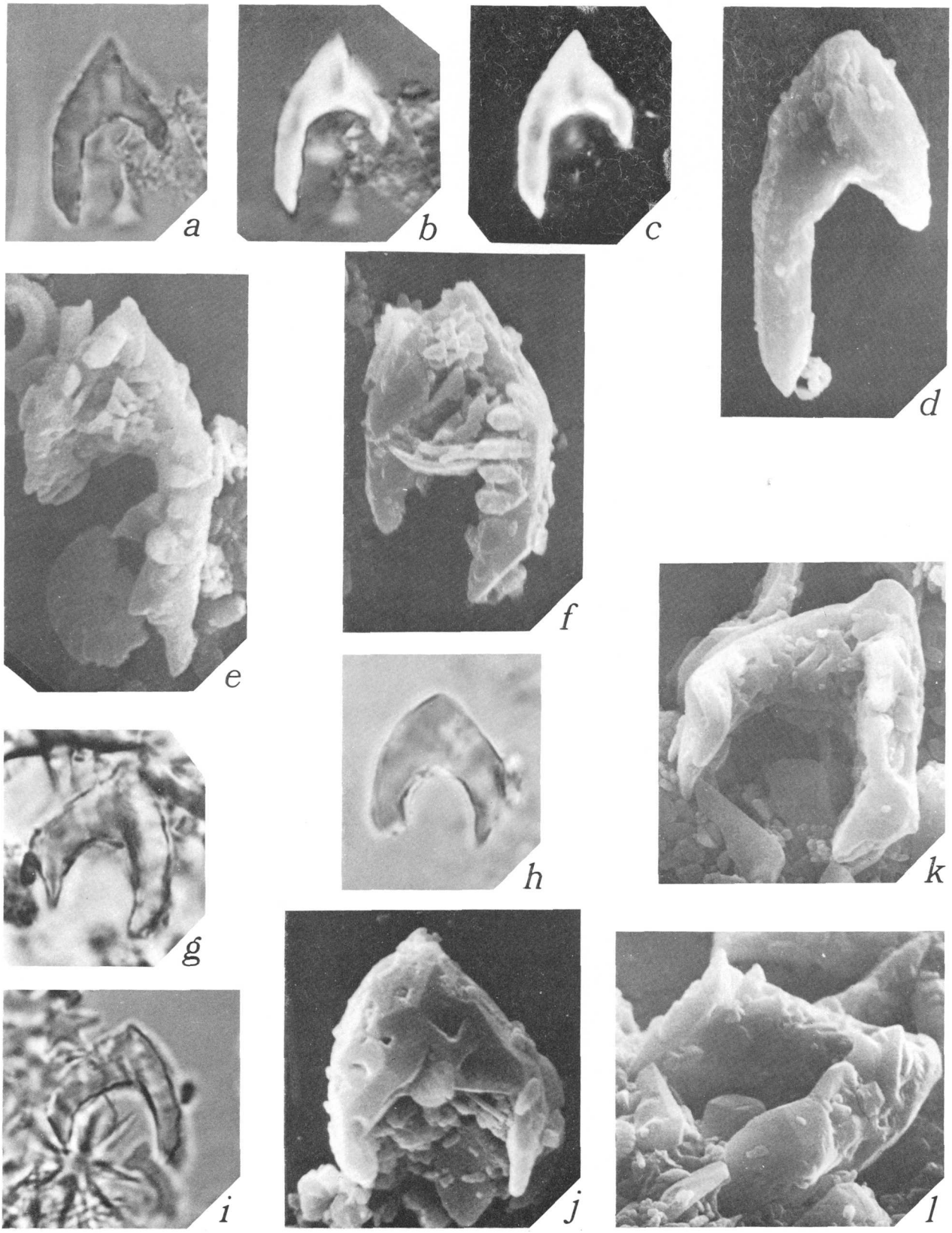

FIGURE 6.—*Ceratolithus* and *Amaurolithus*.

a–f. *Ceratolithus acutus* Gartner and Bukry. Pliocene Indian Ocean.

a–c, Photomicrographs, × 2,400. *a*, Transmitted light. *b*, Interference contrast. *c*, Cross-polarized light. *d–f*, Scanning electron micrographs, × 4,700.

g–l. *Amaurolithus amplificus* (Bukry and Percival) n. comb. *g–i*, Photomicrographs, × 2,400, transmitted light, Pliocene. *g*, Western Atlantic. *h*, Indian Ocean, *i*, Central Pacific. *j–l*, Scanning electron micrographs of the same specimen, × 4,700, Pliocene, Indian Ocean.

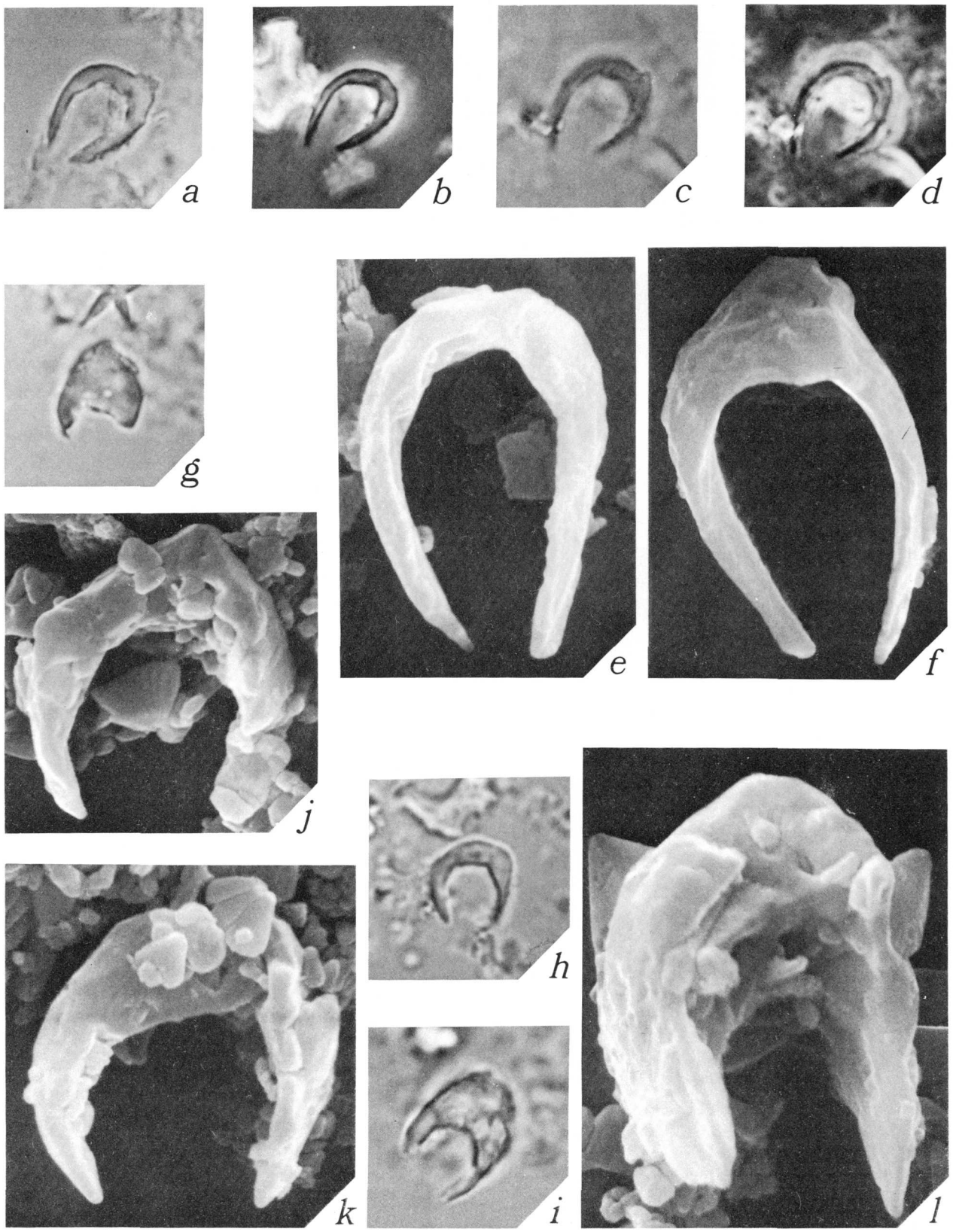

FIGURE 7—*Amaurolithus*.

a–f. *Amaurolithus delicatus* n. sp.
a–d, Photomicrographs, × 2,400, late Miocene. *a,c*, Transmitted light. *a*, Indian Ocean. *c*, Central Pacific. *b,d*, Phase contrast, late Miocene, central Pacific. *e,f*, Scanning electron micrographs, × 9,400, late Miocene, Indian Ocean.

g–l. *Amaurolithus primus* (Bukry and Percival) n. comb.
g–i, Photomicrographs, × 2,400, transmitted light, late Miocene. *g*, Indian Ocean. *h,i*, Central Pacific, *j–l*, Scanning electron micrographs, × 9,400, late Miocene, Indian Ocean.

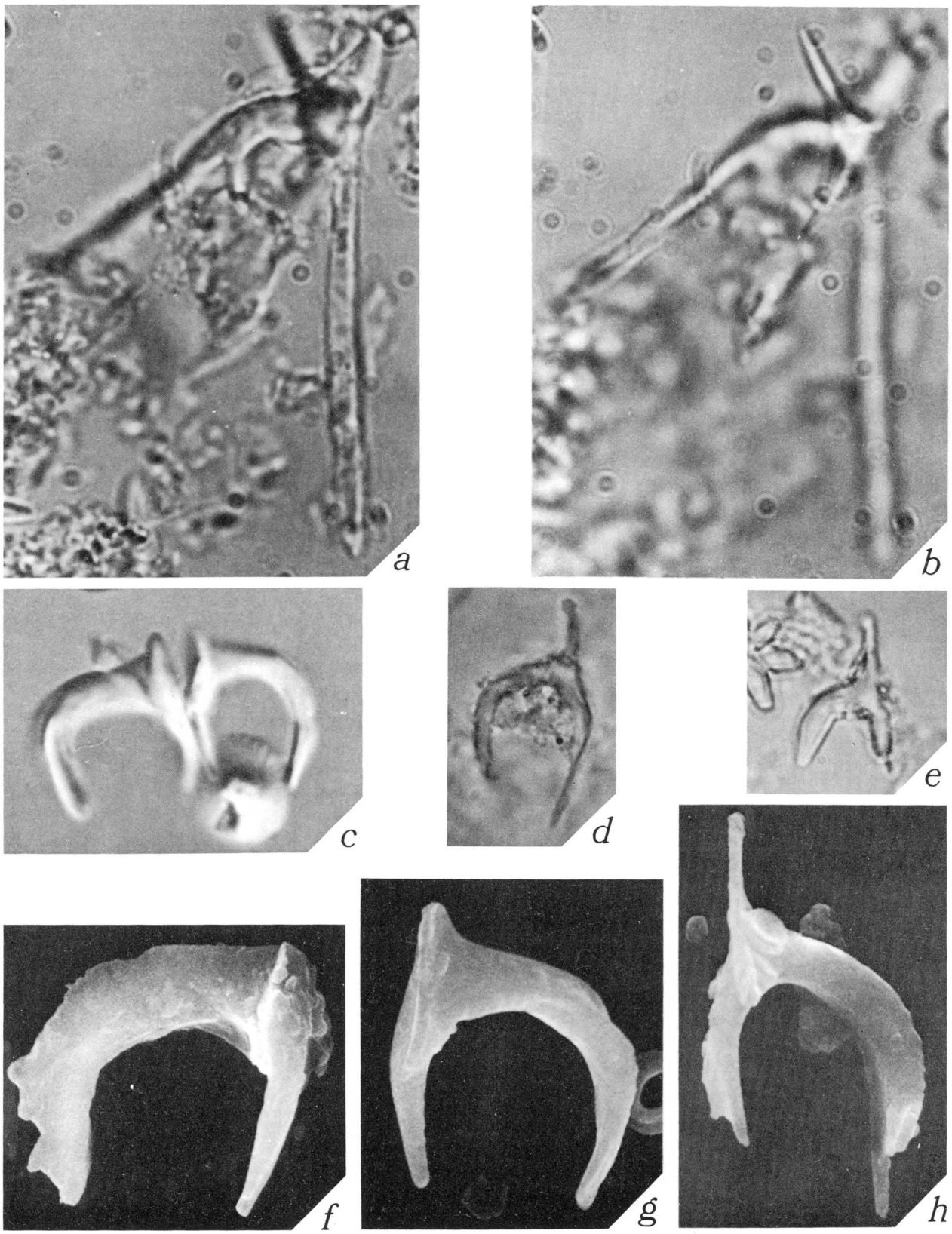

FIGURE 8—*Amaurolithus.*

a,b. *Amaurolithus bizzarus* (Bukry) n. comb.
Photomicrographs, × 2,400, Pliocene, western Pacific.

c–h. *Amaurolithus tricorniculatus* (Gartner) n. comb.
c–e, Photomicrographs, × 2,400, Pliocene. *c,* Interference contrast, Gulf of Mexico. *d,e,* Transmitted light. *d,* Sicily. *e,* Western Pacific. *f–h,* Scanning electron micrographs, × 4,700, Pliocene, Gulf of Mexico.

Jour. Research U.S. Geol. Survey
Vol. 3, No. 4, July–Aug. 1975, p. 467–473

RADIOCHEMICAL DETERMINATION OF VERY LOW CONCENTRATIONS OF NICKEL IN ROCKS AND MINERALS

By ROBERT A. ZIELINSKI, Denver, Colo.

Abstract.—A radiochemical procedure has been developed for the determination of very low concentrations of nickel in rocks and minerals. Sensitivity is 0.01 μg Ni. Accuracy and precision is estimated to be ±5 percent to levels as low as 0.1 μg Ni—a marked improvement over other analytical techniques. Samples are irradiated, combined with nickel carrier, and treated by a series of chemical procedures: (1) collection of nickel in a lead bead using a fire-assay technique, (2) refusion of the lead bead and precipitation of basic element hydroxides, (3) anion-exchange chromatography, and (4) precipitation of nickel dimethylglyoxime. The nickel precipitate is weighed to determine chemical yield and counted for β activity of Ni^{65} along with a precipitate from irradiated nickel standard solution.

Numerous techniques are available for rapid, quantitative determinations of nickel in natural materials. Most reported nickel analyses of rocks and minerals are by X-ray fluorescence, atomic absorption, colorimetric procedures, or emission spectrography. Detection limits and expected accuracy and precision for each of these techniques are reported elsewhere (Rader and Grimaldi, 1973; Bastron and others, 1960; Perkin-Elmer Corp., 1966). Generally, precision of the above methods is ±10 percent or better for replicate determinations of samples with >10 ppm Ni. At lower nickel concentrations, precision deteriorates and so, to be reliable, determinations must be performed on nickel concentrates. Concentration procedures require dissolution of large volumes of material and are therefore inappropriate for analysis of hard-won samples. Such samples may include rocks from extraterrestrial, mantle, and ocean-floor environments, as well as mineral separates. Separates are particularly pertinent in the light of recent interest in accurate determination of trace-element distributions between mineral phases and groundmass material.

The procedure described herein was developed to provide the capability of performing high-precision, accurate nickel analyses at concentrations less than 10 ppm. Samples are subjected to neutron irradiation, and then after addition of nickel carrier, samples undergo radiochemical separation of nickel and counting for β activity of Ni^{65}. Chemical yields are determined by weighing a final precipitate of Ni DMG (nickel dimethylglyoxime). A similar approach was attempted by Smales, Mapper, and Wood (1957); their purification technique relied on an involved sequence of precipitations but the reported precisions and sensitivities were limited by less sensitive β-detection systems. Other radiochemical procedures based on incomplete purification of nickel followed by γ-ray detection and resolution using NaI detectors have been described (Ehmann, 1960; Allen and others, 1970; Wanke and others, 1970). These procedures, though useful, are considerably less sensitive than procedures utilizing modern β-detection apparatus, as discussed below.

Acknowledgments.—The author thanks H. T. Millard for suggesting lead-bead formation as a novel means of collecting nickel and for providing chemical equipment and counting facilities. Thanks also go to the staff of the U.S. Geological Survey TRIGA [1] reactor for doing the sample irradiations and to Claude Huffman for atomic absorption analysis of the nickel standard solution.

REAGENTS AND APPARATUS

Nickel stock solution, 1 mg Ni/ml: Dissolve 318.13 mg of spectrographically pure NiO in ≈100 ml of redistilled 6 *N* HNO_3. Dilute to 250.0 ml with distilled and deionized water. Store the solution in a polyethylene bottle.

Nickel standard solution, 10 μg Ni/ml: Transfer 10.0 ml of stock solution to a 1-litre volumetric flask containing ≈50 ml of redistilled 6 *N* HNO_3. Dilute to the mark with distilled, deionized water. Store an aliquot of the solution in a polyethylene bottle. Fresh standards should be prepared periodically. (See discussion below.)

Dimethylglyoxime solution: Dissolve 0.7972 g of DMG in 100 ml of pure ethyl alcohol.

Nickel carrier solutions, 5 mg and 10 mg Ni/ml: Dissolve 2.208 g of reagent-grade $NiCl_2$ in 200.0 ml and in 100.0 ml 2*N* HCl. Store in polyethylene bottles.

[1] Training Research, Isotope General Atomic.

Tartaric acid solution, 50 wt percent: Dissolve 63 g tartaric acid in 100 ml distilled, deionized water.

Flux mixture: Mix 1.08 g reagent-grade PbO with≈3 g fused sodium borate (borax glass).

Anion-exchange apparatus: Fill a 25-ml buret to a height of 20 cm with Bio Rad AG1–X8 anion-exchange resin, chloride form, 100–200 mesh, which has been previously equilibrated with 12 *N* HCl.

Counting apparatus: A Beckman Widebeta II gas-flow proportional counter system with automatic sample changer and teletype readout. Anticoincidence circuitry lowers background levels to ≈2 c/min (counts per minute).

Graphite rods: Pencil "lead."

Hydrochloric acid: 12 *N*, 6 *N*, and 2 *N* solutions.

Nitric acid: Redistilled 6 *N* solution.

Ammonium hydroxide: Concentrated and 2 *N* solutions.

Sodium hydroxide: Pellets; 1 *N* solution.

Zirconium crucibles: 30 ml with covers.

Millipore filter disk: 8 μm, 25-mm diameter.

PROCEDURE

Sample irradiation.—Add 1.00 ml of Ni standard solution (10 μg Ni/ml) to a 4-dram polyethylene vial which has been previously rinsed with 2 *N* HCl and distilled, deionized water. Add 0.5 g of powdered sample to another 4-dram polyvial. Heat-seat the vials and irradiate at a neutron flux of $\approx 2.5 \times 10^{12}$ $n \cdot cm^{-2} \cdot s^{-1}$ for 1 h. For these experiments, irradiations were performed at the U.S. Geological Survey TRIGA reactor lazy-susan facility. Samples are allowed to decay for ≈1 h prior to delivery.

Unloading and precipitation of standard.—Open the polyethylene vial containing the standard solution of nickel and rinse it with 2 *N* HCl into a beaker containing 100 ml H_2O, 15 ml 12 *N* HCl, 3 ml 50 percent tartaric acid, and 5 mg Ni carrier. Make the solution slightly basic with 15 ml concentrated NH_4OH. If the solution is cloudy, reacidify with HCl and add more tartaric acid to complex any ions such as Fe^{+3}, Al^{+3}, and REE (rare earth elements), and again make basic with NH_4OH. If the basic solution is clear, make slightly acid with 12 *N* HCl and heat to ≈80°C. Add about 10 ml DMG solution and then 2 *N* NH_4OH drop by drop while stirring. A red precipitate of Ni DMG forms. Continue addition of NH_4OH until the solution is slightly basic. Cool the solution and pass it through a tared 8-μm Millipore filter using a suction flask and filter chimney. Wash the precipitate with cold distilled water. Remove the filter disk and precipitate and allow to air-dry to constant weight.

Fusion of the rock sample.—Open the vial containing the rock powder and transfer the powder to a 30-ml zirconium crucible containing 10 mg Ni carrier (10 mg Ni/ml carrier solution evaporated on a NaOH pellet). Add ≈5 g Na_2O_2, cover and sinter for 3 min over a Meker burner. Raise heat and fuse for ≈5 min. While mixture is still molten, add bits of graphite to a total of 0.2 g (1 stick of pencil lead) to destroy excess peroxide. Replace cover; if the melt is too hot, initial graphite will sputter and may be ejected unless the crucible is covered. Cool the melt until partly solidified and add the flux mix of 1 g PbO and 3 g borax glass. Raise the temperature slowly until the mix is uniform and molten. Add 1 g KCN in small increments over a 5-min period, periodically swirling melt and tapping the crucible bottom to promote lead metal collection at the bottom. Cover and heat for ≈5 min.

Dissolution of fusion cake.—Cool the fusion cake in air for 10 min. Transfer the crucible to a warm 500-ml beaker and add a few millilitres of water and then ≈20 ml 6 *N* HCl. Stir occasionally. When the reaction subsides, siphon off supernatant to a radioactive-waste bottle and add more 6 *N* HCl. Repeat addition and siphoning of HCl until the fusion cake is dissolved (30 min) and only a lead bead remains. Remove the bead, wash with water, and dry.

Fusion of lead bead.—Transfer the bead to a 30-ml zirconium crucible. Add 10 g Na_2O_2 and two pellets of NaOH. Cover and heat over a Meker burner until fusion is complete. Cool until cake solidifies. Transfer the crucible and cake to a 500-ml beaker containing 50 ml H_2O. After the cake dissolves, rinse the crucible with ≈5 ml aliquots of 2 *N* HCl and H_2O. Combine rinsings with solution, cool, and centrifuge.

Separation of hydroxides of basic elements.—Decant the liquid, combine precipitates of basic element hydroxides, and wash twice with 20 ml 1 *N* NaOH. Dissolve the precipitates in a minimum (≦1 ml) of 12 *N* HCl and transfer to a small beaker. Heat gently if precipitate of insoluble sodium chloride appears.

Anion exchange.—Load the solution onto the anion-exchange column and elute with 15 ml 12 *N* HCl into a 250-ml beaker.

Nickel DMG precipitation.—Add water and tartaric acid, and perform Ni DMG precipitation according to the previous description. Filter, wash, and air-dry the precipitate.

Chemical yield determination.—Weigh the dried precipitates of Ni DMG resulting from standard and sample solutions. The weight of recovered nickel is 0.2032 times the weight of the precipitate. Calculate yields of carrier nickel based on a starting weight of 5 mg Ni (standard) and 10 mg Ni (sample).

β counting of precipitates.—Heat-seal the precipitates and filter papers in polyethylene plastic and mount on aluminum planchets for β counting of Ni^{65} activity (half-life, $T_{1/2}=2.56$ h). Monitor decay curves and background decay for 24–48 h. Purity of nickel separation is determined from the half-life of decay. Check possible contributions of long-lived contaminants by monitoring the activity for times after which all Ni^{65} has decayed. This long-lived decay contribution may be extrapolated back to any time and subtracted from total counts during Ni^{65} decay.

Calculation of nickel concentration of sample.—Nickel content of the sample is calculated from the following equation:

$$\mu g \text{ Ni in sample} = 10\ \mu g\ \text{Ni} \times \frac{\text{c/min of sample minus background}}{\text{chemical yield of sample}} \times \frac{\text{chemical yield of standard}}{\text{c/min of standard minus background}}$$

Activities of standard and sample, as well as background contributions, are taken for the same time as read from the plotted decay curves.

DISCUSSION

Major radioactivity upon delivery of irradiated rock or mineral powders is due to Na^{24} ($T_{1/2}=15$ h) and Mn^{56} ($T_{1/2}=2.58$ h). Concentration of these elements in the sample, as well as irradiation and "cooling" periods, determines the radioactivity at delivery.

Additional information regarding the procedure for lead-bead formation and recovery was presented by Millard and Bartel (1971). That procedure is based on a well-known fire-assay technique for recovery of noble metals. In theory, the lead bead should contain siderophile elements which are at least as reducible as lead. Elements known to enter the lead bead include Au, Ag, Pt, Ru, Ir, Os, Cu, and Pd. Efficiency of lead reduction and recovery may be checked by weighing the bead: 1.0 g Pb metal represents 100 percent yield from the added 1.08 g PbO. Yields of associated metals may vary considerably but high lead recovery generally correlates with high recovery of associated metals. Sometimes numerous smaller beads form instead of one large bead, or one large bead forms, along with many tiny beads. Recovery of tiny beads is difficult, and generally the large bead or beads represent >90 percent of the total reduced lead.

Nickel yields by the above procedure are variable, ranging from 10 to 50 percent. Tracer experiments indicate that virtually all nickel loss occurs during the lead-bead formation. Lead-bead yields for all the fire assays performed ranged from 70 to 92 percent and did not seem strongly correlated with nickel yields. Further work is needed to identify the variables responsible. A rough qualitative determination of major radioactivities present at various stages of the chemical procedure was determined by counting γ activities on a Ge(Li) detector. Copper, manganese and iron appear to enter the bead in some amounts and sodium probably is contained in undissolved slag. Refusion and precipitation reduce most of these activities below the detection limit of the counter. Whatever manganese and iron come down with the hydroxide precipitate are efficiently removed during anion exchange and Ni DMG precipitation. Total activity of the lead bead is low enough that subsequent chemistry should be performed in areas suitable for low-level radiation.

The anion-exchange column was calibrated using $NiCl_2$ solutions. With concentrated HCl eluent, nickel is not absorbed and washes through in the first 15 ml. Literature determinations of the behavior of other elements indicate that all the siderophile elements as well as copper, zinc, and mercury are strongly retained by such a column in equilibrium with 12 *N* HCl. After use, the column is rinsed with water and reequilibrated with 12 *N* HCl. In some runs, sodium chloride reprecipitated after loading but this had no effect on the operation of the column.

Calculated chemical yields of nickel based on weights of Ni DMG precipitates were routinely 96–98 percent for the solutions of standard and carrier. Relative nickel yields were checked by reirradiating Ni DMG precipitates of standard solutions and samples, then by γ counting of Ni^{65}. Agreement was within ±2 percent. Cu, Co, Mn, Zn, or Fe^{+2} can interfere with the precipitate if present in large amounts but these elements are efficiently removed during previous steps. Alcohol or acetone cannot be used for rapid drying of the precipitate, because Ni DMG is soluble in these solvents.

Because of similar half-lives and β energies, the presence of Mn^{56} β activity in the Ni DMG precipitates cannot be distinguished from Ni^{65} β activity. Manganese activity in sample precipitates leads to systematically high nickel values. A separate experiment evaluated possible manganese blanks. Solutions containing 1×10^{-4} and 1×10^{-8} g Mn were irradiated for 1 h in the TRIGA reactor. The solution containing 1×10^{-4} g Mn was combined with spectrographically pure silica and nickel carrier and taken through the chemical procedure. The first 15 ml from the anion-column elution was concentrated and counted for γ activity along with 1×10^{-8} g Mn standard solution. Remaining activity corresponded to 0.2×10^{-8} g Mn. No β activity attributable to Mn^{56} was determined

from the subsequent Ni DMG precipitate 6 h after irradiation. A separate experiment using manganese tracers to determine the efficiency of manganese decontamination during Ni DMG precipitation indicated that only 0.009 percent of manganese activity in solution is carried by the precipitate. This could be further lowered by adding manganese holdback carrier to the precipitation solution.

Additional blanks were run by performing Ni DMG precipitations with nickel carriers and β counting (1) the rinsings of an irradiated 4-dram polyethylene vial and (2) the rinsings of an irradiated polyvial containing 1.0 ml of a distilled HNO_3 and distilled deionized H_2O mixture equivalent to that used for the nickel standard solution. Resulting β activities of Ni DMG precipitates are plotted as a function of time in figure 1. Both blanks are higher than the instrumental background of 2–3 c/min and show a long half-life. The polyvial and solution blank is significantly higher than the polyvial blank. Sources of the long-lived ($T_{\frac{1}{2}}$=10–25 h) blank remain to be evaluated. An element is required which follows the Ni DMG precipitate and is easily leached from the polyvial or which is present in larger concentrations in the irradiated solution. Preliminary investigation indicates Na^{24} to be the contaminant. The short-lived background component is unknown but appears to decay before samples are usually counted (ΔT=6 h).

Accuracy and precision of the procedure were checked by analyzing a synthetic sample composed of 0.5 g spectrographically pure SiO_2 plus 1.0 ml of 10 μg Ni/ml standard solution. β decay curves of the irradiated, chemically treated synthetic sample, a standard rock, and a precipitated standard solution are shown in figure 2. All samples show short-lived decay dominated by Ni^{65} ($T_{\frac{1}{2}}$=2.5 h). The chemically treated synthetic sample and standard rock decay to a lower background, reflecting the efficiency of the full procedure for producing chemically pure nickel separates. The precipitated standard solution decays to a background similar to the solution blank in figure 1. Calculation of the micrograms of nickel gave a value of 9.6 μg Ni for the synthetic rock. A repeat experiment gave a calculated value of 9.1 μg Ni. At ΔT=6h, sensitivity for nickel based on the standard solution concentration of 10 μg Ni is 500 (c/min)/μg Ni, compared to $\approx$80 (c/min)/μg Ni using a 3×3 NaI detector (Allen, 1970). Long-lived backgrounds for chemically treated rocks are $\approx$10 c/min extrapolated back to ΔT=6 h. If we assume $\pm 3\sigma$ variation in this background, detection limits for nickel are approximately 0.01 μg.

Precision was further tested by performing same-bottle replicate analyses of standard rocks with low nickel concentrations (table 1). Average coefficient of variation for the replicate pairs is $\approx$3 percent. Precision seems unaffected by the fact that most replicates were done on different days and with different chemical yields. Measured values are at the low range of nickel concentrations reported for these standard rocks. This may reflect small systematic low values from this technique and (or) generally high values in other splits. Reduced precision of the other analytical techniques at low nickel levels probably contributed to the wide range of reported values. Also, nickel contamination during analysis could cause some of the nonradiochemical values to be systematically high. Radiochemical techniques eliminate the likelihood of postirradiation contamination because only the radioactive fraction of the element is measured.

The above results for synthetic samples and standard

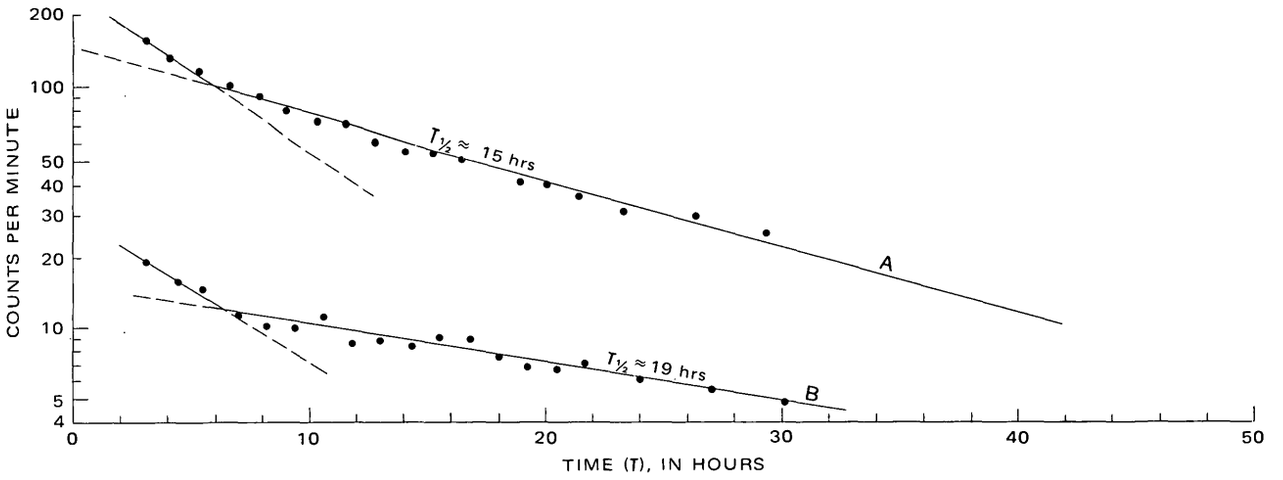

FIGURE 1.—β-decay curves of Ni DMG precipitates resulting from radiochemical treatment of (A) an irradiated solution of deionized water and (B) a water rinse of an irradiated polyethylene vial.

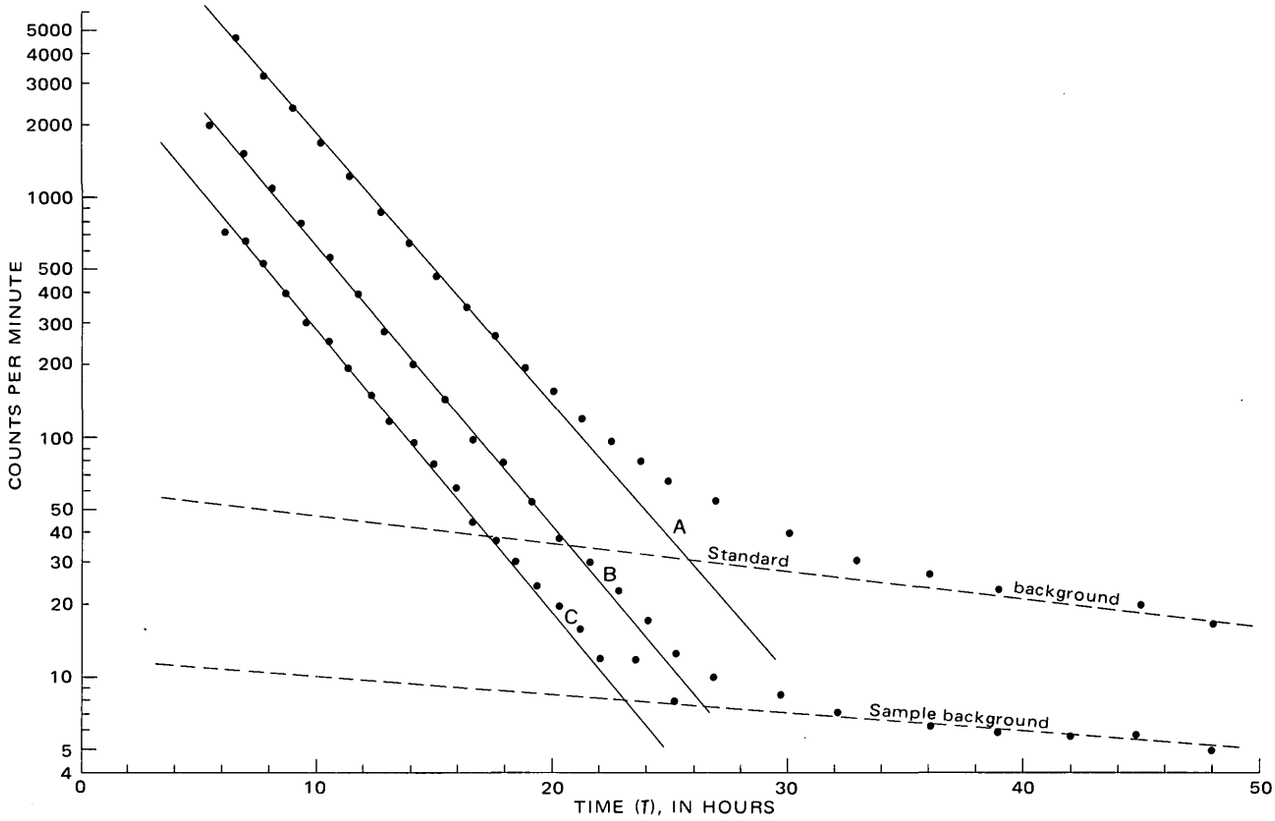

FIGURE 2.—β-decay curves of Ni DMG precipitates resulting from radiochemical treatment of (A) a nickel standard solution, (B) a nickel standard solution plus 0.5 g spectrographically pure SiO_2 and (C) standard rock BCR-1. $T_{1/2}$= 2.5 h.

TABLE 1.—*Results of nickel determinations in standard rocks, rhyolite groundmass, and synthetic standards*

Rock	Chemical yield (percent)	Nickel content (ppm)	Estimated coefficient of variation (percent)	Literature values	
				Average [1, 2]	Range [2]
G–2	22	2.3	±3.1	5.1	2–14
	48	2.4			
GSP–1	19	6.8	±1.0	12.5	3–25
	23	6.9			
AGV–1	10	15.0	±1.4	18.5	11–27
	45	15.3			
BCR–1	21	9.5	±6.4	15.8	8–30
	26	10.4			
JB–1	52	124	-----	[3] 139	-----
BHVO–1	26	110	-----	[3] 114	-----
Rhyolite groundmass.	18	.73	±3.5	----	-----
	21	.695			
Synthetic samples (10 μg Ni + 0.5 g SiO_2).	31	9.1 μg	±3.5	----	-----
	36	9.6 μg			

[1] Flanagan (1972).
[2] Flanagan (1969).
[3] USGS basalt standards. Preliminary X-ray fluorescence data.

rocks prompted further investigation of the technique on the assumption that a systematic error was generating ≈5 percent low values. Inspection of the equation shows that, for such a systematic error to be operative recorded counts for the sample, concentration of the standard, or standard chemical yield are too low, and (or) sample chemical yields or counts for the standard are too high.

Standard solution concentrations were analyzed twice by atomic absorption at a 2-mo interval. Analyses were by two chemists using different instruments and standard solutions. In both analyses the concentration was 10±0.1 ppm indicating the solution was of the correct concentration and stable over a 2-mo interval.

Discrepancies between the ratio of counts in the standard and sample and the Ni concentration ratio are symptomatic of (1) different neutron doses or nickel shielding during irradiation or (2) different degrees of β-particle self absorption or backscattering during counting. Samples and standard were irradiated in adjacent positions in the lazy-susan facility while being rotated around the reactor core at a speed of 1.2 r/min. In this arrangement, samples of similar geometry undergo the same neutron flux gradients and transients during irradiation. Shielding effects due to thermal neutron absorption in powdered rock samples,

discussed by Steinnes (1971), are unimportant so long as rock powders are <100 mesh. Table 2 presents results of an experiment testing the effects of varying concentration and matrix (SiO_2, H_2O) on the neutron-induced activity of simultaneously irradiated samples. γ-ray activity of Ni^{65} shows no dependence upon these variables above the level of counting statistics. Relative differences in absorption of Ni^{65} β particles by the Ni DMG precipitates are minimized by the uniformity of precipitate dimensions and counting geometries. Changes in precipitate thickness due to variable chemical yields apparently do not affect the results within the stated precision (table 1). Also, weights of precipitates are generally smaller for samples (20–50 percent yield of 10-mg carrier) than for standards (96–98 percent yield of 5-mg carrier). If self absorption of β particles by thicker Ni DMG precipitates is important, errors produced should give systematically lower counts for the standard and high nickel calculations. This, however, is opposite to the suspected trend.

TABLE 2.—*Neutron-induced activity of nickel-65 as determined from γ-counting*

Irradiated sample	Counts per minute[1]	
	366 keV	1,115 keV
1.0 mg Ni solution	1,393	1,555
1.0 mg Ni solution + 0.5 g SiO_2	1,430	1,548
10.0 mg Ni solution	14,180	15,430
10.0 mg Ni solution + 0.5 g SiO_2	13,850	15,117

[1] Counts per minute of γ-ray peak, minus background, corrected to the same point in time. Samples counted as solutions of equal volume. SiO_2 samples dissolved in concd HF.

Chemical yields of the standard, if low, are only low by a few percent, inasmuch as at least 96–98 percent Ni in the standard solution is recovered. Sample chemical yields may be systematically high if there is a finite chemical blank for nickel introduced by reagents. This interpretation was tested by duplicating the procedure in the absence of rock powder or nickel carrier. Five milligrams of nickel carrier was added for the Ni DMG precipitation. Any weight in excess of that expected for 98-percent yield of the 5 mg was attributed to the reagent nickel blank. The resulting 0.2 mg Ni blank causes systematic errors of +2 percent in chemical yields calculated, assuming a 10.0 mg Ni carrier. Procedures using 20 mg Ni carrier will reduce this blank contribution.

For the total procedure, estimated random errors amounting to ±5 percent standard deviation are based on generous estimated errors in (1) weighing of precipitates, (2) pipetting stock and standard solutions, (3) preparations of standard and stock solutions, (4) counting statistics, and (5) background determinations. No calculations were performed using experiments with nickel yields below ≦ 20 percent. Errors in determination of low nickel yields generate larger errors in calculated nickel contents. Background data become more critical for samples with very low nickel contents (<0.1 ppm). This ±5 percent estimate is in general agreement with observed precision over a large range of nickel concentrations. Accuracy of reported numbers may be systematically low by 2–5 percent.

Analyst time for setup, chemistry, calculations, and cleanup amounts to 5 h, or 2.5 h per sample. Total time, including sample irradiation and cooling plus precipitate drying, is 7 h. An additional 24 h is required for β counting. Time from reactor to β counting is ≈6 h (2.3 half-lives of Ni^{65}).

Although the procedure should expand the measurable range of nickel in natural samples, some materials do have nickel contents below the 10-ppb detection limit. One such specimen analyzed was a phenocryst feldspar separate from rhyolite groundmass of 0.7 ppm Ni concentration. The distribution coefficient for nickel between these phases is <0.014. Sensitivity of the technique is improved by using larger sample weights, longer irradiation times, shorter cooling times, and decreasing nickel losses in the lead-bead step.

REFERENCES CITED

Allen, R. O., Haskin, L. A., Anderson, M. R., and Muller, O., 1970, Neutron activation analysis for 39 elements in small or precious geologic samples: Jour. Radioanal. Chemistry, v. 6, p. 115–137.

Bastron, Harry, Barnett, P. R., and Murata, K. J., 1960, Method for the quantitative spectrochemical analysis of rocks and minerals, ores, and related materials by d-c arc technique: U.S. Geol. Survey Bull. 1084–G, p. 165–182.

Ehmann, W. D., 1960, Nickel in tektites by activation analysis: Geochim. et Cosmochim. Acta, v. 19, p. 159–155.

Flanagan, F. J., 1969, U.S. Geological Survey Standards, II—First compilation of data for the new U.S.G.S. rocks: Geochim. et Cosmochim. Acta, v. 33, p. 81–120.

——— 1972, Values for international geochemistry reference samples: Geochim. et Cosmochim. Acta, v. 37, p. 1189–1200.

Millard, H. T., Jr., and Bartel, A. J., 1971, A neutron activation analysis procedure for the determination of the noble metals in geological samples *in*, Brunfelt, A. D., and Steinnes, E., eds., Activation analysis in geochemistry and cosmochemistry: Oslo, Universitetsforlaget, p. 353–358.

Perkin-Elmer Corporation, 1966, Analytical methods for atomic absorption spectrophotometry: Norwalk, Conn., Perkin-Elmer Corp.

Rader, L. F., and Grimaldi, F. S., 1973, Chemical analyses for selected minor elements in Pierre Shale: U.S. Geol. Survey Prof. Paper 391–A, 45 p.

Smales, A. A., Mapper, D., and Wood, A. J., 1957, The determination by radioactivation of small quantities of Ni, Co, Cu in rocks, marine sediments and meteorites: Analyst, v. 82, p. 75–88.

Steinnes, E., 1971, Epithermal neutron activation analysis of geological material: *in* Brunfelt, A. O., and Steinnes, E., eds., Activation analysis in geochemistry and cosmochemistry: Oslo, Universitetsforlaget, p. 113–128.

Wanke, H., Begemann, F., Vilesek, E., Rieder, R., Teschke, F., Born, W., Quijano-Rico, M., Voshage, H., and Wlotzka, F., 1970, Major and trace elements and cosmic-ray produced radioisotopes in lunar samples: Science, v. 167, p. 523–525.

Jour. Research U.S. Geol. Survey
Vol. 3, No. 4, July–Aug. 1975, p. 475–478

DETERMINATION OF TUNGSTEN IN GEOLOGIC MATERIALS BY NEUTRON ACTIVATION ANALYSIS

By FREDERICK O. SIMON and CARL L. ROLLINSON,[1]
Menlo Park, Calif., College Park, Md.

Abstract.—A method is described for the determination of tungsten in geologic materials. After fusion with sodium peroxide, tungsten is isolated by extraction into chloroform with α-benzoinoxime, back extraction into aqueous potassium hydroxide, and precipitation with α-benzoinoxime. The activities of the 0.13 and 0.48 MeV gamma rays are measured. The activity of the 0.155 MeV gamma ray of ^{188}Re (^{188}W), added prior to the fusion, is measured to determine the yield; yields normally range from 40 to 90 percent. The coefficients of variation for less than part-per-million concentrations of tungsten are normally <20 percent; the limit of detection is 0.005 ppm for a 100-mg sample.

Examination of the literature reveals that very little is known about the distribution of tungsten in nature; normal semiquantitative spectrographic methods do not possess adequate sensitivity to determine tungsten in geologic materials. If large samples are available, tungsten can be determined spectrophotometrically (Sandell, 1959), but this method cannot be used for small samples of minerals (100 mg or less).

Johansen and Steinnes (1970) determined tungsten in rocks by neutron activation analysis using anion-exchange separations; yields were determined by reirradiation. Hamaguchi and others (1961) separated tungsten from other elements in silicate rocks by precipitation with α-benzoinoxime prior to neutron activation analysis. Morrison and others (1969) used anion exchange to separate a group containing tungsten for gamma-ray counting with a Ge(Li) detector.

In the method described here, tungsten is extracted into chloroform with α-benzoinoxime, stripped from the chloroform with potassium hydroxide, and precipitated with α-benzoinoxime. The 0.13 and 0.48 MeV gamma rays of ^{187}W are counted. Tungsten-188, added prior to the fusion of the samples, is used to determine the chemical yield. Fourteen samples and 4 monitors were processed in 6 h. Several counting techniques have been investigated with varying degrees of success.

EXPERIMENTAL METHOD

Detectors and electronics

Data were collected with one of three germanium detectors: a 15-cm^3 coaxial detector, FWHM (full width, half maximum) = 4.7 keV (at 1.33 MeV); a 30-cm^3 trapezoidal detector, FWHM = 3.0 keV; and a large (efficiency = 12 percent when compared to a 3- by 3-in NaI detector) coaxial detector, FWHM = 2.4 keV. Signals from the detectors were processed through a preamplifier and amplifier and stored in a 1024-channel pulse-height analyzer; the data were read with a teletype or line printer. The method described by Covell (1959) was used for all calculations. Three sodium iodide detectors and their associated electronic components were assembled (fig. 1) in order to measure double and triple coincidence events.

Samples and irradiations

Samples (≈0.1 g) and monitors were sealed in 0.4-dram polyethylene vials and irradiated for 1 h in the

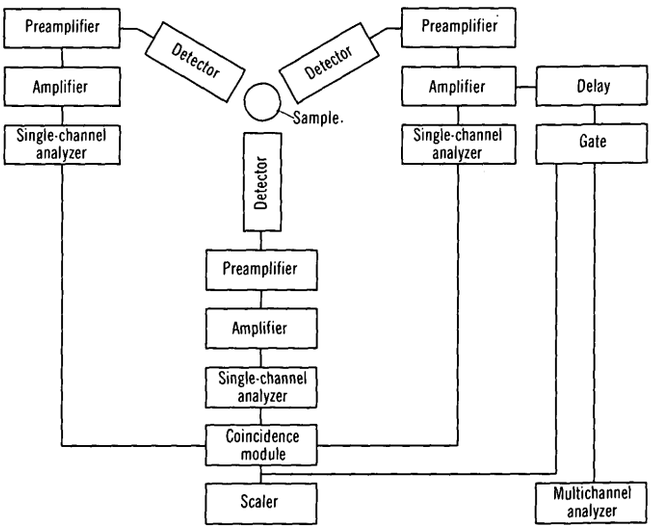

FIGURE 1.—Schematic diagram of coincidence-counting apparatus.

[1] University of Maryland.

National Bureau of Standards reactor in a thermal neutron flux of 5×10^{13} n·cm^{-2}·s^{-1}. The samples were allowed to decay for 24 h before the chemical separations were started.

A 0.100-ml aliquot of a standard tungsten solution (prepared by dissolving $NaWO_4$ in 0.1 percent KOH and diluting so that the working solution contains 10 ppm W) was evaporated on 0.1 g CaO to make a flux monitor. The tungsten content of the calcium oxide was found to be 0.013 ppm.

Procedure for determining tungsten in geologic materials

One millilitre of carrier solution (1 mg W and 0.5 mg Mo), containing sufficient ^{188}W to determine the chemical yield, was evaporated in a zirconium crucible. The irradiated sample was fused with 2 g Na_2O_2, the melt leached with water, 10 ml α-benzoinoxime solution (2 percent in alcohol) added, and the solution acidified with sulfuric acid (final concn, 3 N H_2SO_4). Tungsten was extracted into 50 ml $CHCl_3$, stripped into 20 ml KOH (5 percent) precipitated with α-benzoinoxime from dilute sulfuric acid, and filtered.

The activities of the 0.13 and (or) the 0.48 MeV gamma rays of ^{187}W in the precipitates were measured using a Ge(Li) detector. After 1 week to allow ^{187}W (24-h half-life) to decay and ^{188}W (65-d half-life) to equilibrate with ^{188}Re (17-h half-life), the chemical yields were determined by measuring the activity of the 0.155 MeV gamma ray of ^{188}Re. An alternate method of determining the yield is to irradiate the tungsten α-benzoinoxime precipitates and count either the 0.13 or 0.48 MeV gamma rays of ^{187}W.

RESULTS AND DISCUSSION

The procedure for determining tungsten is based on the extraction of tungsten into chloroform with α-benzoinoxime and measurement of the activity of ^{187}W. The chemical yield is determined by measuring the activity of ^{188}Re in equilibrium with ^{188}W, which was added at the start of the chemical separations. Fourteen samples and 4 monitors were processed in 6 h; this does not include the counting time, which will vary with the tungsten content of the samples and with the efficiency of the germanium detector.

Yield determination

The use of ^{188}W to determine the chemical yield has several advantages over other procedures such as reirradiation of the final tungsten precipitates: (1) Less handling is required because the precipitates do not have to be packaged to be inserted in the reactor, (2) this method is more precise because the variation of the neutron flux is not a factor in the yield determination, and (3) if the reactor is not on site, a second trip to the reactor is eliminated.

The amount of ^{188}W added to determine the yield should be kept to a minimum. Rhenium-188 has several gamma rays at 0.478 MeV that could interfere with the 0.48 MeV gamma ray of ^{187}W. However, the 0.155 MeV gamma ray of ^{188}Re is 20 times greater than the 0.478 MeV gamma rays, and therefore no interference will occur if the amount of ^{188}W added is just sufficient for the yield determination. In practice, we found that an initial ^{188}W (^{188}Re) activity for the 0.155 MeV photopeak of 10–20 counts per minute was sufficient. Yields ranged from 40 to 90 percent.

Variation of the neutron flux

Flux monitors (1–2 mg of silver wire) were taped to each vial, and the activity of the 0.66 MeV gamma ray of ^{110m}Ag determined. Flux correction factors were applied to all calculations.

Counting geometry and efficiency

Tungsten oxide (9.75 μg) was irradiated and counted by various techniques. The results, presented in table 1, indicate that double and triple coincidence counting methods offer no advantage over normal counting methods using Ge(Li) detectors. The highest counting rate was obtained with a sodium iodide detector, but the poor resolution of this detector led to results 10 times too high when standard samples were analyzed. Attempts to further decontaminate the tungsten precipitate were not successful, and germanium detectors were substituted with excellent results. The 0.06 MeV X-ray of ^{187}W is the most sensitive, but the 0.13 and 0.48 MeV gamma rays were selected in order to avoid absorption problems with the low energy peak.

Nuclear interferences

No interference was detected with either the 0.48 or the 0.13 MeV gamma rays of ^{187}W by examining the spectra and by measuring the rate of decay for a variety of samples. Atkins and Smales (1960) found that the production of ^{187}W by the reactions $^{140}Os(n, \alpha)$

TABLE 1.—*Comparison of counting efficiencies*

[Geometries of the coincidence and noncoincidence counting systems were not equivalent]

Detector(s)	Coincidence	Energy (MeV)	Counts per minute per microgram
NaI(Tl)	None	0.48	20462
	Double	Integral	276
	Triple	Integral	20
Ge(Li)	None	.06	5700
	None	.13	2550
	None	.48	970

^{187}W and $^{187}Re(n, p)$ ^{187}W is negligible. Only 1.3 and 3.5 ppm W were found when pure osmium and rhenium were irradiated; since these elements are present in rocks at levels several orders of magnitude lower than tungsten, no interference will be found.

Tantalum-182 occasionally interfered with the yield determination in sphenes, which can contain up to several tenths of a percent tantalum. The 0.152 and 0.156 MeV gamma rays of ^{182}Ta interfered with the 0.155 MeV gamma ray of ^{188}Re (decay product of ^{188}W). The interference was immediately obvious, and the yield for these samples was determined by reirradiation.

Another possible interference is the production of ^{188}W by the double (n, γ) reaction

$$^{186}W(n,\gamma)^{187}W(n,\gamma)^{188}W.$$

An upper limit of this interference was calculated from equation 1.

$$N_b = \frac{\sigma_a \Phi N_a}{\lambda_a}[1-\exp(-\lambda_b t)] \qquad (1)$$

where N_b is the number of atoms produced, N_a is the number of target atoms, σ_a is the cross section of the target in square centimetres, Φ is the neutron flux, λ_a and λ_b are the decay constants, and t is the irradiation time. For the irradiation and counting times used, there will be no interference with the yield determination.

Tungsten content of the U.S. Geological Survey standard rocks

The procedure was tested on 11 U.S. Geological Survey standard rocks. The results, presented in table 2, are in reasonable agreement with those of Hamaguchi and others (1962) but are somewhat lower than the spectrophotometric results of Chan and Riley (1967). The results are systematically higher than those of Johansen and Steinnes (1970), although the differences between the two sets of results are not great.

TABLE 2.—*Tungsten content, in parts per million, of U.S. Geological Survey standard rocks*
[For additional results, see Flanagan (1969)]

Sample	Number of determinations	This Work	1	2	3
Diabase W-1	5	0.58±0.10	0.58	0.38	----
Granite G-1	2	0.40	.50	----	----
Granite G-2	5	0.10±0.03	----	.04	0.4
Basalt BCR-1	5	0.35±0.06	----	.24	.7
Grandodiorite GSP-1	6	0.30±0.07	----	.12	.5
Andesite AGV-1	5	0.57±0.07	----	.45	1.1
Peridotite PCC-1	5	0.007±0.002	----	----	----
Dunite DTS-1	5	0.016±0.002	----	----	----
Quartz latite QLO-1	2	0.62	----	----	----
Syenite STM-1	2	3.8	----	----	----
Rhyolite RGM-1	6	1.50±0.12	----	----	----

1. Hamaguchi and others (1962), neutron activation analysis.
2. Johansen and Steinnes (1970), neutron activation analysis.
3. Chan and Riley (1967), spectrophotometric analysis.

The decay of ^{187}W was checked for at least one half-life for all samples. The decay curves of ^{187}W for sample W-1 and a monitor are shown in figure 2, and the gamma-ray spectra are shown in figure 3. The coefficient of variation at the less than part-per-million concentration level in geologic materials was normally <20 percent, and the 3σ detection limit is 0.005 ppm for a 100-mg sample.

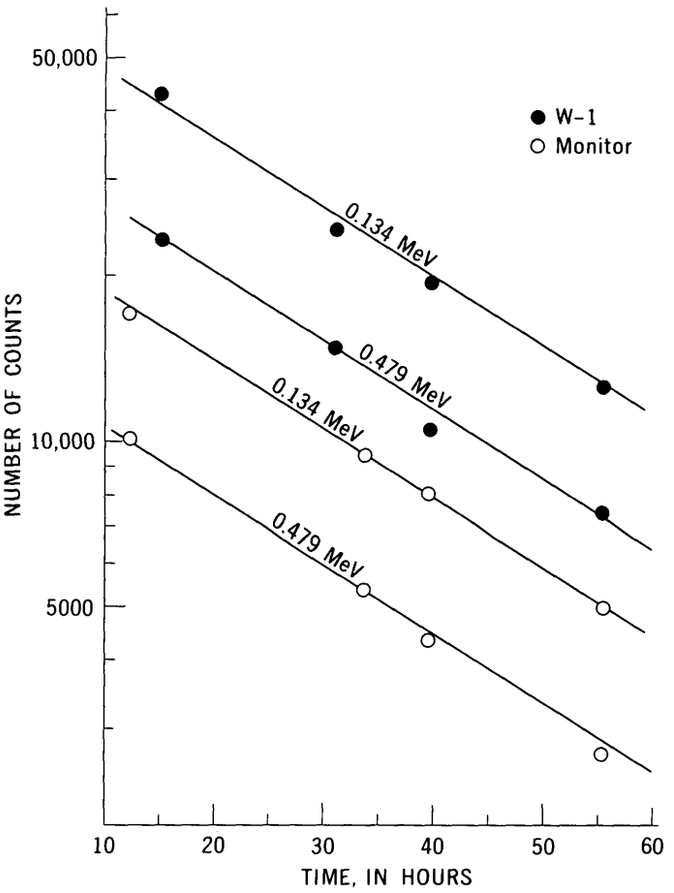

FIGURE 2.—Decay curves of ^{187}W for sample W-1 (live time, 4,000 s) and a monitor (live time, 100 s).

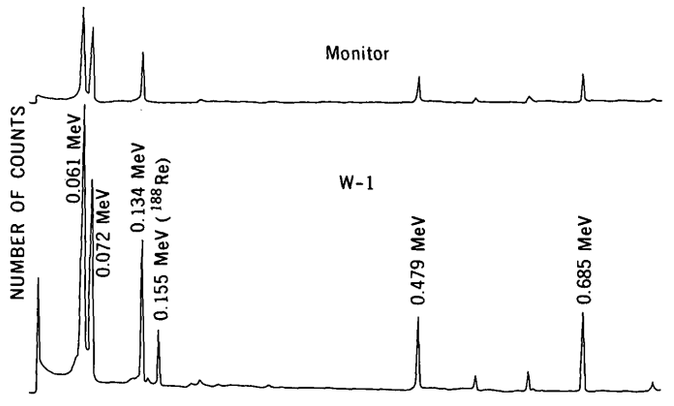

FIGURE 3.—Gamma-ray spectra of ^{187}W for a monitor (live time, 100 s) and sample W-1 (live time, 4,000 s).

REFERENCES CITED

Atkins, D. H. F., and Smales, A. A., 1960, The determination of tantalum and tungsten in rocks and meteorites by neutron activitation analysis: Anal. Chim. Acta, v. 22, p. 462–478.

Chan, K. M., and Riley, J. P., 1967, Determination of vanadium, molybdenum and tungsten in the new series of U.S. Geological Survey analyzed samples: Chem. Geology, v. 2, p. 171–172.

Covell, D. F., 1959, Determination of gamma-ray abundance directly from the total absorption peak: Anal. Chemistry, v. 31, p. 1785–1790.

Flanagan, F. J., 1969, U.S. Geological Survey Standards, II—First compilation of data for the new U.S.G.S. rocks: Geochim. et Cosmochim. Acta, v. 33, p. 81–120.

Hamaguchi, Hiroshi, Kuroda, Rokuro, Shimizu, Tsuneo, Sugisita, Ryuichiro, Tsukahara, Iwao, and Yamamoto, Ryuichi, 1961, Neutron activation analysis of molybdenum, tin, tantalum, and tungsten in silicates: Japan Atomic Energy Soc. Jour., v. 3, p. 800–805.

Hamaguchi, Hiroshi, Kuroda, Rokuro, Shimizu, Tsuneo, and Yamamoto, Ryuichi, 1962, Values for trace elements in G–1 and W–1 with neutron activation analysis—II; Mo, Sn, Ta, W: Geochim. et Cosmochim. Acta, v. 26, p. 503–505.

Johansen, O., and Steinnes, E., 1970, Determination of Co, Cu, Fe, Ga, W, and Zn in rocks by neutron activation and anion-exchange separation: Talanta, v. 17, p. 407–414.

Morrison, G. H., Gerard, J. T., Travesi, A., Currie, R. L., Peterson, S. F., and Potter, N. M., 1969, Multi-element neutron activation analysis of rock using chemical group separations and high resolution gamma spectrometry: Anal. Chemistry, v. 41, p. 1633–1637.

Sandell, E. B., 1959, Colorimetric determination of traces of metals: New York, Interscience Publishers, 1,032 p.

Jour. Research U.S. Geol. Survey
Vol. 3, No. 4, July–Aug. 1975, p. 479–485

LITHIUM IN SEDIMENTS AND BRINES—HOW, WHY, AND WHERE TO SEARCH

By JAMES D. VINE, Denver, Colo.

Abstract.—The possibility of using lithium in batteries to power electric vehicles and as fuel for thermonuclear power has focused attention on the limited resources of lithium other than in pegmatite minerals. The Clayton Valley, Nev., subsurface lithium brine has been the major source of lithium carbonate since about 1967, but the life of this brine field is probably limited to several more decades at the present rate of production. Lithium is so highly soluble during weathering and in sedimentary environments that no lithium-rich sedimentary minerals other than clays have been identified to date. The known deposits of lithium, such as the clay mineral hectorite and the lithium-rich brines, occur in closed desert basins of the Southwest in association with nonmarine evaporites. However, the ultimate source for the lithium in these deposits may be from hydrothermal solutions. The search for previously unreported deposits of nonpegmatitic lithium should consider its probable association, not only with nonmarine evaporite minerals, but also with recent volcanic and tectonic activity, as well as with deposits of boron, beryllium, fluorine, manganese, and possibly phosphate.

A revised estimate of the lithium resources in brine at Clayton Valley, near Silver Peak, Nev. (Kunasz, 1975), represents a significant reduction from previous estimates and hence requires a reappraisal of the total resources in the United States as reported by Norton (1973, p. 372). Although the total resources of lithium in brine are probably large, the amount that can be regarded as proved as well as probable recoverable reserves may be only about one-tenth of the total United States reserves of lithium. The remaining resources of brine would come under the categories of submarginal or undiscovered and therefore would not be regarded as economic at present. The major reserves of lithium in the United States occur in spodumene-bearing pegmatites at Kings Mountain, N.C., which have been estimated to contain about 440 million kilograms of lithium (Norton, 1973, p. 372). Spodumene is a silicate mineral, which is ideally suited for the ceramic industry but costly to reduce to other commodities such as lithium carbonate. The Clayton Valley brine has been the principal source of lithium carbonate in the United States since about 1967. The discovery of additional large brine fields or bedded lithium deposits will be required if the United States is to use lithium batteries for load leveling of off-peak power, or to sustain an automobile industry based on lithium batteries as a source of power, or to construct a thermonuclear power industry based on lithium fuel. This report is intended to further explain the need to search for new deposits of nonpegmatite lithium, to review the geological occurrence and geochemical distribution of lithium in sedimentary environments, and to speculate on the prospects for finding new deposits.

PRODUCTION AND USE

The use and production of lithium minerals and chemicals have increased steadily since the first lithium minerals were produced more than 75 years ago. Prior to 1938, lithium was obtained almost exclusively by handpicking large lithium-bearing crystals from granite pegmatites, where it occurs in both silicate and phosphate minerals. The principal, commercial lithium-bearing mineral, spodumene ($LiAlSi_2O_6$), is purified and used directly in making glass and ceramics where its value is related to both the strength and the thermal expansion of the product. Beginning in 1938, lithium phosphate has been produced from the brine at Searles Lake, Calif., where it is a minor by-product recovered during the production of trona, sulfate minerals, potash, and borates. Lithium carbonate has been produced as a primary product from subsurface brine at a desert playa in Clayton Valley, Nev., since about 1967. The estimated total production of lithium from pegmatite minerals and lithium salts derived from brine amounted to about 2¼ million kilograms of lithium[1] in 1968 and was valued at slightly more than $5 million (Cummings, 1970). Although exact production figures have not been published, it seems reasonable to assume that the Clayton Valley brine field accounted for nearly half of this amount.

[1] In comparing production data for lithium it is essential to specify the basis for calculation. as different sources will report Li_2O, Li_2CO_3, LiCl, or LiOH. The most convenient basis for calculation, which is used throughout this report, is elemental (metallic) lithium (Li) to which all the others can be converted; for example the amount reported for Li_2O multiplied by 0.464 gives the amount of lithium.

In addition to its uses in the glass and ceramic industries, lithium is used in multiple-purpose greases and in a great variety of industrial chemicals, including salts, the hydroxide, organic compounds, and as metallic lithium. The administration of lithium carbonate in the treatment of various mental illnesses has led to the speculation that trace quantities of lithium may be desirable in human nutrition. An increasing amount of lithium is used each year in primary lithium batteries of the dry-cell type (Grady, 1974), and one industry authority has indicated that this use alone will consume half a million kilograms annually by 1977 and a rapidly increasing amount thereafter.

Several potential new uses for lithium may completely alter the resource and demand outlook in the near future. The Argonne National Laboratory and others are currently working on the design of lithium batteries for the storage of off-peak power and to power electric vehicles of various sorts as an alternative to the pollution-producing internal combustion engine. One design model intended for an automobile would require a total of about 45 kg of lithium in the electrolyte and electrodes. The manufacture of 50,000 electric vehicles requiring 45 kg of lithium in each vehicle battery would take an entire year's production of lithium at the 1968 rate of production. The number of vehicles required to ameliorate the smog problem in our major cities would probably be several times 50,000 vehicles each year for a number of years.

Thermonuclear powerplants now being designed will require lithium to produce tritium, a primary fuel for the reaction. Different reactor designs will require more or less lithium, depending on the relative amounts of lithium and beryllium used in the neutron-absorbing blanket. One design would require 2.8 kg of lithium per megawatt of electrical power, MW(e), whereas another might require 920 kg/MW(e). For an ultimate capacity of perhaps 500,000 MW(e) by the year 2020 A.D., the first would require 1,400 t of lithium; the second would require 920,000 t of lithium (Locke Bogart, written commun., 1974).

LITHIUM INDUSTRY

Can industry increase the production of lithium at the rate necessary to meet the growing demand? The answer to this question requires a careful look at the industry and the technical problems associated with the extraction of lithium from known deposits and potential future resources.

Three companies in the United States account for all the domestic lithium production. The Foote Mineral Co. of Exton, Pa., is the largest producer of lithium minerals and chemicals. It produces spodumene ($LiAlSi_2O_6$) from pegmatite mines at Kings Mountain, N.C., and lithium carbonate from lithium-bearing brines that are pumped from the subsurface at Clayton Valley, near Silver Peak, Nev. Kerr-McGee Chemical Corp. (formerly American Potash and Chemical Corp.) recovers lithium phosphate as a byproduct of solar evaporation for other saline minerals at Searles Lake near Trona, Calif. Lithium Corp. of America, Inc., a subsidiary of Gulf Resources and Chemical Corp., produces lithium minerals from pegmatites in North Carolina. Several years ago they announced plans to extract lithium as a byproduct of solar evaporation from Great Salt Lake, Utah, but the plan was canceled, apparently because they could not get a firm contract for the sale of magnesium, which would have to be precipitated before the lithium could be produced. Several other companies, including NL Industries, have indicated an interest in the byproduct recovery of lithium from Great Salt Lake but to date this has not been accomplished.

Lithium-bearing pegmatite minerals such as spodumene will probably continue to be the source of much of the lithium used in the glass and ceramic industries. Although the Kings Mountain area, North Carolina, supplies most of the U.S. requirement for lithium-bearing pegmatite minerals, Canada and Rhodesia also have large reserves and resources of lithium in pegmatites (Norton, 1973, p. 372), but only South America is known to have even potential resources of lithium in brine. Lithium carbonate produced from brines will probably be the most satisfactory source for metallic lithium and lithium salts required in vehicle batteries and for lithium uses in industries other than ceramics.

ESTIMATES OF LITHIUM-BEARING BRINE RESERVES

When the Clayton Valley, Nev., brine field was being developed in the middle 1960's there were no data from which to estimate the quantity of brine that might ultimately be recovered. Reserve estimates were based on the average geochemical abundance of lithium-bearing sediment calculated from a few core holes and extrapolated to 1,000-ft depth and for the entire floor of the valley, some 32 mi^2 in area. Although these estimates made no allowance for recoverability of the brine, they seemed reasonable enough to be accepted and quoted in several reports of the U.S. Geological Survey and the U.S. Bureau of Mines as recently as 1974. After more than 8 yr of development and production history with the brine field at Clayton Valley, the Foote Mineral Co. has calculated and released a new estimate of lithium resources (Kunasz, 1975). Although this new estimate represents a significant reduction from previously published figures, the added

statement that only part of the total lithium resource can ever be recovered may have equal or greater significance.[1] Analysis of the available data indicates why this may be true.

The nature and distribution of the brine-bearing permeable strata in alluvium in Clayton Valley have not been described. Close analogies with other brine fields such as Searles Lake, Calif., where the brine is pumped from permeable salt beds (W. C. Smith, 1966; G. I. Smith, oral commun., February 1974), and Bonneville Salt Flat, Utah, where brine is derived from shallow clay fractures (Turk and others, 1973), have been denied by Ihor Kunasz (oral commun., May 1974). It follows that permeability in the Clayton Valley sediments is probably associated with the fine-grained detrital sediments that characterize the bulk of the sediments in the playa. The technique of drilling wells to a depth of as much as 600 ft implies recovery of brine throughout a section of alluvium as much as 600 ft thick. Consideration of the 10-mi^2 area of the brine field and the 600-ft depth of the producing wells suggest that the total volume of sediment from which lithium-bearing brine is pumped is about 5 km^3. If an average permeability of 3 percent is assumed, the volume of lithium-bearing water can be estimated to be about 150 million cubic metres. If the density of the water is about 1.1 this would be equivalent to about 165 million tons of brine. Published data indicate an average concentration of about 300 ppm lithium in the brine, for a total quantity of about 50 million kilograms of lithium.

Recharge to the brine aquifer is by ground- and surface-water flow from the surrounding mountains and pediment gravels and to a much lesser extent from precipitation on the playa surface. The ground-water flow, in particular, may bring with it a moderate amount of dissolved mineral matter including a minor amount of lithium. If the spring waters along the margin of the playa are representative of recharge from ground-water sources, they may carry a few tens of parts per million of lithium into the aquifer. The life of the deposit will be a function of the rate of production of the original 50 million kilograms of lithium plus lithium added from ground-water recharge until the concentration of lithium is reduced to a level that is no longer economic to pump. This may be two-thirds or three-fourths of the total, but production will cease before all the lithium is depleted because the price of the finished product must be balanced against the cost of pumping, maintenance of the evaporating ponds, precipitation, and drying of the lithium carbonate.

[1] After this report was in page proof, I. A. Kunasz (oral commun., 1975) submitted a revised estimate of 44,500 tons for the recoverable reserves of lithium at Clayton Valley, Nev.

OCCURRENCE OF LITHIUM

Lithium is associated chiefly with the clay fraction of sedimentary rocks (Horstman, 1957; Tardy and others, 1972), and it is known to occur in anomalously high concentrations primarily in the arid regions of the Western United States. Lithium is an essential constituent of a bentonitic clay from the Mojave Desert near the railroad stop of Hector (fig. 1, loc. 1), about 56 km east of Barstow, Calif. (Foshag and Woodford, 1936; Ross and Hendricks, 1945). The unusual properties of this clay attracted interest among the clay mineralogists who have given it the name hectorite and speculated as to its origin and the source of the 0.5 percent lithium and 4.75 percent fluorine that it contains (Ames and others, 1958). Hectorite is a trioctahedral montmorillonite belonging to the high magnesium (saponite) end of the smectite group. These minerals are low in aluminum and can be distinguished from the more common dioctrahedral smectites by the position of the 060 reflection near 62° 2θ on the X-ray diffraction pattern. Table 1 and figure 1 list the localities where hectorite or a clay mineral similar to hectorite have been reported. All are in nonmarine Cenozoic rocks or sediments, most occuring in the late Cenozoic.

GEOCHEMISTRY

The geochemical behavior and mineralogy of lithium in pegmatites is well documented (Heier and Adams, 1964; Heier and Billings, 1972), but its behavior and mineralogy in the sedimentary cycle is less thoroughly documented. Lithium is the lightest of all metals and a member of the alkali group of metals. It is a minor element, having a crustal abundance of about 20 ppm, similar to such elements as lead, gallium, and lanthanum. In minerals, univalent lithium can substitute to some extent for divalent magnesium and iron, but its smaller ionic size does not permit its substitution to any significant extent for the chemically related more abundant alkalies, sodium and potassium. All the common cations are able to dislodge Li^+ from base-exchange material, hence base-exchange reactions tend to bring lithium into solution (Hem, 1959, p. 134). Moreover, the simple salts of lithium are highly soluble, so there is little opportunity for their precipitation, except possibly under the most arid climatic conditions. Lithium tends to remain in the residual brine during evaporation of seawater and is not generally concentrated in marine halite. The lithium released from the primary minerals as the Li^+ cation is readily transported to sea where it becomes dispersed in the fine-grained argillaceous sediments in amounts generally less than 100 ppm. Locally higher concentra-

TABLE 1.—*Hectorite localities in the United States*

Locality (fig. 1)	Name	Location	Rock unit	Reference
1	Hector	San Bernardino, Calif. (sec. 35, T. 18 N., R. 5 E.).	Unnamed (Pliocene?)	Foshag and Woodford (1936), Ross and Hendricks (1945), Ames and others (1958).
2	Kramer borate	Kern, Calif. (secs. 13, 14, and 24, T. 11 N., R. 8 W.).	Tropico Group (Oligocene? and Miocene).	Dibblee (1967), Morgan and Erd (1969).
3	Unnamed (25 km NE. of Amboy).	San Bernardino, Calif. (not known).	Unknown	Foshag and Woodford (1936).
4	Spor Mountain (roadside claims).	Juab, Utah (sec. 8, T. 13 S., R. 12 W.).	Unnamed (Pliocene?)	Shawe, Mountjoy, and Duke (1964), Starkey and Mountjoy (1973).
5	Lyles lithium deposit	Yavapai, Ariz. (sec. 12, T. 13 N., R. 6 W.).	Unnamed (upper Cenozoic).	Norton (1965).
6	Peeples Valley	Yavapai, Ariz. (NE ¼, T. 11 N., R. 4 W.).	Unknown	Norton (1969).
7	Shadow Mountain	Teton, Wyo. (sec. 1, T. 43 N., R. 115 W.).	Teewinot Formation (Pliocene).	J. D. Love (written commun., 1973).
8	Roan Cliffs, (Uinta Basin).	Duchesne, Utah (sec. 12, T. 11 S., R. 10 E.; sec. 27, T. 6 S., R. 8 W.).	Green River Formation (Eocene).	Dyni (1973).
9	Clayton Valley	Esmeralda, Nev. (sec. 35, T. 1 S., R. 40 E., unsurveyed).	Alluvium (Quaternary).	Kunasz (1970).

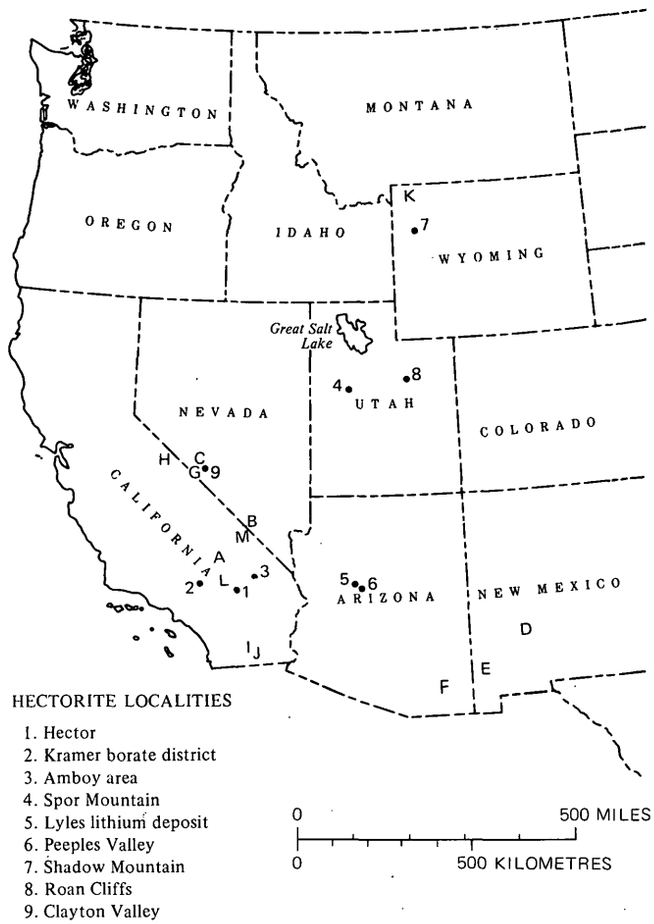

FIGURE. 1.—Index map showing hectorite localities in the United States. Other localities mentioned in text: A, Searles Lake; B, Amargosa Desert; C, Columbus Salt Marsh; D, Truth or Consequences; E, South Alkali Flat; F, Willcox Playa; G, Nivloc mine; H, Mono Lake; I, Salton Sea; J, Imperial Valley; K, Yellowstone National Park; L, Mojave Desert; and M, Death Valley.

tions are associated with nonmarine sediments, especially in arid climates and in oil-field brines where several tens of parts per million are known. In humid climates, lithium tends to become concentrated in kaolinitic clays associated with bauxite, where as much as 340 ppm lithium has been reported (Ronov and others, 1970). Magnesian silicates, such as sepiolites, stevensites, and hectorites that have formed authigenically during arid periods in lagoonal environments, and the associated limestones, dolomites, and detrital rocks, yield the largest amounts of lithium, ranging from 400 to 6,000 ppm (Tardy and others, 1972). Natural lithium salts are not known to exist; however, if they do exist, recognition might be difficult especially if they are fine grained and mixed with other fine-grained minerals. Lithium substitution for Mg^{+2} or Fe^{+2} might not be recognized in carbonates and other salts.

Anomalous concentrations of lithium have been reported in various plants, waters, and soils collected from desert regions of the Western United States. Sievers and Cannon (1974) expressed concern for the health problem of Pima Indians living on the Gila River Indian Reservation in central Arizona because of the anomalously high lithium content in water and in certain of their homegrown foods. Cannon (unpub. data, 1974) identified the Amargosa Desert area along the border between Nevada and California as another area of anomalously high lithium. Papke (1972) reported on the occurrence of sepiolite derived from saponite clay near Ash Meadows in this same area, and I have found as much as 500 ppm lithium in clay at the abandoned claypits at Clay City, Nev., also in the same area.

Other areas of anomalously high lithium are as follows: Alluvial sediments associated with an old borate mine at the south end of Columbus Salt Marsh, Esmeralda County, Nev.; a deposit of limonite and quartz resulting from the alteration of limestone at Geronimo Hot Spring, near the center of Truth or Consequences, N. Mex.; alluvial sediment from the surface of several dry lakes in San Bernardino County, Calif.; Sevier Lake in Millard County, Utah; South Alkali Flat in Hidalgo County, N. Mex.; Willcox Playa in Cochise County, Ariz.; and a quartz-calcite vein sample from the Nivloc mine, near Silver Peak, Nev.

The lithium content of natural waters is highly variable and bears only a slight relation to the content of sodium or total dissolved solids (Bradford, 1963). Table 2 lists the content of lithium and sodium and the lithium-sodium ratio for some selected natural waters. The average content of lithium in seawater is shown to be less than that of the freshwater of Lake Tanganyika in Africa. Moreover, the ratio of lithium to sodium in seawater is only about one-tenth that of the ratio of these elements in the Earth's crust. White, Hem, and Waring (1963, p. F10–F11, and tables 19 and 29) suggested that the highest lithium-sodium ratio probably occurs in acid sulfate-chloride spring waters associated with active or recent volcanism. They further suggested that a high ratio may reflect a high content of lithium in certain volcanic emanations. Recent stable isotope studies of hydrothermal minerals and fluid inclusions such as those from Tonopah and Goldfield, Nev., provide evidence of the quantitative importance of meteoric water relative to primary magmatic water in epithermal gold-silver mineralization (Taylor, 1974). The igneous intrusion serves as a source of heat energy to power a convective circulation of meteoric water in permeable country rock. In such a system, lithium might be leached from the country rock and concentrated in adjacent playa basins. The same mechanism might help to explain the difference in chemical composition of brines in adjacent basins within the same geologic province.

PROSPECTING FOR LITHIUM

Because concentrations of lithium have not as yet been reported from marine sediments, including marine evaporites, authors commonly state that lithium is dispersed among the clay minerals during marine sedimentation. The fate of lithium during deposition of marine evaporites is certainly not obvious. If lithium is concentrated in the residual brine and the brine becomes buried with the sediment, there should be a chance of finding such a lithium-rich brine among the ancient sediments. Saline minerals generally form impervious rocks as a result of deep burial so any residual brine originally buried with the evaporites is probably pressed out into the surrounding more permeable clastic sediments where equilibrium reactions may greatly alter the composition of the brine. Whether or not lithium may enter into such reactions is unknown. Perhaps the Michigan basin brine from the Sylvania Sandstone listed in table 2 is such a residual brine.

Nonmarine environments appear more favorable for the concentration of lithium brine during evaporation and precipitation of saline minerals because of the examples, such as Clayton Valley, where this has occurred. However, there is no adequate explanation yet as to why the brine at Clayton Valley should contain so much more lithium than do brines in other valleys of the same region. An explanation possibly lies in the answers to the following questions for which data are not now available: Is there a source for an unusually abundant supply of lithium within rocks that crop out in the drainage area of Clayton Valley? Is there a source of lithium at depth from the residual liquid of a cooling magma chamber? Is lithium that is extracted from country rock by meteoric waters kept in circulation by a deep-seated source of heat? Is there something unique or distinctive about the structure and geomorphic history of this basin, the type of volcanic activity and lithology of the volcanic rocks, the chemistry and mineralogy of the weathering products within the basin, or the hydrologic character of the basin?

TABLE 2.—*Lithium and sodium content of natural waters*

Water source	Lithium (ppm)	Sodium (ppm)	Li : Na ratio	Reference
Seawater	0.17	10,500	0.00001	Goldberg (1963).
Great Salt Lake, Utah	56	92,200	.0006	Cohenour (1966, p. 211).
Lake Tanganyika, Africa (700 m depth)	.8	64.2	.012	Livingstone (1963, table 84).
Laguna Escantado, Peru	7.6	694	.011	Do.
Mono Lake, Calif	8.5	21,400	.0004	Do.
Salton Sea, Calif	1.9	6,249	.0003	Do.
Searles Lake, Calif. (brine from upper salt)	81	110,000	.0007	White, Hem, and Waring (1963, table 84).
Clayton Valley, Nev. (subsurface brine)	300	66,200	.0045	Kunasz (1970, p. 114).
Michigan basin (brine from Sylvania Sandstone)	70	22,500	.003	White, Hem, and Waring (1963, table 13).
Niland well, Imperial Valley, Calif	18	7,280	.0025	White, Hem, and Waring (1963, table 18).
Norris Basin, Yellowstone National Park, Wyo	8.4	439	.019	White, Hem, and Waring (1963, table 17).

The existence in pegmatites of several lithium phosphate minerals, including Li_3PO_4 plus several more complex compounds of iron, aluminum, and manganese, suggests the possibility that some sedimentary phosphates might also contain significant amounts of lithium. Those phosphates formed in closed basins might be the most favorable.

Lithium is also known to occur in manganese oxide minerals such as lithiophorite (Fleischer and Faust, 1963), which can be distinguished from psilomelane or wad by a characteristic X-ray powder pattern. Lithiophorite is probably a common mineral and has been reported from both hydrothermal and supergene deposits. It occurs in the weathering products of magnesium-rich ultramafic rocks and as black stains and encrustations on quartz, sandstone, and chert.

A maximum of 200 ppm lithium from iron-rich sedimentary rocks was reported by James (1966, table 32), but this value did not include lithium in manganese nodules from the sea floor because no such data were available.

Lithium in sedimentary environments is associated with a characteristic suite of other minor elements. One of these associations is that with boron in the borate deposits of the Mojave Desert and Death Valley areas. Another association is with fluorine, beryllium, and manganese at Spor Mountain, Utah. These same suites of minor elements are also associated with lithium in pegmatites and in lithium-bearing greisen, both of which form from crystallizing magma at relatively high temperatures. The occurrence of the same suites of elements in both high-temperature and low-temperature environments is rather unusual and therefore deserving of an explanation. One possibility is that the sedimentary lithium deposits include a significant contribution from solutions derived from the residual fluids of a differentiated magma. Such a contribution could be derived from thermal springs associated with igneous intrusion or volcanism, especially acid volcanic rocks, which may be the end products of a differentiated magma. This possibility is also consistent with the suggestion for a hydrothermal origin for the hectorite in the Mojave Desert (Ames and others, 1958), the lithium-bearing brine at Clayton Valley (Kunasz, 1970), and the lithium-bearing beryllium deposits at Spor Mountain, Utah (Shawe and others, 1964; Lindsey and others, 1973).

The desert region of the Southwest includes the largest number of known concentrations of lithium in the form of hectorite deposits, lithium-rich brines, and anomalous concentrations of lithium in rocks and sediments. This area may be regarded as a lithium-rich province that is nearly coincident with the Basin and Range structural province. Clearly the desert climate affords the greatest opportunity for concentration of lithium at or near the surface where it may be observed because of an excess of evaporation over precipitation. However, the association of lithium with the Basin and Range structural province may have genetic significance for other reasons as well. For example, the deep-seated faults may provide pathways for the deep circulation of ground water; the volcanic activity provides a source of heat energy to drive ground-water convection cells; and the block faulting interrupts the drainage, forming local basins that serve as hydrologic sinks from which the soluble constituents of surface and ground water cannot escape. Together these features serve to concentrate and trap the lithium in near-surface sedimentary environments where any deposits are most easily discovered. The potential role of lithium-rich source rocks such as alkali-rich volcanics has yet to be evaluated. So also has the role of different clay minerals formed during weathering in causing the concentration or dispersal of lithium in the associated sediments and ground waters.

The prospects for discovering previously unreported deposits of nonpegmatite lithium in any given area can be evaluated empirically by assigning appropriate weight to a list of factors such as the following:

Anomalous concentrations of lithium in surficial materials
Desert climate
Evaporite minerals
Topographic closure
Structural closure
Basin and Range faults
Types of igneous rocks
Volcanic activity
Intrusive activity
Hydrothermal alteration
High Li : Na in water
Thermal springs
Late Cenozoic tectonism
Base or precious metal mineralization
Deposits of boron, beryllium, fluorine, tin, strontium, or tungsten
Deposits of manganese or phosphate
Noncarbonate aquifers
Proportions of clays and zeolites in weathered rocks

More experience in searching for nonpegmatite lithium deposits will be required before the relative importance of these various factors can be determined. Meanwhile, any search for nonpegmatite lithium deposits should be conducted with these factors in mind and an effort should be made to rank their relative importance.

REFERENCES CITED

Ames, L. L., Sand, L. B., and Goldich, S. S., 1958, A contribution on the Hector, California, bentonite deposit: Econ. Geology, v. 53, p. 22–37.

Bradford, G. R., 1963, Lithium survey of California's water resources: Soil Sci., v. 96, no. 2, p. 77–81.

Cohenour, R. E., 1966, Great Salt Lake, Utah, and its environment, *in* 2d symposium on salt—Volume 1, Geology geochemistry, mining: Cleveland, Northern Ohio Geol. Soc., p. 201–214.

Cummings, A. M., 1970, Lithium, *in* Mineral facts and problems: U.S. Bur. Mines Bull. 650, p. 1073–1081.

Dibblee, T. W., Jr., 1967, Areal geology of the western Mojave Desert, California: U.S. Geol. Survey Prof. Paper 522, 153 p.

Dyni, J. R., 1973, Trioctahedral smectite in the Green River Formation, Duchesne County, Utah: U.S. Geol. Survey open-file rept., 25 p.

Fleischer, Michael, and Faust, G. T., 1963, Studies on manganese oxide minerals—[Pt.] 7, Lithiophorite: Schweizer. Mineralog. u. Petrog. Mitt., v. 43, no. 1, p. 197–216.

Foote Mineral Company, 1967, Is there enough lithium?: Foote Prints, v. 36, p. 22–23.

Foshag, W. F., and Woodford, A. O., 1936, Bentonitic magnesian clay-mineral from California: Am. Mineralogist, v. 21, no. 4, p. 238–244.

Goldberg, E. D., 1963, Composition of sea water, *in* Hill, M. N, ed., New York, Interscience Publishers, v. 2, p. 3–25.

Grady, H. R., 1974, The lithium battery moves center stage: Foote Prints, v. 41, no. 1, p. 2–12.

Heier, K. S., and Adams, J. A. S., 1964, The geochemistry of the alkali metals, *in* Ahrens, L. H., and others, eds., Physics and chemistry of the earth: New York, Macmillan Co., v. 5, p. 253–381.

Heier, K. S., and Billings, G. K., 1969, Lithium, Chap. 3 [sec. B–0], *in* Wedepohl, K. H., ed., Handbook of geochemistry: New York, Springer-Verlag, v. 2, no. 1.

Hem, J. D., 1959, Study and interpretation of the chemical characteristics of natural water: U.S. Geol. Survey Water-Supply Paper 1473, 269 p.

Horstman, E. L., 1957, The distribution of lithium, rubidium, and caesium in igneous and sedimentary rocks: Geochim. et Cosmochim. Acta, v. 12, nos. 1–2, p. 1–28.

James, H. L., 1966, Chemistry of the iron-rich sedimentary rocks: U.S. Geol. Survey Prof. Paper 440–W, 61 p.

Kunasz, I. A., 1970, Geology and geochemistry of the lithium deposit in Clayton Valley, Esmeralda County, Nevada: Pennsylvania State Univ. Ph.D. thesis (thesis 71–16, 629, available from University Microfilms, Ann Arbor, Mich.), 113 p.

——— 1975, Lithium raw materials, *in* Industrial minerals and rocks (1975 revision): Am. Inst. Mining, Metall., and Petroleum Engineers. p. 791–803.

Lindsey, D. A., Ganow, Harold, and Mountjoy, Wayne, 1973, Hydrothermal alteration associated with beryllium deposits at Spor Mountain, Utah: U.S. Geol. Survey Prof. Paper 818–A, 20 p.

Livingstone, D. A., 1963, Chemical composition of rivers and lakes: U.S. Geol. Survey Prof. Paper 440–G, 64 p.

Morgan, Vincent, and Erd, R. C., 1969, Minerals of the Kramer borate district, California: California Div. Mines and Geology Mineral Inf. Service, pt. 1, v. 22, no. 9, p. 143–153; pt. 2, 22, no. 10, p. 165–172.

Norton, J. J., 1965, Lithium-bearing bentonite deposit, Yavapai County, Arizona, *in* Geological Survey research 1965: U.S. Geol. Survey Prof. Paper 525–D, p. D163–D166.

——— 1969, Lithium, *in* Mineral and water resources of Arizona: U.S. 90th Cong., 2d sess., Senate Comm. Interior and Insular Affairs, Comm. Print (also Arizona Bur. Mines Bull. 180), p. 206–211.

Norton, J. J., 1973, Lithium, cesium, and rubidium—the rare alkali metals, *in* Brobst, D. A., and Pratt, W. P., eds., United States mineral resources: U.S. Geol. Survey Prof. Paper 820, p. 365–378.

Papke, K. G., 1972, A sepiolite-rich playa deposit in southern Nevada: Clays and Clay Minerals, v. 20, no. 4, p. 211–215.

Ronov, A. B., Migdisov, A. A., Voskresenskaya, N. T., and Korzina, G. A., 1970, Geochemistry of lithium in the sedimentary cycle: Geochemistry Internat., v. 7, p. 75–102.

Ross, C. S., and Hendricks, S. B., 1945, Minerals of the montmorillonite group, their origin and relation to soils and clays: U.S. Geol. Survey Prof. Paper 205–B, 77, p.

Shawe, D. R., Mountjoy, Wayne, and Duke, Walter, 1964, Lithium associated with beryllium in rhyolitic tuff at Spor Mountain, western Juab County, Utah, *in* Geological Survey research 1964: U.S. Geol. Survey Prof. Paper 501–C, p. C86–C87.

Sievers, M. L., and Cannon, H. L., 1974, Disease patterns of Pima Indians of the Gila Indian Reservation of Arizona in relation to the geochemical environment, *in* Hemphill, D. D., ed., Univ. Missouri Symposium on Trace Elements in Environmental Health: v. 7, p. 57–61.

Smith, W. C., 1966, Borax and other boron compounds, *in* Mineral and water resources of California, pt. 1: U.S. 89th Cong., 2d sess., Senate Comm. Interior and Insular Affairs, Comm. Print (also California Div. Mines and Geology Bull. 191), p. 104–111.

Starkey, H. C., and Mountjoy, Wayne, 1973, Identification of a lithium-bearing smectite from Spor Mountain, Utah: U.S. Geol. Survey Jour. Research, v. 1, no. 4, p. 415–419.

Tardy, Yves, Krempp, Gérard, and Trauth, Norbert, 1972, Le lithium dans les minéraux argileux des sédiments et des sols: Geochim. et Cosmochim. Acta, v. 36, no. 4, p. 397–412.

Taylor, H. P., Jr., 1974, The application of oxygen and hydrogen isotope studies to problems of hydrothermal alteration and ore deposition: Econ. Geology, v. 69, no. 6, p. 843–883.

Turk, L. J., Davis, S. N., and Bingham, C. P., 1973, Hydrogeology of lacustrine sediments, Bonneville Salt Flats, Utah: Econ. Geology, v. 68, p. 65–78.

White, D. E., Hem, J. D., and Waring, G. A., 1963, Chemical composition of subsurface waters: U.S. Geol. Survey Prof. Paper 440–F, 67 p.

Jour. Research U.S. Geol. Survey
Vol. 3, No. 4, July–Aug. 1975, p. 487–494

EFFECTS OF SEDIMENT CONTROL ON SEDIMENT TRANSPORT IN THE NORTHWEST BRANCH ANACOSTIA RIVER BASIN, MONTGOMERY COUNTY, MARYLAND

By THOMAS H. YORKE, College Park, Md.

Work done in cooperation with the Maryland–National Capital Park and Planning Commission (Montgomery County and Prince Georges County Planning Boards), the Washington Suburban Sanitary Commission, the District of Columbia Department of Environmental Services, the Montgomery County Department of Environmental Protection, and the Maryland Department of Natural Resources

Abstract.—Streamflow and sediment were monitored in an urbanizing drainage basin in southeastern Montgomery County, Md., from 1962 to 1972. During this period, urban construction areas averaged about 3 percent of the 21.1 mi² (54.6 km²) basin. Urban land increased from 3.5 percent in 1959 to 20 percent in 1971. Virtually all the suspended sediment was transported during storms; three-fourths of it, during large storms. High sediment yields were observed in February, March, June, and August; and low yields, generally from September through January. The decrease in sediment discharge in the latter half of the study period is attributed to a sediment-control program. Sediment discharge decreased 35 percent between 1967 and 1972, when effective control measures were installed on about half the construction sites.

Sediment control has become an integral part of urban construction in the Baltimore-Washington area. In the early 1960's, local government agencies became increasingly aware of the sediment problems associated with urban construction activities, and several programs were instituted to control sediment. Studies by Guy and Ferguson (1962), Keller (1962), Wolman (1964), Guy (1965), and Vice, Guy, and Ferguson (1969) provided information on sediment movement in urban areas which resulted in the adoption of sediment-control programs in Maryland. These early studies were concerned primarily with the magnitude of sediment entering streams from construction sites. This report presents preliminary results from a study begun in 1962 to define urban sediment problems and expanded in 1966 to evaluate response to sediment-control practices in urban construction areas.

DESCRIPTION OF BASIN

The study area is in the headwaters of the Anacostia River which drains parts of Montgomery County and Prince Georges County, Md., and enters the Potomac River in the District of Columbia. The part of the basin being studied is drained by the Northwest Branch north of Glenmont in Montgomery County (fig. 1). The drainage area is 21.1 mi² (54.6 km²) and is bounded approximately by the towns of Glenmont, Norbeck, Olney, Ashton, and Colesville. The altitude of the basin above mean sea level ranges from 320 ft (97.5 m) at the gaging station to 560 ft (170.7 m) near Olney. The main channel slope is 19.3 ft/mi (3.66 m/km).

The basin is in the eastern division of the Piedmont physiographic province and is characterized by a rolling topography. Igneous and metamorphosed igneous rocks underlie the area. The Manor-Chester-Glenelg soil association is predominant in the area. These soils are moderately deep; depth to substratum ranges from about 18 to 40 in (46 to 102 cm). Surface soils range in thickness from 0 to 8 in (0 to 20 cm) and are mostly silt loams and gravelly and channery silt loams. The subsoils are predominately silty clay loams and silt loams. The soils are highly susceptible to erosion, and in some parts of the basin much of the surface soil and part of the subsoil have been removed by erosion.

The study area has a temperate and rather humid climate. The mean annual temperature is about 13°C. The 86-yr Environmental Data Service record of pre-

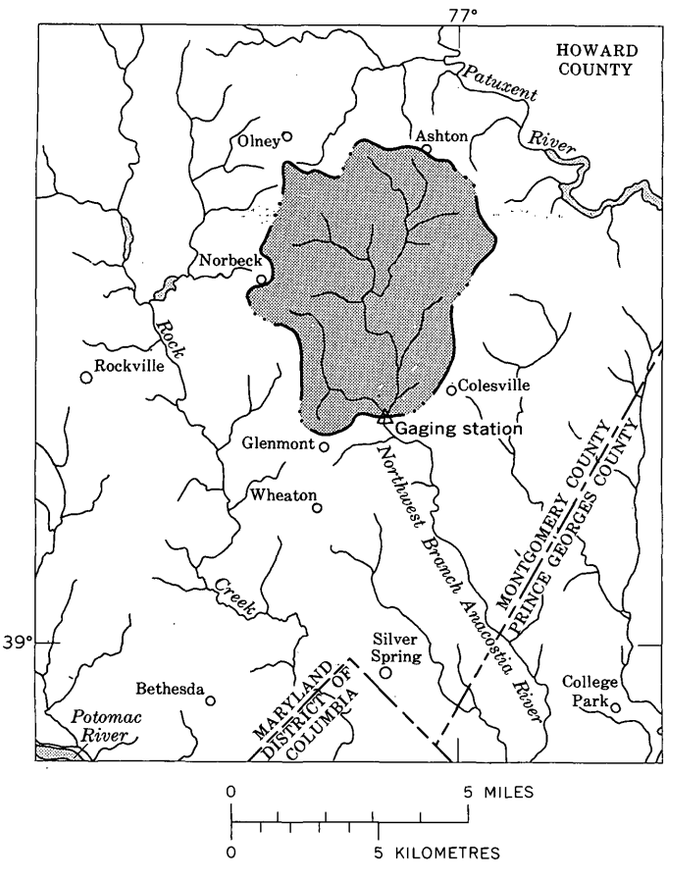

FIGURE 1.—Location of Northwest Branch Anacostia River basin (stippled).

cipitation at College Park, Md., indicates the average annual precipitation is 43.47 in (1,104 mm), occurring mostly as rainfall. The precipitation is evenly distributed throughout the year, ranging from 2.70 in (69 mm) in February to 5.15 in (130 mm) in August. Summer precipitation is characterized by short, high intensity rainfalls from convective storms, and winter precipitation is derived primarily from frontal storms.

LAND USE

Land use in the study area has changed rapidly in the last decade. In 1959, the basin was largely rural, with 66 percent of the drainage area under cultivation or in pasture and another 30 percent in woodlands. Only 3.5 percent was occupied by housing and commercial structures, which were generally located in small towns at highway intersections on the perimeter of the basin. A housing boom began in the drainage basin in 1962. Developers subdivided the land, and new houses were built throughout the basin. Most of the early development was centered in the lower quarter of the basin; however, housing developments were scattered throughout by 1968. The developments generally consist of detached houses on half-acre (0.2 ha) or smaller lots and some townhouses and apartments. Housing construction was accompanied by construction of schools, shopping centers, highways, and recreational facilities to meet the needs of the enlarged population.

Land-use changes in the basin were determined from aerial photographs by the dot-grid-sampling method. The data summarized in table 1 indicate that construction activity was fairly constant from 1963 to 1972. Since 1963, the land under construction has gradually increased from about 2 percent to an average between 3 and 4 percent each year. The basin has been transformed from a rural area with some development on the relatively flat drainage divides to a suburban area with residences and commercial property occupying 20 percent of the basin. Impervious surfaces totaled 977 acres (3.95 km²) or 7.2 percent of the basin in 1971.

TABLE 1.—*Land use, in percentage of drainage area, in the Northwest Branch Anacostia River basin, Montgomery County, Md., 1959–71*

Date	Cultivated	Grass	Woodland	Suburban	Construction
November 1959	33.3	33.1	29.6	3.5	0.5
March 1963	24.6	37.5	28.5	6.5	2.9
March 1964	24.5	37.8	28.5	7.0	2.2
December 1964	---	---	---	--	1.6
July 1965	---	---	---	--	2.7
June 1966	14.6	38.3	30.0	13.8	3.3
June 1967	14.6	37.3	29.3	15.0	3.8
June 1968	14.3	37.1	29.1	16.4	3.1
June 1969	13.6	36.4	29.0	17.4	3.6
June 1970	13.0	36.5	29.2	18.0	3.3
June 1971	13.2	35.4	29.0	19.8	2.6

NOTE.—Suburban category in this report represents all residential and commercial area. The urban category in a previous report, Yorke and Davis (1972), represented commercial area and residential area with lots half an acre or less

Much of the development has occurred on land that was previously under cultivation; however, some of the grass and woodland observed in 1959 has been developed. The grass category has not changed appreciably because some of the previously cultivated land has gone fallow and some of the woodland has been converted to grass for golf courses and other recreational facilities. The woodland category, likewise, has not changed appreciably since 1959 because some of the land previously cultivated or in grass has gradually reverted to scrubby hardwood growth and has been reclassified as woodland.

SEDIMENT CONTROL

The urban sediment-control program in Montgomery County was one of the first in the Nation. This pro-

gram evolved gradually through the efforts of many individuals and local agencies in the Washington, D.C. area. One of these organizations, The Interstate Commission on the Potomac River Basin, initiated a study (Guy and others, 1963), which was the impetus for the Montgomery County program and others in Maryland and Virginia. The study group recommended that sediment control become the stated policy of local governments, that urban development be planned carefully, and that local ordinances be adopted to require developers to employ erosion-control measures on construction sites.

Urban sediment control was implemented with guidelines and principles similar to those used for many years to control erosion and sediment transport on agricultural lands. The basic principles were to fit development to the natural topography, expose the least amount of land possible, provide protection for bare soils, prevent surface runoff from critical sites, and trap eroded materials before they could be transported from the construction sites. Some of the commonly used control measures include scheduled grading to limit the amount of soil exposed at any one time; mulch protection and temporary vegetation to protect bare soils; diversion berms, level spreaders, and stabilized waterways to reduce erosion on critical slopes; and sediment basins to trap eroded sediments on site.

The program was implemented in several phases. In 1965, the Montgomery County Council adopted a program that encouraged developers to include sediment-control provisions voluntarily when new subdivision plans were submitted for approval. This program was not initially effective because many of the projects, which were developed in subsequent years, had been approved prior to 1965, and sediment controls were not included. Moreover, many of the developers and grading contractors were not familiar with methods of sediment control. The program was reinforced in 1967 when the county council passed an ordinance requiring that erosion- and sediment-control plans be submitted with preliminary subdivision plans. The Montgomery County Soil Conservation District reviewed the sediment-control plans and assisted developers in planning adequate controls. An increasing number of sediment-control devices were installed at construction sites after 1967, but there were still several problems with the program. The two major problems between 1967 and 1971 were that some controls were not properly installed and many others were not adequately maintained.

The third phase of the program was begun in 1971 when Montgomery County established a Sediment Control Section within the Department of Environmental Protection. This section was assigned the responsibility of reviewing plans and inspecting sediment controls. For the first time there was a provision to follow up office review of plans with field inspection of control measures by trained inspectors.

STREAMFLOW AND SEDIMENT DISCHARGE

Streamflow has been measured at the gaging station on the Northwest Branch Anacostia River near Colesville since 1923. The gaging station is operated as part of the nationwide streamflow-monitoring network using standard stream-gaging procedures described by Carter and Davidian (1968). Suspended sediment has been monitored since 1960. Suspended-sediment concentration data has been collected manually and with automatic samplers. Generally, depth-integrated samples only are collected during baseflow periods, whereas automatic samples from a single-stage sampler and a pumping sampler, supplemented by manual samples, are collected during storms. Ten or more samples are normally used to define the variation of sediment concentration during runoff periods. The continuous record of water discharge and sediment concentration are used to compute the sediment discharge transported during storms. A detailed description of this computational procedure was prepared by Porterfield (1972). Sediment discharge records are available from 1960 to 1972, daily records from October 1962 to September 1972.

During October 1962 to September 1972, variation in precipitation and streamflow was considerable. Annual precipitation at College Park averaged 41.64 in (1,058 mm) compared to the 86-yr average of 43.47 in (1,104 mm). Precipitation ranged from 32.81 in (833 mm) in 1966 to 53.34 in (1,355 mm) in the 1971 water year. Runoff during the same period averaged 13.35 in (339 mm) compared to the 49-yr average of 14.09 in (358 mm). Suspended-sediment discharge averaged 16,600 tons (15,100 t) per yr and ranged from 9,500 tons (8,620 t) in 1969 to 38,300 tons (34,700 t) in the 1972 water year.

Most of the sediment was transported by the stream during large storms. A duration curve of daily sediment discharge indicates that the sediment discharge was greater than 500 tons (454 t) 2.4 percent of the time (86 days). The sediment discharge for those days represents 76 percent of the 10-yr total. The daily sediment discharge was greater than 1,000 tons (907 t) 1.2 percent of the time (44 days), accounting for 60 percent of the total. In contrast, the daily sediment discharge was less than 0.3 and 2.0 tons (0.27 and 1.81 t) 50 and 80 percent of the time, respectively.

Seasonal variation of suspended sediment

The timing of large storms has a considerable impact on the monthly variation of sediment discharge. Average monthly sediment discharge during 1963–72 ranged from 718 tons (651 t) in December to 3,800 tons (3,450 t) in June (fig. 2). Average sediment discharges for September through January were below the mean monthly discharge of 1,380 tons (1,250 t), and the sediment discharges for February, March, June, and August were above the mean. This variation is consistent with normal weather patterns and storm conditions. October through January is characterized by low precipitation, low-intensity storms, and some precipitation in the form of snow, none of which cause heavy erosion and sediment transport. The higher sediment discharges in February and March are the result of high runoff generally from a combination of high soil-moisture levels, occasional snowmelt, and rainfall. The high sediment discharges in June and August are the result of intensive rainfall from convective storms that causes severe erosion. The sediment discharge for July is below the monthly mean; however, the long-term discharge is probably comparable to those of June and August because the rainfall, soil conditions and other erosion factors are comparable. This seasonal distribution of suspended-sediment discharge approximates the distribution of erosion index values for the Atlantic coast area (Guy, 1964). The erosion hazard is highest in June, July, and August and tapers off to a low in December and January.

The contribution of large storms and the monthly variation of sediment discharge are important factors in planning and designing methods of controlling sediment. The principles of sediment control, as outlined by the Maryland–National Capital Park and Planning Commission (1967), include the use of artificial or vegetal cover to protect exposed soils and using structures to limit and retain the sediment in transport; however, they do not include the optimum time for installation of protective measures. The time distribution of sediment transport in the Anacostia River basin indicates that the late fall and early winter months have the lowest erosion potential and are apparently the best time for initial grading and construction work. If major grading work was completed in the fall and all protective measures were installed by midwinter, there would be protection during high runoff in the spring and during the intense summer storms. The quantity and size of control measures are as important as the timing of their installation. Large storms account for much of the sediment transported by local streams, and sediment-control measures must be able

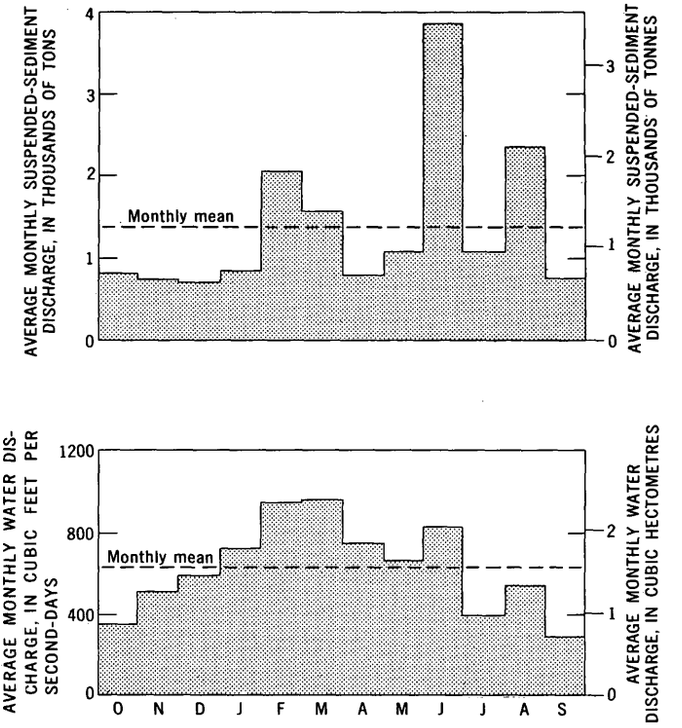

FIGURE 2.—Monthly variation of water and suspended-sediment discharge, Northwest Branch Anacostia River near Colesville, Md. 1963–72.

to accommodate the runoff from these storms for the program to be fully effective.

The monthly and annual summaries of water discharge and suspended-sediment discharge are shown in tables 2 and 3. The data in the tables indicate that water and sediment discharge increased substantially during the second half of the data-collection period. Runoff averaged 10.24 in/yr (261 mm/yr) from 1963 to 1967 and 16.42 in/yr (417 mm/yr) from 1968 to 1972. The average annual sediment discharge during the same periods increased from 14,700 to 18,400 tons. (13,300 to 16,700 t). Most of the increase in sediment can be attributed to high runoff in the 1971 and 1972 water years and the effects of Hurricane Agnes in June 1972. The suspended sediment transported on June 21–22, 1972 was 20,100 tons (18,200 t), which is greater than any previous annual discharge.

Effects of sediment control

Although sediment discharge increased during the study period, the increase was not proportional to the increase in water discharge. Figure 3 is a double mass curve of storm runoff and suspended-sediment discharge for all significant storms between October 1962 and September 1972. A substantial break in the relation occurred between the 1967 and 1968 water years

TABLE 2.—*Monthly and annual water discharge, in cubic feet per second-days, Northwest Branch Anacostia River near Colesville, Md., 1963–72*

[1 (ft^3/s)·d equals 2,447 m^3]

Water year	October	November	December	January	February	March	April	May	June	July	August	September	Annual
1963	149.8	521.7	304.5	565.8	553.9	1,276.8	361.3	267.2	771.5	121.7	317.4	176.2	5,387.8
1964	117.0	807.3	448	1,531	871	998	976	485.3	263.1	151.9	116.6	79.4	6,844.6
1965	134.8	193,9	513.4	609.6	619.7	1,297	527	328.4	204.7	148.3	349.0	143.0	5,068.8
1966	526.9	160.4	158.4	226.2	1,153.7	505.4	650.9	530.3	184.8	73.3	31.2	936.3	5,137.8
1967	576.0	305.0	451.6	595	514.5	1,266	467	669	302.1	309.4	1,122	161.1	6,738.7
1968	227.1	267.5	1,114.7	947	370.6	989.6	440	633.1	680.0	289.5	105.1	123.9	6,188.1
1969	177.8	445.2	403.8	362.2	453.9	457.7	337.8	283.4	338.3	280.2	919.8	365.3	4,825.4
1970	215.9	309.9	1,024	665.8	784	673	1,559	759	693.9	882.0	321.5	167.8	8,055.8
1971	225.6	877.3	718.5	717	2,149.8	867	716	1,184	548.3	401.8	1,724.9	627.1	10,757.3
1972	1,132.0	1,149.0	789.0	884	2,027	1,340	1,556	1,382	4,244	1,403	530.6	296.3	16,732.9
Mean	348.29	503.72	592.59	710.36	949.81	967.05	759.10	652.17	823.07	406.11	533.81	307.64	7,573.72

TABLE 3.—*Monthly and annual suspended-sediment discharge, in tons, Northwest Branch Anacostia River near Colesville, Md., 1963–72*

[1 short ton equals 0.9072 t (tonne)]

Water year	October	November	December	January	February	March	April	May	June	July	August	September	Annual
1963	38.1	655.6	14.2	317.8	1,038.9	2,967.2	6.5	24.3	6,331.6	24.5	4,573.1	818.8	16,811.4
1964	3.0	2,994.9	326.6	5,141.5	835.6	700.7	885.0	68.3	62.2	153.7	309.9	114.9	11,596.3
1965	23.0	511.4	1,702.3	665.9	2,444.7	5,446.9	21.7	47.3	68.9	669.1	4,113.0	175.1	15,889.1
1966	3,042.2	0.6	2.3	45.1	4,354.2	192.6	1,091.2	978.4	51.0	105.2	68.0	4,471.2	14,402.0
1967	2,102.6	173.0	60.2	609.8	207.4	3,148.1	26.0	1,152.5	706.7	1,268.0	5,543.1	11.9	15,009.3
1968	344.33	135.29	2,255.50	812.82	62.62	1,561.52	45.62	1,550.84	2,758.80	600.97	5.44	364.71	10,498.46
1969	123.64	330.37	193.01	200.18	233.95	34.79	8.68	797.29	2,593.77	570.88	3,668.42	703.60	9,458.58
1970	84.80	100.49	1,925.36	88.37	684.68	121.61	3,823.02	2,753.00	3,652.57	3,253.04	560.71	222.58	17,270.23
1971	124.62	1,248.46	512.86	133.38	6,405.08	243.81	146.00	1,963.48	224.27	966.43	3,847.01	737.62	16,553.92
1972	2,209.38	1,179.91	191.90	95.72	4,325.41	1,380.66	1,936.92	1,538.62	21,849.45	2,955.40	635.75	10.15	38,309.27
Mean	809.57	733.00	718.42	811.06	2,059.25	1,579.79	799.16	1,087.41	3,829.93	1,056.72	2,332.44	763.05	16,579.85

indicating either a decrease in suspended-sediment discharge or an increase in storm runoff. This change in the relation was tested with an analysis of covariance. Storm runoff and sediment discharge were accumulated at 3-mo intervals, then divided into two periods, October 1962 to September 1967 and October 1967 to September 1972, to determine if the relation between the two variables was significantly different during the periods. An F-ratio of 5.28 indicated that the observations would not fit one regression line at the 99-percent confidence level. This means that the change in the relation observed in the mass curve is statistically significant and that the break in the mass curve would occur by chance alone once in 100 times.

As mentioned above, the break in the relation between suspended-sediment discharge and storm runoff could have occurred because of a decrease in sediment or an increase in storm runoff. Logically, storm runoff would increase as the amount of impervious area in the basin increased; however, because the impervious area has increased gradually during the study period, the storm-runoff rate would probably also increase gradually. On this basis, the break in the relation between suspended-sediment discharge and storm runoff probably occurred because of a decrease in sediment rather than a sharp increase in runoff.

Several conditions could account for the reduced sediment discharge from the basin. One logical explanation would be a decrease in the number of sediment-source areas. An inspection of the land-use records, however, indicates that the change in sediment-source area has been insignificant since 1965. Cultivated land has decreased, but this is compensated for by an increase in construction area during the same period. Suburban land area increased from 15 to 20 percent of the basin between 1967 and 1971, but this would not result in any substantial decrease in sediment discharge for the erosion potential of suburban land is probably comparable with that of other stable land uses. Actually, an increase in suburban land could increase sediment discharge because of accelerated streambank erosion as channels of small tributaries enlarge to accommodate increased runoff from impervious surfaces.

Migration of construction activities further upstream could also account for a decrease in sediment discharge. With a larger intervening area between the sediment source on construction sites and the sampling point, a substantial part of the sediment load could be deposited in the channel and flood plain. This would be particularly true if the soils in the source area had a high sand content. However, the source material and

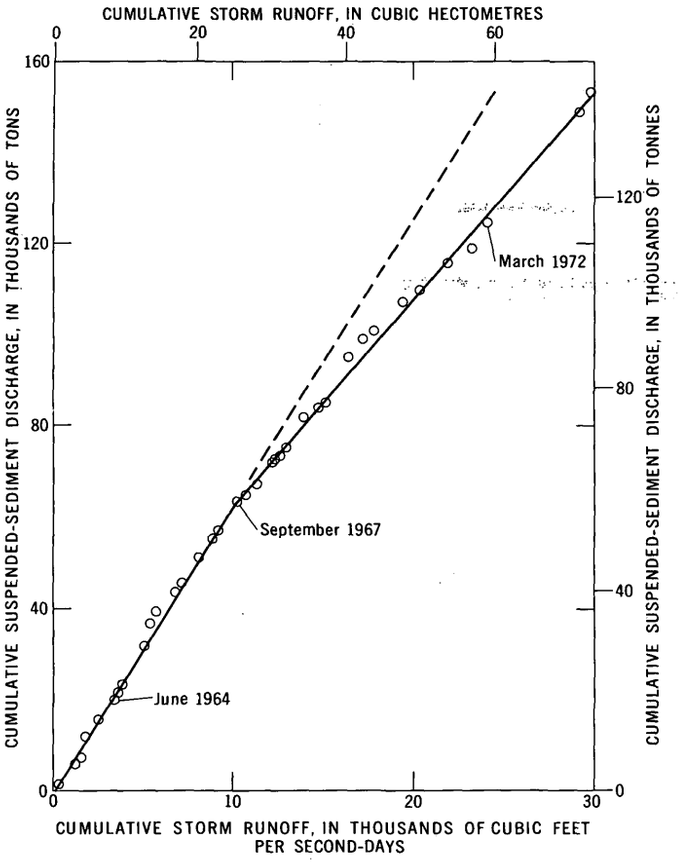

FIGURE 3.—Cumulative storm runoff and suspended-sediment discharge, Northwest Branch Anacostia River near Colesville, Md., 1963–72.

the sediment transported from the basin are largely clay and silt, and it is unlikely that much of the fine material in suspension is deposited within the basin.

The factor most likely responsible for the decreased sediment load between 1968 and 1972 is the sediment-control program begun in 1965. The program started making substantial gains after 1967. Land-use surveys in 1966 and 1967 indicate that 1.3 and 9.1 percent of the construction areas in the basin had controls. These surveys were based on design only and did not evaluate the efficiency of the controls. Subsequent countywide surveys of construction sites by the Montgomery County Sediment Control Task Force in 1968 and 1970 and by the Montgomery County Sediment Control Section in 1972 included onsite inspections. These surveys indicated that most of the developments had implemented sediment controls but that many of the controls were installed improperly or were not properly maintained. During the respective surveys, 36, 41, and 56 percent of the active construction area within the county was judged to have adequate sediment controls. Data are not available to determine similar percentages for the Anacostia River basin, but they are probably comparable with those observed countywide.

The effect of the increased use of sediment controls is further illustrated in figure 4. Figure 4*A* is a plot of sediment discharge and storm runoff for growing-season storms during the 10-yr study period. The solid lines represent the least-squares regression curves for the indicated periods. Figure 4*B* is a similar plot for dormant-season storms. The shift of the regression curves for the periods 1968–70 and 1971–72 to the right of the curves for 1963–67 indicates a decrease in sediment discharge for a given volume of storm runoff. An analysis of covariance was used to test if the differences observed in the curves were statistically significant. The adjusted means of the dormant-season sediment loads for the three periods were determined to be significantly different from each other. The growing-season adjusted mean for the period 1971–72 was significantly different from the means for the 1963–67 and 1968–70 periods; however, there was not a significant difference between the growing-season means for the 1963–67 and 1968–70 periods.

The higher efficiency of sediment controls observed during dormant seasons in the initial phase of the sediment-control program was to be expected because of the nature of storms in the fall and winter. These are generally frontal storms with low-intensity rainfall compared with that associated with convective storms in the summer. Sheet erosion and runoff peaks are low, and sediment-control structures are able to control the runoff and retain the sediment on the construction sites. In contrast, the intense rainfall in the summer causes severe erosion and high runoff rates that commonly exceed the capacity of control structures. The general improvement in the control program after 1971 is reflected by the large shift to the right of the regression curve for the 1971–72 growing seasons (fig. 4*A*). Apparently, control structures that were properly installed and adequately maintained were able to provide adequate control for a greater percentage of the summer storms.

Overall, the sediment-control program has been effective in reducing the suspended-sediment load transported from the Anacostia River basin. The load that would have been transported from the basin between 1968 and 1972 without the control program was estimated to be 110,000 tons (99,800 t). The runoff observed between 1968 and 1972 and the regression equations developed for the seasonal sediment loads between 1963 and 1967 were used to make this estimate. The estimated load for Hurricane Agnes (June 21–22, 1972) was excluded because the Agnes runoff far exceeded the range of runoff sampled between 1963 and

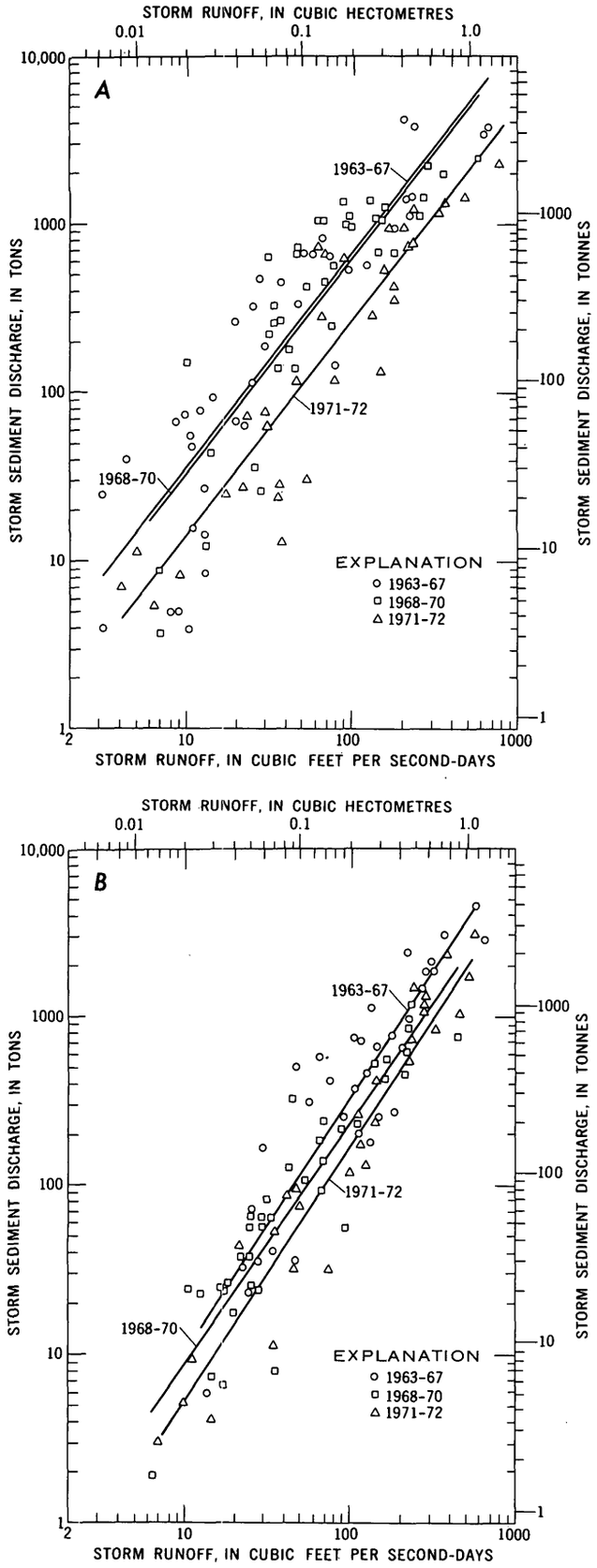

FIGURE 4.—Relation between suspended-sediment discharge and runoff for (*A*) growing-season and (*B*) dormant-season storms in the Anacostia River basin, 1963–72.

1967. The suspended sediment actually measured between 1968 and 1972, excluding the 20,100 tons (18,200 t) from Hurricane Agnes, was 70,000 tons (63,500 t). This represents a 35-percent reduction, which is surprisingly high considering that the amount of construction area in the county with adequate controls ranged from 36 percent in 1968 to 56 percent in 1972.

SUMMARY

The suspended sediment transported by the Northwest Branch Anacostia River near Colesville, Md., was monitored from 1962 to 1972. There were substantial physical changes within the basin that are reflected in the sediment discharge. An average of 3 percent of the basin was under construction each year, and the urban land area increased from 3.5 to 20 percent of the basin between 1959 and 1971. The suspended sediment transported from the basin during the 10-yr period is characterized by the following statements:

1. Total suspended-sediment discharge was 166,000 tons (151,000 t).
2. Virtually all the sediment load was transported during storms. Seventy-six percent of the sediment was transported on 86 days, or 2.4 percent of the time.
3. Fall and early winter (October to January) was a period of low sediment discharge, and early spring and summer were periods of high sediment discharge.
4. Sediment discharge in relation to water discharge decreased during the 10-yr period. Sediment discharge during significant storms between 1968 and 1972 was 70,000 tons (63,500 t), about 35 percent less than that estimated by regression equations based on sediment and runoff data collected between 1963 and 1967.

The decrease in sediment discharge observed between 1968 and 1972 is probably the result of the sediment-control program adopted by Montgomery County in a series of regulations between 1965 and 1971. The 35-percent decrease in sediment in the early stages of the program when less than half the construction sites were adequately controlled indicates that a fully implemented program can provide a high degree of sediment control. The data indicate that further control can be achieved if most of the major grading is scheduled for periods of low erosion potential and if structures are designed to control sediment and runoff during large storms.

REFERENCES CITED

Carter, R. W., and Davidian, Jacob, 1968, General procedures for gaging streams: U.S. Geol. Survey Tech. Water-Resources Inv., book 3, chap. A6, 13 p.

Guy, H. P., 1964, An analysis of some storm-period variables affecting stream sediment transport: U.S. Geol. Survey Prof. Paper 462–E, 46 p.

———1965, Residential construction and sedimentation at Kensington, Maryland, *in* Federal Inter-Agency Sedimentation Conference Proceedings, 1963: U.S. Dept. Agriculture Misc. Pub. 970, p. 30–37.

Guy, H. P., and Ferguson, G. E., 1962, Sediment in small reservoirs due to urbanization: Am. Soc. Civil Engineers Proc., Jour. Hydraulics Div., v. 88, no. HY2, p. 27–37.

Guy, H. P., and others, 1963, A program for sediment control in the Washington metropolitan region: Interstate Comm. Potomac River Basin Tech. Bull. 1963–1, 48 p.

Keller, F. J., 1962, Effect of urban growth on sediment discharge, Northwest Branch Anacostia River basin, Maryland: U.S. Geol. Survey Prof. Paper 450–C, p. 129–131.

Maryland–National Capital Park and Planning Commission, 1967, Sediment control program for Montgomery County, Maryland: Maryland–National Capital Park and Planning Commission, 6 p.

Porterfield, George, 1972, Computation of fluvial-sediment discharge: U.S. Geol. Survey Tech. Water-Resources Inv., book 3, chap. C3, 66 p.

Vice, R. B., Guy, H. P., and Ferguson, G. E., 1969, Sediment movement in an area of suburban highway construction, Scott Run basin, Fairfax County, Virginia, 1961–64: U.S. Geol. Survey Water-Supply Paper 1591–E, 41 p.

Wolman, M. G., 1964, Problems posed by sediment derived from construction activities in Maryland—Report to the Maryland Water Pollution Control Commission, Annapolis, Md.: 125 p.

Yorke, T. H., and Davis, W. J., 1972, Sediment yields of urban construction sources, Montgomery County, Maryland: U.S. Geol. Survey open-file rept., 39 p.

Jour. Research U.S. Geol. Survey
Vol. 3, No. 4, July–Aug. 1975, p. 495–500

THE EFFECT OF A FUEL OIL SPILL ON BENTHIC INVERTEBRATES AND WATER QUALITY ON THE ALASKAN ARCTIC SLOPE, HAPPY VALLEY CREEK NEAR SAGWON, ALASKA

By JON W. NAUMAN and DONALD R. KERNODLE, Anchorage, Alaska

Abstract.—Samples of aquatic organisms and water were collected upstream and downstream from leaks and spills of arctic diesel fuel oil into Happy Valley Creek near Sagwon, Alaska. All groups of benthic invertebrates were reduced in abundance at the downstream boundary of the spill area, whereas invertebrates at an upstream site were unaffected.

This report is auxiliary to a study of seasonal water-quality characteristics to determine baseline conditions of selected streams along the trans-Alaska pipeline corridor. Several small arctic diesel fuel oil spills and leaks beginning in December 1970, including an estimated 3,750-litre leak during the winter of 1972, have been reported by Alaska Construction News, Inc. (1972). The oil seeped into Happy Valley Creek at Alyeska Pipeline Service's Happy Valley construction camp (lat 69°08′50″ N., long 148°49′50″ W.) in the northern foothills of the Brooks Range (fig. 1). A study of Happy Valley Creek was conducted to determine to what extent benthic invertebrates and chemical quality of water were affected by arctic diesel fuel oil.

Happy Valley Creek, originating from a series of small thaw lakes, has a drainage area of 89.4 km². The elevation drops approximately 230 m from the creek's source to the confluence of the creek and the Sagavanirktok River.

Bedrock underlying the Happy Valley Creek basin is sandstone and conglomerate. Along hillslopes the bedrock is overlain by colluvium and alluvium. The active flood plain consists of unconsolidated sand, gravel, and boulders. Ferrians (1965) reported that this area is underlain by continuous permafrost.

The area drained is arctic tundra, the dominant vegetation consisting of dwarf willow bushes (*Salix* sp.) along the streambanks and cotton grass tussocks (*Eriophorum* sp.) on the hillslopes.

Meteorological records for the 1972 water year for Happy Valley camp show air temperatures ranged from −47.7° to 27.2°C and the monthly average ranged from −28.9° to 9.7°C. Monthly precipitation ranged from zero during December to a high of 33 mm in June. Stream discharge varied from zero flow dur-

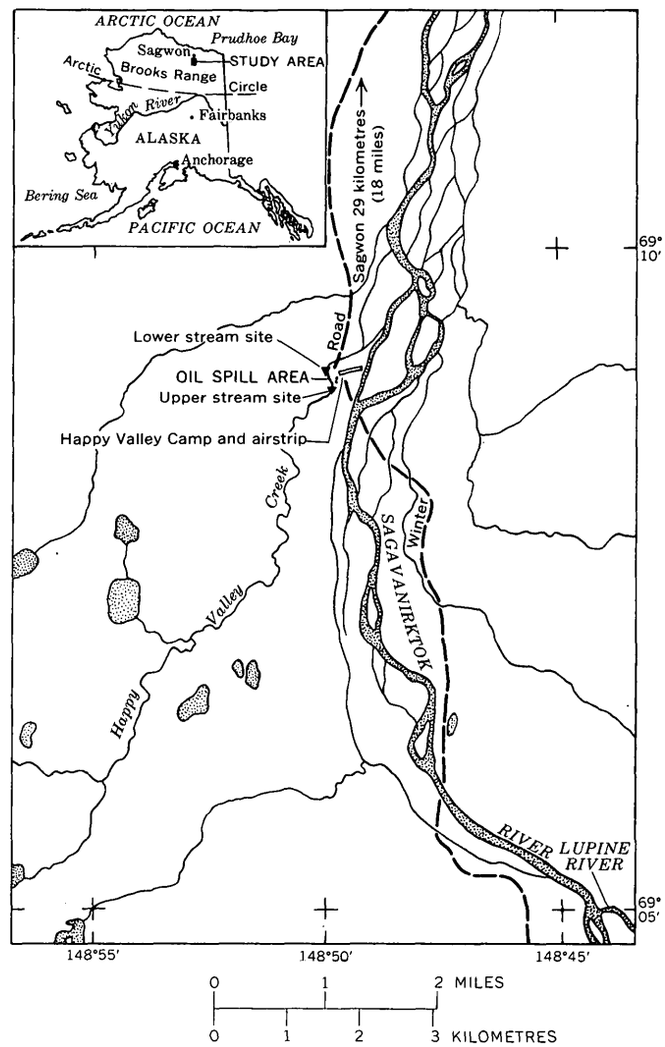

FIGURE 1.—Location of study area, Happy Valley Creek, near Sagwon, Alaska.

ing winter, when the stream was frozen solid, to an estimated flow greater than 14 m^3/s during the 1972 spring breakup.

Two sites were selected for this study, one is approximately 70 m upstream of the Happy Valley camp pumphouse and a second is approximately 250 m downstream at the boundary of the seepage area (fig. 2). With the exception of the right bank adjacent to the oil seepage area, the streambanks and adjacent gently sloping hills were covered with undisturbed tundra vegetation.

The underground fuel oil line, between the bladder tanks and the camp buildings, broke and allowed fuel oil to seep to the creek through an area measuring approximately 2,800 m^2. Three collection trenches were dug in the seepage area to collect and stop the oil flow into the creek. The collected oil was burned or removed for disposal. At the time of this study nearly 21 mo had passed since the first spills occurred and nearly 6 mo had passed since a large leak was first detected. During the time of the study an oil film was noted along the seepage area shoreline.

Adjacent to and upstream of the seepage area is a retention pond for holding secondary treated domestic camp sewage effluent. At the time of this study the sewage treatment plant was treating approximately 3,800 l/d. No chlorination of the treated effluent was performed, although a chlorinator was installed. Most of the effluent seeped through the gravel base of the pond, and excess effluent flowed to a small drainage ditch that extended for a short distance down the hillslope towards the creek.

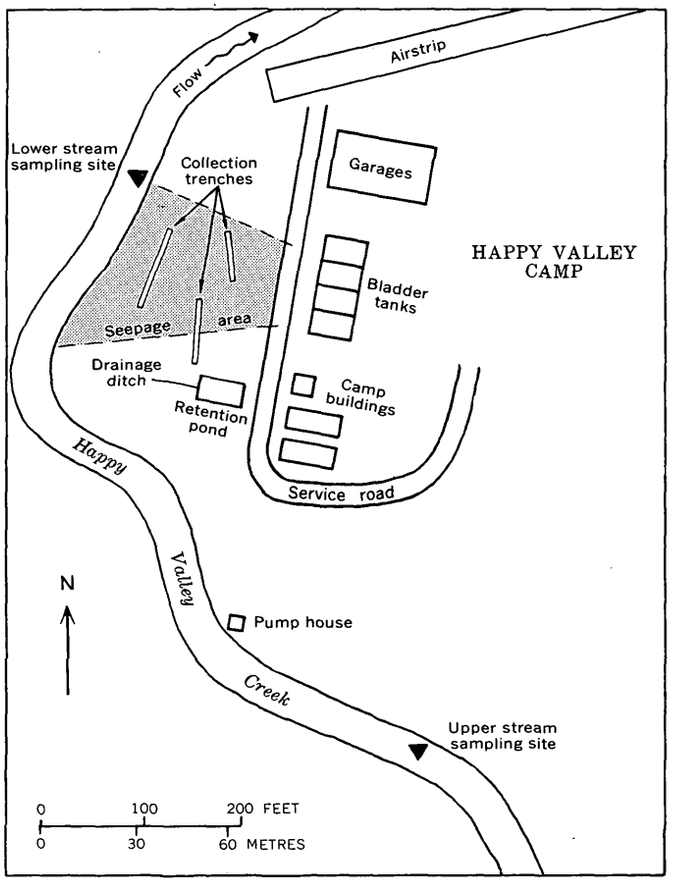

FIGURE 2.—Sampling sites on Happy Valley Creek.

This report lists the benthic invertebrates and other miscellaneous aquatic organisms collected on August 12 and 13, 1972, and includes field water-quality information, analysis of oil and grease in water samples collected during the study, and onsite observations on August 13 and 14, 1972.

METHODS

Physical and chemical sampling and results

Water temperature was measured to the nearest 0.1°C by using a bucket thermometer. Specific conductance was measured by an Industrial Instrument Model RM3 Solu Bridge featuring a cell constant of 0.2. Alkalinity was determined by titrating a measured 50-ml water sample with 0.01639 N H_2SO_4 to pH 4.3.

Dissolved oxygen was determined by the Winkler method (Brown and others, 1970). Chlorophyll *a* was determined by filtering 500 ml of stream water in the field through 0.45-mm Whatman GF/C glass filters. The fluorometric method of Strickland and Parson (1968) for chlorophyll extraction was followed in laboratory analysis. Turbidity was analyzed in the field by using a Hach Chemical Co., Model DR3450–B turbidimeter.

Water stage was measured to the nearest 3.0 mm by using a temporary staff gage. Discharge was measured by standard U.S. Geological Survey procedures (Buchanan and Somers, 1969).

In addition, in order to sample small amounts of fuel oil (arctic diesel oil is a light oil containing few heavy hydrocarbons and having a pour point of −45°C or below [1]) in water, visible oil at the lower site was skimmed from the surface with a clean rectangular enameled sorting pan. The skimming was repeated until a total of 1 litre of oil and water was collected. Although no oil was visible at the upper site, the same sampling procedure was followed there. After the samples were collected and an HCl fixative was added, they were transported to the laboratory for analysis where the procedure of Rainwater and Thatcher (1960), applicable to a range of 5 to 1,000 mg/l of extractable oil, was followed.

[1] Fuel oil supplied by Petro Products Co., Inc.

Biological sampling and results

Benthic invertebrates were collected by the following two methods:

1. The Surber stream-bottom sampler, sometimes used quantitatively (Slack and others, 1973), was modified with a 1-m-long net constructed of nylon screen cloth having mesh openings of 210 μm. A cross section of the stream at the upper and lower sites was visually divided into thirds. One sample was collected from each third, corresponding to the right, middle, and left parts of the stream cross sections.
2. Ten streambed rocks ranging from 15 to 30 cm in diameter were randomly selected at each site. As each rock was lifted off the bottom, a U.S. standard sieve No. 70 (210-μm mesh opening) was immediately slipped under the rock from the downstream position to minimize loss of organisms. The rocks were then scrubbed with a brush in a bucket of water and the loose material was caught and concentrated on the sieve.

A third set of samples was collected by dip net; however, because of the subjectivity of the method, the resultant data were excluded from this report.

Benthic invertebrate samples were preserved with 40 percent isopropyl alcohol in the field. In the laboratory, invertebrates were separated and counted by handpicking aided by density separation, differential staining, and subsampling (Slack and others, 1973). Enumeration and identification was done using a stereoscopic microscope. Limitations of time precluded identification of all invertebrate forms to species, hence the specimens were identified only to the level of the various invertebrate taxa listed in table 2. These taxa were placed in separate vials, preserved in 40 percent isopropyl alcohol, and labeled according to taxon, identification number, date, and sample origin.

OBSERVATIONS

Forty-one hours elapsed, including a part of August 12, all of August 13, and part of August 14, from the beginning of the study to its completion. Water stage monitored during the elapsed time dropped steadily for a total of 85 mm from the maximum value measured at the beginning. A discharge of 1.6 m^3/s was measured at the upper site at 1100 hours on August 13. The stream at the upper site measured 6.9 m wide, had an average depth of 0.3 m and an average current velocity of 0.7 m/s. The bottom was covered with small boulders, cobbles, and coarse gravel that created a continuous riffle from the upper to the lower site. No discharge measurements were made at the lower site for the two sites appeared to have the same width, depth, and bottom characteristics.

During the study, field water-quality data were collected 11 times at the upper site and 3 times at the lower site. These data are presented in table 1. The water in Happy Valley Creek is a calcium bicarbonate type with very low specific conductance.

The total number of individual aquatic organisms collected by the two methods at each site is shown in table 2. Numbers in parentheses are percentages of the total number of individuals collected by each method. A summary of the Surber samples presented as a percentage occurrence of major groups for the right, middle, and left parts of the cross sections, is shown in figure 3; figure 4 shows the percentage occurrence for the 10-rock samples, total for combined Surber samples, and total numbers of individuals for major grouping for the two methods for each site.

DISCUSSION

The data, despite the small number of samples and the short time of collection, indicate that the general

TABLE 1.—*Meteorological and water-quality data for Happy Valley Creek, Alaska, August 12–14, 1972*

[Jtu, Jackson turbidity unit; upper, site above oil seepage area; lower, site adjacent to oil seepage area]

Date	Time		Water temperature (°C)		Conductance (μmho)		pH		Alkalinity (mg/l)		Dissolved oxygen: Milligrams per litre		Dissolved oxygen: Percent saturation		Turbidity (Jtu)		Chlorophyll *a* (μg/l)		Stage (ft)		Discharge (ft^3/s)	
	Upper	Lower	Upper	Lower	Upper	Lower	Upper	Lower	Upper	Lower	Upper	Lower	Upper	Lower	Upper	Lower	Upper	Lower	Upper	Lower	Upper	Lower
Aug. 12	1515	----	----	----	----	----	----	----	----	----	----	----	----	----	----	----	----	----	9.16	----	----	----
	1800	----	----	----	----	----	----	----	----	----	----	----	----	----	27	----	----	----	9.14	----	----	----
Aug. 13	0700	----	8.3	----	21	----	6.8	----	12	----	10.8	----	95	----	----	----	0.7	----	9.04	----	----	----
	0800	----	8.3	----	21	----	6.8	----	12	----	----	----	----	----	22	----	.7	----	9.02	----	----	----
	0930	----	8.6	----	21	----	6.8	----	11	----	10.6	----	93	----	18	----	.7	----	9.02	----	----	----
	1100	----	9.3	----	21	----	6.8	----	13	----	10.6	----	95	----	21	----	.7	----	9.02	----	5.50	----
	----	1130	----	----	----	30	----	6.9	----	18	----	----	----	----	----	24	----	0.7	----	----	----	----
	1400	----	10.0	----	21	----	6.9	----	12	----	10.4	----	93	----	24	----	.6	----	8.99	----	----	----
	1630	----	10.5	----	21	----	6.9	----	12	----	10.4	----	96	----	20	----	.6	----	8.96	----	----	----
	----	1700	----	----	----	26	----	7.0	----	15	----	10.3	----	94	----	21	----	----	----	----	----	----
	1730	----	10.7	----	22	----	6.8	----	15	----	10.2	----	94	----	19	----	.6	----	8.86	----	----	----
	2000	----	10.6	----	22	----	6.7	----	13	----	10.2	----	94	----	22	----	.6	----	8.84	----	----	----
Aug. 14	0200	----	10.0	----	22	----	6.5	----	17	----	10.2	----	93	----	20	----	.6	----	8.92	----	----	----
	0610	----	9.7	----	23	----	6.6	----	13	----	10.4	----	94	----	21	----	.5	----	8.90	----	----	----
	----	0630	----	----	----	22	----	6.6	----	13	----	----	----	----	----	20	----	.6	----	----	----	----
	0730	----	10.1	----	23	----	6.7	----	12	----	10.3	----	94	----	20	----	.5	----	8.88	----	----	----

TABLE 2.—*Biological data given in number of taxa collected from Happy Valley Creek, Alaska, August 13–14, 1972*
[Percentage of total number of individuals collected by each method is given in parentheses; minus in parentheses indicates <1 percent]

Taxa	Surber samples						10-rock samples	
	Upper site cross section			Lower site cross section			Upper site	Lower site
	Right	Middle	Left	Right	Middle	Left		
Nematoda	16 (—)	276 (7)	164 (5)			20 (2)	243 (4)	47 (44)
Oligochaeta	12 (—)	196 (5)	8 (—)		4 (—)		243 (4)	
Crustacea:								
Cladocera	1,536 (63)	616 (15)	712 (24)	32 (80)	400 (71)	752 (76)	47 (—)	22 (21)
Ostracoda	8 (—)		4 (—)	4 (10)	8 (1)	4 (—)	7 (—)	
Copepoda	16 (—)	96 (2)	108 (4)		48 (8)	60 (6)	150 (2)	14 (13)
Mollusca: Gastropoda	40 (2)	84 (2)	40 (1)		12 (2)	16 (2)	20 (—)	1 (1)
Insecta								
Chironomidae (larvae)	748 (32)	2,620 (64)	1,864 (63)	4 (10)	64 (11)	92 (9)	5,699 (88)	15 (14)
Chironomidae (pupae)	12 (—)	16 (—)	4 (—)		8 (1)		15 (—)	1 (1)
Tabanidae (larvae)		24 (—)	8 (—)				16 (—)	
Muscidae (larvae)							5 (—)	
Plecoptera (nymphs)	4 (—)	36 (1)	24 (1)			4 (—)	1 (—)	
Collembola		4 (—)	4 (—)		12 (2)	20 (2)		1 (1)
Hemoptera							1 (—)	
Trichoptera		44 (1)					44 (1)	
Arachnoidea: Hydracarina	28 (1)	68 (1)	20 (1)		4 (1)	24 (2)	6 (—)	5 (5)
Total individuals	2,420	4,080	2,960	40	560	992	6,497	106
Total taxa	9	11	12	3	8	9	13	7

effect of the oil spill was the overall reduction of aquatic organisms at the lower site. Benthic invertebrates usually are immobile and are unable to escape deleterious environmental changes. They, therefore, reflect the effect of the oil in alteration of normal species composition and species abundance. Of all the taxa in the samples, the most abundant were the Chironomidae larvae and Cladocera, and both of these decreased at the lower site. The relative percentage difference in abundance, between the upper and lower sites, was greater for the Chironomidae than for the Cladocera (figs. 3 and 4). Cladocera generally are not considered indicators of environmental stress. Surber samples from both the upper and lower sites apparently indicate a dissimilarity of aquatic organism populations in each of the three parts of the cross section (table 2); however, samples from the downstream site apparently show the effects of the greater concentration of oil at the right bank. The number of organisms per sample increases from the right bank to the left bank. Surber samples from the upstream site show a much smaller reduction in numbers of organisms at both banks relative to the center.

Reports by Bury (1972) and Watson (1941) verified the toxic effects of diesel fuel and oil on stream aquatic organisms subjected to long-term exposures. The fact that oil was known to be seeping into Happy Valley Creek for some time, that it was noted in the creek at the time of this study, and that bottom material, when disturbed, produced an oil film on the water surface, coincident with a total reduction in abundance of aquatic organisms (mostly Chironomidae, Trichoptera, and Plecoptera larvae), suggests that arctic diesel fuel oil is toxic to some forms of benthic invertebrates at the concentrations existing in the creek.

Although oil was visually observed at the lower site and its odor was apparent in the samples of water and organisms collected there, oil was not detected in the water samples by the analytical method available at the laboratory. The gravimetric extraction analysis method that was used is considered to be unreliable for the more volatile oil fractions. However, Giles McDonald, Bureau of Land Management, Alaska Pipeline Office (written commun., 1973) indicated that studies made on August 13, 1973, using the dimethylchloride extraction method did detect low concentrations of total oils. Concentrations of 1.0 and 7.9 mg/l were found above and below the spill area, respectively. However, a visible light-oil sheen may indicate a concentration of oil on the water surface of 10–20 mg/l (S. L. Bugbee, Environmental Protection Agency, Surveillance and Analysis Div., Kansas City, Kans., written commun., Aug. 13, 1974).

No significant differences in field water-quality characteristics were found between the two sites. The slight differences in water quality which occurred (table 1) may be attributed to diurnal variations, sampling techniques, and effluent from the retention pond. Because the effluent was fully treated and unchlorinated, the only anticipated effects might be nutrient enrichment in the immediate area of the confluence of the creek and the effluent ditch. During June 1972, Nauman and Kernodle (1973) reported chlorophyll *a* concentrations of 115.0 and 0.4 μg/l for the retention pond and the creek, respectively.

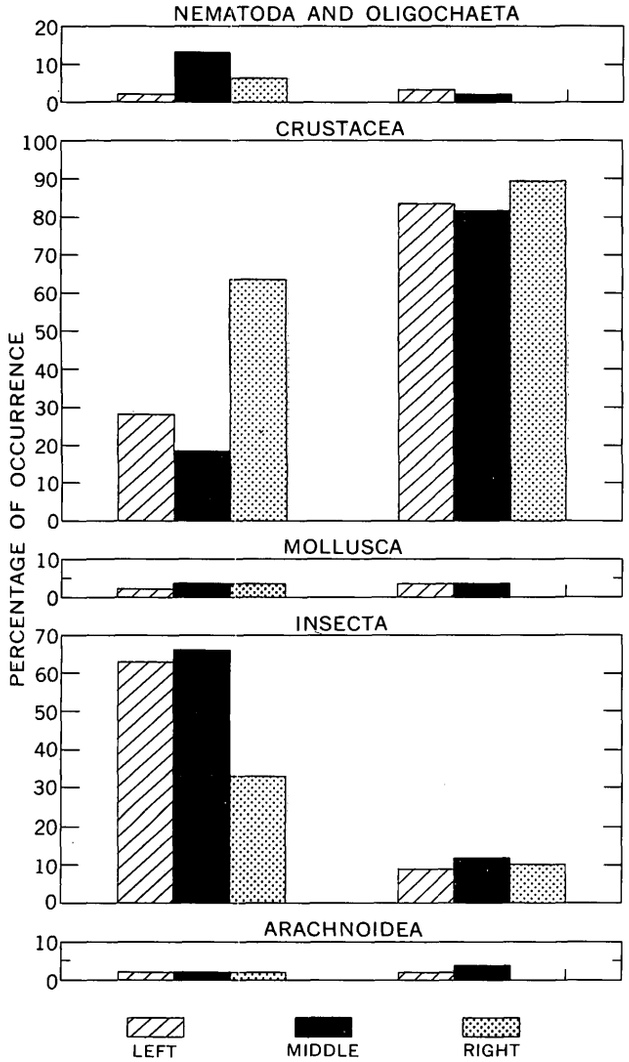

TOTAL INDIVIDUALS COLLECTED			
UPPER SITE		LOWER SITE	
LEFT	2,960	LEFT	992
MIDDLE	4,080	MIDDLE	560
RIGHT	2,420	RIGHT	40
TOTAL	9,460	TOTAL	1,592

FIGURE 3.—Percentage of occurrence of aquatic organisms collected with the Surber sampler.

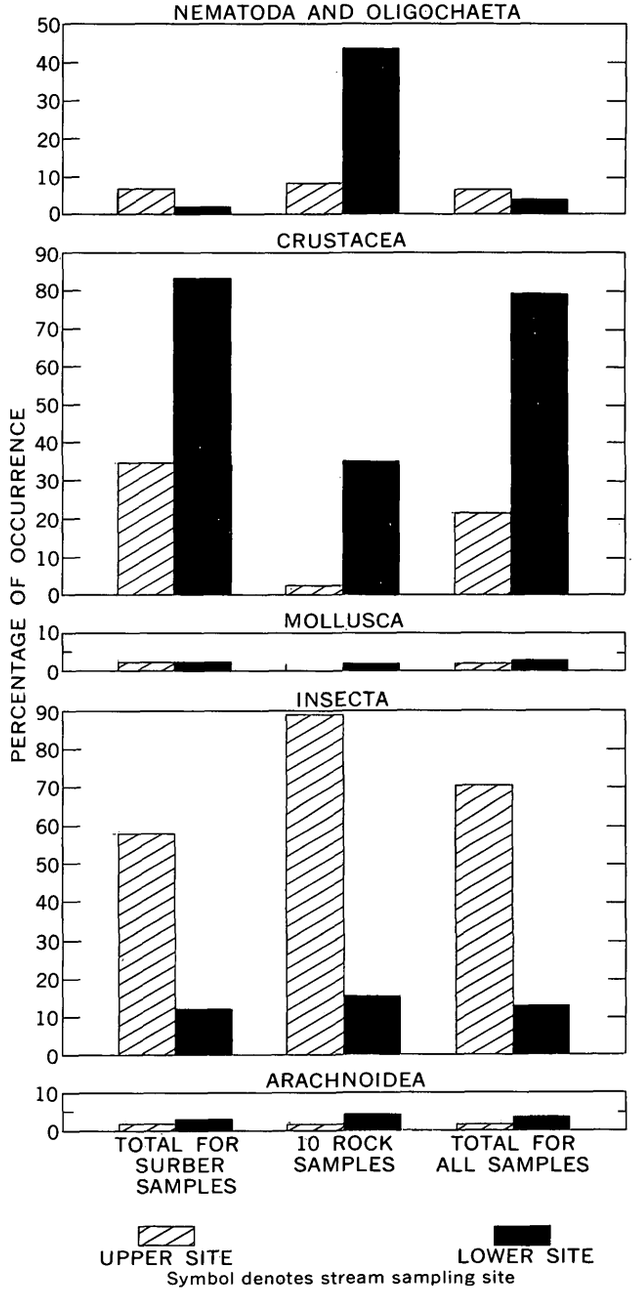

TOTAL INDIVIDUALS			
UPPER SITE		LOWER SITE	
SURBER SAMPLES	9,460	SURBER SAMPLES	1,592
10 ROCK SAMPLES	6,497	10 ROCK SAMPLES	106
TOTAL	15,957	TOTAL	1,698

FIGURE 4.—Percentage of occurrence of aquatic organisms collected by the Surber-sample and the 10-rock sample methods and total numbers of individuals collected.

CONCLUSION

Although the data are inconclusive, benthic invertebrates of all taxonomic groups were reduced in numbers at the lower site immediately adjacent to the oil seepage area relative to those at the upper site unaffected by the oil. This reduction may be attributed to the accumulation of arctic diesel fuel oil, which was visually detected in the water adjacent to the seepage area and on bottom substrates and was reported in water samples collected during the period of this study.

REFERENCES CITED

Alaska Construction News, Inc., 1972, All about the "disaster" in Happy Valley: Alaska Construction and Oil, v. 13, no. 10, Oct., p. 50–52, 54.

Brown, Eugene, Skougstad, M. W., and Fishman, M. J., 1970, Methods for collection and analysis of water sampled for dissolved minerals and gases: U.S. Geol. Survey Techniques Water-Resources Inv., book 5, chap. A1, 160 p.

Buchanan. T. J., and Somers, W. P., 1969, Discharge measurements of gaging stations: U.S. Geol. Survey Techniques Water-Resources Inv., book 3, chap. A8, 65 p.

Bury, R. B., 1972, The effects of diesel oil on a stream fauna: California Fish and Game, v. 58, no. 4, p. 291–295.

Ferrians, O. J., Jr., 1965, Permafrost map of Alaska: U.S. Geol. Survey Misc. Geol. Inv. Map I–445.

Nauman, J. W., and Kernodle, D. R., 1973, Field water-quality information along the trans-Alaska pipeline corridor, September 1970 through September 1972: U.S. Geol. Survey open-file rept., 22 p.

Rainwater, F. H., and Thatcher, L. L., 1960, Methods for collection and analysis of water samples: U.S. Geol. Survey Water-Supply Paper 1454, 301 p.

Slack, K. V., Averett, R. E., Greeson, P. E., and Lipscomb, R. A., 1973, Methods for collection and analysis of aquatic biological and microbiological samples: U.S. Geol. Survey Techniques Water-Resources Inv., book 5, chap. A4, 165 p.

Strickland, J. D. H., and Parson, T. R., 1968, A practical handbook of seawater analysis: Fisheries Research Board of Canada Bull. 167, 311 p.

Watson, G. I., 1941, A physiological study of mosquito larvae which were treated with antimalarial oils: Bull. Entomol. Research, v. 31, 319 p.

Jour. Research U.S. Geol. Survey
Vol. 3, No. 4, July–Aug. 1975, p. 501–503

INJECTION-PIPE SYSTEM FOR ARTIFICIAL RECHARGE

By HAROLD O. REEDER, St. Paul, Minn.

Abstract.—An injection-pipe system was designed to utilize pipe friction rather than a remote-control valve in the well to maintain positive pressure and to eliminate gas release and air entrainment in the injection water. The size of the injection pipe was selected on the basis of obtaining a unit friction head loss per equal-unit length of pipe for the desired injection rates. The injection rates are 70 gallons per minute (4.4 litres per second) through a 1¼-inch (32-mm) heavy duty pipe and 106 gal/min (6.7 l/s) through a 1½-in (38-mm) heavy duty pipe. A diagram shows flow rates through other pipe sizes.

A major problem in some recharge experiments has been plugging of the formation or wells with bubbles. Entrainment of air in the recharge water and release of dissolved gasses from the water are the sources of bubbles that enter the formation. The cause can be attributed primarily to decreased pressures or negative pressures that may prevail in closed-pipe recharge or air entrainment when water is allowed to fall freely down a well. Sniegocki and Reed (1963) discuss the principles and effects of siphons in detail. The problem is solved by maintaining a full injection pipe with positive pressure throughout its length. In some experiments a control valve was placed below the water level in the injection well to maintain a full pipe and positive pressure. However, placing a valve down-hole requires a large-diameter well and a means for controlling the valve from the ground surface.

The U.S. Geological Survey has completed an experiment in West St. Paul, Minn., to test the feasibility of artificially recharging fissured carbonate rocks through wells.

DESIGN OF INJECTION-PIPE SYSTEM

In the experiment, the injection system was designed to use pipe friction instead of a valve to maintain positive pressure in the pipe. The pipe size was selected on the basis of the desired injection rate and of the maximum flow that a pipe can carry when the friction causes a unit head loss for an equal unit of pipe length. The following form of the Hazen-Williams formula, King (1939, p. 176) was used in the computation:

$$v = 1.318 C r^{0.63} s^{0.54} \qquad (1)$$

in which v is the mean velocity of the water, in feet per second; C is the Hazen-Williams roughness coefficient of the pipe; r is the mean hydraulic radius $= d/4$; s is the head loss, the mean slope of the hydraulic gradient, in feet per foot length of pipe; and d is the inside diameter of the pipe, in feet. The form of the equation can be modified to solve for the rate of flow as $Q = vA$, in which A is the cross-sectional area of the pipe. The formula for round pipe becomes:

$$Q = 1.318 C \frac{\pi d^{2.63} s^{0.54}}{4^{1.63}} \qquad (2)$$

With the design head loss gradient due to friction of $s = 1$, then $s^{0.54} = 1$, and the formula becomes:

$$Q = \frac{1.318 \pi C d^{2.63}}{4^{1.63}} = 0.432 C d^{2.36} \qquad (3)$$

in which d is the inside diameter of the pipe, in feet, and Q is rate of flow, in cubic feet per second. (Multiply Q by 28.32 to convert to litres per second.)

Two pipes, 1¼-in (32-mm) and 1½-in (38-mm) diameter heavy duty wrought iron black pipe, were installed from the supply pipe, with a static pressure of 125 ft (38 m), to 75 ft (23 m) below the water level in the well. The pressure head in the injection pipe at the top of the well remained fairly uniform at about 97 ft (30 m) after the valve was fully opened during injection. The water level in the well (in which the injection pipe was submerged) fluctuated barometrically but did not have a long-term rise or decline after the initial buildup of about 6 ft due to injection. This means that the injection head loss (difference in entrance and exit pressure heads) remained about the same after the first day of injection. The computed maximum (uncontrolled by valve) injection rates, with a friction loss gradient of 1 with this system are: 70 gal/min, or 4.4 l/s through the 1¼-in (32-mm) pipe, 106 gal/min (6.7 l/s) through the 1½-in (38-mm) pipe, and 176 gal/min (11.1 l/s) through both pipes together, based on a C value of 130 for new steel or cast-iron pipe. A graph of flow rates for small pipes, with the Hazen-Williams roughness coefficients, C, of 100 and 130 and a friction head loss of gradient of 1, is shown in figure 1. These values generally are not shown in published pipe-friction tables because the flow rates and head losses exceed those normally con-

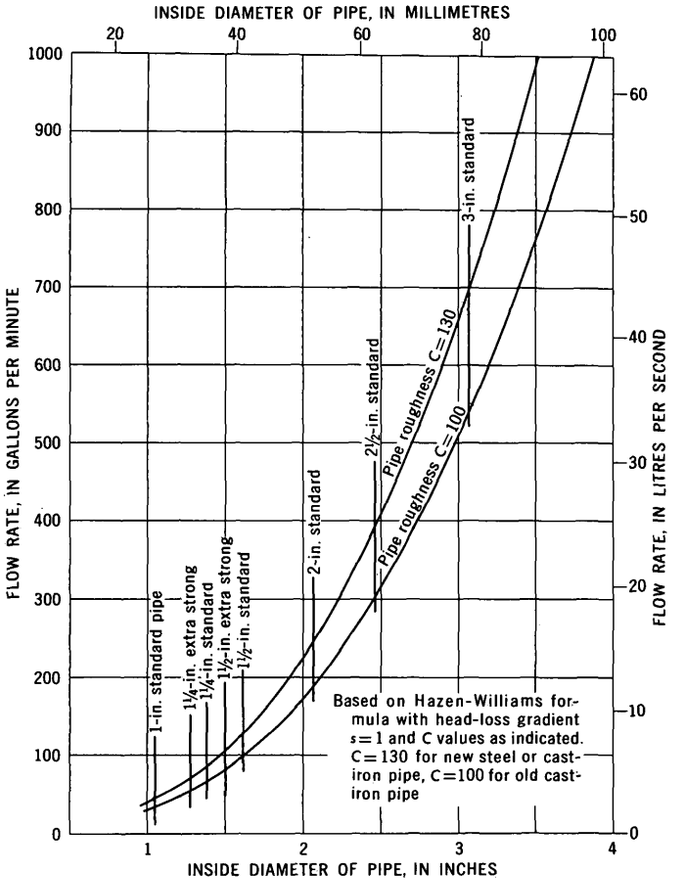

FIGURE 1.—Graph of flow rates in small pipes, with unit head loss per unit length of pipe.

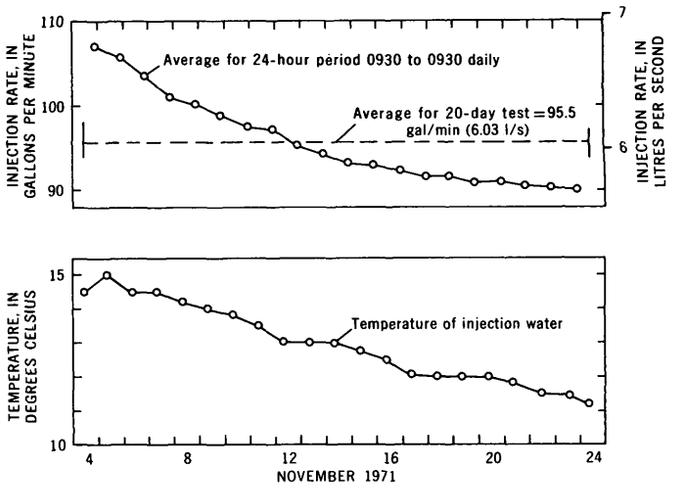

FIGURE 2.—Graphs of injection rate and temperature of injection water during injection test.

sidered in pipeline design. Olson (1966, p. 248) presents a nomograph of pipe flow for the Hazen-Williams formula, with $C=100$, in the range of rates and head losses used in pipeline designs. By extending the head-loss scale to 1,000 ft (304.8 m) of head loss per 1,000 ft (304.8 m) of pipe, approximate values could be determined comparable to those shown in figure 1.

During the test using only the 1½-in (38-mm) pipe, the rate of injection started at 108 gal/min (6.8 l/s) and gradually decreased to 90 gal/min (5.7 l/s). Temperature of the injected water during the 20-day test declined gradually from 15.0° to 11.2°C, giving an apparent cause for the gradual decrease in injection rate. Part of the decrease in flow rate can be accounted for by assuming that discharge is inversely proportional to the kinematic viscosity of the water at its prevailing temperature. For example, based on this assumption and data after the inlet valve at the well head was fully opened, a water-temperature change from 14.0° to 11.2°C would decrease the flow rate in the 1½-in (38-mm) pipe from 100 gal/min (6.31 l/s) to a computed 93.8 gal/min (5.92 l/s), as compared with 90.0 gal/min (5.68 l/s) measured. Figure 2 shows graphs of injection rate and water temperature. As part of the variation may be due to the change in water temperature, it is suggested that a viscosity correction is needed in the above equations, at least for the range of pipe sizes and friction head losses used in the computations. Other factors, such as change in pipe roughness, may have caused part of the decrease in flow rate. A gradual change in the roughness coefficient, C, from 130 to 110 would account for a decrease in flow rate from 108 to 91.6 gal/min (6.8 to 5.78 l/s), which is nearly the actual decrease. It does not seem likely that a roughness would change that much during the 20 days of the test, but perhaps the relatively high velocities cause corrosion, pitting, or other roughening of the pipe.

The Hazen-Williams formula is most applicable for pipes of 2 in (50 mm) or larger and velocities less than 10 ft/s, or 3 m/s (Chow, 1964, p. 7–18). However, results from the formula in this design were valid. An advantage to using this formula is that all problems have direct solutions. The Darcy-Weisbach equation and the Moody resistance diagram take into account viscosity of the water and roughness of the pipe, but changes in the two cannot be separated with the data available.

CONCLUSIONS

Air entrainment and release of dissolved gasses from water that accompanies a head drop can be avoided by using small-diameter pipe utilizing the pipe friction, a scheme that also reduces the cost of the injection-pipe system. The expense of an injection system can be further reduced by using pumped wells also as injection wells. Many production wells are large enough to

accommodate one or more small pipes beside the pump column and could be used alternately as production wells and injection wells.

REFERENCES CITED

Chow, Ven Te, ed., 1964 ,Handbook of applied hydrology: New York, McGraw-Hill Book Co., Inc., p. 7–18.

King, H. W., 1939, Handbook of hydraulics: New York, McGraw-Hill Book Co., Inc., 617 p.

Olson, R. M., 1966, Essentials of engineering fluid mechanics: Scranton, Pa., International Textbook Co., 448 p.

Sniegocki, R. T., and Reed, J. E., 1963, Principles of siphons with respect to the artificial-recharge studies in the Grand Prairie region, Arkansas: U.S. Geol. Survey Water-Supply Paper 1615–D, 19 p.

☆ U.S. Government Printing Office 1975: 585-407/6

RECENT PUBLICATIONS OF THE U.S. GEOLOGICAL SURVEY

(The following books may be ordered from the U.S. Geological Survey, 1200 South Eads Street, Arlington, VA 22202 (an authorized agent of the Superintendent of Documents, Government Printing Office). Prepayment is required. Remittances should be sent by check or money order payable to U.S. Geological Survey. Give series designation and number, such as Bulletin 1368–A, and the full title. Prices of Government publications are subject to change. Increases in costs make it necessary for the Superintendent of Documents to increase the selling prices of many publications offered. As it is not feasible for the Superintendent of Documents to correct the prices manually in all the publications stocked, the prices charged on your order may differ from the prices printed in the publications and in this list)

Professional Papers

716–F. Geology of the Parachinar quadrangle, Pakistan, by C. R. Meissner, Muzaffar Hussain, M. A. Rashid, and U. B. Sethi. 1975. p. F1–F24; plate in pocket. 95¢.

758–B. Geology and mineral deposits of the Upper Chulitna district, Alaska, by C. C. Hawley, and A. L. Clark. 1974 (1975). p. B1–B47; plates in pocket. $2.75.

763. Stratigraphy of the Inyan Kara Group and localization of uranium deposits, southern Black Hills, S. Dak. and Wyo., by G. B. Gott, D. E. Wolcott, and C. G. Bowles. 1974 (1975). 57 p.; plates in pocket. $5.10.

810. Geophysical surveys of Liberia with tectonic and geologic interpretations, by J. C. Behrendt and C. S. Wotorson. 1974 (1975). 33 p. $3.80.

842. Type sections of the Madison Group (Mississippian) and its subdivisions in Montana, by W. J. Sando and J. T. Dutro, Jr. 1974 (1975). 22 p.; plate in pocket. $1.70.

847. Quaternary stratigraphy and extent of glaciation in the Mount Rainier region, Washington, by D. R. Crandell and R. D. Miller. 1974 (1975). 59 p.; plates in pocket. $1.60.

852. Evolution of the Platoro caldera complex and related volcanic rocks, southeastern San Juan Mountains, Colo., by P. W. Lipman. 1975. 128 p. $3.25.

862. Quaternary stratigraphic nomenclature in unglaciated central Alaska, by T. L. Péwé. 1975. 32 p. $1.25.

868. Post-Paleocene Tertiary rocks and Quaternary volcanic ash of the Wet Mountain Valley, Colo., by G. R. Scott and R. B. Taylor. 1975. 15 p.; plate in pocket. $1.55.

883. Discrimination of rock types and detection of hydrothermally altered areas in south-central Nevada by the use of computer-enhanced ERTS images, by L. C. Rowan, P. H. Wetlaufer, A. F. H. Goetz, F. C. Billingsley, and J. H. Stewart. 1974 (1975). 35 p. $1.55.

908. Simulated effects of oil-shale development on the hydrology of Piceance basin, Colorado, by J. B. Weeks, G. H. Leavesley, F. A. Welder, and G. J. Saulnier, Jr. 1974 (1975). 84 p.; plate in pocket. $3.15.

Bulletins

1387. Checklist of North American late Paleozoic coral species (Coelenterata, Anthozoa), by W. J. Sando. 1974 (1975). 36 p. 70¢.

1390. Monazite placers in the southeastern Atlantic States, by J. B. Mertie, Jr. 1975. 41 p. 80¢.

1395–A. Changes in stratigraphic nomenclature by the U.S. Geological Survey, 1973, by G. V. Cohee and W. R. Wright. 1975. p. A1–A68. 95¢.

Water-Supply Papers

1880–B. Floods of September-October 1967 in south Texas and northeastern Mexico, by E. E. Schroeder, R. U. Grozier, D. C. Hahl, and A. E. Hulme. 1974 (1975). p. B1–B111; plates in pocket, $3.55.

2029–E. An appraisal of potential water salvage in the Lake McMillan delta area, Eddy County, N.Mex., by E. R. Cox and J. S. Havens. 1974 (1975). p. E1–E26; plates in pocket. $1.50.

2032. Ground water in the Corvallis-Albany area, central Willamette Valley, Oreg., by F. J. Frank. 1974 (1975). 48 p.; plates in pocket. $1.95.

2097. Quality of surface waters of the United States, 1968—Part 8, Western Gulf of Mexico basins. 1974 (1975). 473 p. $3.45.

2132. Surface water supply of the United States, 1966-70—Part 12, Pacific slope basins in Washington—Volume 1, Pacific slope basins in Washington except Columbia River basin. 1974 (1975). 640 p. $4.40.

2140. Ground-water levels in the United States, 1968-72—Northeastern States. 1974 (1975). 207 p. $1.75.

2142. Quality of surface waters of the United States, 1969—Part 2, South Atlantic slope and eastern Gulf of Mexico basins. 1974 (1975). 625 p. $4.35.

2145. Quality of surface waters of the United States, 1969—Part 6, Missouri River basin. 1974 (1975). 441 p. $3.25.

2146. Quality of surface waters of the United States, 1969—Part 7, Lower Mississippi River basin. 1974 (1975). 540 p. $3.85.

2147. Quality of surface waters of the United States, 1969—Part 8, Western Gulf of Mexico basin. 1974 (1975). 567 p. $4.

2148. Quality of surface waters of the United States, 1969—Parts 9 and 10, Colorado River basin and the Great Basin. 1974 (1975). 348 p. $2.65.

2159. Quality of surface waters of the United States, 1970—Part 11, Pacific slope basins in California. 1974 (1975). 397 p. $3.60.